Investigating centriole orientation in the *Drosophila* embryo



Nicole Liew Syuen Li

St. Catherine's College

University of Oxford

A thesis submitted for the degree of Doctor of Philosophy

Michaelmas Term 2023

Table of Contents

Acknowledgements ..... **V**

Abstract ..... **VII**

Abbreviations ..... **VIII**

Introduction **1**

1.1 Centrioles **1**

1.1.1. Centriole Structure 2

1.1.2. Centriole Duplication 4

1.1.3. Centrioles as Basal Bodies in Ciliogenesis 7

1.1.4. The Evolution of Centrioles 8

1.2. The PCM and the centrosome **10**

1.2.1. Centrosome Composition and Growth 11

1.2.2. Centrosomes as MTOCs 14

1.2.3. Interactions between the Centrosome and Actin 15

1.3 The distal end **18**

1.3.1. Distal Appendage Proteins 18

1.3.2. Conservation of DAPs in *Drosophila* 20

1.3.3. Distal Cap proteins 21

1.4. Centriole and Centrosome Positioning **25**

1.4.1. Asymmetric Division 25

1.4.2. Cell Migration 27

1.4.3. Cell Polarity 28

1.4.4. Putative Roles for Centriole Orientation 30

1.5. Neural Networks **33**

1.5.1. How ANNs Work 34

1.5.2. Types of Neural Networks 34

1.5.3. Calculating and Minimising Network Error 37

1.6. Thesis Overview **39**

1.7. Aims **40**

2. Materials and Methods **41**

2.1. Fly Husbandry **41**

2.1.1. Fly Handling 41

2.1.2. *Drosophila* stocks 41

2.2. Biochemistry and Cell Biology **43**

2.2.1. Embryo Fixation for Differential Fluorescence Labelling 43

2.2.2. SDS-PAGE and western blotting 44

2.3. Experiments in living embryos **46**

2.3.1. Embryo Handling for live-imaging 46

2.3.2. Drug injection 46

2.4. Microscopy **47**

2.4.1. Zeiss 880 Laser Scanning Microscope 47

2.4.2. OMX V_3 Blaze with 3D-structured illumination 47

2.4.3. Olympus Super Resolution Confocal Microscope 47

2.5. Data Analysis **48**

2.5.1. Processing of fixed images for differential fluorescence labelling 48

2.5.2. Radial Profiles 48

2.5.3. Processing of movies 48

2.5.4. Centrilyze 49

2.5.5. Implementing a Hidden Markov Model to quantify centriole stability 49

2.5.6. Processing Centrilyze and HMM data 50

2.6. Statistics **50**

3. Centrioles appear preferentially distally-oriented with respect to the embryo cortex **52**

3.1. Introduction **52**

3.1.1. Distal end components of centrioles in mammalian and *Drosophila* cells 52

3.1.2. Key Findings 55

3.2. Results **56**

3.2.1. An assay to determine the orientation of *Drosophila* centrioles 56

3.2.2. Centrioles appear preferentially oriented with their distal-end facing the cell cortex 58

3.3. Discussion 64

4. Establishing an assay to quantify centriole orientation and stability 69

4.1 Introduction 69

4.1.1 Advantages of using a live assay to measure centriole orientation 69

4.1.2. Measuring centriole orientation using an ANN 70

4.1.3. Key Findings 72

4.2 Results 73

4.2.1 Developing an imaging pipeline 73

4.2.2. Developing a high-throughput analysis pipeline to quantify centriole orientation 80

4.2.3. Calculating centriole stability over time 86

4.3. Discussion 92

4.3.1. Imaging syncytial embryos in S-phase 92

4.3.2. Usage of Centrilyze to quantify centriole orientation 93

4.3.2. Explaining the presence of Bar and Slanted states given that centrioles have a preference to be oriented as Rings 94

5. Mechanisms establishing and maintaining centriole orientation 97

5.1 Introduction 97

5.1.1. A need to understand why centrioles are oriented 97

5.1.2. The importance of microtubules and actin in centrosome function 98

5.1.4. The roles of distal cap proteins CP110 and Cep97 99

5.1.5. Key Findings 101

5.2 Results 102

5.2.1. Role of cytoskeletal components in centriole orientation 102

5.2.2. The role of Cnn and the PCM in centriole orientation 110

5.2.3. Distal cap proteins appear to help orient centrioles 116

5.3. Discussion 125

5.3.1. The subtle effects of actin depletion on centriole orientation and stability 125

5.3.2. The effect of centriole movement on the stability of centriole orientation in *cnn*^{f} embryos 127

5.3.3. The discrepancy between Cep97$^{-/-}$ and CP110$^{-/-}$ embryos 127

5.3.4. Ring-oriented centrioles are the default state 129

5.3.5. A preliminary model for centriole orientation 130

6 Discussion 133

6.1. Summary of Key Findings 133

6.2. Quantifying highly subjective measurements 134

6.3. Centriole orientation as an ancient function of the centriole itself 136

6.5. Future Directions 138

6.5.1. Improving methods of actin depletion in *Drosophila* embryos 139

6.5.2. Exploring other ways to deplete the PCM 139

6.5.3. Investigating centriole orientation in embryos where proteins implicated in centriole positioning have been depleted 140

6.5.4. Further experiments investigating a Cep97 led mechanism of centriole orientation 141

6.5.5. Exploring centriole orientation in other *Drosophila* tissues 141

6.5.6. Understanding centriole orientation in non-ciliated systems 142

References 143

Appendix 166

Acknowledgements

I would first of all like to express my thanks for my supervisor, Jordan Raff, for guiding me from a very lost rotation student to a little less lost Dphil student. He has taught me to think carefully and specifically about the experiments I do, altogether shaping me into a better scientist and planner. I cannot overstate how patient he has been with me through this complicated project and tough time in my personal life, and beyond the science I will always be grateful for that patience. I would also like to express my gratitude to the Wellcome Trust for their generous funding throughout the course of my Dphil, as well as the Oxford Medical Sciences Training Centre for waiving my international tuition fees upon entry into the program. It is because of their generosity that more people from other countries get to pursue science at such a prestigious university. To my program coordinator Matthew Whitby, as well as Louise Samson, thank you for always being on hand to answer all my questions and helping me through the tedious tasks of extension application and Visa renewal throughout my Dphil.

Thank you to the members of the Raff lab, who have accommodated me through my presence and absence through the years as well as provided important scientific insights, Yanis Guimard, Ines Alvares Rodrigo, Ed Rea, Mustafa Aydogan, Mo Mofatteh, Laura Hankins, Tess Harrison, Emma Roberts, Chang Chia Chun, Nada Mohamad, Zach Wilmott, João Monteiro and Zsofi Novak, a lot of the interpretation within my thesis would not have been possible without conversations I have had with all of you. Thanks to Thomas Steinacker for providing me with the NG-Asl fly line which I have used throughout this thesis and Saroj Saurya for help with western blots and being a slice of home away from home. I would also like to thank Isaac Wong for performing the preliminary experiments that jumpstarted our interest in centriole orientation, writing the python scripts and being a generally inspirational human being, I will always be in awe of your ideas and your resolve to do anything you set your mind to. To Conor Wild for writing Centrilyze, without which this thesis would not exist. I apologize for all the short notice and thank you for so kindly teaching me about a subject many people (Biologists) find intimidating (Statistics). You have worked very closely with me to create a network that is accessible yet robust and I am very happy with what we've been able to do together. I would also like to extend a special thanks to Alan Wainman for his endless knowledge in microscopy but more importantly, for believing in me when I didn't believe in myself. It can be hard staying motivated in such a long project, and your enthusiasm and reassurance helped me keep going.

Mam and Papa (Agnes Yoong and Liew Chuw Yee respectively), if you had not taken the leap of faith to agree to send me to the UK alone at the age of sixteen, I would not be here, so thank you for believing in me and through all these years continuing to financially support me. You both have also continued to allow me to pursue science to this high level, which I am grateful for and I hope you are proud of what I have achieved. Lai Sook (Lau Ken Poh), thank you for doing so much heavy lifting while I chaotically moved in near the end of my Dphil so I had more time to focus on my writing. Finally, Jason Liew, thank you for telling me that 'you are not your work', a mantra that I have repeated time and time again throughout this process. You have always tried your best to see where I'm coming from and give some of the most succinct, slap-you-over-the-head advice that I think of daily. I truly could not have asked for a better brother.

Progression of my Dphil coincided with COVID-19 as well as mental health issues. During this time, I have found that the presence of found family can be deeply healing. As such, I would like to thank Cynthia Zhang, Anna Mckie, Ainhoa Santos Goicoechea, Domenic Suntrapak, Rowan Moore, Geraint Hoggan, George Andrews, Daniel Antoine-Donatein and William Brilliant, all some of the best writers and creatives I know. It sounds corny, but you all have whisked me away to fantastical worlds when I needed it most and provided some very real consolation when we came back from our adventures. I would also like to thank Valentine

and Hemlock, my cats, who remind me to wake up, take breaks and get sleep with their timely and incessant meowing. Their presence has been immensely calming as they constantly remind me to be present in my surroundings.

Lastly, Peyton Cherry, my other half, who I did not plan to meet at the start of this Dphil and has been the reason my life has taken so many unexpected turns. It is to you that I would like to extend the biggest thanks. Every day, you show me how to be a better person and inspire me with your love for the natural world that continues to keep my own love of science alive. Thank you for all your hot takes and warm encouragements throughout my Dphil, for all the tissues, and glasses of water, and the biscuits you have brought me, for all the dinners you have cooked and chores you've taken over since I started writing. For every sleepless night and panic attack and vet emergency room… I would not be here in any capacity without you and because you are by my side, I can firmly say throughout these chaotic years that I regret nothing.

Abstract

Investigating centriole orientation in Drosophila embryos

Nicole Liew Syuen Li

St. Catherine's College / Sir William Dunn School of Pathology

A thesis submitted for the degree of Doctor of Philosophy, Michaelmas 2023

Centrioles are barrel shaped organelles that are known to nucleate microtubules (MT) contributing to the mitotic spindle and act as basal bodies during ciliogenesis. Mammalian centrioles possess distal appendage proteins (DAPs) which allow them to anchor to the cell cortex via their distal end. This distal ended orientation often plays a functional role within the cell. In many other cell types, centrioles are specifically positioned close to the cell cortex. However, we do not yet understand how centrioles may be oriented in these systems. Our lab has long observed that in *Drosophila* embryos, which do not possess DAPs or make cilia, that most centrioles appear upright. Using a fixed assay and differential fluorescence labelling, I show that most centrioles have a preference to be upright with their distal end pointing towards the cell cortex, much like in mammalian cell types where centriole orientation is known. In collaboration with a statistician, we develop an assay to image embryos in real-time using super-resolution microscopy and analyse spatiotemporal aspects of their orientation using a neural network. Initial analysis further showed that centrioles have a preferential upright, "Ring" oriented state that is mostly stable over S-phase. Using a combination of drug- and candidate-based approaches, my data suggests that centrioles may indirectly be pushed and pulled into different orientations gradually by a balance of surrounding forces from microtubules and the centriole's surrounding pericentriolar material. However, I also uncover a possible role for scaffold protein Centrosomin (Cnn) and distal cap proteins, most strikingly distal cap protein Cep97, which may be instrumental in maintaining the distal ended orientation of centrioles. My data strongly suggests that distally oriented centrioles are the default state in *Drosophila* embryos and there is an active mechanism maintaining this orientation.

Abbreviations

γ-TuRC	Tubulin Ring Complex
μm	Micrometer
3D-SIM	OMX 3D-Structured Illumination Microscopy
Ana	ANAstral spindle
ANN	Artificial Neural Network
APC	Antigen Presenting Cell
ARP2/3	Actin Related Protein 2/3 complex
Asl	Asterless
BLAST	Basic Local Alignment Search Tool
BSI	Back Side Illuminated
BTIF	Big TIFF File format
C_B	Clear Bar
C_R	Clear Ring
CC-E	Cross Entropy loss function
CDK	Cyclin-dependent kinase
CDK5RAP2	Cdk5 Regulatory subunit-Associated Protein
Cep	Centrosomal Protein
CM	Centrosomin Motif
Cnn	Centrosomin
CNN	reCurrent Neural Network
cnn^{f}	*Cnn^{f04547} ; NG-Asl* genotype
CP1	Capping Protein 1
CP110	Centrosomal Protein of 110kDa
CPAP	Centrosomal P4.1-Associated Protein
CRISPR	Clustered Regularly Interspaced Short Palindromic Repeats
CSV	Comma-Seperated Values
CyO	Curly Oster (Balancer)
DAG	Diacyglycerol
DAPI	4′,6-DiAmidino-2-PhenylIndole
DMSO	DiMethyl SulphOxide
EGTA	Ethylene glycol-bis(β-aminoethyl ether)-N,N,N',N'-tetraacetic acid
EM	Electron Microscopy
FBF1	Fas Binding Factor 1
FIJI	FIJI Is Just Imagej
Fz-PCP	Frizzled-Planar Cell Polarity
GFP	Green Fluoresent Protein
HMM	Hidden Markov Model
hr	hour
HRP	Horse Radish Peroxidase

ID	Identification
if	Irregular Facets
IFT	IntraFlagellar Transport
IS	Immune Synapse
Jup	Jupiter
kDa	kilodaltons
LAP	Linear Assignment Problem
LECA	Last Eukaryotic Common Ancestor
mch	mCherry
mg	milligram
min	minute/ minutes
ml	mililitre
mM	millimolar
mm	micrometer
mM	Micromolar
mRNA	Messenger RiboNucleic Acid
ms	milisecond
MT	Microtubules
MTOC	MicroTubule Organising Centre
NA	Numerical Aperture
NG	NeonGreen
nM	nanomolar
nm	nanometer
NuMA	Nuclear Mitotic Apparatus
ODF1	Outer Dense Fibre of sperm tails 1
P_B	Perceived Bar
P_R	Perceived Ring
PAGE	PolyAcrylamide Gel Electrophoresis
PAR	Protease-activated receptor
PBS	Phosphate-Buffered Saline
PBST	PBS + 0.2% Tween-20
PCM	PeriCentriolar Material
PLC	PhosphoLipase C
Plk	Polo-like kinase
PLP	Pericentrin-Like Protein
pUbq	Ubiquitin Promoter
Resnet18	Residual Neural Network 18
RT	Room Temperature
S	Slanted
Sas	Spindle ASsembly Abnormal
Sced	Scrambled
SCLT1	Sodium Channel and CLaThrin Linker 1
SD	Standard Deviation

sDAP	sub-Distal Appenage Protein
SDS	Sodium Dodecyl Sulphate
sec	second/ seconds
SoRa	Olympus Super Resolution SpinSR Spinning Disk Confocal microscope
Spd	SPindle-Defective
TBS	Tris-Buffered Saline
TIFF	Tag Image File Format
TRIM37	TRIpartite Motif-containing protein 37
TTBK2	Tau TuBulin Kinase 2
TZ	Transition Zone
U	Unidentified
WT	Wild-Type

Introduction

1.1 Centrioles

Centrioles are polar, barrel shaped organelles made up of MTs and many other proteins (Paintrand et al., 1992). Centriole duplication is controlled by the cell cycle, with "daughter" centrioles growing orthogonally to "mother" centrioles during S-phase (Nigg and Holland, 2018). In many cell types mother daughter pairs are surrounded by a proteinaceous matrix of Pericentriolar Material (PCM) (Mennella et al., 2012). A centrosome consists of a centriole pair together with their surrounding PCM (Fig 1.1A).While centrosomes are most well-known for nucleating many of the MTs that constitute the mitotic spindle, it is likely that the most ancient conserved function of centrioles is in ciliogenesis (Carvalho-Santos et al., 2011).

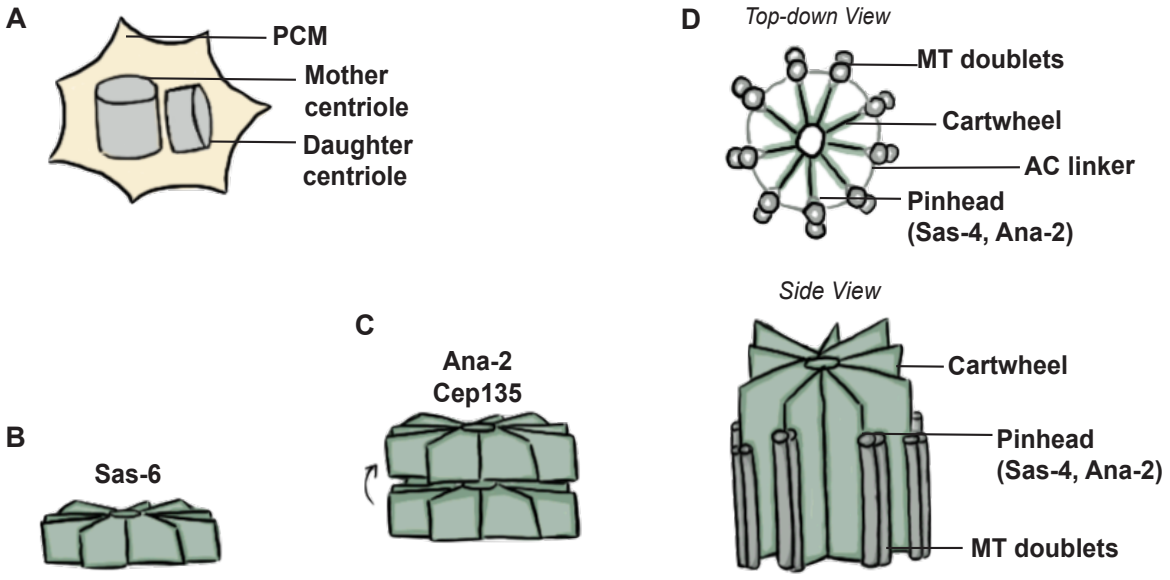

Figure 1.1. Centriole Structure

(A) Simplified schematic of a centrosome showing an upright mother centriole (*grey*) and a daughter centriole growing orthogonally to it, both surrounded by pericentriolar material (PCM, *yellow*). **(B)** Illustration depicting a 9-fold ring of Sas-6 homodimers (*dark green*) forming a cartwheel structure. **(C)** Illustration depicting 2 9-fold rings of Sas-6 homodimers stacking over one another via Ana-2 and Cep135. **(D)** Illustration depicting growth of a *Drosophila* centriole showing a completed Sas-6 cartwheel with microtubule (MT) doublets (*grey*) starting to elongate around the ends of each cartwheel spoke. Top-down view shows that each doublet is connected to the cartwheel by a pinhead structure and connected to each other via an AC linker.

1.1.1. Centriole Structure

Centrioles consist of a central "cartwheel" surrounded by MTs (Paintrand et al., 1992). Although there are slight differences in structure, centrioles in animals have several conserved elements (Carvalho-Santos et al., 2010). The central cartwheel consists mainly of a Spindle Assembly Abnormal protein 6 (Sas6) which homodimerizes through its coiled-coil domain into a 9-fold ring with coiled-coil domains pointing outwards, like spokes on a wheel (Fig. 1.1B) (Guichard et al., 2013; Kitagawa et al., 2011; van Breugel et al., 2011). The cartwheel elongates by stacking Sas-6 cartwheels. This process is aided by Anastral Spindle 2 (Ana2—STIL in humans) and Cep135 (Fig. 1.1C) (Guichard et al., 2017). The central cartwheel is then connected to outer MTs by a "pinhead" structure made up of Sas4 (CPAP in humans) and Ana2 (Fig 1.1D) (Gönczy, 2012).

MTs are an essential part of the cell cytoskeleton, usually forming long filaments that facilitate transport and maintain structural integrity of cells (Goodson and Jonasson, 2018). They also make up the outer barrel of centrioles. MTs are assembled from α and β-tubulin subunits into long protofilaments that are laterally associated into a closed, hollow tube, usually consisting of 13 protofilaments (Fig 1.2A). They are typically nucleated from a specialised protein complex consisting of γ-tubulin known as the γ-Tubulin Ring Complex (γ-TuRC) (Kollman et al., 2011; Moritz et al., 1995b). Due to the specific way in which α and β-tubulin subunits dimerize, resulting MT filaments are polar (Fig 1.2A). In *Drosophila*, MTs assemble into doublets attached to the central cartwheel by pinheads (Fig 1.1D). They consist of a partial B-tubule attached to 13-fold complete A-tubule (Fig. 1.2B). This unusual confirmation is made possible by abundant post-translational modifications to α and β-tubulin subunits, as well as by specialised δ and ε-tubulins (Fig. 1.2A) (Winey and O'Toole, 2014; Guichard et al., 2023). In mammalian systems, predictions of where δ and ε-tubulins might make contact with α and β-tubulins have been made based on sequence homology (Fig. 1.2A) (Stathatos et al., 2021). However, it is yet unclear if δ and ε-tubulins are part of the centriolar tubulin code, or if they are only required in centriolar MT assembly to decrease the angle of curvature between doublet MT protofilaments when forming the outer barrel of the centriole (Fig. 1.2C) (Guichard et al., 2023; Loubresse et al., 2001).

Centrioles in some organisms, such as *Caenorbabditis elegans* (*C. elegans*) consist of MT singlets, whereas mammalian centrioles consist of MT triplets (Winey and O'Toole, 2014). Due to the polarity of MTs, the centriole is an inherently polar structure which is exacerbated by the differences in accessory proteins at the proximal and distal ends (Guichard et al., 2013; Uzbekov and Alieva, 2018).

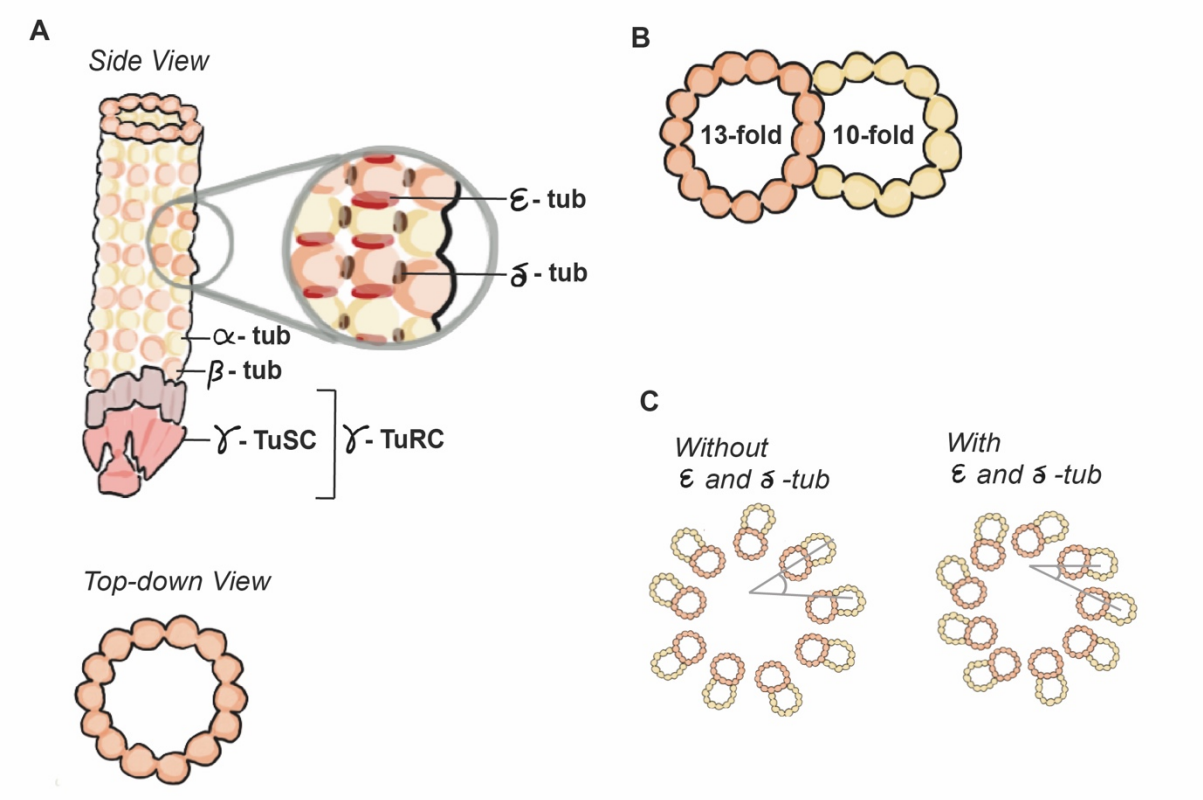

Figure 1.2. Microtubule Structure

(A) Illustration depicting a side view of an MT filament including γ-TuRC (*red*) and protofilaments of α (*pale yellow*) and β-tubulin (*pale orange*) connected laterally into a 13-fold hollow tube. Circular enlarged section shows predicted locations of δ and ε-tubulins within the protofilament. Top-down view shows a hollow ring of β-tubulins arranged in a 13-fold confirmation. **(B)** Top-down view of MT doubles in *Drosophila* embryo showing an A-tubule with 13-fold symmetry (*pale orange*) and a B-tubule (*pale yellow*) connected to it which is formed of an incomplete MT ring with only 10 protofilaments. **(C)** Illustration depicting a top-down view of centriolar MT doublets arranged in a 9-fold structure. In the presence of δ and ε-tubulins, the curvature between doublets decreases (*grey* lines), increasing the stability of the centriole (adapted from Guichard et al., 2023).

Mammalian and *Drosophila* centrioles differ in a few key ways. One of these differences is in size. Mammalian centrioles are 100-500nm in length with a 250nm diameter whereas *Drosophila* centrioles are much smaller at 150nm in length and diameter (Fig 1.3A) (Azimzadeh and Marshall, 2010; Winey and O'Toole, 2014). The diameter of *Drosophila* centrioles is beyond the resolution limit of many conventional widefield microscopes. Therefore, their structure is best observed using super resolution microscopy, a technique which has also been widely used to characterise structural details of and around vertebrate

centrosomes (Bowler et al., 2019; Gartenmann et al., 2017; Sonnen et al., 2012). Another key difference between mammalian and *Drosophila* centrioles is the composition of accessory proteins around fully mature centrioles (Fig 1.3B). At their distal ends, centrioles in most vertebrates possess Distal Appendage Proteins (DAPs) that organise into 9 "cone" like complexes around the centrioles (Fig 1.3B) (Ishikawa et al., 2005; Yang et al., 2018). DAPs are responsible for docking centrioles to the cell membrane in a distal ended orientation during ciliogenesis (Graser et al., 2007; Tanos et al., 2013). Slightly more proximal to DAPs are sub-distal appendage proteins (sDAPs), which have a less organised structure (Chong et al., 2020; Huang et al., 2017). sDAPs have roles in various centrosome functions including ciliogenesis and orienting the mitotic spindle (Mönnich et al., 2018; Shinohara et al., 2013; Veleri et al., 2014).

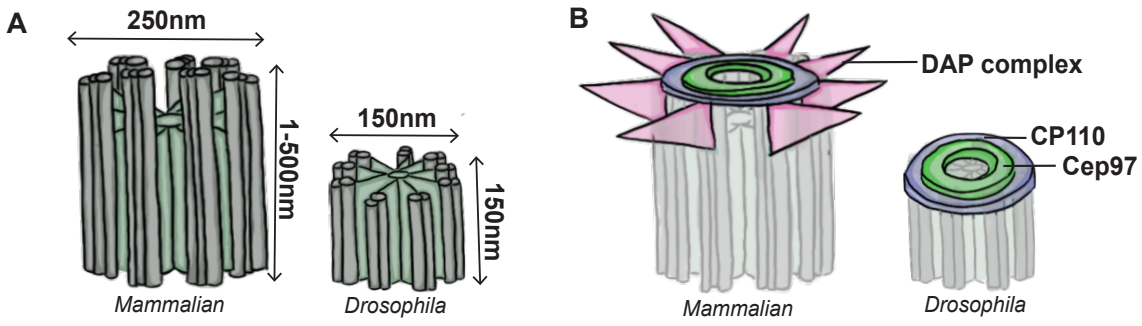

Figure 1.3. Differences between mammalian and *Drosophila* centrioles

(A) Illustration of mammalian and *Drosophila* centrioles side by side with cartwheel in *green* and MTs in *grey*. Not to scale. Showing the differences in length and width between them. Mammalian centrioles also have triplet MTs around their central cartwheel that grow beyond the cartwheel. **(B)** Illustration of mammalian and *Drosophila* centrioles showing the differences in accessory proteins on the distal ends of centrioles. Mammalian centrioles have 9 Distal Appendage Protein (DAP) complexes in cone shapes around the centriole (*pink*), with CP110 (*purple*) and Cep97 (*green*) capping the distal end. *Drosophila* centrioles do not have DAP complexes but the distal cap is conserved.

1.1.2. Centriole Duplication

While it is possible for centrioles to be generated *de novo* (Dzhindzhev et al., 2010; Nabais et al., 2021), *in vivo* new daughter centrioles usually grow orthogonally from the proximal side of old mother centrioles (Fig 1.1C) (Paintrand et al., 1992). A complex system of feedback loops connected to the cell cycle ensures that centrioles duplicate only once per cell cycle, and grow to the same size each time (Aydogan et al., 2018; Nigg and Holland, 2018). In interphase, a site for daughter centriole growth is determined by Polo-like-kinase 4 (Plk4) which is recruited to the outer wall of mature centrioles by Asterless (Asl, Cep152 in humans) (Fig. 1.4A). Asl is a protein that coats the MT walls of centrioles and shown to be both essential and sufficient for daughter centriole growth (Dzhindzhev et al., 2010). It binds Sas4 at its C-terminus and Plk4 at its N-

terminus, thus allowing the mother centriole to specify the general location of daughter centriole growth. Plk4 interacts with Ana2 (STIL in humans) to recruit Sas6 which forms the central cartwheel (Dzhindzhev et al., 2014; Moyer et al., 2015). Once the cartwheel has formed, MTs are added, attached by the pinheads (Fig. 1.1B). MTs elongate from the proximal end of the forming daughter centriole and are eventually capped by CP110 and Cep97 (Fig. 1.3B) (Gartenmann et al., 2020; Schmidt et al., 2009).

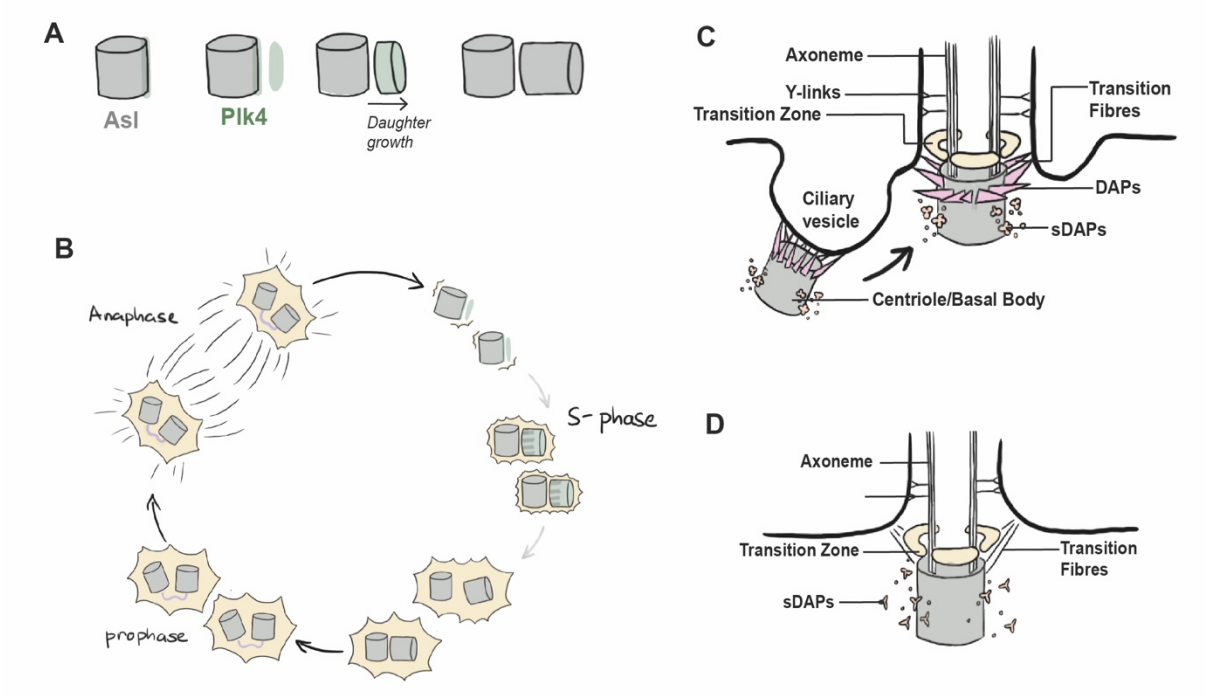

Figure 1.4. Centriole duplication and centrioles as basal bodies

(A) Schematic showing how the site of daughter centriole growth is defined orthogonally to the mother centriole in *Drosophila* by Plk4 (*green*). **(B)** Schematic showing centriole growth at different cell cycle stages where low levels of PCM (*yellow*) are nucleated in S-phase as daughter centrioles (*green*) grow, represented by *grey* arrows. Near mitosis the PCM expands and in Anaphase the proteinaceous linker (*purple*) between mother and daughter centrioles is severed, forming an old and new mother centriole. **(C)** Illustration of centriole (*grey*) recruitment to the site of ciliogenesis in mammalian cells where DAPs (*pink*) attach to the ciliary vesicle with the help of Sub-Distal Appendage Proteins (sDAPs, *orange*) which fuse with the cell membrane to attach basal bodies by their distal end. Then a transition zone (*yellow*) forms as the axoneme extends from basal body MTs and is attached to the ciliary membrane by Y-links. **(D)** Illustration of ciliogenesis in *Drosophila* cells. Transition fibres attach centrioles to the cell membrane where a transition zone forms. Even though DAPs are not conserved, basal bodies are decorated by various sDAPs.

Plk4 specifying a site for future daughter centriole growth and its role in controlling centriole number has been an exciting field of study in the last decade (Nigg and Holland, 2018). It has been observed that once recruited to the mother centriole wall, Plk4 condenses to a dot on the proximal end of mother centrioles (Ohta et al., 2014). One attractive model for how this occurs relies on interactions between Plk4 and Ana2, and the ability of Plk4 to phosphorylate itself, facilitating its own degradation (Lopes et al., 2015; Ohta et al., 2014; Yamamoto and Kitagawa, 2019). Plk4 initially localises as a ring around mother centrioles and

acts to phosphorylate Ana2 which recruits Sas6, the central component of the centriole cartwheel (Dzhindzhev et al., 2014; Ohta et al., 2014). The interaction between Plk4 and Ana2 is thought to stabilize Plk4 at a single location (Arquint et al., 2015; Ohta et al., 2014). As Plk4 is allowed to accumulate at all other locations unprotected by Ana2, it continues to phosphorylate itself which increases its own instability by increasing the likelihood of ubiquitination and degradation (Holland et al., 2010; Klebba et al., 2013).

The importance of Plk4 in the field of centriole biology cannot be overstated. Recently, it has been studied as a potential target in cancer therapy following data uncovering the regulatory dynamics between it and checkpoint ubiquitin ligase TRIM37 (Domínguez-Calvo et al., 2021; Meitinger et al., 2016; Meitinger et al., 2020; Nigg and Holland, 2018; Yeow et al., 2020). The autocatalytic degradation of Plk4 has been shown to be directly responsible for controlling the copy number of centrioles per cell cycle (Holland et al., 2012; Lopes et al., 2015; Nigg and Holland, 2018). Roles and interactions between Plk4, Ana2 and Sas6 also appear to be conserved across a variety of organisms (Kitagawa et al., 2011; Stevens et al., 2010).

The timing of centriole growth is deeply connected to the cell cycle, with new daughter centrioles forming during S-phase and disengaging into old and new mother centrioles in late mitosis (Fig. 1.4B) (Nigg and Holland, 2018). When a daughter centriole has formed orthogonally to the mother, centriole reduplication is blocked by the engagement of mother and daughter centriole, which are in close proximity to each other (Tsou and Stearns, 2006). In early mitosis, centrioles start to disengage from each other and move apart with the help of Polo-like kinase 1 (Plk1), a mitotically controlled kinase (Shukla et al., 2015). Proteinaceous connection between mother and daughter is later severed in late mitosis, which allows Asl to be loaded onto the new mother centriole (Fig. 1.4A, B) (Tsou and Stearns, 2006). Asl loading therefore licences this new mother centriole for duplication at the onset of interphase (Nigg and Holland, 2018; Novak et al., 2014). Plk4 and Ana2 are then activated by Cyclin Dependent Kinase 1 (Cdk1), allowing Plk4 to be recruited by Asl and daughter centriole growth to be initiated (Novak et al., 2016; Steinacker et al., 2022). As Cdk1 activity oscillates through the cell cycle, the timing of centriole duplication is tightly controlled (Aydogan et al., 2018).

1.1.3. Centrioles as Basal Bodies in Ciliogenesis

Cilia are finger-like organelles that protrude from the cell surface as cells exit the cell cycle and become quiescent. They are used to sense the environment, to increase surface area for nutrient absorption and in cell motility (Avidor-Reiss and Leroux, 2015; Vertii et al., 2016). Loss of cilia leads to a class of diseases known as ciliopathies that are often associated with mechanosensory defects, microcephaly, obesity, cystic kidneys and skeletal malformations (Baker and Beales, 2009; Chavali et al., 2014).

Cilia are templated by a specialised centriole known as a basal body (Carvalho-Santos et al., 2011; Ishikawa and Marshall, 2011). MTs that elongate from basal body MTs form the growing axoneme which makes up the core of the cilium (Sánchez and Dynlacht, 2016). The cilium membrane is continuous with the cell membrane and the axoneme is connected to the ciliary membrane via Y-links (Fig. 1.4C). At the base of the axoneme is a specialised domain called the transition zone (TZ) which facilitates protein transport between cilium and cell cytoplasm, termed Intraflagellar transport (IFT) (Fig. 1.4C) (Ishikawa and Marshall, 2011; Reiter et al., 2012). Depending on the organism and function of the cilium being built, there are a few structural differences. For example, in motile cilia the MT motor protein dynein attaches itself between the outer wall of the axoneme and the cell membrane, providing force for cilia to bend. These cilia also have two extra MT filaments within their axoneme to increase structural integrity during bending (Klena and Pigino, 2022).

In mammalian cells, ciliogenesis begins with a centriole attaching itself to a primary ciliary vesicle via its DAP complexes. DAPs and sDAPs aid trafficking of the ciliary vesicle to the site of ciliogenesis (Joo et al., 2013; Sorokin, 1962; Ye et al., 2014). The vesicle then fuses with the cell membrane, where the attached centriole is converted into a basal body (Fig. 1.4C) (Reiter et al., 2012). DAPs form transition fibres, which anchor the centriole to the cell membrane (Fig. 1.4C) (Tanos et al., 2013; Wei et al., 2015). Notably, this is one of the few centriole functions studied where we know centriole orientation to play a role. Basal bodies are distally oriented when they are anchored to the cell membrane (Mansour et al., 2021; Tanos et al., 2013), and this distal orientation is essential to allow axoneme extension from the plus ends of basal body MTs (Avidor-Reiss and Leroux, 2015; Reiter et al., 2012; Sánchez and Dynlacht, 2016; Wei et al., 2015).

In organisms where most DAPs are not conserved such as *Drosophila* (Hodges et al., 2010), transition fibres anchor centrioles directly to the cell membrane without need for a ciliary vesicle (Fig. 1.4D) (Gottardo et al., 2018; Jana et al., 2018; Roque et al., 2018). The process by which this occurs is poorly defined (Ishikawa and Marshall, 2011; Jana et al., 2018), yet the requirement for distal ended centriole orientation is just as apparent in this system. Two separate studies have used Scanning Electron Microscopy to show that when centrioles are unable to dock due to TZ- or PCM-related mutations, fibrous extensions are still observed between the centriole and the cell membrane (Roque et al., 2018; Vieillard et al., 2016), highlighting the robustness of transition fibre formation in *Drosophila* and a need to further understand how centrioles attach to the cell membrane without DAPs.

1.1.4. The Evolution of Centrioles

Centrioles are an ancient organelle that was likely present in our Last Eukaryotic Common Ancestor (LECA), and subsequently lost from specific lineages, such as higher plants and some fungi (Azimzadeh et al., 2012; Carvalho-Santos et al., 2011). Current theory based on RNA sequencing proposes that this ancient structure would have had a 9-fold symmetric structure and the ability to form a basal body to nucleate motile flagella (Carvalho-Santos et al., 2011; Carvalho-Santos et al., 2010). Although the ability to nucleate MTs contributing to the mitotic spindle is the most well-known function of the centriole, it would seem as though cilia formation is its most ancient conserved function (Azimzadeh, 2014; Marshall, 2009). In line with these comparisons, some cell types can divide in the absence of centrosomes (Nigg and Holland, 2018). For example, *Drosophila* embryos deficient for Sas4 without centrioles are able to develop to adulthood (Basto et al., 2006). Microsurgical ablation of centrosomes in vertebrate cell culture has also shown the ability of cells to undergo mitosis by forming acentrosomal clusters of MTs which nucleate MTs contributing to the mitotic spindle in place of centrosomes (Khodjakov et al., 2000). Additionally, some cell types naturally divide without centrosomes. For example. plants nucleate MTs contributing to the mitotic spindle from acentrosomal sites (Hamada, 2014). Specific vertebrate cell types at certain stages of development, such as female cells undergoing meiosis, also do so without centrosomes (Mogessie et al., 2018). In contrast, centrioles are essential for ciliogenesis and an inability to form cilia leads to highly debilitating ciliopathies.

Indeed, a significant number of known ciliopathy genes encode proteins associated with centrioles (Chavali et al., 2014; Kumar et al., 2021).

However, it is also worth noting that while cells can divide without centrioles, such divisions are often associated with tumorigenesis where cells divide through acentrosomal MT-nucleating sites (Bazzi and Anderson, 2014; Domínguez-Calvo et al., 2021; Meraldi, 2016; Sir et al., 2013). Acentrosomal division in cancer cells has recently been leveraged to target centrosome proteins which led to the selective depletion of cancerous cells, highlighting the potential of centriole biology in discovering novel therapeutic targets in cancer treatment (Domínguez-Calvo et al., 2021; Meitinger et al., 2020; Yeow et al., 2020). Altogether, while the functions of centrioles and centriolar proteins are crucial to ensure regulated cell divisions, evidence suggests that the evolution of the centrosome and roles in mitotic division may have been more recent compared to the roles of centrioles in ciliogenesis.

1.2. The PCM and the centrosome

Most centrioles are surrounded by PCM. Centrioles and their PCM is collectively called the centrosome. The PCM is made up of structural and signalling proteins that form scaffolds which recruit and maintain hundreds of other components needed for core centrosome functions (Alves-Cruzeiro et al., 2014). Centrosomes mainly function as a MT Organising Centre (MTOC) (Kuriyama and Borisy, 1981). In interphase, the position of centrosomes can help determine cell polarity and establish intracellular trafficking hubs (Vertii et al., 2016). In mitosis, centrosomes nucleate MTs contributing to the mitotic spindle and ensure sister chromatids are pulled into resulting daughter cells in anaphase (Kuriyama and Borisy, 1981). Orientation of the mitotic spindle via the MT binding capabilities of the PCM is also known to facilitate asymmetric division (Januschke et al., 2011; Rebollo et al., 2007). During these processes, centrosomes may also nucleate actin and facilitate MT/actin crosstalk (Farina et al., 2016).

In addition to their roles in MT nucleation, centrosomes are also important coordination centres within cells (Vertii et al., 2016). The size and maturation of the centrosome is tightly controlled by the cell cycle (Fig. 1.4B), however the centrosome itself also appears to be the origin of signalling cascades that trigger the onset of key cell cycle stages, such as prophase and anaphase (Basu et al., 2020; Grallert et al., 2013). As centrosomes are important MT nucleators, it also makes sense that centrosomes themselves are able to interact with intracellular trafficking machinery and cytoskeleton remodelling proteins (Cheng et al., 2019; Hehnly et al., 2012).

It is theorised that a PCM-like structure may have evolved independently in several eukaryotic lineages upon basal body forming centrioles (Azimzadeh, 2014). However, during ciliogenesis, the PCM has also evolved to aid in basal body localisation and docking to the cell membrane. For example, the MT-nucleating roles of centrosomes also function to increase trafficking to the site of a growing cilium (Jurczyk et al., 2004; Roque et al., 2018). Taken together, the PCM confers vast functionality upon the centrosome, evolving centrosomes into key positional organisers within cells while also bolstering the ancestral function of the centriole in basal body formation.

Many centrosome functions rely on push and pull forces from both the actin and MT cytoskeleton, both in terms of centrosomes nucleating and reorganising these cytoskeletal filaments, as well as actin and MTs determining centrosome position within a cell (see section 1.4). These push and pull forces from actin and MT on centrosomes may also be indirectly changing the orientation of centrioles.

1.2.1. Centrosome Composition and Growth

The PCM is a dense proteinaceous matrix which consists of an underlying scaffold structure made up of proteins that are able to homodimerize via their long coiled-coil domains. Homodimers then interact with each other to form a fibrous matrix (Fig. 1.5A), which allow proteins that confer centrosome function to be recruited and maintained (Lawo et al., 2012; Mennella et al., 2012). Much of the work done to elucidate PCM components has been done in *Drosophila.* These key mechanisms of PCM assembly appear to be conserved in humans despite the presence of additional scaffold proteins (Alves-Cruzeiro et al., 2014; Fry et al., 2017; Vasquez-Limeta and Loncarek, 2021). Conserved scaffold proteins consist of mainly Centrosomin (Cnn) and Spd2 (Cep192 in humans). When either Spd2 or Cnn are mutated, the size of the PCM is dramatically reduced (Conduit et al., 2014b). Furthermo.re, Fluorescence Recovery After Photobleaching analyses have also shown that while many other PCM components are highly dynamic at the PCM, Cnn and Spd2 are relatively stable, especially in mitosis (Conduit et al., 2014b; Conduit et al., 2015). These observations provide strong evidence that Cnn and Spd2 are not just part of the PCM but form a mesh-like scaffold (Woodruff et al., 2014).

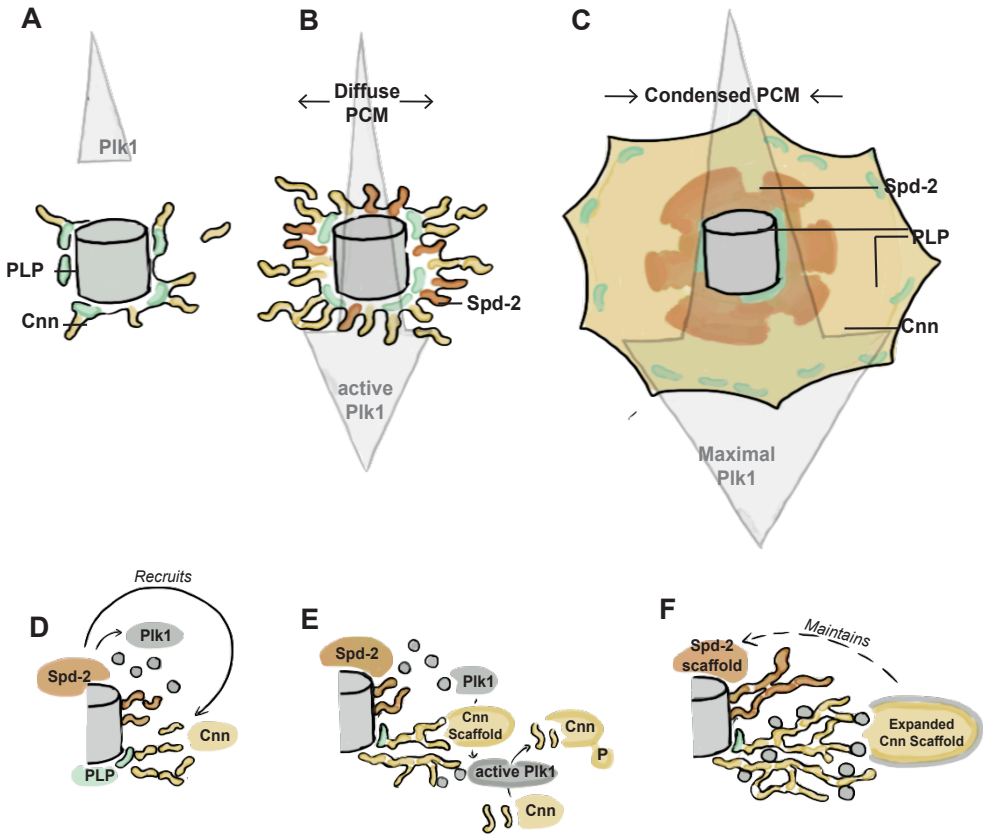

Figure 1.5. Centrosome growth

(A - C) Schematic showing the recruitment of Spd-2 (*orange*) and Centrosomin (Cnn, *yellow*) scaffold in interphase leading up to mitosis. (A) PLP (*cyan*) binds to the centriole (*grey*) walls and recruits Cnn, which is capable of binding to both PLP and Sas-4 within the pinhead structure between MTs and the central cartwheel. Spd-2 is also weakly recruited by Sas-4 but at this stage both Cnn and Spd-2 are unstably bound to the centriole. (B) As the cell gets closer to mitosis, more Polo-like-kinase 1 (Plk1, *grey* arrow) is activated which activates Spd-2. Activated Spd-2 can recruit more Cnn which is also phosphorylated by Plk1 to increase scaffold formation. (C) In mitosis, the PCM is greatly condensed with a weaker Spd-2 scaffold close to the centriole and a stable Cnn scaffold that expands further out from the centriole. PLP continues to be present close to the centriole wall and also at the ends of the Cnn scaffold, aiding in its stability. **(D)** Spd-2 binds Sas-4 and recruits both Plk1 and Cnn to the centriole wall. **(E)** As Cnn accumulates, it dimerises and forms a scaffold. This retains and activates Plk1 which phosphorylates Cnn, allowing Cnn to form an even more stable and expanded scaffold. **(F)** While Cnn cannot recruit more Spd-2, it aids to maintain the Spd-2 scaffold as well as bind and retain Plk1.

In most organisms, the PCM scaffold originates from the outer centriole wall (Conduit et al., 2015; Woodruff et al., 2014). In interphase, PLP (Pericentrin [PNCT] in humans) forms 9-fold complexes around centrioles and weak fibrous extensions into the cytoplasm (Lawo et al., 2012; Mennella et al., 2012). At this cell cycle stage, scaffold proteins Spd2 and Cnn are also weakly associated with the PCM, with Spd2 lying close to the centriole and Cnn forming diffuse fibres at the periphery of the centrosome (Fig. 1.5B) (Conduit et al., 2015; Giansanti et al., 2008; Lerit et al., 2015; Woodruff et al., 2014). Some cell types are able to organise the mitotic spindle from acentrosomal sites. Two examples of such cells include the slime mould

Dictyostelium discoideum (Azimzadeh, 2014), and cancer cells from neuroblastomas and certain breast cancers. This occurs by the formation of acentrosomal foci scaffolded by Spd2 and Plk4 (Meitinger et al., 2016). These foci appear in certain types of cancer cells where Plk4, which controls centriole copy number, is catalytically inactive and allow cells to undergo mitosis in the absence of centrioles (Meitinger et al., 2020). These cells also tend to have high expression of the ubiquitin ligase TRIM37 which targets Spd2 for degradation (Meitinger et al., 2020), presumably causing acentrosomal foci to rely on catalytically inactive Plk4 to form and continue dividing (Domínguez-Calvo et al., 2021; Meitinger et al., 2020). Recent studies have identified Plk4 as a potential target in cancer therapy given the roles of TRIM37 (Yeow et al., 2020). In cancer cells which divide by acentrosomal foci, TRIM37 tends to be highly expressed due to its other cancer promoting functions and position in a highly upregulated genomic region. These cells appear to be highly sensitive to Plk4 inhibition (Wong et al., 2015), which abolishes the formation of acentrosomal foci and allows TRIM37 to act as a checkpoint protein, leading to an increase in mitotic errors which triggers p53 mediated G1 arrest (Domínguez-Calvo et al., 2021; Meitinger et al., 2016). These studies highlight the flexibility of PCM components in forming a stable MTOC as well as the importance of regulating of centrosome PCM assembly.

During mitosis, the PCM greatly expands (Fig. 1.5C). It is believed that expansion occurs due to a positive feedback loop between Cnn, Spd2 and Plk1, timed by the cell cycle (Alvarez-Rodrigo et al., 2019; Conduit et al., 2014a; Wong et al., 2022). The process in which the PCM grows in relation to the cell cycle is a topic of interest in the Raff Lab. They propose that Spd2 is able to form an unstable scaffold close to centrioles, but as it binds, it is able to recruit Cnn and Plk1 (Fig. 1.5D) (Alvarez-Rodrigo et al., 2021; Conduit et al., 2014a). During mitosis, Plk1 binds to PCM scaffolding proteins through its Polo-box-domain, which causes a conformational change that relieves its kinase inhibitory region, allowing further activation of its kinase ability during mitosis (Fig. 1.5E) (Colicino and Hehnly, 2018). Activated Plk1 then phosphorylates Cnn, allowing Cnn to form a larger, more stable scaffold around the centriole (Fig. 1.5E) (Conduit et al., 2015; Feng et al., 2017). While Cnn is unable to recruit more Spd2, its presence aids in maintaining the inner Spd2 scaffold (Fig. 1.5F) (Conduit et al., 2014b; Lucas and Raff, 2007). This greatly expanded and highly condensed PCM allows centrosomes to nucleate the mitotic spindle.

1.2.2. Centrosomes as MTOCs

As described previously, MTs are an essential part of the cell cytoskeleton and are inherently polar structures, usually with a γ-TuRC stabilised minus end and a fast growing plus end (Fig. 1.2A) (Mitchison and Kirschner, 1984; Moritz et al., 1995b). The length and stability of growing MTs are regulated by a suite of Microtubule Associated Proteins (Wieczorek et al., 2015). When unstable, MTs lose lateral connections between protofilaments resulting in MTs peeling apart as they depolymerise. This phenomenon is known as MT catastrophe (Fig. 1.6A) (Goshima et al., 2005; Tournebize et al., 2000). Stable MT filaments form cellular "highways" which, via specialised motor proteins, allow the trafficking of membrane bound organelles, vesicles for exocytosis, mRNA. They are split into two different classes: kinesins which typically move towards the plus end of MTs (with the exception of the kinesin13 family) and dyneins which move towards the minus end (Goodson and Jonasson, 2018).

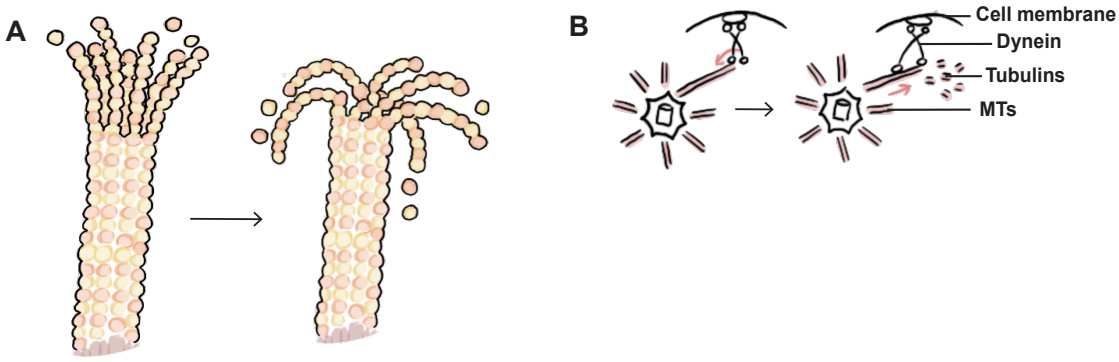

Fig 1.6. MT depolymerisation

(A) Illustration showing MTs (coloured as in 1.2A) catastrophe as lateral connections are lost between αβ-tubulin protofilaments causing them to peel apart. **(B)** Illustration showing the movement of dynein towards the negative end of MTs (*red*) causing MT catastrophe as it walks along MTs thus bringing centrosomes closer to the cell membrane (*red* arrows) where dynein is attached.

The centrosome is best-known as an MTOC and its MT-nucleating abilities are mostly provided by the PCM. MTs are nucleated from the centrosome or centrosomal MTs via γ-tubulin containing complexes such as γ-TuRC. These are recruited in a variety of ways including through PLP, Cnn and Augmin (Martinez-Campos et al., 2004; Tariq et al., 2020; Zhang and Megraw, 2007; Zimmerman et al., 2004). Cnn in particular binds γ-TuRC through its highly conserved centrosomin motif 1 (CM1) domain (Choi et al., 2010; Fong et al., 2008; Kuriyama and Borisy, 1981; Zhang and Megraw, 2007). Organisms that do not possess centrioles

nucleate MTs through acentrosomal sites that may recruit γ-TuRC or a smaller complex within it called the γ-Tubulin Small Complex (γ-TuSC) (Fig. 1.2A) (Hayward et al., 2014). This is the case for higher plants and some fungi that have lost centrioles (Hamada, 2014). However, cell types with centrioles can also nucleate MTs from non-centrosome sites (Efimov et al., 2007; Espigat-Georger et al., 2016). In these cell types, the presence of centrioles may balance centrosome and acentrosomal nucleation (Cheng et al., 2019). For example, MTs may be nucleated from the centrosome then released and captured by other MTOCs. Centrosomal proteins may also be relocated to other intracellular locations to facilitate MT nucleation at acentrosomal sites (Espigat-Georger et al., 2016; Ríos et al., 2004). The MTOC nucleating capabilities of centrosomes are important in interphase cells to establish cell polarity and facilitate intracellular trafficking (see section 1.4.). In mitosis, expansion of the MT network requires both direct nucleation from the centrosome and nucleation from Augmin, which attaches itself onto the sides of MT filaments as well as chromosomes (Goshima et al., 2007; Hayward et al., 2014; Tariq et al., 2020).

In mitosis, centrosomes have a greatly expanded PCM and migrate to opposite poles of the cell to nucleate the mitotic spindle (Choi et al., 2010; Fong et al., 2008; Moritz et al., 1995a). Centrosomes are anchored to the cell membrane by dynein binding to the plus ends of MTs and the cell cortex (Fig. 1.6B) (Kotak and Gönczy, 2013). Specialised membrane zones recruit dynein, which specifies centrosome position and therefore determines spindle pole orientation (Kotak and Gönczy, 2013; McNally, 2013). This mechanism is especially important during asymmetric division (Kiyomitsu and Cheeseman, 2012). Distal end centriole proteins also contribute to centriole anchoring in mitosis, for example the sDAP Ninein in mammalian cells (Delgehyr et al., 2005; Shinohara et al., 2013). At the cell cortex as dynein walks back towards the minus end of MTs at the centrosome, MT catastrophe occurs behind it, shortening the MT and bringing centrosome towards the cell cortex (Fig. 1.6B).

1.2.3. Interactions between the Centrosome and Actin

In addition to being an MTOC, centrosomes have also recently been shown to nucleate actin (Farina et al., 2016). Actin is made up of globular actin (G-actin) subunits loaded with GTP which increases their capability to polymerise into a polar, 2-strand twisted filament with a slow growing minus-end and a fast growing plus-

end (F-actin, hereafter known simply as actin), also known as the pointed- and barbed-ends respectively (Fig. 1.7A) (Oda et al., 2009; Vavylonis et al., 2006). Together with bundled motor protein myosin, actomyosin contractions provide mechanical forces essential for a variety of cellular processes (Pollard and Cooper, 2009). Actin may be nucleated by a stable actin nucleus consisting of several G-actins, or through branching complexes such as ARP2/3 (Fig. 1.7A) (Oda et al., 2009). It was found that human centrosomes were able to nucleate actin *in vitro* through centriolar satellite component PCM1 binding to ARP2/3 (Farina et al., 2016). At mitosis, overexpression or inhibition of ARP2/3 levels subsequently increased or decreased actin nucleated at centrosomes (Plessner et al., 2019). Decreased levels of actin nucleation led to mitotic defects, showing that organisation of actin at centrosomes is important in to ensure proper nuclear divisions.

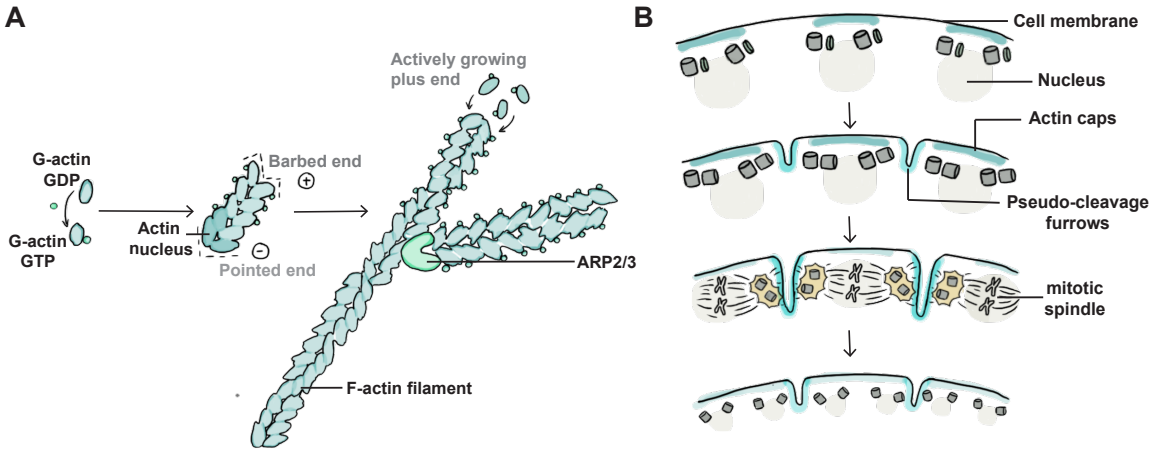

Figure 1.7. The roles of centrosomes in the embryo involving actin

(A) Schematic showing actin nucleation and growth. GTP (*cyan*) is attached to Globular actin (G-actin, *blue*) allowing it to polymerise in a polar manner nucleated by a stable actin nucleus (*deeper blue*) containing several G-actins the minus end is called the pointed end and the plus end is called the barbed end. Over time it forms a two-twist F-actin strand with a stable slow-growing pointed end and a fast-growing barbed end where G-actin GTP is being added to the strand. ARP2/3 (*green*) is a complex that attaches to the sides of F-actin and can also nucleate F-actin filaments, its presence facilitates a more branched actin network. **(B)** Illustration showing the syncytial *Drosophila* embryo cell cortex with centrioles (*grey*) close to the cell cortex which determine the position of cortical actin caps (*pale blue*). The position of actin caps thereby positions pseudo-cleavage furrows (*bright blue*) which deepen during mitosis and prevent centrosomes from interacting with centrosomes associated with neighbouring nuclei. As mitosis ends, these pseudo-cleave furrows recede.

In syncytial *Drosophila* embryos, actin plays a highly specialised role in cell division and nuclear spacing, orchestrated by centrosomes (Foe et al., 2000; Raff and Glover, 1989). As nuclei are distributed across the cell cortex, actin caps form above each centrosome (Fig. 1.7B). The establishment and maintenance of these caps are dependent on the interaction between PCM components and actin binding proteins. Upon depletion of PCM, actin caps fail to form (Kao and Megraw, 2009). During mitosis, a pseudo cleavage furrow forms

from each actin cap to prevent centrosomes from interacting with spindles of neighbouring nuclei (Fig. 1.7B). This seems to be a mechanism to reduce genomic instability as nuclei divide in a syncytium. At cycle 14, actin furrows deepen as the embryo cellularises. The spacing between each furrow ensures that each resulting cell contains only one nucleus and centrosome pair (Kotadia et al., 2010). This example underlines how centrosomes may act to position actin, as well as actin's role in regulating nuclear division.

MTs and actin also often work together in various cellular processes (Baker et al., 1993; Inoue et al., 2019; Royou et al., 2004; Sullivan and Theurkauf, 1995). For example, during mitosis, MTs interact with cortical actin in order to position the mitotic spindle through a complex of MT plus end binding proteins (Buttrick et al., 2008; Cliffe et al., 2004; McCartney et al., 2001). A similar mechanism between cortical actin domains and centrosomes is observed in the *C.elegans* embryo during symmetry breaking (Cowan and Hyman, 2004). However, centrosomes may also able to organise actin independently of MTs. For example, it has been found that the binding site for centrocortin, an actin interacting protein, in Cnn is separate from its γ-TuRC binding site. Mutating this binding site specifically impairs cleavage furrow formation due to its inability to interact with centrocortin without affecting MT nucleation (Kao and Megraw, 2009; Zhang and Megraw, 2007). These investigations highlight the propensity of centrosomes to interact with cortical actin, a feature that is highly conserved across multiple organisms (Calvo and Izquierdo, 2021; Cowan and Hyman, 2004; Farina et al., 2016; Garrido-Jimenez et al., 2018; Kotak and Gönczy, 2013; Zhang and Megraw, 2007). These examples demonstrate that both MTs and actin are involved in positioning centrosomes close to the cell cortex.

Due to the myriad of forces exerted on the centrosome by MTs which interact with cortical actin in the context of the *Drosophila* embryo (Buttrick et al., 2008; Kao and Megraw, 2009), and the connection of the PCM to the centriole wall (Conduit et al., 2014b; Feng et al., 2017; Lerit et al., 2015), it is likely that the centriole may be indirectly pulled into different orientations as a result of MT and actin-based forces. This is because MTs are nucleated from the centrosome in all directions and there is no known stable docking mechanism between centrosomes and the cell cortex in interphase (Delgehyr et al., 2005; Giansanti et al., 2008; Ojas et al., 2021). Therefore, it is possible that centriole orientation is random as a result of multidirectional cytoskeletal forces pushing and pulling centrosomes into position.

1.3 The distal end

Centrioles are inherently polar organelles, with a proximal and distal end that comprise of different proteins for different functions. While the proximal end of mother centrioles is responsible for nucleating the growth of new daughter centrioles from its side (Ohta et al., 2014; Paintrand et al., 1992), the distal end tends to be involved in centrosome positioning and ciliogenesis (Carvalho-Santos et al., 2011; Tanos et al., 2013). DAP complexes which emanate from the distal end attach centrioles to the cell membrane in both ciliated and some non-ciliated systems (Fig. 1.3B) (Stinchcombe et al., 2015; Tanos et al., 2013). Additionally, there have been suggestions throughout the literature that centrioles are distally oriented in a variety of different contexts (Cassioli and Baldari, 2019; Delgehyr et al., 2005; Shinohara et al., 2013), presumably via DAP complexes (Kasioulis et al., 2017; Shao et al., 2020; Stinchcombe et al., 2015). However, these studies do not explain how centrioles may be oriented in organisms where DAPs are not conserved.

The distal end also contains functionally conserved distal cap proteins CP110 and Cep97 (Paintrand et al., 1992). Both are known to be co-regulated and act as a complex with Cep97 recruiting CP110 on and off the centriole (Spektor et al., 2007). Their presence is thought to physically inhibit further growth of centriole MTs, which is why their removal is key to ciliogenesis initiation (Song et al., 2022; Spektor et al., 2007; Tsang et al., 2008). In *Drosophila* embryos where centrioles lie close to the cell cortex, CP110 and Cep97 are the distalmost known proteins and so are physically the closest centriolar proteins to the cell surface (Aydogan et al., 2022; Dobbelaere et al., 2020). This places them as potential candidates for a putative centriole orientation mechanism.

1.3.1. Distal Appendage Proteins

DAPs comprise a group of 9-13 proteins that lie at the distalmost end of mammalian centrioles. They form complexes around the 9-MT blades of the centrioles that resemble cone-like structures (Yang et al., 2018). Several key DAPs include CEP83, CEP89, SCLT1, FBF1 and CEP164 (Chong et al., 2020; Yang et al., 2018). They assemble in a hierarchical fashion starting with CEP83 recruited by centriolar satellite protein CEP90 (Fig. 1.8A) (Kumar et al., 2021). CEP83 and CEP89 then recruit SCLT1 and CEP164 that form the

cone structures (Fig. 1.8A). Finally, FBF1 is recruited in between the cones (Fig. 1.8A) (Bowler et al., 2019; Yang et al., 2018).

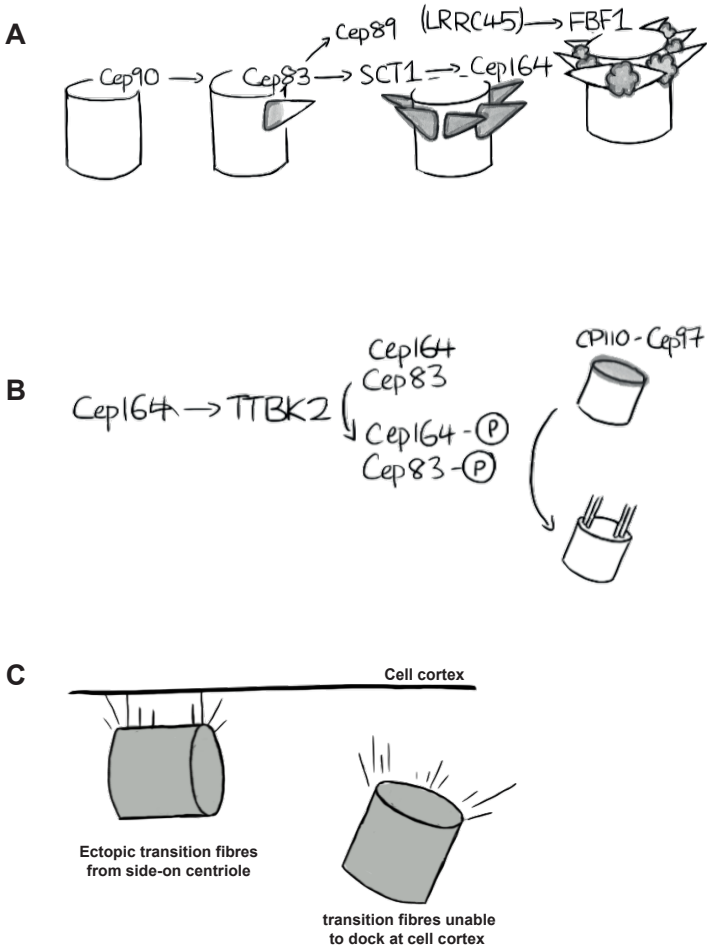

Figure 1.8. Distal Appendage Proteins and transition fibres

(A) Schematic showing hirearchial recruitment of DAPs to form 9 cone-like DAP complexes around the centriole. This starts with centriolar satellite protein CEP90 recruiting CEP83. LRRC45 is in brackets as while it is loaded onto the DAP complexes while they are formed, it unloads as DAPs are completed. The last DAP to be loaded is FBF-1 which is positioned in between cones. **(B)** Schematic showing that CEP164 recruits TTBK2 to phosphorylate CEP164 and CEP83, enabling the removal of the CP110-Cep97 distal cap complex, allowing axoneme elongation from centrioles during ciliogenesis. **(C)** Illustration showing transition fibres forming from *Drosophila* basal bodies when PCM is reduced (left) or when transition zone proteins are mutated (right). These examples highlight how robust transition fibres are and the importance of distal ended orientation of centrioles in ciliated cells. Adapted from Roque et al., 2018 and Vielliard et al., 2016 respectively.

Of all the DAPs currently identified, CEP164 appears to be the most abundant and well characterised with indispensable roles in all stages of ciliogenesis (Bowler et al., 2019; Čajánek and Nigg, 2014; Tanos et al., 2013; Wu et al., 2018). As centrioles bind to the ciliary vesicle, CEP164 facilitates MT network remodelling which facilitates centriole movement to the site of cilium formation (Fig. 1.4C) (Pitaval et al., 2017; Wu et al., 2018). It then recruits Tau tubulin kinase 2 (TTBK2), which, alongside CEP83, removes the ciliogenesis inhibitor CP110 (Fig. 1.8B) (Čajánek and Nigg, 2014; Goetz et al., 2012). As the transition zone forms, CEP164 and other DAPs anchor the basal body to the cell cortex via transition fibres (Fig. 1.4C) (Tanos et al., 2013). CEP164 has also been found to maintain stable IFT between the cytoplasm and cilium via interacting with Rab8 and Rab11 endosomes as well as recruiting other key IFT proteins (Čajánek and Nigg, 2014; Hehnly et al., 2012). We understand DAPs to be essential for ciliogenesis, as several DAP genes have

been identified as causative mutations for various ciliopathies. For example, CEP83 has been directly linked to a cystic kidney ciliopathy called Nephronophthisis (Mansour et al., 2021). As CEP83 nucleates DAP complex formation, mutating CEP83 results in DAP complexes being unable to form, even though expression of other DAPs is unaffected. (Shao et al., 2020).

DAPs also show roles in centriole to membrane docking in non-ciliated cells. An example in Radial Glial Progenitor cells show that DAP complex attachment to the cell membrane is important for maintaining cortical tension via formation of ring-shaped MT structures adjacent to cell junctions (Kasioulis et al., 2017; Shao et al., 2020). In absence of DAP complexes, mechanosensitive signalling pathways are activated which results in over-proliferation of cells (Shao et al., 2020). Interestingly, while DAPs are required for cell cycle regulation (Kobayashi et al., 2020; Mansour et al., 2021), they appear to be dispensable in mitotic spindle orientation. During mitosis, DAP levels are actually reduced at centrosomes (Bowler et al., 2019), and mutations in DAPs do not appear to affect cell division directly (Ma et al., 2023; Shao et al., 2020). Rather it seems that centrosomes in mitosis are anchored to the membrane by MT attaching to cortical actin via MT plus end binding proteins or proteins that interact with both MTs and actin (Buttrick et al., 2008; Cliffe et al., 2004; McCartney et al., 2001; McNally, 2013). This process is regulated by highly conserved sDAPs Ninein and Cenexin (Delgehyr et al., 2005; Hung et al., 2016; Ma et al., 2023; Shinohara et al., 2013). But as sDAPs do not form regular complexes like DAPs (Chong et al., 2020; Uzbekov and Alieva, 2018), and given the astral nature of MTs nucleated from centrosomes, it is unclear if centrioles have a regulated orientation during mitosis when they are presumably anchored at cell poles.

1.3.2. Conservation of DAPs in *Drosophila*

While most DAPs are conserved in humans, mice and zebrafish, they are often not conserved in *Xenopus* or invertebrates such as *Drosophila* and *C.elegans* (Callaini et al., 1997; Jana et al., 2018; Mansour et al., 2021; Tischer et al., 2021). The only DAPs that show some sequence homology with *Drosophila* proteins are FBF1, CEP164 and CEP89 (Hodges et al., 2010). However, my own BLAST searches show that the human sequence for CEP164 has more sequence homology to the NuMA ortholog Mud, a nuclear tethering protein, as compared to *Drosophila* CEP164 (data not shown). In line with these observations, it appears these three

conserved DAPs are only somewhat functionally conserved. Like in mammalian cells, CEP89, FBF1 and CEP164 localise to the transition zone during ciliogenesis, but they are only required for membrane docking in neuronal ciliogenesis and not in spermatocytes. CEP164, arguably the most important DAP in mammalian cells, is completely dispensable for ciliogenesis (Hou et al., 2023; Tischer et al., 2021). Unlike mammalian DAPs, *Drosophila* DAPs are also not consistently present on mature mother centrioles (Gartenmann et al., 2017; Lattao et al., 2017).

Despite the lack of DAPs it has been shown that *Drosophila* basal bodies do form transition fibres that anchor basal bodies to the cell cortex (Fig. 1.4D) (Gottardo et al., 2018). However, it is unclear what these fibres are composed of. While a study has shown that FBF1 mutant flies are uncoordinated with late ciliogenesis defects related to IFT (Hodge et al., 2021), their localisation does not match that of transition fibres (Basiri et al., 2014; Hou et al., 2023; Lapart et al., 2019). Transition fibres in *Drosophila* are also highly robust and difficult to perturb. Mutations that drastically reduce PCM in spermatocytes show that centrioles become oriented side-on to the cell cortex, however fibrous extensions are still able to form between the outer centriolar wall and the cell cortex (Fig. 1.8C) (Roque et al., 2018). Mutations in key transition zone proteins that disrupt centriole docking also show that fibres are still able to form from the distal end of the centriole, but cannot attach to the membrane (Fig. 1.8C) (Vieillard et al., 2016). These examples show that while basal body docking at the cell membrane likely requires a combination between stable centriolar components, PCM components and specialist ciliogenesis proteins (Hou et al., 2023; Lapart et al., 2019; Wu et al., 2020), there are gaps in our knowledge of how this process occurs.

1.3.3. Distal Cap proteins

The distal cap consists of CP110 and Cep97 which are well-known inhibitors of ciliogenesis in various organisms (Schmidt et al., 2009; Song et al., 2014; Spektor et al., 2007; Tsang et al., 2008; Walentek et al., 2016). Removal of CP110 by Cep97 is essential for ciliogenesis to occur (Fig. 1.8B) (Nagai et al., 2018; Song et al., 2022; Spektor et al., 2007). This may be partially due to the physical inhibition of plus end MTs when CP110 is present, its removal therefore allows axoneme extension from basal body MTs (Aydogan et al., 2022; Spektor et al., 2007). In *Drosophila* the role of CP110 in ciliogenesis does not appear to be fully

conserved, as *CP110*$^{-/-}$ flies appear viable and healthy. However, another cell conserved role for the distal cap is in centriole length control in both ciliated and non-ciliated cells (Aydogan et al., 2022; Delgehyr et al., 2012; Schmidt et al., 2009). While CP110 and Cep97 are commonly known to act together, recent data suggests that they may also function independently of each other (Delgehyr et al., 2012; Dobbelaere et al., 2020).

1.3.3.1. CP110

CP110 removal from the distal end of centrioles is an important step in its conversion into a basal body in vertebrate cells, allowing ciliogenesis to occur. Depletion of CP110 in typically unciliated cells *in vitro* has been shown to cause ectopic cilium growth, even as cells continued to undergo mitosis (Spektor et al., 2007). While these results have been corroborated by many more studies which continue to elucidate CP110's inhibitory roles in ciliogenesis (Song et al., 2014; Song et al., 2022; Tsang et al., 2008), some reports also observe that loss of CP110 is not sufficient to initiate ciliogenesis, even in typically ciliated cells (Walentek et al., 2016; Yadav et al., 2016). Moreover, *CP110*$^{-/-}$ mice develop ciliopathic defects and lack cilia. An analysis of primary fibroblasts from *CP110*$^{-/-}$ mice shows that while MTs were able to dock potential basal bodies to the cell membrane at the site of ciliogenesis, this attachment did not last more than 20 minutes, suggesting that CP110 is important in maintaining membrane attachment (Yadav et al., 2016). This observation is in line with an independent study in *Xenopus in vivo* showing that CP110 interacts with actin remodelling proteins to mediate membrane docking during ciliogenesis (Walentek et al., 2016). Taken together, it is likely that an optimum level of CP110 is required in order to facilitate and maintain distal ended docking of future basal bodies to the cell membrane.

Despite its storied roles in ciliogenesis, *CP110*$^{-/-}$ flies show minimal ciliogenesis defects (Franz et al., 2013). This suggests that in *Drosophila* CP110 is dispensable for ciliogensis. Instead, CP110 in *Drosophila* is most often implicated in centriole length control by interacting with proteins that promote centriolar MT polymerising or depolymerising, such as Sas4 and kinesin-13 family proteins respectively (Delgehyr et al., 2012; Franz et al., 2013; Shoda et al., 2021). The roles of CP110 in centriole length control appear to be highly conserved (Kobayashi et al., 2011; Kohlmaier et al., 2009; Schmidt et al., 2009). Indeed, the formation of ectopic cilia in non-ciliated cells depleted of CP110 is more recently been thought to be centriolar MT

extensions due to the lack of CP110 capping the distal end (Kohlmaier et al., 2009; Spektor et al., 2007). However, depending on the cell type and organism, loss of CP110 may lengthen or shorten centrioles due to the imbalance of MT growth regulators (Delgehyr et al., 2012; Franz et al., 2013; Kobayashi et al., 2011). In *Drosophila* embryos, CP110 levels are tightly regulated by the cell cycle such that it's level peaks at a similar point in each cell cycle (Aydogan et al., 2022). While CP110 mutants do not show severe differences in centriole length or cell division in fly embryos, it is nevertheless highly expressed and caps all mature mother centrioles in the embryo syncytium (Aydogan et al., 2022; Franz et al., 2013). Due to its position at the distal end and well-studied roles in membrane docking, CP110 is a potential candidate in a putative centriole orientation mechanism.

1.3.3.2. Cep97

Cep97 is typically known to function in a complex with CP110 such that they are co-regulated, with depletion of one from centrioles usually resulting in the depletion of the other (Aydogan et al., 2022; Carvalho-Santos et al., 2011; Spektor et al., 2007). Cep97 is required in order to recruit CP110 onto the centriole (Spektor et al., 2007). Competition between Cep97 and other CP110 interactors has been shown to decrease the ability of Cep97 to bind as frequently to CP110, increasing the chance of CP110 removal from the distal cap (Song et al., 2022). Ubiquitination mediated depletion of Cep97 was further shown to destabilise CP110's presence at the centriole (Nagai et al., 2018). Like CP110, Cep97 has been reported to be a ciliogenesis inhibitor in vertebrate cells as it recruits CP110 to the distal cap (Bettencourt-Dias and Carvalho-Santos, 2008). Cep97 and CP110 have also been shown to be co-regulated in centriole length control (Kobayashi et al., 2011; Schmidt et al., 2009). These examples highlight the dependency of CP110 on Cep97.

In contrast to these roles, recent evidence suggests that Cep97 may have independent functions from CP110, exemplified by Cep97 mutants showing more severe defects than CP110 mutants in some cell types (Delgehyr et al., 2012; Dobbelaere et al., 2020; Franz et al., 2013). Furthermore, while removal of a CP110-Cep97 complex from centrioles allows ciliogenesis to occur, fluorescence imaging shows that Cep97 alone is only transiently removed from resulting basal bodies, suggesting additional ciliogenesis-related functions for Cep97 (Delgehyr et al., 2012; Dobbelaere et al., 2020). As described in section 1.3.3.1., CP110 mutants

show minimal defects in ciliogenesis in *Drosophila*, however, Cep97 mutant flies are notably more uncoordinated and show missing cilia from neuronal tissues despite the presence of basal bodies. In these images, basal bodies were often not docked and found side-on with respect to the cell cortex (Dobbelaere et al., 2020), showing that membrane docking and thus centriole orientation in ciliated cells is perturbed when Cep97 is deleted. These results may be in conflict with other published data showing that CP110 and Cep97 act together (Aydogan et al., 2022; Kobayashi et al., 2011; Schmidt et al., 2009). However, it is possible that Cep97 possesses both CP110 dependent and independent roles. Like CP110, Cep97 is highly expressed in *Drosophila* embryos where it caps the distal end. Together with its roles in membrane docking and ciliogenesis in the same organism, it too represents an ideal candidate for a putative centriole orientation mechanism in embryos.

1.4. Centriole and Centrosome Positioning

Centrosomes are key positional organisers within cells which possess them. In previous sections, I have discussed how centriole position and orientation is important in ciliogenesis (sections 1.1.3 and 1.3), I have also introduced centrosomes as nucleators of MTs contributing to the mitotic spindle (section 1.2.2.). Additionally, I have provided examples of how the position of centrosomes as MTOCs and actin nucleators influence the direction of trafficking and organelle position (sections 1.2.2. and 1.2.3.). It is possible that aspects of these mechanisms may also influence centriole orientation. Hence, in this section I detail our understanding of the mechanisms behind centriole positioning in different systems.

1.4.1. Asymmetric Division

Centrosomes nucleate the mitotic spindle; therefore, the position of centrosomes affects the orientation of cell division (Cabernard and Doe, 2009). This is especially important during asymmetric division where resulting daughter cells can be of different sizes and contain different cytoplasmic components (Cabernard and Doe, 2009; Cowan and Hyman, 2004; Noatynska and Gotta, 2012; Rebollo et al., 2007). This was first clearly observed in the asymmetric division of the single celled *C.elegans* embryos (Cowan and Hyman, 2004; Noatynska and Gotta, 2012). In *Drosophila,* a well-studied example of this mechanism is in neuroblasts whereby positioning of centrosomes in interphase leads to asymmetric division, producing another neuroblast and a ganglion mother cell that goes on to differentiate into neurons (Homem and Knoblich, 2012; Januschke et al., 2011). In this system, the new mother centriole is attached to the apical cell cortex of the neuroblast, recognised by the young centriole marker Centrobin (Januschke et al., 2013). The centriole is held in place by a protein complex bound to the cell membrane by PAR proteins, which are known to establish cell polarity through specialised cortical domains during development (Cowan and Hyman, 2004; Feldman and Priess, 2012). The protein complex facilitating centriole attachment to the cortex contains proteins Pins and Mud (Izumi et al., 2006). Mud is expressed in other cell types such as *Drosophila* embryos and is a functional homologue of NuMA, a protein which attaches centrosomes to the nuclear membrane in non-polar, cycling cells (Bowman et al., 2006). Both NuMA and Mud are able to promote MT polymerisation and force generation in order to position centrosomes (Knoblich, 2010; Merdes et al., 1996). In line with their broadly conserved mechanism of action (Elric and Etienne-Manneville, 2014; Morin and

Bellaïche, 2011), Pins and Mud have also shown functionality in cellularised *Drosophila* embryos to organise and orientate the mitotic spindle (Camuglia et al., 2022; Izumi et al., 2006). These functions could potentially implicate Pins and Mud in centriole orientation.

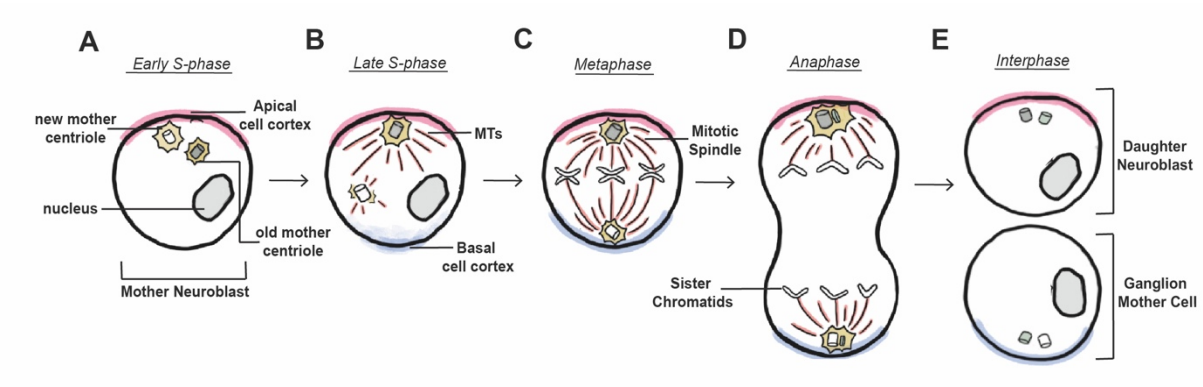

Figure 1.9. Asymmetric division in the *Drosophila* neuroblast

(A) Schematic showing an asymmetrically dividing neuroblast that is polarised and maintains the old mother centriole (*white*) at the apical cell cortex (*pink*) while the new mother centriole (*grey*) loses PCM (*yellow*). **(B)** As the daughter centriole nucleates less MTs (*red*) it is more mobile allowing it to drift until it is captured by the basal side (*violet*) of the cell. **(C)** This determines the orientation of the mitotic spindle (*orange*), **(D)** as well as protein composition of resulting daughter cells as sister chromatids are segregated in anaphase. **(E)** The daughter cell which inherits the new mother centriole goes on to differentiate into a Ganglion Mother Cell, while the daughter cell which retained the old mother centriole remains as a neuroblast.

The PCM also facilitates centrosome positioning during asymmetric division. In *Drosophila* neuroblasts as new mother centrioles are retained at the apical end (Fig 1.9A), old mother centrioles are mobile and drift across the nucleus where they are eventually localised at the basal cell cortex by PAR proteins (Fig. 1.9B) (Januschke et al., 2011). Decrease of Cnn at the old mother PCM decreases PCM size and MT-nucleating ability (Conduit and Raff, 2010), allowing old mother centrioles to drift away from the apical cell cortex (Fig. 1.9B) (Rusan and Peifer, 2007; Wang et al., 2009a). These specifically positioned centrioles in interphase later define the orientation of the mitotic spindle during asymmetric cell division (Fig. 1.9C, D). Asymmetric division results in the daughter cell which inherited the new mother centriole to differentiate into a Ganglion Mother Cell, while the daughter cell that retained the old mother centriole remains as a neuroblast (Fig. 1.9E). A similar requirement for other PCM components in retaining centrioles at the apical cortex to orient the mitotic spindle for asymmetric division have been demonstrated in various systems (Ramdas Nair et al., 2016). This makes sense, as the PCM facilitates MT attachment to centrioles, allowing MT and membrane interacting proteins such as Pins and Mud to bind and, together with a motor protein like

dynein, pull centrosomes into position (Fig. 1.6B) (Goshima et al., 2005; Hunter and Wordeman, 2000; Knoblich, 2010; Merdes et al., 1996).

Given that Pins and Mud are binding to MTs which emanate from centrosomes as an aster, centrosomes would presumably adopt random orientations at the apical surface. However, in other systems where centrosomes are positioned at the apical cortex such as the *Drosophila* embryo, most centrosomes appear upright (Aydogan et al., 2018; Gartenmann et al., 2017). This suggests that there are still gaps in our knowledge as to how centrioles position themselves, and emphasises importance of the inherent polarity of the centriole in this process.

1.4.2. Cell Migration

During the migration of slow-moving cells such as patrolling leukocytes or macrophages, centrosome position is maintained at a constantly evolving leading edge, both to position other organelles and facilitate intracellular trafficking (Elric and Etienne-Manneville, 2014; Luxton and Gundersen, 2011). As cells extend filipodia or lamellipodia in the direction of a chemoattractant, a leading edge is formed with a highly branched actin network, thus polarising the cell in the direction of the attractant (Fig. 1.10A, B). During this process, centrosomes are recruited to the leading edge by MT attachment to rigid cortical actin and dynein mediated pulling of centrosomes (Fig. 1.10A, B) (Higginbotham et al., 2006; Solecki et al., 2004; Solecki et al., 2009). This position allows astral MTs nucleated from the centrosome to extend into the cell and towards the leading edge, aiding in increased intracellular trafficking to maintain dynamic actin polymerisation and efficient responses to chemoattractants (Kuijpers and Hoogenraad, 2011). As centrosomes are maintained at the leading edge, they also pull along other organelles such as the nucleus. In migrating olfactory bulb neurons, centrosomes form a MT cage around the nucleus and drag it forward (Fig. 1.10C) (Solecki et al., 2004; Solecki et al., 2009). In this mechanism, MT/actin crosstalk is especially important in maintaining centrosome position at a constantly changing leading edge as cells migrate (Fig. 1.10D) (Solecki et al., 2009). While not all migratory cells have centrioles positioned at the leading edge, most show regular and defined centriole positioning that is likely optimised for the cell's microenvironment (Gudima et al., 1988; Renkawitz et al., 2019).

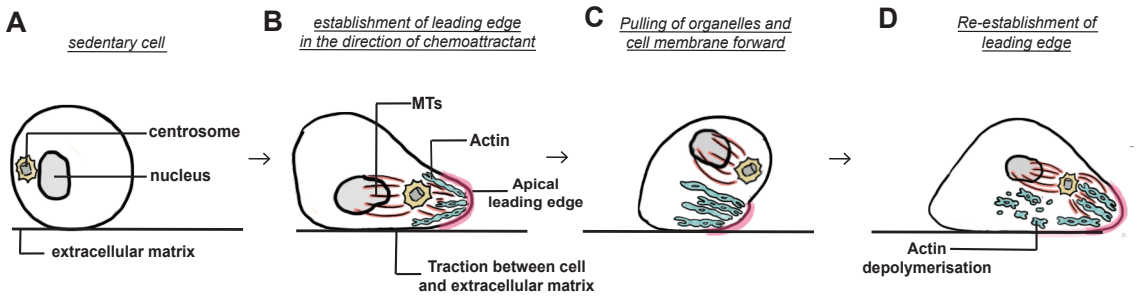

Figure 1.10. Cell migration in a slow-moving white blood cell

(A) Schematic showing a cell migrating towards a chemoattractant (right). Centriole in *grey* with *yellow* PCM and nucleus in *grey.* **(B)** A leading-edge forms that polarises the cell (*pink*) in the direction of the attractant, actin (*blue*) gathers at the leading edge to form a protrusion (filapodia/lamellipodia). Crosstalk between MTs (*red*) and actin draws the centrosome (*grey* with *yellow* PCM) to the leading edge. **(C)** The centrosome forms a cage around the nucleus, pulling it along as the cell moves. **(D)** The leading edge is redefined as the previous leading edge makes contact with the extracellular matrix and the centrosome is dynamically repositioned as the new leading edge forms.

1.4.3. Cell Polarity

Previous sections have shown the importance of specific centrosome positioning in various cell types, as well as some insight into how centrosome positioning is achieved. In many scenarios, protein complexes establishing polar cell membranes recruit centrosomes via MT and actin linked motors. However, there are also cases where centrosome positioning is involved in establishing the polarity of the cell itself. This is usually facilitated by repositioning the centrosome to the cell cortex where it acts as an MTOC as the cell becomes polarised along the MTOC axis. However, centriolar MTs from more centrally positioned centrosomes can also establish cell polarity in a similar manner (Siegrist and Doe, 2007). One example of apically positioned centrioles facilitating cell polarity is in terminal intestinal cell division in *C.elegans* where centrosomes do not typically function as a main MTOC. Centrosomes are trafficked to the future apical surface with polarity establishing proteins PAR3 and PAR6. Live cell analysis showed that once at the future apical membrane, centrosomes recruit MTOC components and condense γ-tubulin as it takes over the main MTOC role in the cell, thereby aiding in the process of cell polarisation (Feldman and Priess, 2012). Furthermore, drug-mediated inhibition of MTs stalled centrosome and PAR protein travel, resulting in PAR3, PAR6 and the centrosome adhering to the cell membrane in the middle of the cell instead of the future apical end. As a result, these cells failed to polarise.

Another example showing the importance of centrosome positioning in establishing cell polarity is in immunological synapse (IS) formation. An IS is formed when a T cell is activated through cell-to-cell contact with an antigen presenting cell (APC) (Fig. 1.11A). A key event in proper formation of the IS is repositioning and distal ended docking of the centrosome to the cell cortex (Fig. 1.11B) (Stinchcombe et al., 2015). Repositioning of the centrosome is achieved by membrane-bound molecule diacylglycerol (DAG) which is cleaved from phospholipids upon IS formation. Photoinactivation of PLC-γ, which produces DAG, results in lateral positioning of the centrosome (Quann et al., 2009). In this system, centrioles are docked at the cell membrane via DAPs (Fig. 1.11C) (Stinchcombe et al., 2015; Tsun et al., 2011). These distally oriented centrosomes have been suggested to polarise activated T-cells along the axis formed by the IS (Fig. 1.11D) (Liu and Huse, 2015; Quann et al., 2011). This polarisation through the directionality informed by the centrosome has further been suggested to control capacity of trafficking to the IS (Fig. 1.11E) (Stinchcombe and Griffiths, 2014; Stinchcombe et al., 2006; Tamzalit et al., 2020). Forces pulling the centrosome to the IS are so strong that the connected membranes of the T-cell and target cell will invaginate as an IS forms until it contacts the centrosome (Fig. 1.11C) (Yi et al., 2013), which may be travelling from the nucleus where centrosomes are usually tethered. This particular example highlights the importance of centriole positioning at the cell cortex and its role in polarity establishment.

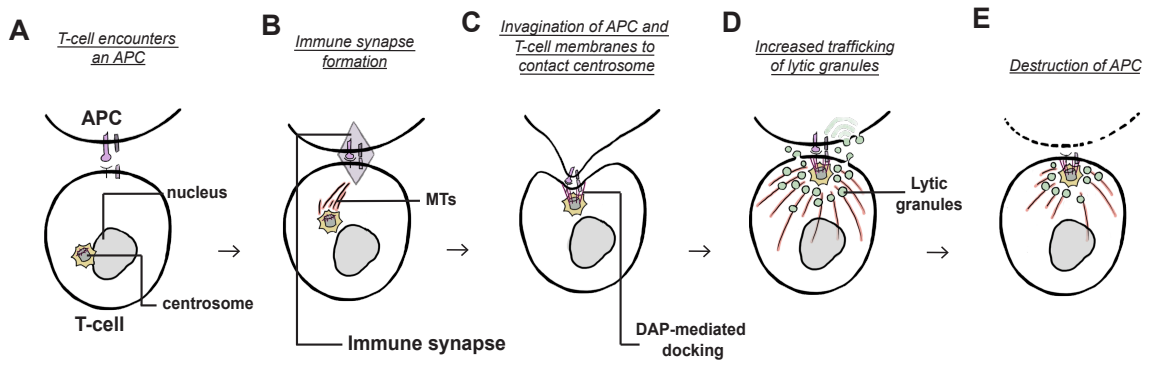

Figure 1.11. Immune Synapse formation

(A) Schematic showing a T-cell contacting an Antigen Presenting Cell (APC) and forming an Immune Synapse (IS, *purple*). With centriole in *grey* with *yellow* PCM and nucleus in *grey*. **(B)** Formation of the IS recruits the centrosome (*grey* with *yellow* PCM and *pink* DAPs) to the IS via MTs (*red*) and docks via DAPs (*pink*). **(C)** The force from pulling the centriole towards the IS invaginates the T-cell and APC membrane towards the centriole. **(D)** The centriole at the IS polarises the cell in the direction of the APC. This increases intracellular trafficking to the area as MTs are nucleated at the IS via the centrosome. **(E)** This allows lytic granule vesicles (*green*) to travel to the immune synapse where they are exocytosed and destroy the attached APC.

Previous examples have focused on mammalian cells, however there is also evidence of centrosome positioning being important in the establish of cell polarity in *Drosophila* wing-disc epithelia (Carvajal-Gonzalez et al., 2016a). Wing-disc epithelial cells are polar and on the apical side form actin-rich hairs. Establishment of polarity and thus proper formation of these hairs is achieved by interactions between the centrosome and the Frizzled-Planar Cell Polarity signalling pathway (Fz PCP). When the Fz-PCP pathway was disrupted, fewer cells were able to form hairs and of those that do, centrioles were commonly seen uncoupled from hairs and further from the apical cortex (Carvajal-Gonzalez et al., 2016a; Carvajal-Gonzalez et al., 2016b). The same group later identified a role for actin in positioning centrosomes close to the future apical cell cortex. They propose that actin confined centrioles to a specific subcellular location, which then allows centrioles to be further positioned close to the cell cortex and interact with the Fz-PCP pathway, resulting in polarised cells (Garrido-Jimenez et al., 2018). This theory was corroborated by an independent study which proposed that concentric rings of actin define a subcellular location for centrosomes. MTs nucleated by the centrosome then associate with these actin rings and through MT pulling forces fine tune centrosome position within the cell (Jimenez et al., 2021).

Unlike studies in immune cells, it is unknown how centrioles may be oriented in this cell type. However, given the functionality of centriole orientation in other polarised epithelia involves building specialised structures (IS formation, ciliogenesis), and the ancient conserved functionality of centriole orientation in ciliogenesis (Carvalho-Santos et al., 2011), it is possible that centrioles are oriented in this system as well in order to facilitate actin hair formation.

1.4.4. Putative Roles for Centriole Orientation

In ciliated cells, centriole orientation is important to allow ciliogenesis to occur as axonemes extend from the plus ends of centriolar MTs at the distal end of centrioles (Ishikawa and Marshall, 2011). Centrioles also dock at the cell membrane during IS formation to facilitate trafficking of lytic granules (Cassioli and Baldari, 2019). There are many other processes that require centrosomes to be positioned close to the cell cortex. This includes cellular events which require reorganisation of cytoskeletal networks for force generation (such as cell migration), as well as establishing mitotic spindle orientation (such as in asymmetric division) (Elric

and Etienne-Manneville, 2014; Januschke et al., 2011; Quann et al., 2009). However, it is unclear if centrioles are specifically oriented in these contexts, or if any such orientation is functionally significant to centrosome positioning. A possible mechanism for centriole orientation in these other systems may be inferred from what we already understand about centriole orientation in ciliated cells and centriole positioning in polarised cells.

In ciliated cells, the mechanism of centriole docking seems to differ between organisms depending on if DAPs are present (Dobbelaere, 2023; Gottardo et al., 2018; Hou et al., 2023; Tanos et al., 2013). In many vertebrate cell types, DAPs facilitate binding to a ciliary vesicle which brings centrioles to the future site of ciliogenesis (Fig 1.2C) (Pitaval et al., 2017; Wu et al., 2020). DAPs such as CEP164 also function to remove ciliogenesis inhibitors such as distal cap proteins and recruit transition zone proteins (Čajánek and Nigg, 2014; Tanos et al., 2013). In organisms where DAPs are not conserved, centrioles still attach to the cell membrane via transition fibres (Gottardo et al., 2018; Hou et al., 2023). Transition fibre formation seems to depend on a combination between PCM components (Jurczyk et al., 2004; Roque et al., 2018), appropriate levels of distal cap proteins CP110 and Cep97 (Dobbelaere et al., 2020; Yadav et al., 2016), and transition zone proteins that are specifically expressed and recruited to the growing cilium (Vieillard et al., 2016). Of these required proteins, core PCM components such as PLP, Spd2 and Cnn, as well as distal cap components CP110 and Cep97 appear to be well conserved and expressed in both ciliated and non-ciliated cells (Carvalho-Santos et al., 2011; Hodges et al., 2010).

Interestingly, the formation of the IS has been structurally compared to a cilium (Cassioli and Baldari, 2019; Stinchcombe and Griffiths, 2014). Reports have shown that centrioles do indeed dock to the apical cell membrane during IS formation (Stinchcombe et al., 2015; Tsun et al., 2011). Unlike in ciliogenesis, distal cap proteins CP110 and Cep97 remain associated with the centriole as it docks, and inhibition of DAP complex formation not only abolishes ability to dock, but also reduces the efficiency of lytic granule trafficking to the IS (Stinchcombe et al., 2015). Another study showed that distal ended orientation of centrioles serves to guide lytic granule secretion in the direction of the target cell (Liu and Huse, 2015). Such an example would pose a second system in addition to ciliogenesis, whereby the inherent orientation of centrioles plays a role in polarised cell function. A later study contradicted these results, showing that

orientation of centrioles at the IS did not affect the directionality of lytic granule release, but was instead involved in the amount of lytic granules released (Tamzalit et al., 2020). The authors showed that when centrioles were genetically deleted, force generation by synaptic actin decreased, slowing down lytic granule trafficking within the cell and exocytosis from the cell (Tamzalit et al., 2020). However, residual PCM was present despite the lack of centrioles. Thus, while the activity of MTs decreased, acentriolar PCMs were still able to nucleate MTs and provide some directionality to lytic granule release. These studies show that distal-ended orientation of centrioles can have distinct functionality in non-ciliated cell types, notably using proteins that may have been evolutionarily conserved from ciliogenesis (Cassioli and Baldari, 2019; Stinchcombe and Griffiths, 2014). It also highlights that while centriole specific docking and orientation may be important, centrioles work in concert with their PCM. Therefore, it is likely that if centriole orientation has any functional importance in other systems, both centriole and PCM proteins are involved.

It is also possible that centriole orientation is random and facilitated by pushing and pulling forces generated by MTs and actin on the PCM (Knoblich, 2010; Merdes et al., 1996; Yi et al., 2013). MT and actin forces pulling centrosomes into place are likely relying on the attachment of MTs and actin to the PCM and not the centriole itself (Choi et al., 2010; Farina et al., 2016; Woodruff et al., 2014). But, as the PCM is connected to the centriole wall (Conduit et al., 2015; Fu and Glover, 2012; Lerit et al., 2015), centrioles may be indirectly changing orientation depending on the direction it is pulled in. This is especially possible if centrioles are not docked to a membrane such as the nucleus (Bowman et al., 2006), or the cell membrane (Tanos et al., 2013; Tsun et al., 2011).

1.5. Neural Networks

Over the course of my project, I collaborated with Conor Wild from the von Delft lab in developing an ***Artificial neural network*** (ANN) to quantify centriole orientation data. This ANN allowed high throughput, accurate quantification of centriole orientation and forms a major part of my thesis. ANNs are a type of machine learning algorithm based on the structure of the human brain (Hassabis et al., 2017). While ANNs have many different functions, most biological applications use ANNs to categorise data that is daunting or difficult for humans to accurately categorise in a high-throughput manner (Ben Hamida et al., 2021; Zhang et al., 2019). The ANNs used to categorise data are called ***supervised neural networks***. An ANN takes the data we give it, called ***input data***, and approximates it into output categories we define. ANNs sort input data into our desired outputs by learning from a ***training dataset*** consisting of a sizeable set of input data that has ***desired outputs*** for each input (Fig. 1.12A). ANNs then adjust themselves to place input as accurately as possible into output categories using a principle called ***deep learning***.

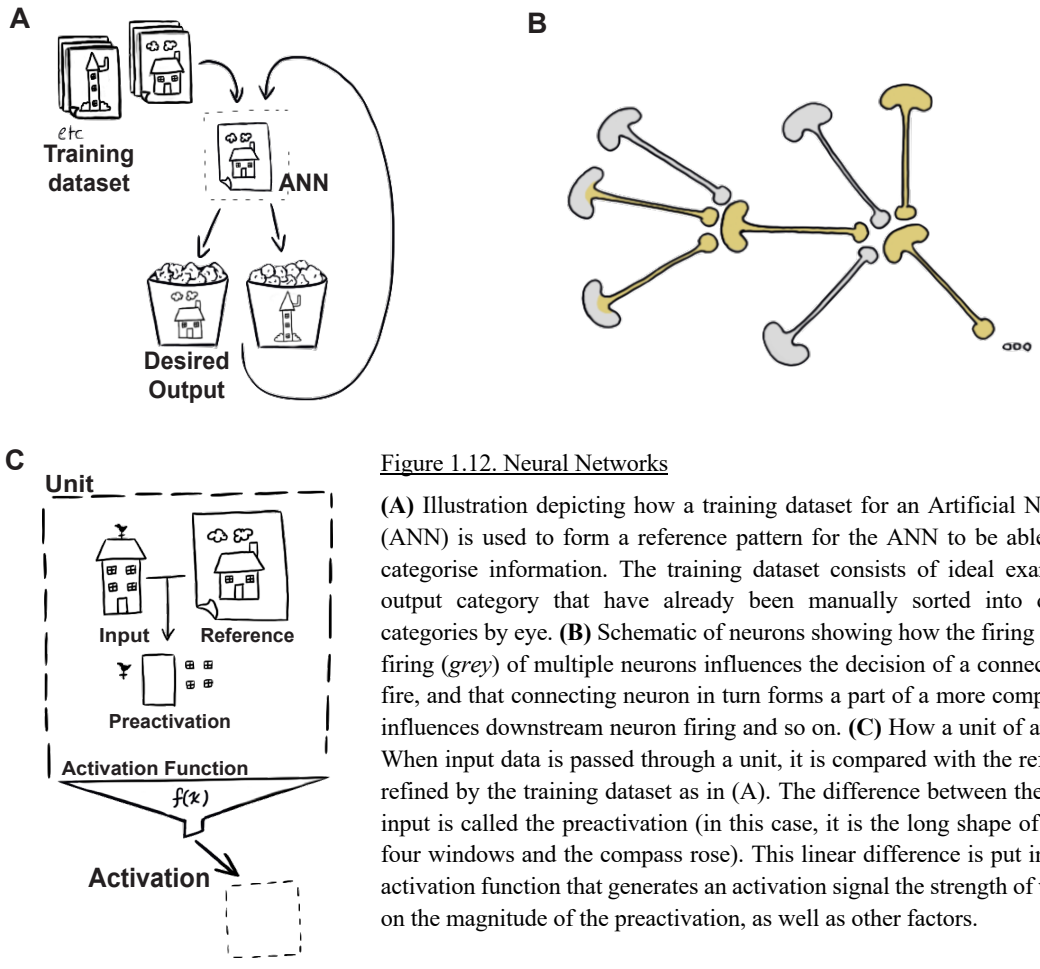

Figure 1.12. Neural Networks

(A) Illustration depicting how a training dataset for an Artificial Neural Network (ANN) is used to form a reference pattern for the ANN to be able to accurately categorise information. The training dataset consists of ideal examples of each output category that have already been manually sorted into desired output categories by eye. **(B)** Schematic of neurons showing how the firing (*yellow*) or not firing (*grey*) of multiple neurons influences the decision of a connecting neuron to fire, and that connecting neuron in turn forms a part of a more complex signal that influences downstream neuron firing and so on. **(C)** How a unit of an ANN works. When input data is passed through a unit, it is compared with the reference pattern refined by the training dataset as in (A). The difference between the reference and input is called the preactivation (in this case, it is the long shape of the house, the four windows and the compass rose). This linear difference is put into a nonlinear activation function that generates an activation signal the strength of which depends on the magnitude of the preactivation, as well as other factors.

1.5.1. How ANNs Work

In the brain, each neuron receives signals through its dendrites. Based on the *multiple* signals a neuron receives, it may fire a *single* action potential down its axon. Its decision to fire then makes up one of multiple signals received by neurons downstream and so on (Fig. 1.12B). Many neurons, each with its own binary output, fired in a particular pattern, allow our brains to come to a single decision. This principle is also applied in ANNs, each decision-making node (equivalent to a neuron) is called a ***unit***. Each unit is coded to interrogate a specific aspect of the input data and based on training data passed through it, forms a ***reference pattern*** which reflects the optimum pattern potential input data could provide (Fig. 1.12A). The closer the input's data matches the reference, the stronger the resulting signal from the unit. The difference between the input and the reference is called the unit's ***preactivation*** and is calculated such that preactivation is maximum if the input data perfectly matches the reference (Fig. 1.12C). The preactivation is passed through the unit's nonlinear ***activation function*** to output an activation pattern (or simply ***activation***). The activation pattern from all units within an ANN determines which output category input data is sorted into (Kriegeskorte and Golan, 2019).

The activation function transforms the preactivation into a value that considers parameters besides the ones interrogated by the single unit from which the preactivation was derived. The function for each unit is described as nonlinear because how each unit interprets its preactivation depends on parameters that themselves change as input data changes, such as activations from other units within the ANN.

1.5.2. Types of Neural Networks

ANNs in their simplest form have a layer of input data, a unit that makes a decision based on its reference pattern as well as additional parameters set by the author, and a layer of output data determined by the unit. Most ANNs have multiple units arranged into a ***hidden layer*** (Fig. 1.13A). As all units are within the same layer, input data is passed through all units concurrently. Each unit interrogates a different aspect of the data using a different activation function. The combination of activation patterns from all units allows the ANN to best approximate the output category for the data that best matches the input. In this way, increasing the

number of units *within* a layer increases the precision of the neural network (Fig. 1.13B) (Kriegeskorte and Golan, 2019).

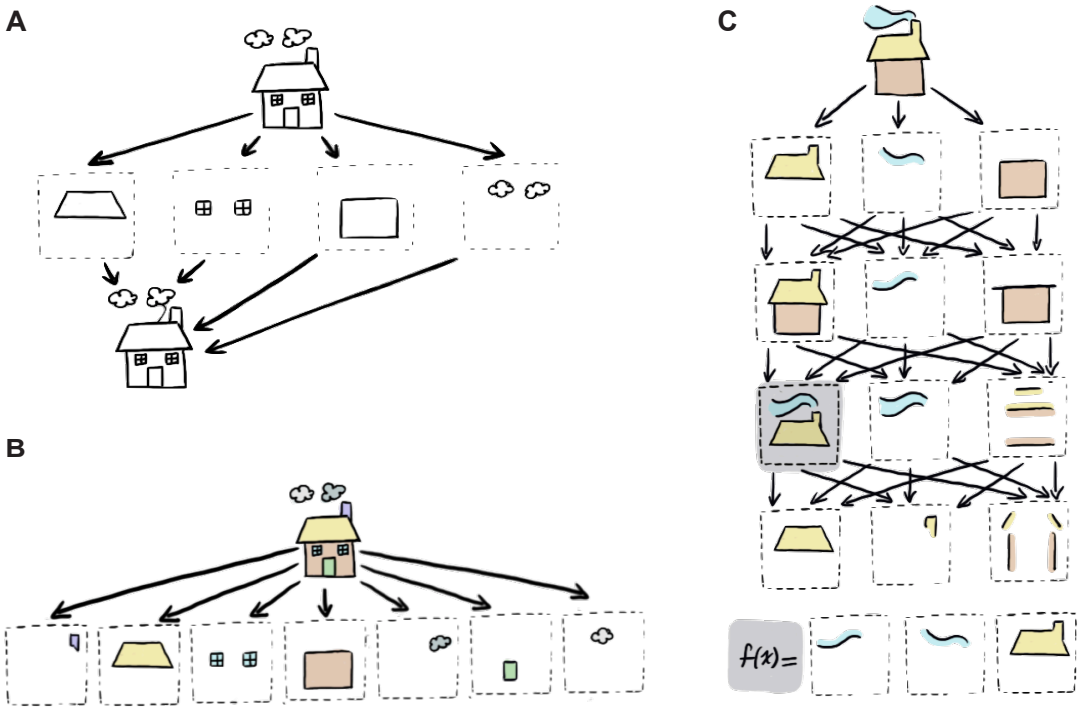

Figure 1.13. The function of Units within an ANN

(A) Units may be organised into a hidden layer consisting of several units, each probing different and unique aspects of the input data. Each unit then contributes to the strength of placing the input data into a particular output category. **(B)** ANNs can achieve higher precision by adding more units to a layer, each probing more and more specific aspects of the input data to more finely tile the input data, thus making a more confident decision as to which output category the input data belongs to. **(C)** ANNs with multiple layers allow the ANN to generalise and approximate data based on less information. This is because units in lower layers can account for experience from layers preceding it, in each layer, sparse input data can be interrogated from a different perspective that takes into account what the ANN has already learned from previous layers. Example is shown by "f(x)=" showing the components of the *grey* unit and how it utilises aspects from other units within the network.

Deep ANNs have multiple hidden layers and are advantageous as they can use "experience" gained in previous layers to inform downstream layers, creating more robust activation functions in downstream units that can more accurately categorise input data with sparse information. For example, if input data had many defining points that directed it to specific outputs, it would be possible to generate many units within a single hidden layer to accurately categorise novel input data (Fig. 1.13B). However, if input data had few defining points, or if we wanted to generalise the usage of an ANN such that there are fewer similar points of interrogation between different inputs, it becomes more difficult to accurately place data into an output category using a single hidden layer. In a deep ANN with multiple layers, a given layer may reuse parts of functions from units in upstream layers and recalculate a similar aspect of the input data in a slightly different context (Fig. 1.13C). This structure allows more reliable approximation of outputs from a fixed budget of

input parameters. The increase in computational power afforded by modern technology, as well as research into arrangement of units within hidden layers and how each unit or layer relies on others, have resulted in the development of highly complex ANNs that can provide increasingly accurate decisions based on less and less input information (Kriegeskorte and Golan, 2019).

ANNs where experience from one layer influences the next layer down are known as ***feedforward*** networks, however there are also ***recurrent/convolutional neural networks***, in which units consider activation from upstream layers as well as other units within their own layer (Fig. 1.14A) (Alzubaidi et al., 2021). In these networks, how activation from upstream ***source*** units is weighted within the activation function of the current ***target*** unit depends on time. Adding a temporal element to ANNs allow them to categorise live data such as speech and videos (LeCun et al., 2015). The type of ANN used is this thesis is a ***residual neural network*** (He et al., 2016). These networks tend to contain many layers, but in addition to using experience gained in units directly preceding the current layer of units, a given target unit may have a source that is multiple layers upstream from itself (Fig. 1.14B). The network used in this thesis, Resnet18, has 18 layers, making it a very good approximator of data with few defining points as each layer has an increasing wealth of experience from preceding layers. "Shortcut" connections to units many layers upstream ensure that layers deep within the ANN perform as well as upstream layers. It also helps Resnet18 preserve the context of data as it is sorted (He et al., 2016).

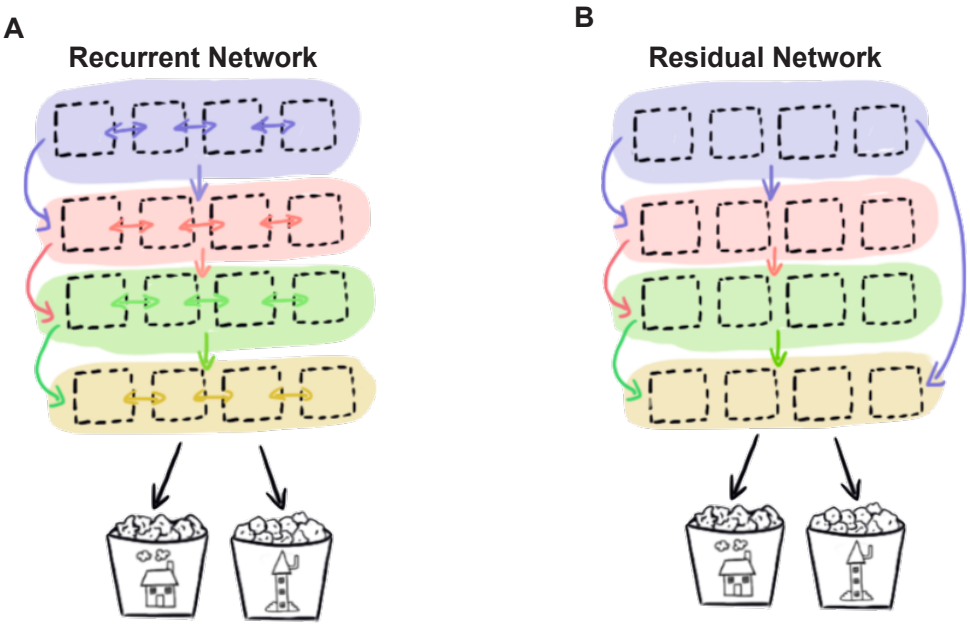

Figure 1.14. Types of ANNs

(A) In Recurrent Networks, units incorporate the activation from upstream layers, but also incorporate activation from units within its layer, adding a temporal aspect to how data is interpreted. **(B)** In Residual Networks, units incorporate the activation from the upstream layer directly preceding the current layer but also "shortcut" connections that allow units to incorporate the activation from units much higher in the ANN. This allows context of the data to be preserved as layers increase. (A, B) layers are *purple, pink, green* and *yellow*.

1.5.3. Calculating and Minimising Network Error

Providing an ANN with a training data set that has input images annotated with desired outputs allows each unit to form a reference that determines its preactivation as input data as received. However, each activation function typically contains other parameters representing connections or biases within a deep ANN. As input that has desired outputs attached to each input image (not training set data) is run through the ANN, we can calculate how well the ANN's outputs match desired outputs; this is known as the error or the ***cost*** of the ANN. The goal of an accurate ANN is to minimise cost (Kriegeskorte and Golan, 2019).

To do this, we calculate how much the cost changes when a parameter in a unit is changed. The change in the cost between changes in a parameter is referred to as the ***cost sensitivity***. It would be highly time consuming to manually change a parameter by small increments and record corresponding changes in cost. Thus, by differentiating a unit's cost sensitivity function, we can plot a curve that extrapolates how the cost would further change given incremental deviations in activation function parameters for a particular unit, this is called the ***partial cost derivative***. In addition to the partial cost derivative, the relationship between a unit and the total cost also depends on sensitivities in units upstream from any one unit (Kriegeskorte and Golan, 2019). Thus, if we start from the last activation function preceding output and work backwards from activation to preactivation in each unit, we can employ a method called ***backpropagation*** which allows all partial cost derivatives from each unit to be accurately calculated (Rumelhart et al., 1985). Through this process, we can computationally find a combination of parameters for each unit that result in the lowest cost (Fig. 1.15A).

The strength of connections between units is also similarly differentiated in order to find the combination of unit-to-unit connections with the lowest overall cost. The analogous situation in the brain is how neurons that often fire together or in sequence with each other become more myelinated (Fig. 1.15B) (Hassabis et

al., 2017). By multiplying the activation from a source unit with the partial cost derivative of the target, we can capture how activation from different source units influence the target unit's effect on the total cost. Units that are synergistic in improving the accuracy of the ANN through lowering cost thus become more biased towards relying on each other (Alzubaidi et al., 2021; Kriegeskorte and Golan, 2019).

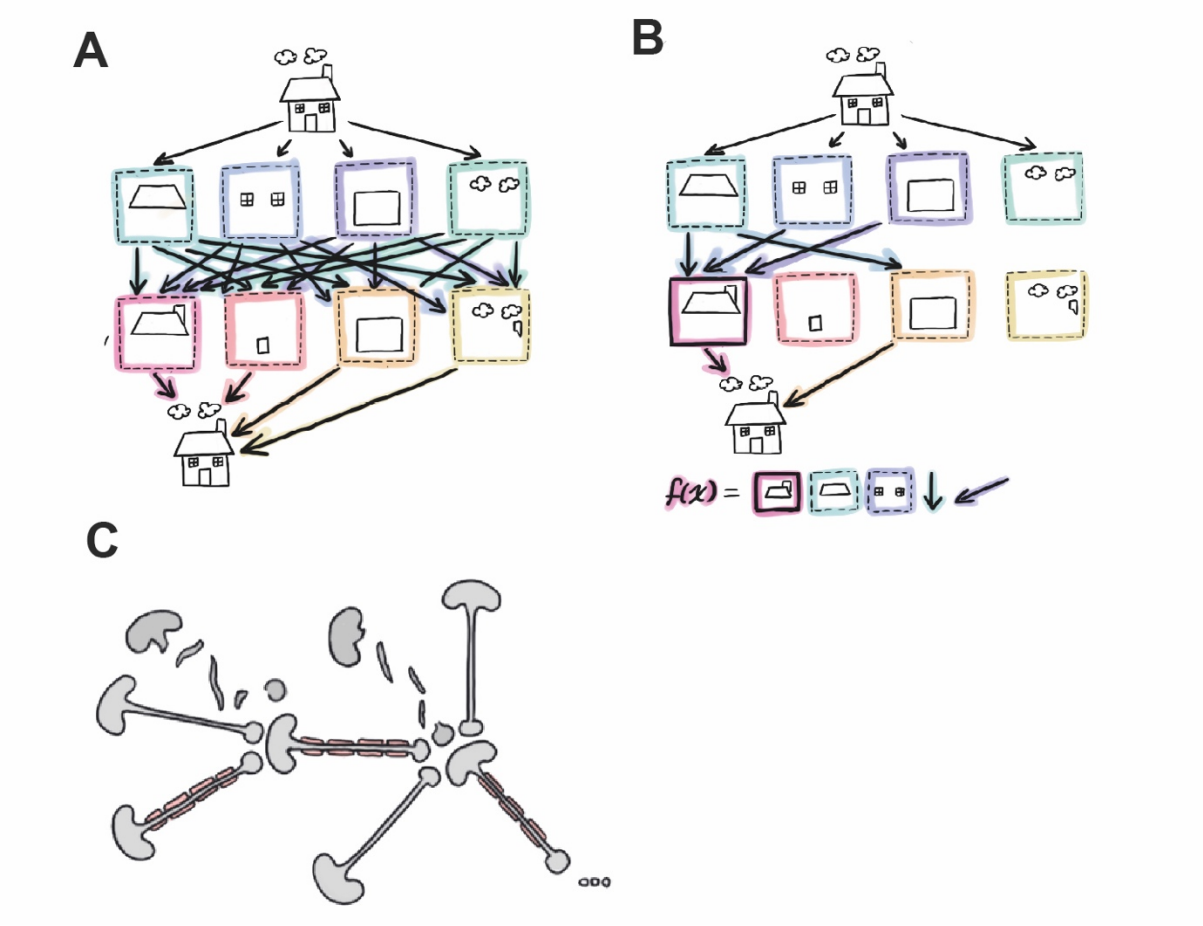

Figure 1.15. Strengthening network connections

(A) As training data is passed through the ANN, units that tend to activate together will play a larger part in each other's activation functions. **(B)** As the ANN is trained, it becomes biased to the activation of other units that tend to activate together with it (for example, houses with long rectangular bases also tend to have gabled roofs). **(C)** This is similar to how connections between neurons are reinforced in the brain, neurons that are frequently used and fire in sequence become myelinated, and neurons that are not often fired are destroyed or become dormant.

1.6. Thesis Overview

In this thesis, I develop methods to measure centriole orientation. I then use these methods to investigate potential candidates and cytoskeletal systems involved in establishing and maintaining centriole orientation. This project began with the observation that centrioles close to the cell cortex in *Drosophila* embryos appear mostly upright, despite not making cilia or having DAP complexes at their distal end. I started by attempting to confirm that centrioles do exhibit a biased orientation in this system by using a fixed antibody labelling assay. I find that centrioles have a preference to be oriented upright with their distal end close to the cell cortex. This mimics centriole orientation in ciliated cells and the few other cell types in mammalian cells where orientation of centrioles has been documented (Stinchcombe et al., 2015; Tanos et al., 2013; Tsun et al., 2011). I then work with a collaborator (Conor Wild, Life Sciences, Diamond Light Source, Oxford) to design an ANN that works in concert with a live imaging assay in order to quantify centriole orientation in an accurate, high throughput manner. Through quantifying centriole orientation over time, we were also able to quantify centriole stability, that is, the propensity for centrioles to change orientation over time. Devising and improving upon our neural network, Centrilyze, was a task with many factors to consider, including how small *Drosophila* centrioles were and how subjective we were being in our categorisation of different centriole morphologies.

Once a live assay and quantification method were established with over 95% confidence with respect to manual quantification, I take a drug-based approach to investigate the effect of loss of actin or MTs on centriole orientation. I find that while loss of MTs somewhat stabilizes centrioles, loss of actin mildly destabilises centrioles. I then employ a candidate-based approach and test the effect of key PCM protein Cnn, and distal cap proteins CP110 and Cep97 on centriole orientation. Cnn^{f} embryos showed a decrease in stability that is likely due to a decrease in inertia provided by a properly formed PCM. However, these changes may also be due to the direct loss of Cnn.

Remarkably, loss of Cep97 results in a majority of centrioles falling onto a stable side-on position with respect to the cell cortex. This suggested that upright, distally oriented centrioles were a default orientation and that in the absence of Cep97, an active centriole orientation mechanism was disrupted, leading to

centrioles falling onto a side-on orientation. However, surprisingly, depletion of the other distal cap protein CP110 showed more moderate effects on centriole orientation. Therefore, while the prospect of distal cap, and in particular, Cep97 involvement is exciting, especially given that not much is known about Cep97 beyond its roles in complex with CP110 in *Drosophila*, additional experiments will be required to form detailed conclusions about the nature of Cep97's role in centriole orientation.

1.7. Aims

1. To investigate if centrioles in *Drosophila* embryos are oriented with their distal end facing the cell cortex like in mammalian cells, in the absence of DAPs or the formation of cilia.

2. To establish an analysis pipeline which can reliably measure centriole orientation over time in live embryos. This method should also allow high through-put quantification of centriole orientation.

3. To identify the main players establishing and maintaining centriole orientation in the *Drosophila* embryo. This includes the cytoskeletal networks responsible for force that may be passively changing centriole orientation, as well as candidate proteins that may be acting in a putative mechanism to maintain orientation.

2. Materials and Methods

2.1. Fly Husbandry

2.1.1. Fly Handling

Flies were fed on *Drosophila* culture medium (0.8% agar, 8% cornmeal, 1.8% yeast extract, 1% soya, 8% malt extract, 2.2% molasses, 0.14% nipagin, and 0.625% propionic acid) in 8 cm x 2.5 cm plastic vials or 0.25 pint plastic bottles. Embryos were collected from apple juice plates (25% apple and raspberry juice, 2.5% sucrose and 2.25% agar) supplemented with a mixture of yeast and water. Standard fly handling techniques were used.

2.1.2. *Drosophila* stocks

Oregon R flies were used as the wild type (WT) stock in all experiments. Balancer chromosomes and markers were used as previously described (Lindsley and Zimm, 1992).

Table 2.1 – Drosophila lines used in this thesis

Genotype	Description	Chapter	Reference
pUbq-CP110-GFP	CP110-GFP expressed from a Ubiquitin promoter	3	(Dobbelaere et al., 2008)
If/CyO;MKRS/TM6B	Double balancer line expressing Curly Oster (CyO) on the second chromosome, as well as TM6B on the third chromosome	3	Raff Lab (pers. comm. Alan Wainman)
If/CyO;pUbq-CP110-GFP/TM6B	Double balancer line expressing CyO on the second chromosome, as well as CP110-GFP expressed	3	Generated by Sam Barry (Raff Lab)

	from a Ubiquitin promoter and TM6B on the third chromosome		
pUbq-PLP-GFP/TM6C	PLP-GFP expressed from a Ubiquitin promoter	4	(Richens et al., 2015)
NG-Asl/TM6B	NeonGreen-Asterless expressed at endogenous levels, balanced by TM6B. Homozygous lethal	4	Generated by Thomas Steinacker (Raff Lab)
NG-Asl/Jupmch	NeonGreen-Asterless expressed at endogenous levels, Jupiter-mcherry	5	This thesis
cnn^{f04547}	PiggyBac insertion in the middle of the *cnn* gene	5	Exelixis stock no. f04547, Exelixis Stock Centre (Harvard Medical School, Boston, MA).
cnn^{f04547}*/CyO;NG-Asl/TM6B*	cnn^{f04547} mutant balanced over CyO also expressing NeonGreen-Asterless	5	Generated by Isaac Wong (Raff Lab)
cnn^{f04547}*/CyO;Jupmch/TM6B*	cnn^{f04547} mutant balanced over CyO also expressing Jupiter-mcherry	5	Generated by Isaac Wong (Raff Lab)
cnn^{f04547}*;NG-Asl/Jupmch*	cnn^{f04547} mutant also expressing NeonGreen-Asterless and Jupiter-mcherry	5	This thesis
$CP110^{-/-}$*;;*	Fly line where the entire *CP110* coding region has been deleted via FLP-induced recombination of two P-element insertions	5	(Franz et al., 2013)

Cp110$^{-/-}$;;NG-Asl/TM6B	*CP110$^{-/-}$* as described above, also expressing NG-Asl	5	This thesis
;Cep97$^{-/-}$;	Fly line where entire *Cep97* coding region has been replaced with the white marker gene vias ends-out gene targeting	5	(Franz et al., 2013)
;Cep97$^{+/-}$ NG-Asl/TM6B	Fly line heterozygous for *Cep97* coding region replacement described above. Also expressing NG-Asl	5	This thesis
;Cep97$^{-/-}$;NG-Asl/TM6B	*Cep97$^{-/-}$* as described above, also expressing NG-Asl	5	This thesis

2.2. Biochemistry and Cell Biology

2.2.1. Embryo Fixation for Differential Fluorescence Labelling

Embryos were collected for one hour on apple juice plates as previously described (section 2.1.1.), then incubated at 25°C for 45 min. Embryos were then washed three times with washing buffer (1x PBS, 0.05% Triton X-100) then dechorionated with 60% bleach for 3 minutes (min) before being washed three times with washing buffer once more. Embryos were washed with 2 ml of heptane into a glass vial containing methanol containing 3% 0.5M EGTA. Embryos were gently swirled to allow them to sink to the bottom of the vial. Excess heptane and embryos floating at the methanol-heptane interface were discarded. Embryos were then washed 3 times with methanol containing 3% 0.5M EGTA and transferred to a new tube containing methanol and left at 4°C overnight.

Methanol was removed from the tube containing embryos before washing 3 times with 1 ml PBS + 0.2% Tween-20 (PBST) for 10 min each while rotating at room temperature (RT). Then embryos were incubated in primary antibody diluted in PBS to 1 ml for two hours at RT or at 4°C overnight. Primary antibody was removed and samples were washed 3 times with PBST as described above. Embryos were then incubated in secondary antibody for one hour at RT. After another 2 washes with 1 ml PBST as described above, they were washed with 1 ml PBS containing Hoechst for 15 min. Embryos were then mounted in 20 µl of VECTASHIELD Antifade Mounting Medium with DAPI (LS Bio LS-J1033) onto slides with glass coverslips on top. Coverslips were sealed twice with clear nail polish and slides were kept in the dark at 4°C.

2.2.2. SDS-PAGE and western blotting

Embryos fixed in methanol as described in 2.2.1 were washed 3 times in 1 ml PBST for 10 min each while rotating at RT. Embryos were then transferred to watch glasses in PBST and embryos in the syncytial blastoderm stage were selected under a light microscope. About 20 embryos were selected for each genotype and resuspended in 20 µl of PBST mixed with 20 µl x2 SDS loading dye. The sample was boiled at 100°C for 10 min and stored at -20°C.

Samples were thawed if necessary and 20 µl was loaded onto a 3-8% NuPAGE Tris-Acecate Protein Gel (Thermo Fisher EA03785BOX) in NuPAGE Tris-Acetate SDS running buffer (Thermo Fisher LA0041). The gel was run at 150V for 60 min in an XCell SureLock Mini-Cell (Thermo Fisher). Samples were then transferred semi-wet onto a nitrocellulose membrane (Bio-Rad 1620112, 0.2 µm) using transfer buffer (25nM Tris pH 7.4, 192 mM glycine, 25% methanol and 1% SDS) and transferred in a Mini Trans-Blot Electrophoretic Transfer Cell (Bio-Rad) at 100V for 90 min. Membranes were then cut to appropriate sizes to allow incubation in different antibodies later on. All membranes were then incubated in blocking buffer (1x PBS, 4% semi-skimmed milk powder, 0.1% Tween-20) at 4°C overnight.

Blocked membranes were moved with plastic tweezers into primary antibody solution and incubated at RT for an hour with gentle shaking. Membranes were then washed 3 times with 1x TBS + 0.1% Tween-20 for 15 min each before incubating with HRP-conjugated secondary antibody solution. Membranes were washed

again as described above, then incubated for 1 min in 50% or 33% SuperSignal West Femto Maximum Sensitivity Substrate, diluted in the manufacturer-provided buffer (Thermo Fisher 34095). Film was then exposed to membranes from 10 sec up to 15 min before developing.

Table 2.2 Primary antibodies used in this thesis

Lab ID	Protein	Raised in	Use in this thesis	Concentration	Source
200	Asterless	Guinea Pig	Fluorescent labelling	1:1000	Eurogentec (animal SKC123)
166	GFP	Llama	Fluorescent labelling	1:500	Chromotek (gba488)
37	Cnn	Rabbit	Western blot	1:500	Eurogentec (animal SK3516)
15	CP110	Rabbit	Western blot	1:500	Eurogentec (animal SK4824)
250	Cep97	Rabbit	Western blot	1:500	Generated by J. Dobbelaere

Table 2.3 Secondary antibodies used in this thesis

Lab ID	Reacts with	Raised in	Use in this thesis	Concentration	Source
41	Guinea pig	Goat	Fluorescent labelling	1:500	Invitrogen (A11075)
39	Rabbit	Swine	WB	1:3000	Agilent (P039901-2)
37	Rabbit	Rabbit	Western blot	1:500	Eurogentec (animal SK3516)

2.3. Experiments in living embryos

2.3.1. Embryo Handling for live-imaging

Embryos were collected for one hour on apple juice plates as previously described (section 2.1.1.) then incubated at 25°C for 45 min. Embryos were dechorionated by hand on double sided tape and mounted onto a strip of glue (made from dissolving the tacky side of Sellotape in heptane) on a 25 mm glass-bottomed Petri dish with 14 mm micro-wells (MatTek). Embryos were dessicated for 30 sec at 25°C then covered in Voltalef H10S oil (ARKEMA), then imaged in S-phase of cycle 12-13 as this is the stage of the cell cycle where centrioles are closest to the cell cortex.

2.3.2. Drug injection

Colchicine in DMSO was diluted in Scheider's medium to 100 μg/ml, while Cytochalasin in DMSO was diluted with ddH_20 to 1mg/ml and pipetted into glass needles. Embryos were prepared as described in section 2.3.1. Embryos were collected for half an hour to an hour then incubated for 30 min. They were dechorionated and mounted as described in section 2.3.1. Embryos were then desiccated for 10 min at 25°C. Embryos at S-phase of cycle 12-13 were injected and imaged from immediately to approximately 6 min post-injection depending on experiment.

2.4. Microscopy

2.4.1. Zeiss 880 Laser Scanning Microscope

Images of embryos were acquired using an inverted Zeiss 880 Laser Scanning Microscope (Zeiss 880) fitted with Airyscan detector and a Plan-Apochromat 63x/1.4-NA oil lens. 488 nm argon and 561 nm diode lasers were used for excitation of GFP, GFP antibody and Alexafluor 568 antibody respectively. Images were acquired in S-phase of cycle 12 or 13 in Z-stacks consisting of 9 to 15 planes using a 0.2 μm step size and 200 ms exposure time per image. Movies were similarly acquired and imaged every 20 seconds (sec). Microscope was manually focused between acquisitions to maintain centrioles in the plane of imagining. Three fields of view were taken per embryo.

2.4.2. OMX V_3 Blaze with 3D-structured illumination

Embryos were imaged using a DeltaVision OMX V3 Blaze Microscope (3D-SIM) with a 60x/1.42-NA oil UPlanSApo Olympus objective. 488 nm diode laser was used for excitation of GFP. Images were acquired as a Z-stack consisting of 6 planes using a 0.125 μm step size and 20 ms exposure time per image.

2.4.3. Olympus Super Resolution Confocal Microscope

Embryos were imaged using an Olympus IX83 microscope with a 60x1.3-NA silicon immersion lens. Super-resolution microscopy was performed using a Yokogawa Super Resolution SpinSR Spinning Disk Confocal (SoRa) disc with an Olympus 3.2 magnification lens and a photometrics BSI camera. Coherant 488 or 561 nm QBIS lasers with 525/50 or 617/75 nm emission bandpass filters respectively were used to excite NeonGreen (NG) and mcherry (mch) respectively. Images were acquired as a Z-stack of 8 to 16 slices using 0.2 μm step size and 200 ms exposure time per image. Movies were taken for 5 min to 6 min 20 sec with images acquired every 20 sec. Movies were processed using super-resolution processing with standard strength, then deconvolved using a constrained iterative deconvolution function with 20 iterations in Olympus CellSense software.

2.5. Data Analysis

2.5.1. Processing of fixed images for differential fluorescence labelling

Images were exported in the TIFF format. The thresholding function in FIJI was used to select centrioles, whose coordinates within the Z-stack were saved as a CSV file. The Z-stack and CSV file were then passed through a custom python script to generate a plot of fluorescence intensity at every slice within the stack with a gaussian curve fitted through the data, as fluorescence intensity around a point tends to follow a normal distribution (Mutch et al., 2007). The peak of fluorescence in each channel was inferred from the gaussian plot and the fluorescence maximum in the red channel was subtracted from the fluorescence maximum in the green channel to obtain the Red/Green difference. Due to the nature in which Z-stacks are taken at the Zeiss 880 microscope, the more negative the Red/Green difference, the closer the green fluorescence maximum to the cell cortex. Chromatic aberration was calculated in a similar way, from images where the same protein was labelled in both green and red.

2.5.2. Radial Profiles

The centre of a Ring-oriented centriole was manually determined and thresholding was used to eliminate as much background fluorescence as possible. Then fluorescence intensity at multiple radii from the centre of the centriole was calculated using the Radial Profile plugin for FIJI by EMBL tools. 70 points of measurement were taken from centre of the centriole outwards. Background fluorescence intensity from 25 radii measurements beyond but adjacent to the centriole were measured and subtracted from centriolar measurements. This was repeated for 20 centrioles selected from over 10 embryos. Control centrioles were always selected from embryos in the same experiment. Measurements were then mirrored and plotted on a line graph.

2.5.3. Processing of movies

Movies were exported in the BTIF format and Z-projected by maximum intensity projection. Brightness and Gain were adjusted for the making of clear figures. For quantification by Centrilyze, the channel containing centrioles was then tracked by TrackMate. A Laplacian of Gaussian detector with a 0.9 μm blob size was

used to detect centrioles. The quality of detection was manually assessed for each image and adjusted to maximize the sensitivity of centrosome detection and remove background particles. Centrioles tracked over each frame in the movie were linked by a LAP tracker with no gaps allowed within each track. The coordinates of each track were saved in a CSV file alongside the maximum z-projected image and passed through a custom python script to generate catalogued, single 28x28 pixel images of each centriole at each frame.

2.5.4. Centrilyze

Full documentation for how Centrilyze was designed is provided in appendix A1 as code was written by my collaborator Conor Wild. Centrilyze is a Convolutional Neural Network implemented in Pytorch with a Resnet 18 architecture. It was trained on centriole images obtained from the python script described in 2.5.3. from 9 WT embryos imaged for 6 min and 20 sec each in cycle 12 or 13 S-phase. This data consisted of approximately 1,200 centrioles and a total of 25,117 centriole images. During training, data is augmented as it is iteratively passed through the network to prevent the network from overfitting, allowing better generalisation of Centrilyze to embryos beyond the training dataset and even embryos from mutant embryos. These augmentations included blurs, transformations to random angles and translations in a 7-pixel range as is typical for ANN training data. Centrilyze was trained with a CC-E lost function for classification convolutional neural networks and optimized with the Adam optimiser set to a learning rate of 0.001. It was then tested on 10,378 images from an additional 5 centrioles and optimized until annotation of centrioles did not differ by more than 5% from my manual annotation. Centrilyze was trained and tested on data annotated into one of seven categories that were later merged into Ring (containing previously defined “Oriented” and “Perceived_Oriented” categories), Bar (containing previously defined “Not_Oriented” and “Perceived_Not_Oriented” categories) and Slanted (containing the “Slanted” category).

2.5.5. Implementing a Hidden Markov Model to quantify centriole stability

Stability analysis was implemented in python using a Hidden Markov Model (HMM) via the hmmlearn model with the MultinomailHMM class (Rabiner, 1989). Stability was trained against Centrilyze quantification of its test dataset (10,378 images as mentioned in 2.5.4.) using fixed emission probabilities

and the Baum-Welch algorithm to produce the transition probability matrix (Rabiner, 1989). Training was performed for 1,000 iterations across the entire training dataset. The Viterbi algorithm was then used in order to determine the most likely series of orientation states for each centriole (Viterbi, 1967). From these measures, the probability of state change was calculated for each orientation state. Further detail is provided in Appendix A2.

2.5.6. Processing Centrilyze and HMM data

Centrilyze outputs the number of centriole images in each orientation category stated above. Orientations are then converted into percentages based on the total number of centriole images per movie. To calculate stability, data from Centrilyze was passed through an HMM to obtain the likelihood that any one centriole will remain in its current orientation state or change orientation states in the next frame (20sec). All combinations of any orientation category moving to any other orientation category were computed as an average probability per embryo. Only the probability of centrioles remaining in their current orientation state in the next frame was plotted for each orientation category. Unidentified data was not included in final graphs, and embryos which possessed more than 40% Unidentified centrioles were discarded from the sample size entirely.

2.6. Statistics

GraphPad Prism 9 software was used to perform all statistical tests. T-tests were used to determine *p*-values. $p<0.05$ indicated that the means of two datasets were statistically significant. Independent T-tests were performed to the same dataset with separate datasets. T-tests were always performed with the Welch correction, which does not assume equal standard deviation between datasets. T-tests are performed on normally distributed, parametric data. In the case of Red/Green differences for fixed data, fluorescence around a point is typically understood to be normally distributed (Kask et al., 1999). In the case of centriole orientation data, pooled sample sizes used are large (>30 points in most cases). Due to

these large sample sizes, the central limit theorem is likely to apply. This states that if the dataset is sufficiently large, data can be assumed to be normally distributed (Kwak and Kim, 2017). Additionally, when performing T-tests Graphpad Prism also performs the D'Agostino-Pearson omnibus normality test to confirm that data is normally distributed before proceeding.

3. Centrioles appear preferentially distally-oriented with respect to the embryo cortex

3.1. Introduction

3.1.1. Distal end components of centrioles in mammalian and *Drosophila* cells

Centrioles have a distinct proximal and distal end. The proximal end contains a site for orthogonal growth of the daughter centriole (Paintrand et al., 1992). In mammalian cells, DAPs mark the distal end of mature centrioles and facilitate centriole attachment to the plasma membrane in several cell types by forming part of transition fibres that anchors a mother centriole to the cell cortex (Jana et al., 2018; Mansour et al., 2021; Tanos et al., 2013; Yang et al., 2018). Interactions between DAPs and the cell cortex have been suggested to aid in defining and maintaining integrity of the apical cell membrane in ciliated cells (Shao et al., 2020). The distal ended orientation of centrioles anchored by DAPs have also shown functionality at the root of a cilium or in directional intracellular trafficking (Tamzalit et al., 2020; Tanos et al., 2013).

In *Drosophila,* most mammalian DAPs identified in mammalian systems are not conserved at the protein level (Hodges et al., 2010; Hou et al., 2023). A previous study has shown that merely three of over ten conserved DAPs: FBF1, CEP164 and CEP89, appear to function in *Drosophila* ciliogenesis, however their roles are only partially conserved (Hou et al., 2023). Non-ciliogenesis functions of CEP89 have been conserved (van Bon et al., 2013). However, CEP164 is completely dispensable for cilia formation, while FBF1 and CEP89 are only essential in sensory neurons and not in spermatocytes (Hou et al., 2023; Tischer et al., 2021). This suggests that *Drosophila* ciliogenesis has in some ways diverged from mammalian cells (Avidor-Reiss and Leroux, 2015). High resolution imaging has further shown that DAPs emanate from the

distal end of mammalian centrioles like conical spokes (Jana et al., 2018; Tischer et al., 2021; Yang et al., 2018), and no such structures have been observed in similar images of *Drosophila* centriole in ciliated or non-ciliated cells (Fu and Glover, 2012; Gartenmann et al., 2017; Roque et al., 2018). If similar structures did exist on *Drosophila* centrioles, they would be using different proteins, or be less electron dense than those formed by DAPs in mammalian cells.

In mammalian cells, DAPs anchor basal bodies to the putative site of ciliogenesis by their distal ends (Tanos et al., 2013). Despite lack of DAP conservation, *Drosophila* basal bodies anchor in the same way (Hou et al., 2023; Roque et al., 2018; Vieillard et al., 2016). DAPs can also anchor centrioles in other non-ciliated cell types (Stinchcombe et al., 2015). However, even though there is evidence that centrioles may be specifically positioned close to the cell cortex in polarised, non-ciliated cells (Carvajal-Gonzalez et al., 2016a; Januschke et al., 2011), orientation of these centrioles is not known. In *Drosophila* embryos the Raff Lab has previously observed centrioles in embryos appear mostly as "Rings" when viewed on an OMX 3D-Structured illumination microscope (Fig. 3.1 A, B) (Aydogan et al., 2018; Gartenmann et al., 2017). Thus, the centrioles in these embryos are presumably oriented with either their distal or proximal end "facing" the cortex, as centrioles are viewed looking down the barrel of the centriole with respect to the cell cortex (Fig. 3.1B). This suggests that, even when not forming cilia, the centrioles may be able to sense the cell cortex and orient themselves with respect to it. If this is the case, then an important point is whether these centrioles are always oriented with their distal-end towards the cortex (as would be the case in ciliated cells), with their proximal ends towards the cortex, or a mixture of both (Fig. 3.1C). In this Chapter I set out to address this question which may provide insight into how centrioles may be oriented in other polarised, non-ciliated cells.

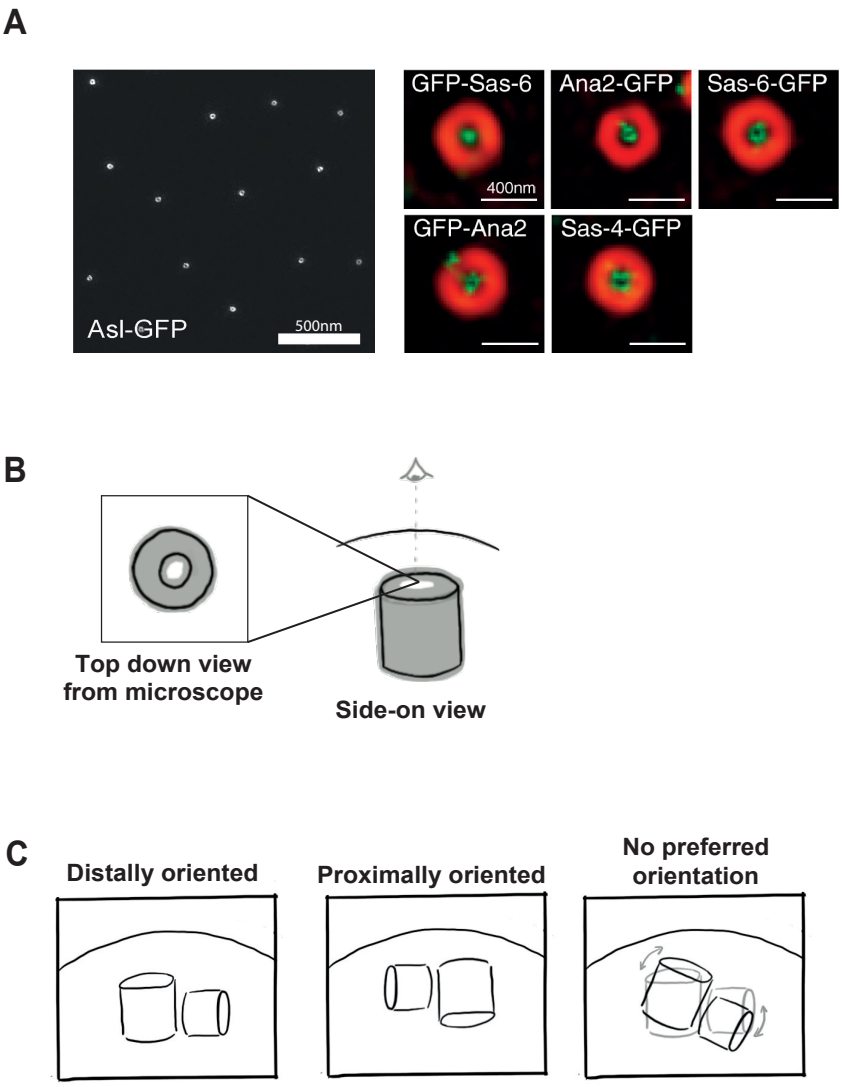

Figure 3.1 Centrioles in *Drosophila* embryos are typically oriented as Rings when seen down the microscope

(A) Images taken from Aydogan et al., 2018 Figure 7A and from Gartenmann et al., 2017 Figure 1C respectively. Both show centrioles labelled with Asterless (Asl, *grey* in the left panel, *red* in the right panels) appearing as Rings taken using an OMX 3D SIM system. **(B)** Illustration showing how the Ring orientation of centrioles allow us to infer that centrioles are oriented upright (and how we are looking down the barrel of the centriole) with respect to the cell cortex. **(C)** Illustration showing three possible ways centrioles could be oriented with respect to the cell cortex. Smaller centriole orthogonal to the larger centriole represents the daughter centriole and thus the proximal end.

In absence of DAPs, the distalmost proteins in *Drosophila* centrioles are CP110 and Cep97 that together make up the distal cap. It is well known that CP110 inhibits ciliogenesis in vertebrates, with its removal thought to be important for basal body maturation (Bettencourt-Dias and Carvalho-Santos, 2008; Cao et al., 2012; Spektor et al., 2007; Xie et al., 2022). However, more recent studies have shown that it may be a positive regulator of ciliogenesis and facilitates attachment to the cell membrane (Walentek et al., 2016; Yadav et al., 2016). CP110 can also regulate centriole length (Delgehyr et al., 2012; Franz et al., 2013;

Schmidt et al., 2009). Cep97 typically acts in complex with CP110, thus it too inhibits ciliogenesis and has roles in centriole length control (Dobbelaere et al., 2020; Lee et al., 2022; Nagai et al., 2018; Spektor et al., 2007). Notably, despite CP110 removal being important for ciliogenesis in vertebrates, centrioles can still dock to the membrane while CP110 is present in other systems (Stinchcombe et al., 2015). Moreover, CP110 has been implicated in centriole length control in *Drosophila*, such that its levels peak at the same time in each cell cycle (Aydogan et al., 2018; Franz et al., 2013). These roles show that CP110 is a core centriolar component that marks the distal end of mature centrioles in both *Drosophila* and vertebrates.

3.1.2. Key Findings

In this chapter, I establish a fixed embryo assay in collaboration with Isaac Wong in the Raff lab to determine the position of the distal end of the centriole in *Drosophila* embryos relative to the rest of the centriole and the cell cortex. This technique involves using fluorescence imaging on a Zeiss 880 spinning disc confocal system (Zeiss 880) to measure the depth of different parts of the centriole in the embryo. The Zeiss 880 has a theoretical resolution of 150 nm and in practice a resolution of ~250 nm (pers. comm. Alan Wainman), which is above the length and width of *Drosophila* centrioles. Therefore, measurements made in this assay will have some degree of inaccuracy. Given these limitations, I use large sample sizes and rigorous controls to ensure that my results are robust. With such measures in place, we find that centrioles in *Drosophila* embryos do indeed have a bias towards being distally oriented.

3.2. Results

3.2.1. An assay to determine the orientation of *Drosophila* centrioles

3.2.1.1. Using the distance between fluorescence maxima to determine centriole orientation

To determine if centrioles are distally oriented, Isaac Wong and I established a technique I call ***differential fluorescence labelling***. This method involves staining fixed embryos with an antibody against a centriole protein that localises along the entire barrel of the outer centriole wall in *red* and one that recognises a distal cap protein in *green* (Figure 3.2A). A complete Z-stack through the entire volume of the cortical centrioles in an embryo was acquired on a Zeiss 880 microscope. The fluorescence intensity of each centriole-marker at each Z-plane was measured to find the arbitrary depth, denoted by Z-stack number, at which the fluorescence of each centriole-marker peaked—known as the ***fluorescence maximum***. The red and green fluorescence maximum represent the midpoint of the centriole and distal cap respectively. The green fluorescence maximum is subtracted from the red fluorescence maximum and the result is defined as the ***Red/Green difference*** (Fig 3.2A). The Red/Green difference gives an approximation of the difference in depth between the centriole midpoint and the distal end midpoint, while the positive or negative nature of this measure indicates if the distal end lies above (-ve) or below (+ve) the centriole midpoint relative to the cell cortex.

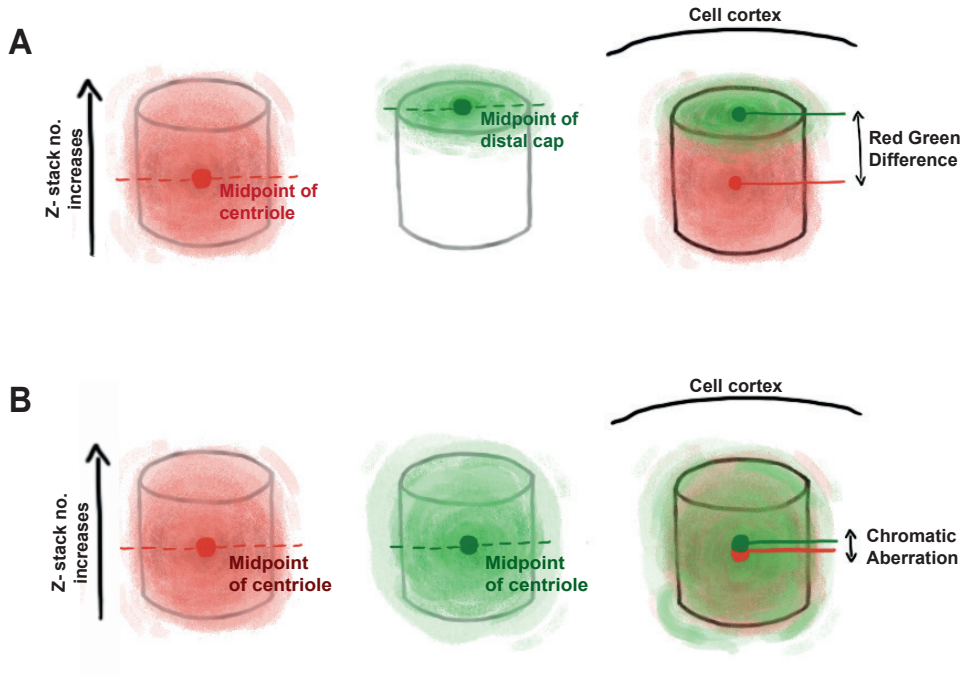

Figure 3.2 Methodology for testing the potential orientation of centrioles relative to the embryo cortex

(A) Illustration showing the centriole wall labelled with Asl in *red* and the distal cap labelled with CP110-GFP in *green.* The closer to the cell cortex, the greater the Z-stack number. Coloured dots represent the depth in which fluorescence is maximum in 586 (*red)* and 488nm (*green*) fluorescence channels, approximating the midpoint of the centriole or distal cap respectively. Difference in depth between fluorescence maxima is called the Red/Green difference. **(B)** Illustration showing centriole labelled with centriole wall marker Asterless (Asl) in *red* and *green*. The closer to the cell cortex, the greater the Z-stack number. Coloured dots represent the depth in which fluorescence is maximum in 586 (*red)* and 488nm (*green*) fluorescence channels respectively, both approximate the midpoint of the centriole. Coloured dots do not co-localise perfectly. Difference in depth between fluorescence maxima is a measure of chromatic aberration in the depth plane.

3.2.1.2. Correcting for chromatic aberration between red and green fluorescence channels

To investigate if centrioles are distally oriented, I use differential fluorescence labelling which requires measuring fluorescence within the embryo using the red and green fluorescence channels. Both these channels have slightly different wavelengths. Because of this, the results have to account for any possible chromatic aberration between the red and green channels in the depth plane. ***Chromatic aberration*** results from each colour on the visible spectrum having slightly different refractive indexes; this means that when two different colours of light are passed through the same lens, they will focus on slightly different locations (Kruger et al., 1993; Thibos et al., 1990). The objectives on modern microscopes are usually designed to minimise these differences, but they exist nevertheless and are potentially significant for this experiment where I am trying to measure very small differences in distance. To measure chromatic aberration, I labelled fixed embryos using antibody against a centriole protein that localises along the entire barrel of the outer

centriole wall. Then, embryos were stained with a mix of red and green secondary antibodies to the same primary antibody and imaged at a Zeiss 880. Red/Green differences were calculated from fluorescence maxima of individual centrioles (Fig 3.2B). In theory, red and green fluorescence should co-localise perfectly as they are labelling the same protein. In practice, any Red/Green difference calculated here represents the chromatic aberration between channels in the depth plane that is inherent to the microscope system. The Red/Green difference in this control experiment can then be used to correct for chromatic aberration in the Red/Green difference from the real experiment.

3.2.2. Centrioles appear preferentially oriented with their distal-end facing the cell cortex

3.2.2.1. Using CP110 and Asl to show that centrioles are distally oriented

I used differential fluorescence labelling to determine if centrioles in *Drosophila* embryos are distally oriented. Differential fluorescence labelling requires a fluorescent centriole wall marker and a distal cap marker in different colours. To this end, I fixed cycle 10-13 embryos expressing CP110-GFP. As mentioned above, CP110 is a distal cap protein that is a well-known marker of mature centrioles and is implicated in centriole length control in both vertebrates and *Drosophila* (Aydogan et al., 2022; Delgehyr et al., 2012; Schmidt et al., 2009). To label the entire centriole, I used Asterless (Asl) which is present along the outer walls of mature centrioles. Asl aids in recruiting Plk4 to the centrosome (Cizmecioglu et al., 2010; Dzhindzhev et al., 2010). Embryos were stained with an α-Asl antibody and an α-GFP nanobody (to enhance the CP110-GFP fluorescence signal). As a control, WT embryos were stained with an α-Asl antibody only, and a mix of green and red secondary antibodies was allowed to bind to the same primary antibody. This control allowed me to identify how much of difference in depth between red and green channels was due to chromatic aberration alone, as described in section 3.2.1. Embryos in S-phase were chosen for imaging as centrioles are closest to the cell cortex at this cell cycle stage and embryos in mitosis are nucleating the mitotic spindle, which may add additional factors to consider when interpreting the orientation of centrioles. Thus, going forward all images and movies of embryos will be taken in S-phase. Visually, in Z-stacks through an entire centriole volume, the CP110-GFP distal cap (*green*, Figure 3.3A) appeared to be displaced

slightly closer to the cell cortex when compared to the Asl centriole wall fluorescence (*red*, Figure 3.3A). These observations suggest that centrioles may be oriented with their distal end facing the cell cortex.

Figure 3.3

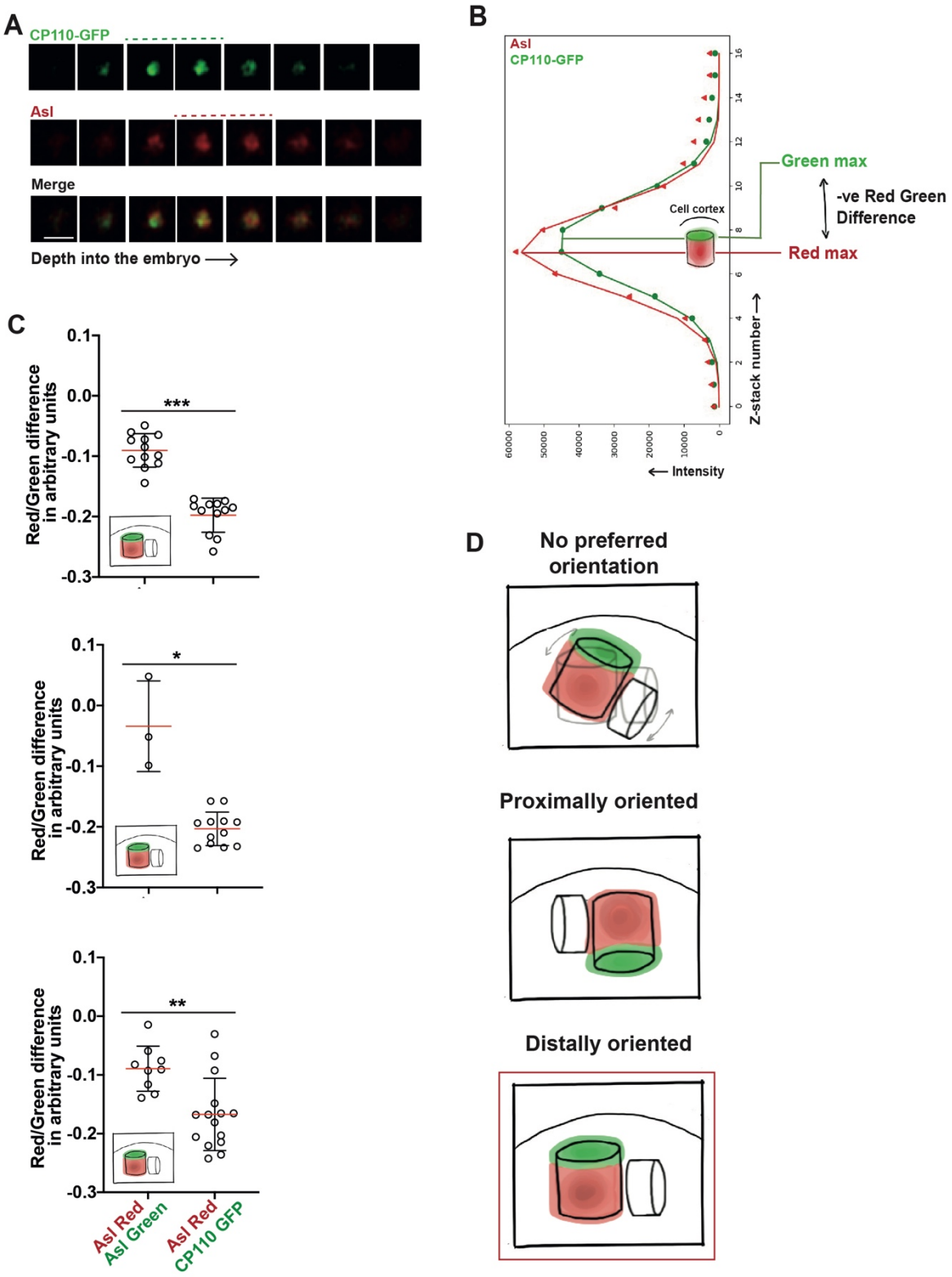

Figure 3.3 Centrioles appear to be preferentially oriented with their distal-end towards the embryo cortex.

(A) Images show individual images from a Z-stack through an entire centriole volume from top (left images, near the cortex) to bottom. The centriole cap is stained with CP110 (*green*) and the bulk-centriole wall is stained with Asl (*red*). Dotted lines

above each set of images highlight the planes where green and red fluorescence is highest. Scale bar = 1μm. **(B)** Graph shows the fluorescence intensity profile through the Z-stack of a single centriole imaged on a Zeiss 880. X-axis shows intensity and Y-axis shows the Z-stack number. Gaussian curves were fitted to the data points using a python script written by Isaac Wong in the Raff lab. The plane in which the fluorescence is maximum corresponds to the middle of the centriole (*red* signal) or the centre of the distal end of the centriole (*green* signal). In this example, the green fluorescence maximum subtracted from the red fluorescence maximum results in a negative Red/Green difference, indicating that the distal-end of the centriole is slightly closer to the embryo cortex. **(C)** Scatter plots show three independent repeats (mean ±SD) calculating the Red/Green difference in arbitrary units between the distal end as compared to the centriole midpoint using differential fluorescence labelling as described in Fig. 3.1. Graphs show Red/Green difference on the y-axis and label combination on the x-axis. Each open circle represents the mean Red/Green difference from all the centrioles measured in a single embryo. Putative orientation of centrioles in each experiment based on the Red/Green difference compared to chromatic aberration is shown in the bottom left corner of each graph. N = 3-15 embryos per experimental repeat; n≥40 centrioles per embryo. T-tests were performed to assess differences between the two datasets in each experimental repeat. *; $p<0.05$, **;$p<0.01$, ***;$p<0.001$**(D)** Illustration showing three possible ways centrioles could be oriented with respect to the cell cortex. Smaller centriole orthogonal to the larger centriole represents the daughter centriole and thus the proximal end. *Red* outline shows that results indicate centrioles have a preference to be distally oriented.

The Red/Green difference was quantified between CP110-GFP and Asl fluorescence maxima. As sample sizes were large, Isaac Wong wrote a python script that calculated the fluorescence intensity in each Z-plane of each centriole in every image-stack. The fluorescence profiles for each centriole were plotted and gaussian curves were fitted across datapoints as fluorescence was believed to be normally distributed (Mutch et al., 2007). Any peaks of fluorescence intensity that happened to lie in between measured Z-planes could then be inferred from the fitted gaussian curves (Fig. 3.3B). The fluorescence maximum in the *red* channel represented the depth of the *centriole midpoint*, while the fluorescence maximum in the *green* channel represented the depth of the *distal cap* in the embryo (Fig. 3.3B). The Red/Green difference was then determined by subtracting green fluorescence maxima from red fluorescence maxima (Fig. 3.3B). Because all Z-stacks were taken with the first plane being deepest into the centriole, the more *negative* the Red/Green difference, the *closer* the green fluorescence maximum is to the cell cortex compared to the red fluorescence maximum.

Results based on 3 independent repeats show that, on average, the Red/Green difference between the distal cap and centriole midpoint is consistently more negative than that caused by chromatic aberration alone is approximately 0.2 arbitrary units. As these units are based on the Z-stack number of each image, we can use the step size between each Z-plane (0.2 μm) to estimate the distance between the centriole midpoint and the distal end as observed by Asl and CP110-GFP fluorescence respectively. Using this method, analysis of Red/Green differences show that the distal end is ~20 nm above the centriole midpoint. These results suggest that on average, the distal ends of centrioles are closer to the cell cortex as compared to the centriole midpoint

(Fig 3.3C). Thus, it seems likely that the centrioles in *Drosophila* embryos, like the centrioles in mammalian cells and ciliated *Drosophila* cells, have a bias to being distally oriented (Figure 3.3D). These results suggest that there is a mechanism that establishes and maintains a preferential distal orientation of the centrioles in non-ciliated *Drosophila* embryos.

3.2.2.3 Centriole orientation may be a readout of embryo health

As centrioles in *Drosophila* embryos are preferentially distally oriented, I hypothesised that centriole orientation could be functionally significant in this non-ciliated cell type. When CP110-GFP flies with a WT background or *if*/*CyO* ; *MKRS*/TM6C double balanced background are stained with an α-Asl antibody and α-GFP nanobody booster as described in 3.2.1.1, flies with a double balanced background exhibit a wider variety in Red/Green differences across multiple embryos as compared to flies in a WT background (Fig. 3.4A, B). If a centriole were to change orientation with respect to the cell cortex, the relative distance between its distal end and the centriole midpoint would decrease, then increase again as the proximal end faced the cell cortex. A wide breadth of Red/Green differences across double balanced embryos may therefore suggest that centriole orientation is more variable (Fig. 3.4 B). This data shows that centriole orientation may be affected by poor embryo health characteristic of flies containing the *CyO* balancer (Miller et al., 2019). However, even though the breadth of Red/Green differences is increased in double balanced flies, the average Red/Green difference is still more negative than chromatic aberration alone (Fig. 3.4B, *black* dashed line compared to *red* dashed line). Thus, it is more likely that centrioles still have a preference to be distally oriented and this orientation is not significantly perturbed by the presence of balancers.

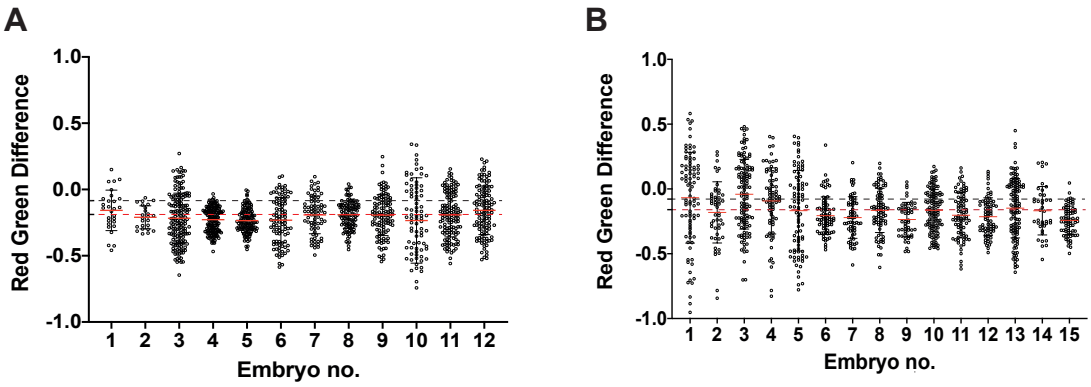

Figure 3.4 Centriole orientation may be a readout of embryo health

(A, B) Scatter plots show the mean (±SD) Red/Green difference in individual embryos (numbered along the x-axis) of embryos expressing CP110-GFP in (A) a WT background (B) *If/CyO; MKRS/TM6C* background. (A, B) *Red* dashed line represents the mean across all embryos, *black* dashed line represents average chromatic aberration. N = 12-15 embryos, n≥40 centrioles per embryo.

3.3. Discussion

In this chapter I established an assay to measure the distance between the centre of a centriole and the distal end using the difference in depth between red and green fluorescence maxima. Because the distance measured was very small (on the scale of nm), I corrected for chromatic aberration in each individual experiment. While measurements were not exact due to resolution limits of the microscope used, large sample sizes and independent repeats showed that the distal end is consistently closer to the cell cortex with respect to the centre of the centriole, strongly suggesting that centrioles have a preference to be oriented with their distal ends facing the cell cortex.

In ciliated *Drosophila* cells, basal bodies are attached to the putative site of ciliogenesis by transition fibres much like in mammalian cells (Fig. 1.3B) (Gottardo et al., 2018). However, while transition fibres in mammalian cells are formed of DAP complexes (Tanos et al., 2013), the mechanism of transition fibre formation and basal body docking to the cell cortex is not well understood in *Drosophila* or other organisms that lack DAPs (Basiri et al., 2014; Hodges et al., 2010; Hou et al., 2023; Lapart et al., 2019), despite its importance in establishing distally oriented centrioles to allow axoneme extension (Roque et al., 2018). Current literature shows a requirement for transition zone proteins and other specialist ciliogenesis proteins for this process (Hou et al., 2023; Lapart et al., 2019; Vieillard et al., 2016), it also highlights an importance for core centrosome components that are highly expressed in other non-ciliated cell types, such as PCM and distal cap proteins (Dobbelaere et al., 2020; Roque et al., 2018). Therefore, understanding how centriole orientation may be important in *Drosophila* embryos, an unciliated cell type and where the centrioles lack DAPs, may provide insights into how centriole and eventually basal body docking is established and maintained in ciliated *Drosophila* cells.

Additionally, such understanding may further illuminate roles for centriole orientation in unciliated cells where centriole positioning is important, such as polarised epithelial cells or asymmetrically dividing neuroblasts (Garrido-Jimenez et al., 2018; Januschke et al., 2013). In *Drosophila* neuroblasts, new mother centrioles are retained at the apical cortex by combination of a nuclear tethering protein Mud (ortholog of human NuMa) and membrane bound PAR proteins that establish cell polarity. In wing-disc epithelial cells,

formation of actin-rich hairs at the apical surface relies on apical localisation of centrioles and their interaction with the Fz-PCP pathway. While it is possible that centrioles are randomly oriented in these other systems, the apparent biased distal-end orientation of centrioles in the polarised embryo suggests that centrioles may also have a preferred orientation in other cell types that are similarly polarised with centrioles close to the cell cortex. Indeed, in vertebrate systems where centriole orientation has been established such as in the IS, orientation is seen to maintain directionality and control the capacity of exocytosed vesicles (Stinchcombe et al., 2015).

In flies with a double balanced background, there is an increase in the breath of Red/Green differences. Centrioles exhibiting Red/Green differences close to 0 may appear more slanted as the distance in the depth plane between the distal end and midpoint of the centriole decreases. Positive Red/Green differences would imply that the distal end is below the midpoint of the centriole and that centrioles are proximally oriented. However, a recent study has shown that in *Drosophila* embryos, the proximal end of centrioles are most likely tethered to the nuclear envelope (Cunningham et al., 2022), which is consistent with the position of centrosomes in other cell types (Tang and Marshall, 2012). Furthermore, balancer lines are healthy enough to undergo mitosis similar to WT embryos and are widely used in generating fly lines (Miller et al., 2019; Sullivan et al., 1993). Therefore, there may be other factors affecting the Red/Green difference in balancer lines that are not related to orientation. One of the factors may that the population of flies used in this experiment was mixed between embryos laid from mothers possessing either one or two copies of *pUbq-CP110-GFP*. This is because in order to generate double balanced flies expressing CP110-GFP, flies with the genotype *if/CyO;pUbq-CP110-GFP;TM6B* were crossed to each other, generating offspring that were half heterozygous and half homozygous for *pUbq-CP110-GFP*. Initially this was not taken into account as CP110-GFP was used purely as a marker of the distal end and heterozygous embryos nevertheless exhibited a strong GFP signal when boosted with the GFP nanobody.

Given that the Red/Green difference relies on the position of GFP attached to a putative distal end protein (CP110) as well as the central nature of the red fluorescence maximum produced by labelling Asl. The size of each protein labelled, as well as the antibody itself, could potentially affect the position of the observed midpoint of the centriole. This would then have an effect on the Red/Green difference. The average

Red/Green difference is ~0.2 arbitrary units, which is about ~20 nm. Asl in particular is a large protein at 120 kilodaltons (kDa) (Varmark et al., 2007), it is then detected by an IgG antibodies that are ~150 kDa (Tan et al., 2015). The IgG antibody itself occupies a length of ~14 nm (which is ~28 nm if accounting for both primary and secondary antibodies) and Asl is estimated to occupy ~150 nm. The direction of which Asl is pointing out from the wall of the centriole and subsequent IgG labelling could significantly influence the accuracy of the centriole midpoint measurement, and thus affect the resulting Red/Green difference (Fig. 3.5A). In future experiments, using a Asl nanobody could potentially provide a more accurate measurement of the centriole midpoint, as the fluorescent moiety would be physically closer to the Asl protein (Fig. 3.5B). However, while protein and antibody sizes may make the observation of the centriole midpoint less accurate, any error caused by Asl positioning is likely systematic assuming Asl is always positioned in a similar direction in each centriole. Additionally, it is likely that multiple antibodies label a single Asl protein (Fig. 3.5C). Therefore, the fluorescence maximum of Asl represents an average of all possible binding positions of antibodies attached to Asl (Fig. 3.5C).

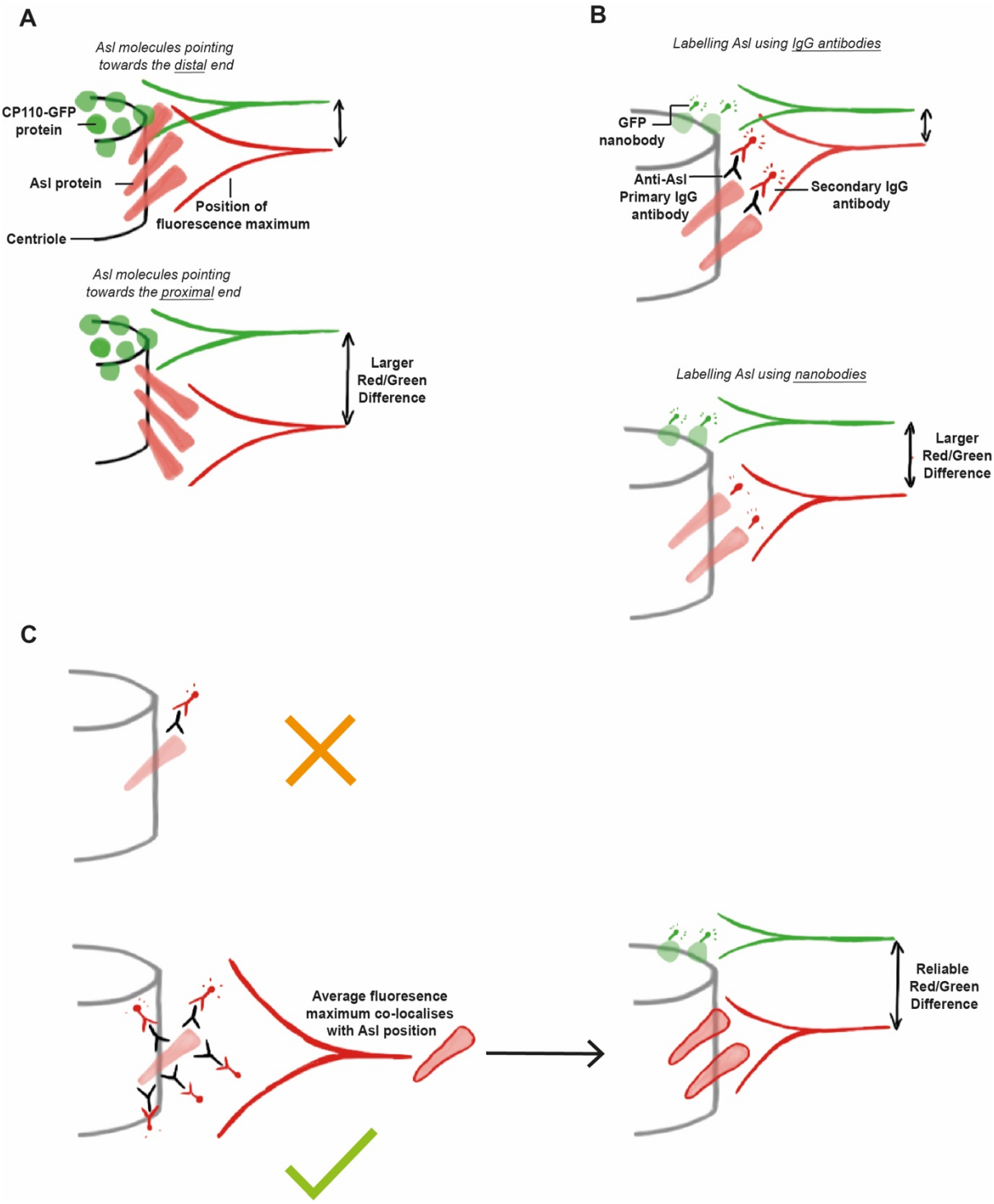

Figure 3.5 The position and size of Asl potentially affecting measurement of the centriole midpoint

(A,B) Illustration showing the approximate position of CP110-GFP protein (*green*) at the distal end of a centriole as compared to Asl protein (*red*) which are pointing towards (top) the distal end, (A) or away from (bottom) the distal end. Depending on how Asl is positioned, the fluorescence maximum of the centriole midpoint (*red* lines) could be significantly different as compared to that of the distal end (*green* lines). This could have a significant effect on the Red/Green difference (B) GFP nanobodies (*green*) allow for fluorescence maximum to be an accurate readout of GFP position. When Asl is labelled with primary (*black*) and secondary (*red*) IgG antibodies (top), the space taken up by antibodies potentially decreases the Red/Green difference. When Asl is labelled with nanobodies (bottom), Red/Green difference is larger as red fluorescence maximum is a more accurate readout of Asl position. **(C)** Illustration showing that it is unlikely for Asl to be labelled with a single primary and secondary antibody (top, *orange* cross). Instead, it is more likely that Asl is labelled with many antibodies (bottom, *green*

tick). The average fluorescence from antibodies then allows the position of Asl to be accurately visualised, resulting in a reliable and large Red/Green difference.

The variation of average Red/Green difference between embryos could also be due to some embryos being imaged in early, as compared to mid and late S-phase. The majority of centrioles in *Drosophila* embryos are upright with respect to the cell cortex, which means as daughter centrioles grow orthogonally to mother centrioles they will appear to be on their side (Fig. 1.4B). At early S-phase, daughters have disengaged from old mother centrioles and have formed new mothers (Fig. 1.4B). However, these new mothers still tend to be side-on with respect to the cell cortex, and eventually flip into an upright ring shape in mid S-phase. Embryos imaged in early S-phase may thus contain higher proportions of centrioles on their side as compared to those in mid S-phase, which may explain why the average Red/Green difference is lower in certain embryos as compared to others.

In the future it would also be useful to investigate if the magnitude and sign of the Red/Green difference is still preserved if alternative markers were used. For example, a combination of Cep97-GFP and Sas4 (a MT and cartwheel pinhead protein that also labels the entire centriole) labelled with red antibody. It may also be useful to have the distal cap labelled in red, while the entire centriole is labelled in green to confirm that the direction of chromatic aberration does not significantly affect the Red/Green difference value. Due to the sizes of Asl and IgG antibodies, perhaps nanobodies that are only 4 nm in length (as opposed to 14 nm IgG antibodies) could be sought out for Asl to potentially achieve a more accurate centriole midpoint measurement in future experiments. Unfortunately, due to time constraints, these experiments could not be performed. However, if this project were to be continued, these proposed experiments would add to the robustness of this fixed centriole orientation assay.

Due to the lack of resolution and temporal context available in this fixed assay, I am unable to draw more specific conclusions on how centrioles are oriented and how orientation may be changing. In the next Chapter I set out to establish a live-cell assay that would allow me to better investigate how centriole orientation is established and maintained in *Drosophila* embryos.

4. Establishing an assay to quantify centriole orientation and stability

4.1 Introduction

4.1.1 Advantages of using a live assay to measure centriole orientation

Various studies have shown centrioles as punctae within *Drosophila* embryos. However, when a protein that is present throughout the entire centriole is labelled, then viewed on a microscope system with sufficient resolution, centrioles in *Drosophila* embryos often appear as Rings (Gartenmann et al., 2017; Mennella et al., 2012). In Chapter 3, I established that these centrioles appear to be preferentially oriented with their distal end facing the cell cortex (Fig. 3.4B). However, previously documented examples of Ring-oriented centrioles tend to come from fixed samples, and the usage of methanol fixative is known to cause sample shrinkage (Rahman et al., 2022). Using organic solvent fixatives on cell culture has also been known to cause loss of membrane integrity and lipids (Hobro and Smith, 2017). Therefore, it is possible that centriole orientation may change through the fixation process, making centriole orientation measurements less accurate in fixed samples. A live assay would provide a better measure of centriole orientation with relatively minimal alteration to the centriolar environment as compared to fixed studies.

Fixed images observed in previous studies and in my own data thus far only provide a "snapshot" of centriole orientation. In contrast, a live-cell assay would measure centriole orientation over time and there is evidence to suggest that centrioles may change orientation over time. Daughter centrioles are born orthogonally to a presumably distally oriented, Ring-oriented mother centriole, and so are instead Bar-oriented and side-on with respect to the cell cortex (Cunningham et al., 2022). Initial observations show that most centrioles appear as Rings (Aydogan et al., 2018). Therefore, a significant percentage of daughter centrioles must at some point presumably flip into a Ring orientation when they mature into mothers.

Once in a Ring orientation, we do not yet know if centrioles change orientation. Understanding this process would help illuminate mechanisms that establish and maintain centriole orientation. These findings may provide important insight into how basal bodies position themselves during ciliogenesis in the absence of DAPs, or how centrioles find and remain at the apical sides of polarised epithelial cells. Once a live-cell assay is established, I would be able to characterise centriole orientation and possible stability further. I intend to employ this assay on flies expressing mutant forms of distal cap or pericentriolar proteins, as well as inject cytoskeleton perturbing drugs into embryos and follow changes in centriole orientation over time.

4.1.2. Measuring centriole orientation using an ANN

Measuring centriole orientation relies on observation of a Ring that is only ~150nm in width (Franz et al., 2013). A characteristic feature of a Ring is that it must have a hollow centre; down the microscope this is represented by an area of absence in fluorescence that is less than 150nm. The lower the resolution of the microscope, the less able I am to see an absence of fluorescence in the middle. This makes Ring-oriented centrioles more difficult to identify using lower resolution microscopes. In the live-cell assay developed in this chapter, an Olympus Super Resolution SpinSR Spinning Disk Confocal microscope (SoRa, methods section 2.4.3.) is used which has a theoretical resolution of 150nm at 488nm wavelength. Even though this confocal system allows Ring or Bar-oriented centrioles (upright or side-on with respect to the cell cortex) to be clearly visualised, lack of resolution still limits the identification of other orientation states in between Rings and Bars. In this chapter, I attempt to better understand how resolution affects my measurements, allowing any conclusions made from this assay to be robust.

While Ring or Bar-oriented centrioles can be manually identified using the live-cell assay developed in this chapter, it is tedious to continually manually annotate centrioles into different orientation categories. For this reason, I work with a collaborator to establish an ANN that can accurately categorise centrioles into different orientations. ***ANNs*** are a type of machine learning algorithm which has a structure inspired by the human brain (See section 1.5). They work by learning from a set of training data consisting of a set of inputs which have desired outputs attached to them (Fig. 1.12A). Through iteratively passing training data through the network, it adjusts its own parameters to find the combination which allows it to best approximate the correct

output category for input images (Fig. 1.14A). The ANN used in this thesis is a Residual Neural Network called Resnet18 which has a layer of input data, 18 hidden layers of units and an output layer which contains desired sorting categories. Residual Neural Networks like Resnet18 have a deep multi-layered structure in which downstream units not only take into account activation from upstream units but may also reuse and reinterpret parts of upstream units in current units, allowing current units to recalculate a similar aspect of the input data from a different perspective (Fig. 1.13C).

A unique feature of Residual Neural Networks is that in addition to taking into account activation from units in the layer directly upstream, these networks have "shortcut" connections which link activation of units several layers upstream to current units (Fig. 1.14B). These shortcut connections preserve the context of data as it reaches deeper layers within the network and better allows the network to converge on an appropriate output category for the data. For example, if a deep ANN had fifty layers, by layer forty-nine the impact of activation from layer two would be very small as the influence of layer two would have been passed through over 40 layers of units before it reaches the units of layer forty-nine. However, the addition of shortcut connections then ensures that the impact from activation in layer two remains relevant for longer, as it passes through fewer units before reaching layer forty-nine (Fig. 1.14B). Since its development, Resnet18 has already shown high performance in biological contexts such as the categorising magnetic resonance images to diagnose necrosis in the brain (Liu et al., 2021). Amongst several ANN types, Resnet18 also emerged as one of the highest performing ANNs in categorising X-ray images for the diagnosis of COVID-19 (Mondal et al., 2021). These examples highlight the utility of Resnet18 in distinguishing subtle changes in the spatial distribution of fluorescence intensity in biological images. Previous use cases thus make Resnet18 in particular ideal to categorise the spread of fluorescence intensity in images of centrioles.

In this chapter we "train" the units within Resnet18 to measure different physical aspects of a centriole image (e.g. circularity, spread of fluorescence over each pixel or number of pixels covered) and based on the image's unique combination of parameter values, Resnet18 will "learn" which orientation category best matches the image (Fig. 1.15A) (Zhang et al., 2019).

4.1.3. Key Findings

In this chapter I develop a live assay to measure centriole orientation over time using a super resolution system that allows for centriole rings to be clearly visualised. I then work with a collaborator to establish an ANN analysis pipeline to automate quantification of centriole orientation. Microscope resolution and the centriole-protein marker used play a significant role when identifying centriole orientation. In the case of the microscope system used, sacrifices to resolution were made in order follow centrioles in living embryos. Nevertheless, the protocol we developed allowed me to automate quantification of centriole orientation in a reliable and reproducible manner.

Using this live-cell assay I then measured centriole-orientation stability over time. Centriole-stability is analysed from ANN quantifications and is defined as the probability for any one centriole to stay in the same orientation state in the next 20 sec. Centrioles mostly appear as Rings but can also appear as Bars, indicating their side on orientation with respect to the cell cortex. Both states appear to be relatively stable, with most centrioles exhibiting only occasional transitions (>20 sec) between the two states through an intermediary ***Slanted*** orientation. Taken together, results suggest that *Drosophila* centrioles show bistable orientation.

4.2 Results

4.2.1 Developing an imaging pipeline

4.2.1.1 Using NeonGreen-Asterless-expressing flies to measure centriole orientation in living embryos

An important aspect of establishing an assay to measure centriole orientation in living *Drosophila* embryos was to determine how best to visualise the centriolar Ring. To this end, 3 fly lines expressing GFP-fusion to PLP and either GFP or NeonGreen (NG) fusion to Asterless (Asl). Asl is a 120 kDa, ~150 nm coiled-coil protein that is attached to the outer centriole wall via its C-terminal binding to the centriole cartwheel component Sas4 (Hatch et al., 2010), while PLP is associated with the outer centriole wall (Fu and Glover, 2012; Lerit et al., 2015). Previous studies have shown that Asl or PLP labelled *Drosophila* centrioles show Clear rings using a 3D-SIM, which has a theoretical resolution as low as 100 nm (methods section 2.4.2.) (Gartenmann et al., 2017; Mennella et al., 2012).

The first fly line tested overexpressed GFP tagged PLP from a Ubiquitin promoter, previously made in the lab (Richens et al., 2015). When imaged on the SoRa, centrioles show diffuse clouds of GFP-positive material around centriolar rings (Fig 4.1A). This localisation is in line with PLP fibrils extending from the centriolar wall into the PCM, as reported by previous studies (Lerit and Rusan, 2013; Richens et al., 2015). While diffuse material around the centriolar rings still allowed Ring-oriented centrioles to be identified by eye, other centriole orientation morphologies became harder to discern, such as Bar-oriented centrioles (indicative of centrioles on their side) (Fig. 4.1B). This is because it was difficult to determine where the centriole was amongst PLP PCM labelling, likely due to PLP being a component of the outer PCM as well as the centriole wall (Lerit et al., 2015; Richens et al., 2015). Due to its PCM staining I decided not to pursue PLP-GFP further as a marker for my live-cell centriole orientation assay.

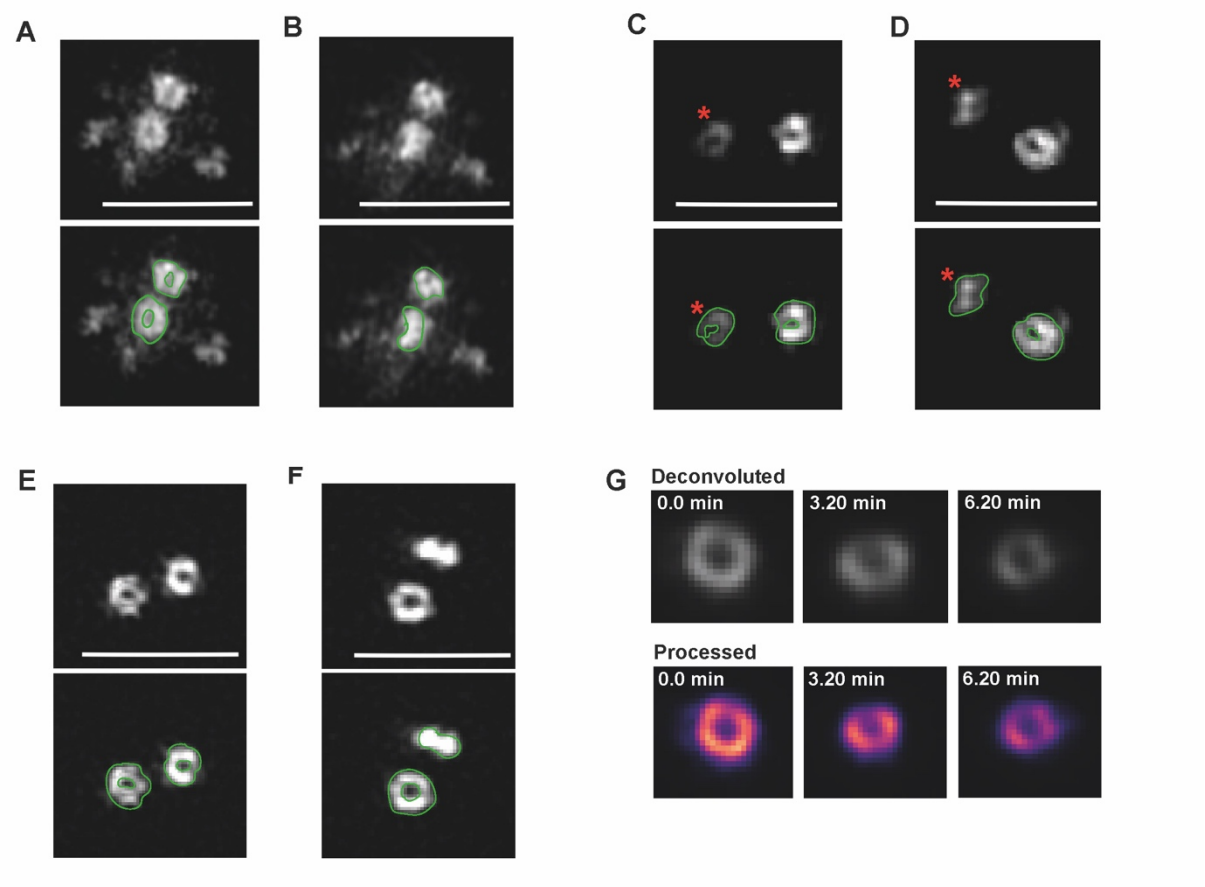

Figure 4.1 Using NeonGreen-Asterless-expressing flies to measure centriole orientation in living embryos

(A, B) Panels show spinning disc confocal images of centrioles from embryos expressing PLP-GFP **(C-F)** Panels show SoRa images of centrioles from embryos expressing (C, D) Asl-GFP (E, F) NG-Asl. (A-F) The lower panels highlight my interpretation of centriole orientation (*green* outline), showing either (A, C, E) two centrioles oriented as Rings or (B, D, F) one centriole as a Ring and one as a Bar. (C, D) *Red* asterisks indicate an example where it was difficult to distinguish between a Ring and Bar-oriented centriole due to similarities in shape. (A – F) Scale Bars = 1μm. **(G)** Left panel shows the first frame of a 20 frame, 6 min 20 sec centriole movie taken at 20 second intervals on the SoRa in NG-Asl-expressing *Drosophila* embryos. Middle panel shows frame 11 and rightmost image shows the frame 20 of the same movie. Images were processed with similar brightness, gain and contrast levels. Time shown in the top left corner as min.sec.

Another line tested overexpressed GFP tagged Asl (Asl-GFP) from a Ubiquitin promoter. Upon imaging Asl-GFP positive embryos at the SoRa, Rings appeared small and thick walled (Fig. 4.1C). In many cases, centriole orientation could not be accurately determined as the dip in fluorescence in the centre of Rings was very small. Moreover, centrioles on their side appeared as thick Bars that were close in shape to some Ring-oriented centrioles (Fig. 4.1C, D; *red* asterisks). These phenotypes were likely due to attachment of GFP to the buried C terminus of Asl. The C terminus of Asl contains a binding site for Sas4 that binds to centriolar microtubule doublets, as compared to the outward pointing N terminus of Asl which contains a Plk4 binding site and actively helps recruit Plk4 to the centriole (Cizmecioglu et al., 2010; Dzhindzhev et al., 2010).

Attachment of GFP to the C terminus therefore resulted in visualisation of a smaller centriolar Ring that could not be consistently resolved by the SoRa.

I then tested a fly line generated by Thomas Steinbacker (Raff lab, Dunn School of Pathology) which expressed a CRISPR/Cas9 knock-in of N-terminal tagged NeonGreen Asl (NG-Asl). When imaged at the SoRa, embryos expressing NG-Asl produced the clearest Rings of all three lines tested (Fig. 4.1E). Different orientation morphologies were often identifiable with centrioles side on with respect to the cell cortex appearing as definitive Bars (Fig. 4.1F). Importantly, in the generation of this line, flies homozygous for NG-Asl did not survive, this suggests that NG-Asl may not rescue WT Asl. However, the benefits of NG-Asl as a label outweigh these possible disadvantages. Rings appear fluorescent despite moderate bleaching over 6 min 20 sec movies and centrioles remain identifiable as rings, especially after images have been processed (Fig 4.1G). For these reasons, I decided to use this NG-Asl line for future centriole orientation experiments.

4.2.1.2 Using an Olympus SoRa to measure centriole orientation over time

The Ring orientation of centrioles indicate that we are looking down the barrel of the centriole, showing that the centrioles are upright with respect to the cell cortex (Fig. 3.1B). Images of such centrioles taken using a 3D-SIM have been documented in previous papers from the lab (Fig. 3.1A) (Aydogan et al., 2018; Gartenmann et al., 2017). However, this method does not allow centriolar movies to be made as the 3D-SIM requires many more photons to hit each sample to produce a single image. This results in samples bleaching significantly after a single Z-stack (pers. comm. from Alan Wainman). Therefore 3D-SIM was deemed unsuitable for creating a live assay.

Instead, the SoRa used achieves a theoretical spatial resolution of 120 nm (Azuma and Kei, 2015). This results in a resolution of 150 nm in practice at 488 nm wavelength (pers. comm. Alan Wainman). This is under the diffraction limit of light and just about matches the ~150nm width of *Drosophila* centrioles (Hayashi and Okada, 2015; Lopez, 2019), allowing Rings to be visualised at multiple timepoints (Fig. 4.2, Movie1). As the SoRa is a spinning disk confocal microscope, it also allows faster image acquisition as compared to other confocal systems (Hayashi and Okada, 2015). This feature makes movies less light

demanding and an ideal choice as an imaging method to develop a live-cell assay as centrioles could be imaged for up to ~6 min 20 sec and orientation still be identifiable (Fig 4.1G).

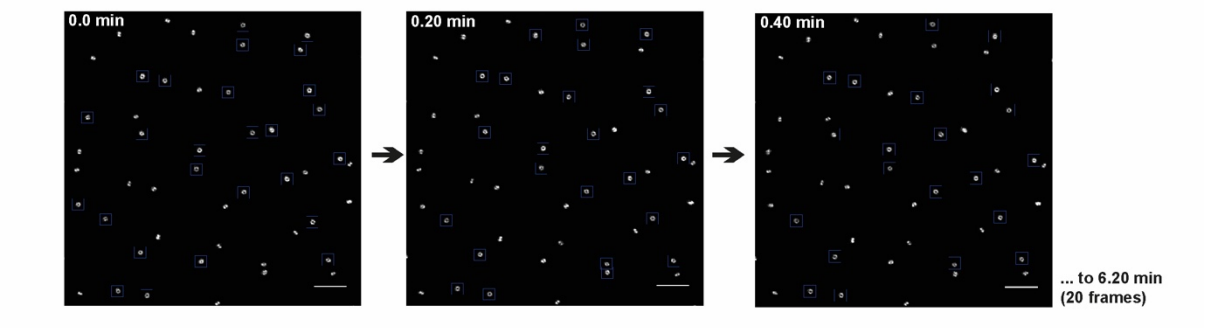

Figure 4.2 Using an Olympus SoRa to measure centriole orientation over time

Panels show three successive images from a movie taken on the SoRa in NG-Asl-expressing *Drosophila* embryos. Time indicated on images as min.sec. Blue boxes show manually identified Ring-oriented centrioles. Scale Bar = 3µn.

4.2.1.3 A significant proportion of Centrioles in Drosophila embryos are oriented

To establish a pipeline for tracking centriole orientation in living embryos, I acquired images of centrioles from *Drosophila* embryos expressing NG-Asl on the SoRa. In an initial pilot experiment, I manually quantified centrioles based on the shape they exhibit when oriented in different positions with respect to the cell cortex, with ***Ring-oriented*** centrioles being upright and ***Bar-oriented*** centrioles being side-on with respect to the cell cortex. I also quantify centrioles that are between Rings and Bars, which I call ***Slanted***. Images were obtained from 10 individual embryos during S-Phase of nuclear cycle 11-13. I found that ~40% of the centriole in these images were clearly visible as Rings, ~40% were Bar-oriented and ~20% resembled flattened rings, scored as Slanted (Fig. 4.3A). I use this terminology to describe centriole orientation throughout the rest of this thesis.

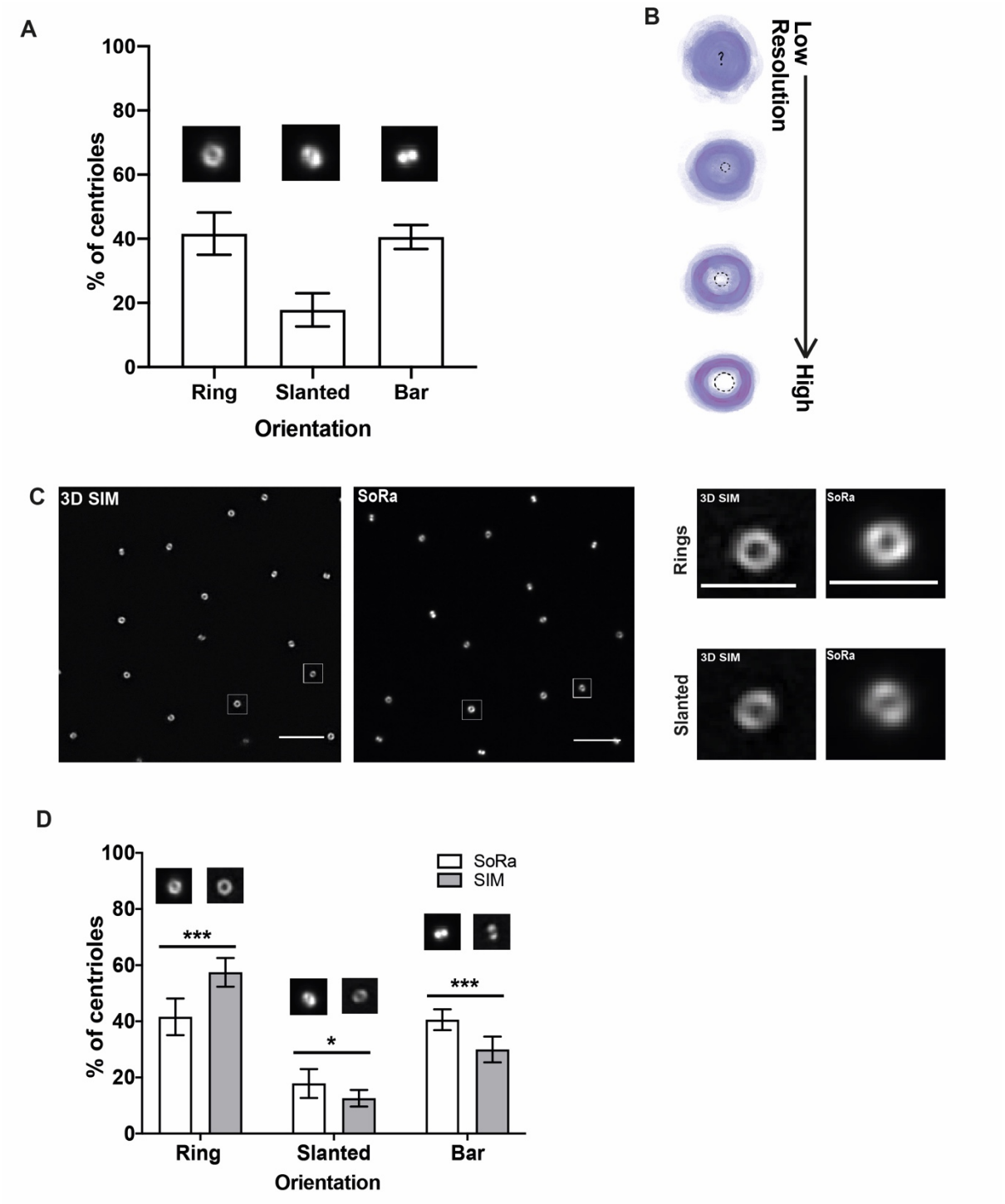

Figure 4.3 Centrioles in *Drosophila* embryos are oriented

(A) Bar graph shows the percentage (mean±SD) of Ring, Slanted and Bar-oriented centrioles based on manually quantified centriole images. The image above each Bar shows an example centriole morphology in that orientation category. Images were taken on the SoRa in NG-Asl-expressing *Drosophila* embryos. N = 9 embryos; n≥10 centrioles per embryo. **(B)** Illustration showing how as resolution increases, it becomes easier to see an absence of fluorescence in the centre of centrioles, making them more clearly identifiable as Rings. Dotted lines indicate perceived absence of fluorescence in the centre of illustrated centrioles. **(C)** Panels show Z-projected centriole images from separate embryos taken on a 3D-SIM (left panel) or a SoRa system in NG-Asl-expressing *Drosophila* embryos. Scale Bars = 3μm. *White* boxes show centrioles that are cropped on the rightmost panel. Top right panel shows an example of a Ring-oriented centriole while the bottom right panel shows an example of a Slanted centriole taken on each microscope. Scale Bars = 1μm. **(D)** Bar graph shows the percentage of Ring, Slanted and Bar-oriented centrioles based on manually quantified centriole images from the same dataset as in A (*white* Bars) compared

to data taken using a 3D-SIM (*grey* Bars). Centriole images above each Bar shows an example centriole morphology in that orientation category. Individual t-tests were performed to assess the statistical differences between the SoRa and SIM datasets. *=p<0,05; ***=p<0.001. N = 8 embryos; n≥10 centrioles per embryo.

This percentage of centrioles I scored as Rings in this initial experiment was lower than expected, as previous observations made by previous lab members from 3D-SIM images showed that a majority of centrioles appear as Rings (Aydogan et al., 2018; Gartenmann et al., 2017). The ability to manually score centrioles as being in a Ring orientation is influenced by the resolution of the images being analysed. The lower the resolution, the less able I am to identify an area of absence of fluorescence in the middle of centrioles, characterising them as Rings (Fig 4.3B). So, I wondered whether the difference in resolution between the 3D-SIM system and the SoRa system might explain this difference. To test this possibility, NG-Asl-expressing embryos were imaged with a 3D-SIM and manually scored for centriole orientation into the same three categories (Ring, Slanted and Bar).

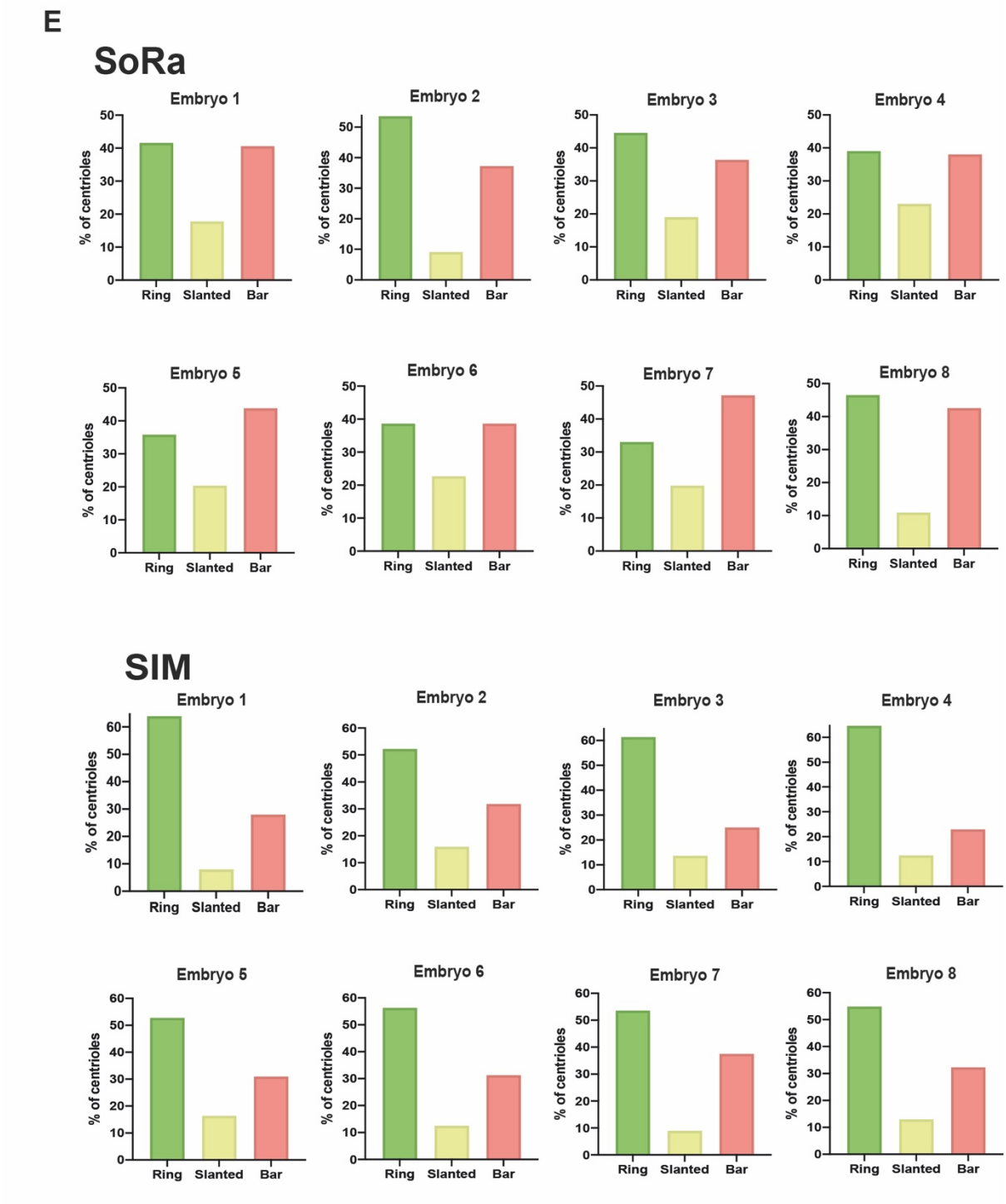

Figure 4.3 Centrioles in *Drosophila* embryos are oriented (Cont.)
(E) Bar graphs showing manual quantification for individual embryos making up D. Each graph shows the percentage of Ring (*green*), Slanted (*yellow*) and Bar-oriented (*red*) centrioles in one embryo imaged at the SoRa (top) or SIM (bottom).

In the 3D-SIM images the proportion of centrioles scored as Rings is ~20% higher, with corresponding decreases in the percentage of centrioles scored as either Slanted or Bars (Fig. 4.3C, D). These differences are larger compared to the variation between embryos taken at the same microscope system (Fig. 4.3E). For

example, the largest difference in centriole orientation measured within a single category between embryos imaged at the SoRa is ~10%, as seen in the Slanted category between Embryo 2 and 4. Moreover, on average the variation between Ring- or Bar-oriented centrioles between embryos imaged at the SoRa is ~5%. This is approximately a quarter of the difference seen between Ring- and Bar- oriented centrioles quantified from images taken at the SoRa as compared to the SIM. These comparisons show that the increase in proportion of Ring-oriented centrioles and the decrease in proportion of Bar-oriented centrioles observed in embryos imaged at the SIM are indeed significantly different compared to quantification from SoRa images. Graphs showing the proportion of Rings, Bars and Slanted centrioles in individual embryos also show that quantification between SIM images is more consistent than that of SoRa images (Fig. 4.3E), further highlighting the importance of resolution in quantifying centriole orientation. It is likely that the increased resolution of the 3D-SIM system made it easier to observe the absence of fluorescence in the centre of centrioles that were oriented as Rings.

However, as mentioned previously, the increased resolution of the 3D-SIM is attained at the cost of many more photons being required to generate a single image, resulting in samples bleaching much more quickly compared to the SoRa. In trial experiments, it was not possible to follow centrioles on the 3D-SIM system for more than 2-3 timepoints, whereas embryos can be imaged on the SoRa system for up to 6 minutes 20 seconds, containing up to 20 timepoints (one image every 20 sec) and retain sufficient image quality to quantify centriole orientation. For these reasons, I decided to continue using the SoRa system in my future experiments, while recognising that analysis will likely be systematically underestimating the true percentage of centrioles oriented as Rings.

4.2.2. Developing a high-throughput analysis pipeline to quantify centriole orientation

4.2.2.1 Establishing a dataset to train a neural network to quantify centriole orientation

I decided to develop an ANN to automate the quantification of centriole orientation in collaboration with Conor Wild (Life Sciences, Diamond Light Source, Oxford). ANNs are a type of machine learning algorithm which has a structure inspired by the human brain (section 1.5. and 4.1.2.). The network architecture used

for this ANN is called Resnet18 which has shown high performance in categorising complex biological images (Fig. 1.14B) (Liu et al., 2021; Mondal et al., 2021).

ANNs learn solely from a set of data provided to them that already has input images matched to the appropriate output; this is referred to as the training dataset (Fig. 1.12A). To establish a training dataset that would provide the ANN with as much information as possible, I took advantage of the multiple centriole orientation morphologies visible in SoRa movies. After much discussion, I decided to split the centriole images into six morphological categories: “Clear Ring”, “Perceived Ring”, “Slanted”, “Perceived Bar” and “Clear Bar”; any centrioles that I could not confidently place into the above 5 categories were placed into a final “Unidentified” category (Fig 4.4A). Each category was characterised by a consistent centriole morphology that represented a centriole appearing as a Clear Ring to a Clear Bar with 3 states in between exhibiting a non-perfect Ring, such as one that’s incomplete or not completely circular (Perceived Ring), a flattened Ring or very thick Bar (Slanted) or a thick Bar (Perceived Bar). The categories from a Clear Ring to a Clear Bar represent how much the distal end of centrioles is facing the cell cortex (appearing as Rings) as compared to the centriole wall (appearing as Bars).

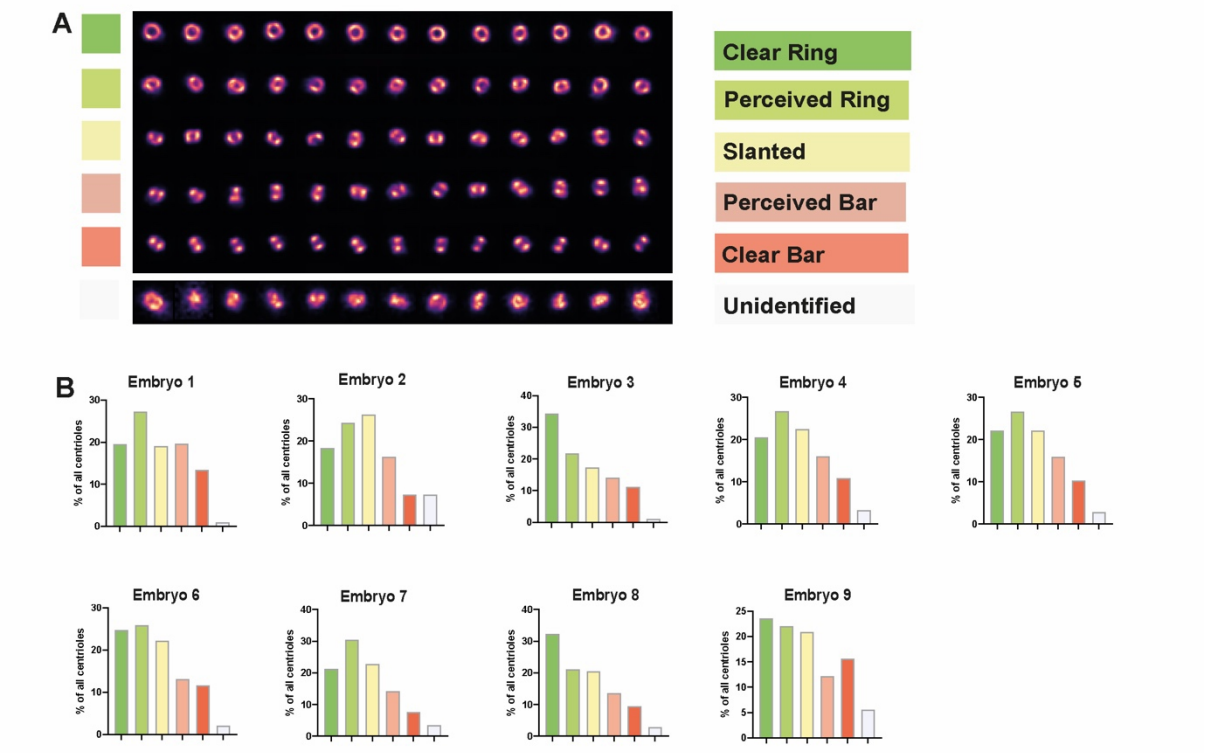

Figure 4.4 Establishing a dataset to train the neural network to quantify centriole orientation

(A) Panels show example images of several individual centrioles that I manually sorted into 6 orientation categories used to train Centrilyze (name of the finalised ANN, colour coded as indicated in the key on the right of the images). **(B)** Bar graphs show the percentage of centriole images in each orientation category in the 9 embryos used to generate a training dataset for Centrilyze. **(A, B)** Based on Centrilyze's training dataset consisting of 25,117 centriole images taken on the SoRa in NG-Asl-expressing *Drosophila* embryos. N = 9, n≥40 centrioles per embryo, each centriole scored at 20 timepoints.

The rationale for such an approach was that separate categories could easily be combined later if this was desirable, but splitting one category into two would be difficult (as it would require retraining the ANN). I generated a training dataset by manually categorizing 14 fields of 40-60 centrioles from 14 WT embryos where I acquired 20 timeframes from each embryo at 20 sec intervals (Fig 4.4B). This was done with the aid of a python script written by Isaac Wong (Raff Lab, Dunn School of Pathology, Oxford) that created a 28x28 pixel montage of every centriole image at every time point observed in a movie, saved as individual images. This process resulted in 35,495 images which I manually sorted into one of the 6 categories described above (producing ***annotated*** images). We then split this data into a set of *training* and *testing* data. We iteratively passed a training dataset of 25,117 annotated images from 9 embryos through the Resnet18 framework (He et al., 2016). As training data was passed through multiple times the network is able to adjust the strength of its connection to other units as well as internal parameters to achieve a reference pattern that would most accurately sort input data (section 1.5.3.). This is similar in principle to how neurons that often fire together gradually become myelinated, while unused connections are degraded over time (Fig. 1.15B). We then tested the network with an unseen set of 10,378 annotated images from 5 embryos which allowed us to check network accuracy using data where the network is not made aware of the annotations (the correct orientation category for each image) as it is with training data. We can then compare the network's annotation to my annotation. This represents a "real" test of the model built using training data. If the network was making consistent errors in testing data, we can go back to the training dataset and re-optimise parameters. As it was developed, we decided to name this network ***Centrilyze***.

4.2.2.2. Testing the neural network's accuracy and reliably

Through vigorous training and re-optimisation employed by Conor (detailed in Appendix A1), Centrilyze was gradually able to achieve accurate sorting of centriole images. However, as experiments progress, not all unseen input images will match each category's reference pattern perfectly (section 1.5.1., Fig. 1.12C). It is possible that when the same image is passed through Centrilyze multiple times, it might be placed into

a different category. Equally, it is also possible for me to occasionally sort centrioles into the wrong orientation through the process of sorting over 10,000 centriole images. Knowing how often centriole images are miscategorised, either by Centrilyze or by me, will give us a measure of how reliable or accurate Centrilyze is respectively. For our purposes, we calculate an error rate. These ***error rates*** are defined as the probability that an image belonging to one category would be reannotated into another category during a speculative round of sorting.

Error rates from two major sources of error aided Centrilyze in categorising data. First, we calculated how likely it was for me to mis-categorize centrioles. I did this by annotating a random set of 783 centrioles a total of 5 times over a week. The likelihood of any particular centriole image being sorted into a different category during each round of annotation was determined. ***Personal error rates*** were calculated as the probability of sorting any one centriole from any one category (underlined on top left of each graph) into other categories (abbreviated on the x-axis) during a speculative round of sorting (Fig 4.5A). Each graph shows the probability that the centriole is sorted correctly into the category it belongs to (Clear Rings into the Clear Ring [C_R] category, Perceived Rings into the Perceived Ring [P_R] category and so on) or incorrectly into any other category. Personal error rates show that while the probability of mis-sorting Clear or Perceived Ring-oriented centrioles as Clear or Perceived Bars and vice versa is very low (less than 0.01, *dark blue* arrows), the probability of mis-sorting *Clear* Ring or Bar-oriented centrioles into their respective *Perceived* categories is relatively high (probability of 0.3 and 0.5 respectively, *light blue* arrows). These errors are more than double compared to the error of sorting Perceived Rings or Bar-oriented centrioles as Slanted (Fig. 4.6A, *light blue* asterisks). This shows that while I can reliably tell the difference between Ring, Bar and Slanted centrioles, it is more difficult to discern which Slanted centrioles are closer to Rings or Bars as compared being Slanted (morphologically in between Rings and Bars).

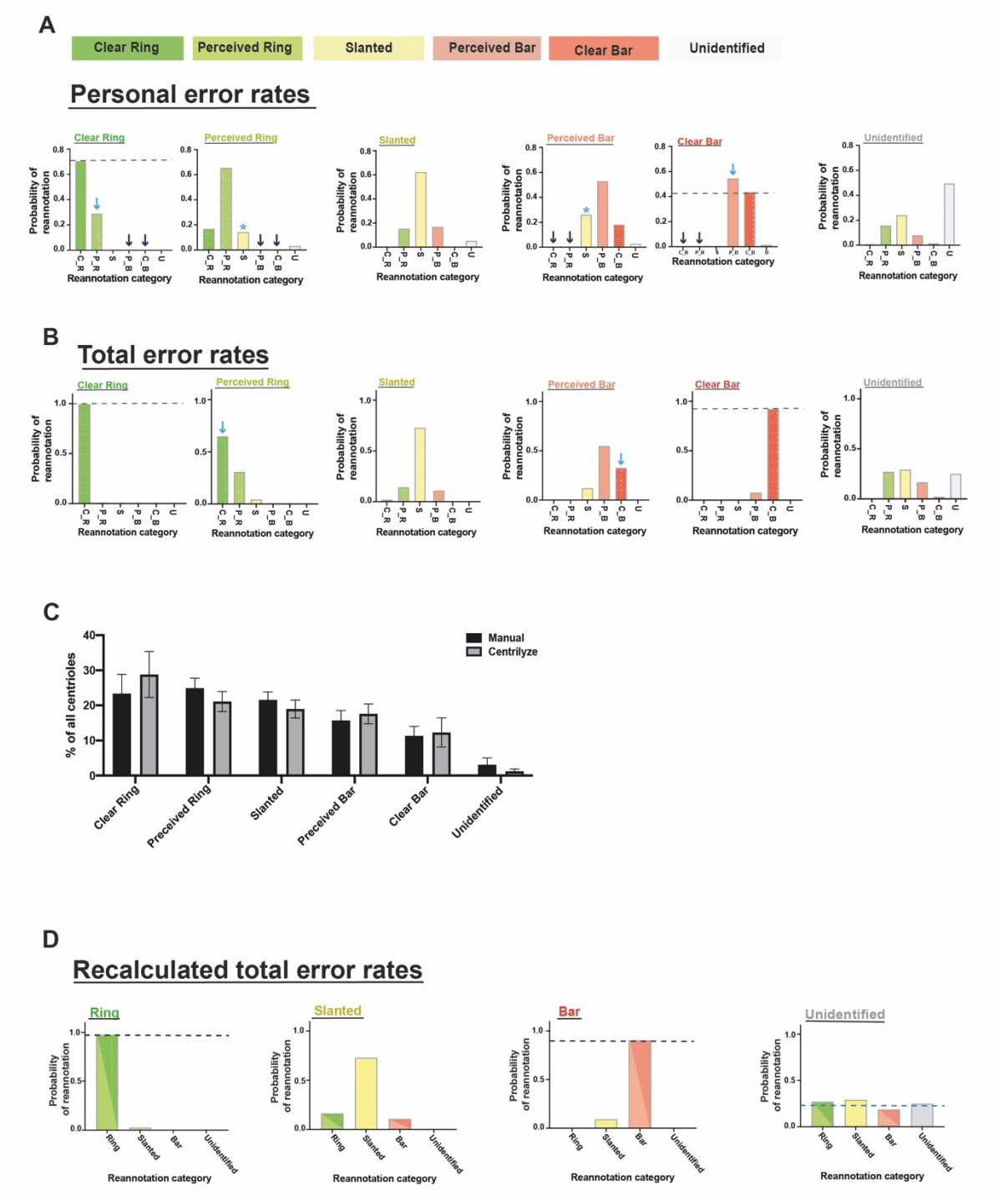

Figure 4.5 Testing the neural network's accuracy and reliability

(A, B) Bar graphs show (A) my personal error rates calculated from 5 reannotations of a dataset consisting of 783 centriole images taken randomly from the Centrilyze's training dataset or (B) Centrilyze's total error rates (that was calculated taking into account my personal error rate) calculated from Centrilyze's training dataset (A, B) expressed as a probability of centrioles in the category shown on the top left of each graph being speculatively reannotated into the categories shown on the x-axis including Clear Ring (C_R, *green*), a Perceived Ring (P_R, *light green*), Slanted (S, *yellow*), a Perceived Bar (P_B, *pink*), a Clear Bar (C_B, *red*) or Unidentified (U, *grey*). (A) *Dark blue* arrows show where the error between sorting Rings as Bars vice versa is very low. *Light blue* arrows show that the error between mis-sorting Clear Ring or Bar centrioles into their respective Perceived category is relatively high. *Blue asterisks* show that Perceived Rings or Bars are most likely to be mis-sorted as Slanted, and these error rates are lower than the error when mis-sorting Clear Rings or Bars into their respective Perceived category (*Light blue* arrows). (B) *Light Blue* arrows show that the error of mis-sorting Perceived Ring or Bar

centrioles into their respective Clear category is relatively high. **(C)** Bar graph showing percentage (mean ±SD) of centrioles annotated as Clear Rings, Perceived Rings, Slanted, Perceived Bars, Clear Bars or Unidentified when annotated manually (*black*) as compared to annotation by Centrilyze (*grey*). Based on annotation of 3,132 images of previously unseen centrioles. **(D)** Centrilyze's total error rate recalculated from Centrilyze's training dataset when orientation categories were merged. Expressed as a probability of centrioles in the category shown on the top left of each graph being speculatively reannotated into the categories shown on the x-axis including Ring (*green* and *light green*), Slanted (*yellow*), Bar (*red* and *pink*) or Unidentified (*grey*). (A, B, D) *Black* Dashed lines show probability that Clear Rings or Bars are sorted correctly when sorted (A) manually. (B) by Centrilyze. (D) by Centrilyze when Clear and Perceived categories were merged and error rate recalculated. *Blue* dashed line represents the average error of Unidentified centrioles into Ring, Slanted or Bar categories, showing that they are relatively equal. (A, B, D) Centrilyze's training dataset consisted of 25,117 centriole images. N = 9, n≥40 centrioles per embryo, each centriole scored at 20 timepoints.

Second, Centrilyze automatically calculates model error rates as the training dataset is passed through it. The model error rate describes how likely it would be for the same centriole image to be sorted into a different category if it were to be passed through the network again. These error rates were combined with my personal error rates to generate Centrilyze's ***total error rates*** (Fig. 4.5B). Similar to my personal error rate, Centrilyze's total error rate was highest when sorting centrioles in Perceived categories. The probability that Centrilyze correctly sorts Perceived Rings or Bars into the correct category is only 0.6. Most of the error in sorting into Perceived categories came from being from mis-sorting *Perceived* Rings or Bars into their respective *Clear* categories (Fig. 4.5B, *light blue* arrows). However, Centrilyze is able to sort centrioles into Clear Ring and Bar categories correctly most of the time (0.9 probability which is 90% of the time) which is over a third higher than my probability in sorting Clear Rings and Bars correctly (Fig. 4.5A, B, dashed lines). These results highlight the ability of neural networks to accurately sort large amounts of data that might be daunting for humans (Currie et al., 2019; Kriegeskorte and Golan, 2019). In line with these observations, and despite the relatively high errors, in Perceived categories my annotation of a previously unseen dataset of 3,132 centriole images in parallel with Centrilyze showed that Centrilyze deviated from my manual annotations by no more than 5% (Fig 4.5C). These results indicated that Centrilyze in this state was already able to replicate my annotations to a high degree of accuracy.

Due to the high error rates seen between *Perceived* categories and respective *Clear* Ring or Bar categories, the Perceived categories were combined with their respective Clear Ring or Bar category and Centrilyze's total error rate was re-calculated. Total error rates decreased across all remaining categories such that centrioles are reliably sorted into Ring or Bar orientation states ≥95% of the time (Fig 4.5D, *black* dashed line showing over 0.95 probability that Rings will be reannotated as Rings and Bars will be reannotated as

Bars). Additionally, there is a similar, ~25% probability that an unidentified centriole gets sorted into any other orientation state (Fig 4.5D, *blue* dashed line). This observation suggests that unidentified centrioles do not preferentially resemble one orientation state and the mis-sorting of unidentified centrioles is a systematic error. Taken together, combining Perceived categories with their respective Clear Ring or Bar categories improved Centrilyze's accuracy and allowed me to simplify interpretation of results going forward.

4.2.3. Calculating centriole stability over time

4.2.3.1. Stability analysis using a Hidden Markov Model

A key advantage of establishing a live-cell assay and automated analysis pipeline was the ability to analyse a lot of data quickly, allowing me to easily measure centriole orientation across multiple timeframes for many centrioles from multiple embryos at once. From this data I observed that centrioles are capable of changing orientation over time. The frequency of such state changes was measured using a ***Hidden Markov Model (HMM)*** that Conor attached to Centrilyze (detailed in Appendix A2). An HMM is a type of statistical model initially developed to recognise speech (Churchill, 1992; Jelinek et al., 1975; Rabiner, 1989). HMMs are used to measure changes in a sequence of different states that are not directly observable (Rabiner, 1989; Rabiner and Juang, 1999). Changes in centriole orientation over time are not directly observable as movies are taken at 20 sec intervals and any orientation centrioles may take in between observed timeframes have to be inferred by the model. However, I have observed that centriole orientation is unlikely to change between 20 sec intervals (section 4.2.3.2.), ensuring that such intervals probably do not result in under sampling changes in centriole orientation over time. Another important feature of an HMM is that the next observable state does not depend on any previous state, but solely on the current state. This approach is suitable for our data as all centriole movies are taken broadly in S-phase, so there is no obvious biological change marking the start or end of each movie (such as nuclear envelope breakdown, or chromatid separation in anaphase). Thus, any one frame in any movie could lie at any point in S-phase, making each subsequent transition in each movie insignificant as it pertains to frame number within the movie (frame 1 to 20).

In summary, an HMM uses the data it is fed to calculate the probability of a centriole transitioning into any orientation state (as defined in Centrylize) in the next frame, depending only on the state it is currently in. In

each embryo, this measure is calculated separately for every sequence of centrioles (20 frames per centriole) in a movie. From these measurements, we can calculate the average probability of any one centriole at any one time transitioning from its current state into any other state. Centriole stability was then defined as the probability of a centriole remaining in the state it is currently in, in the next frame (20 sec).

4.2.3.2. Drosophila centrioles are remarkably stable

As the HMM analyses possible changes in centriole orientation throughout 5 min centriole movies, it was important to ensure the proportion of each orientation state observed throughout centriole movies is not significantly affected by sample bleaching. Annotating centriole orientation in 5 frame intervals throughout movies show that although the proportion of Ring-oriented centrioles decreases by ~5%, relative proportions of Ring, Slanted and Bar-oriented centriole remain the same throughout the entire movie (Fig. 4.6A).

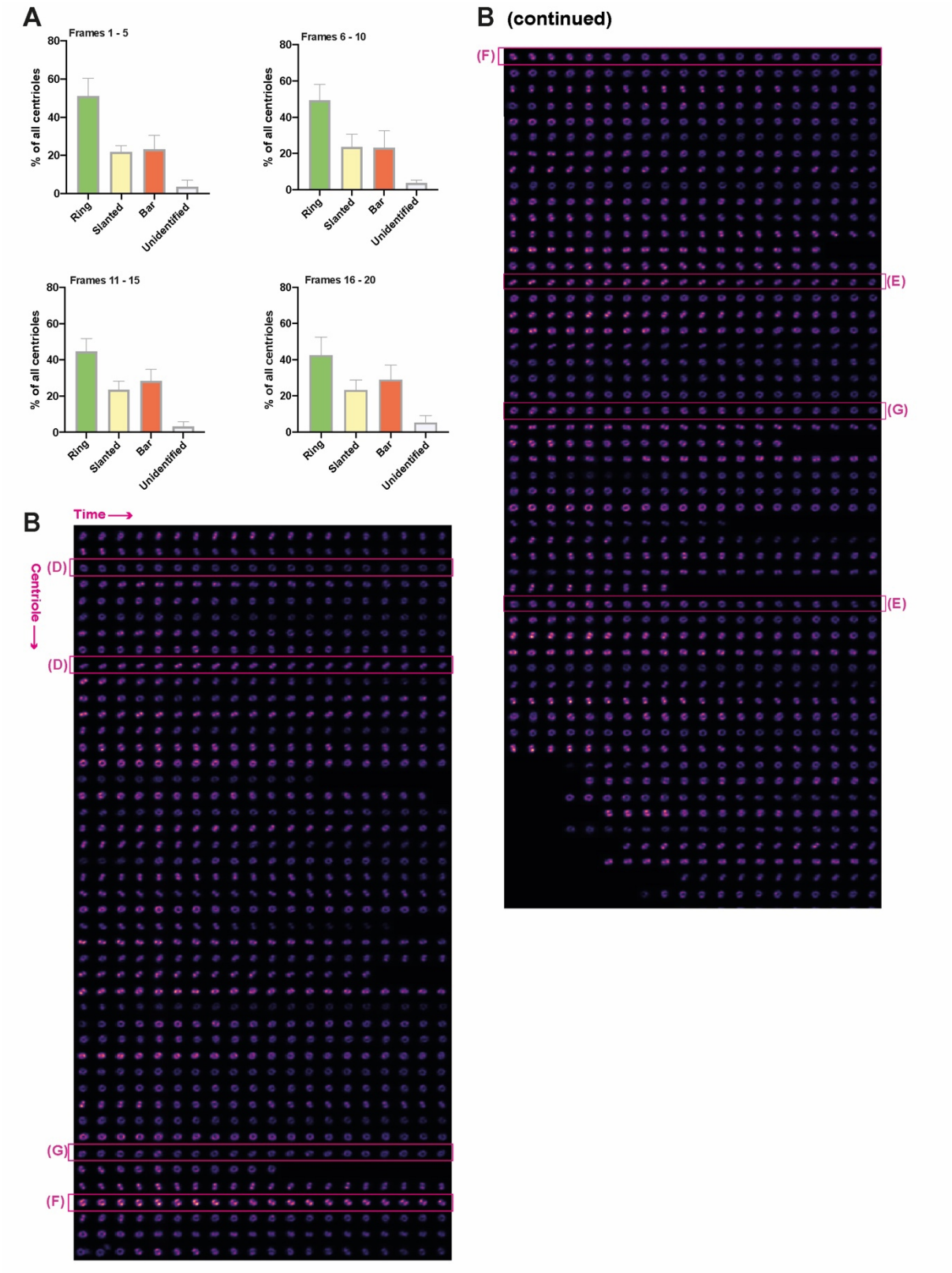

Figure 4.6 *Drosophila* centrioles are remarkably stable

(A) Bar graphs showing percentage of centrioles (mean ±SD) in Ring (*green*), Slanted (*yellow*), Bar (*red*) or Unidentified (*grey*) orientation states in 5 frame increments in a single movie. N≥10, n≥40 centrioles per embryo. **(B)** Timelapse montages of all centriole images in one embryo movie taken on SoRa in NG-Asl-expressing *Drosophila* embryos. Each row shows same centriole at successive timepoints (20 sec intervals). Blank spaces denote that a centriole was not captured at that timepoint. *Pink* boxes show centriole montages used in figures D – G.

Using an HMM applied onto data annotated by Centrilyze, I found that centrioles not only mostly appear as Rings, but are mostly stable. This phenomenon is not only seen visually by how centrioles appear as Rings for most of the 300 second movies they are tracked over (Fig 4.6B), but is also reflected in ≥90% probability that a Ring-oriented centriole will remain a Ring in the next time frame (Fig. 4.6C, D). This result is in line with fixed samples imaged at the 3D-SIM by previous lab members (Aydogan et al., 2018; Gartenmann et al., 2017). The second most stable orientation is Bar-oriented centrioles, which are side on with respect to the cell cortex (Fig. 4.6B, D). Of all orientation states, Slanted centrioles are the most unstable, suggesting that they are a transitionary state between the more stable Ring and Bar-oriented states (Fig. 4.6C). These results are in line with observed data, which typically show Slanted centrioles as Rings transitioning into Bars or vice versa, or when Ring- or Bar-oriented centrioles appear unstable (Fig. 4.6E, F). Both these observations further suggest that neither Ring- or Bar-oriented centrioles are completely stable. We also occasionally observe centrioles that appear to be very unstable and transition rapidly between all 3 states throughout the entire movie (Fig. 4.6G). However, such unstable centrioles were rare, further supporting our conclusion that centrioles are mostly stable (Fig. 4.6B, C). Taken together, Rings being the most common state implies that there is an active mechanism that acts to maintain distally oriented centrioles which appear as Rings. In the next chapter I investigate what key players may be involved in this potential centriole orientation mechanism.

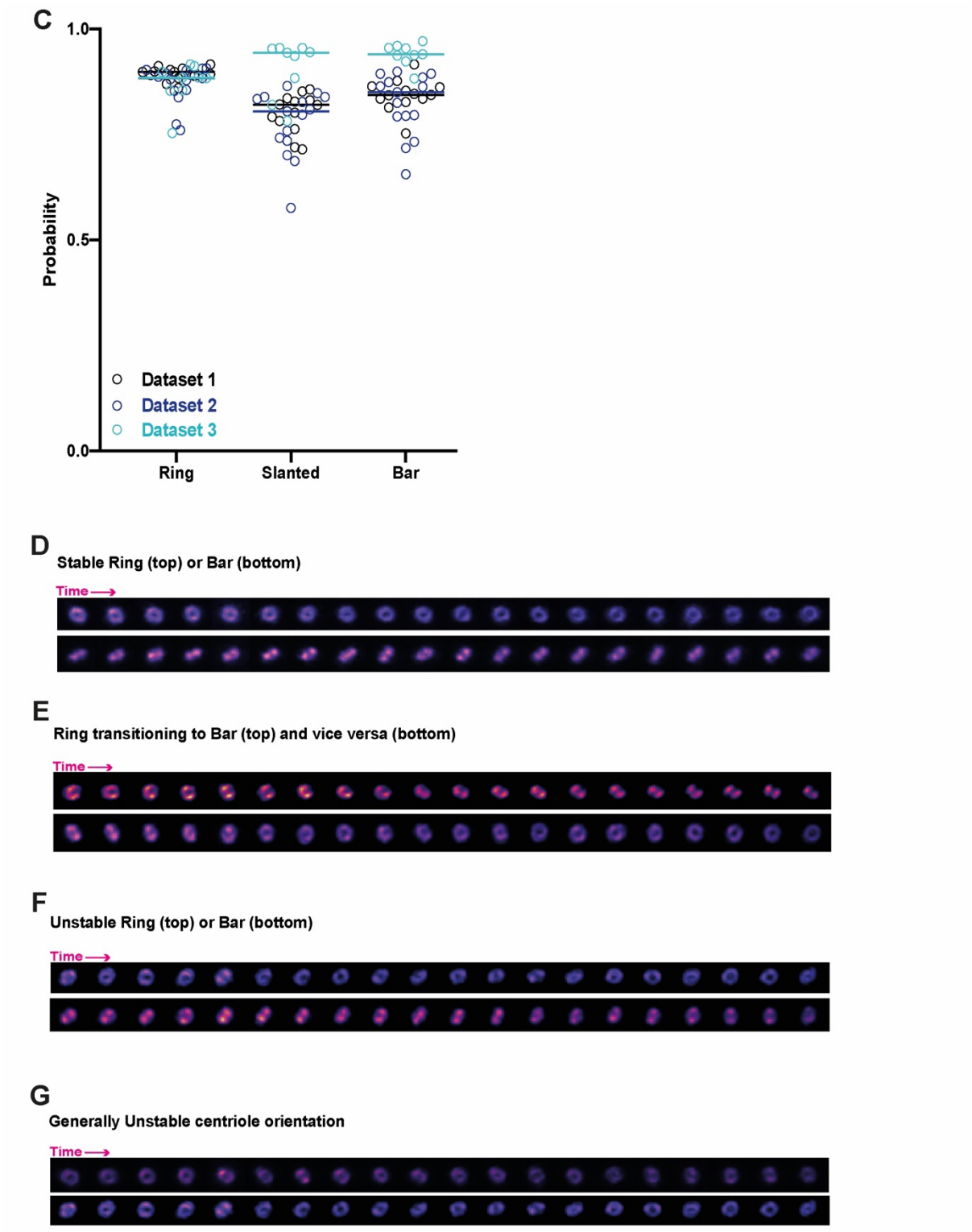

Figure 4.6 *Drosophila* centrioles are remarkably stable (Cont.)

(C) Scatter plot showing centriole stability (mean only) across three datasets. Each open circle shows average probability of any centriole in a single embryo remaining in the Ring, Slanted or Bar orientation state in the next frame (20 seconds). N≥10 embryos, n≥40 centrioles per embryo. **(D)** Examples of 2 stable centrioles are shown. The top panel shows a stable Ring, while the bottom panel shows a stable Bar. **(E)** Examples of 2 centrioles gradually transitioning from one stable state to another. Top panel shows a Ring tilting into a Slanted state then ending as a Bar. Bottom panel shows the opposite with a Bar flipping into a Ring. **(F)** Examples of 2 unstable Ring- or Bar-oriented centrioles. The top panel shows an unstable Ring centriole which is a Ring in most timepoints measured, but flips into a Slanted state every 2-3 frames. The bottom panel shows the same with an

unstable Bar centriole. **(G)** Examples of 2 unstable centrioles. Both centrioles rapidly transition between Ring, Slanted and Bar orientation states.

4.3. Discussion

In this chapter I establish a live-cell assay to measure centriole orientation while minimising bleaching to the sample over time. Then, my collaborators and I establish a quantification workflow that includes extraction of single images of centrioles at every timepoint throughout movies, and sorts them into defined orientation categories using a Resnet18 ANN architecture. We later apply an HMM over quantified data to measure stability of centrioles over time. From preliminary analysis of WT embryos, we find that centrioles in embryos have a preference to be oriented as Rings, which is consistent with previous observations made in the Raff Lab (Aydogan et al., 2018; Gartenmann et al., 2017). We also show that centrioles tend to remain stably oriented through S-phase in the syncytial embryo.

4.3.1. Imaging syncytial embryos in S-phase

Throughout this assay and going forward, I image embryos in S-phase, specifically at cycle 12 or 13. This is because in mitosis, centrosomes nucleate MTs contributing to the mitotic spindle and the presence of spindle forces would give me additional factors to consider when using a drug or candidate-based approach to understand centriole orientation (Chapter 5). In mitosis, centrioles also sink deeper into the embryo, which would lower the clarity of rings as compared to centrioles in S-phase. Finally, I specifically image embryos at cycle 12 or 13 as these stages would allow me the maximal sample size whilst the embryo is still a syncytium. Though preliminary data shows that orientation of centrioles does not significantly change when embryos have cellularised (data not shown), much like imaging centriole orientation during mitosis, imaging orientation in celullarised embryos would add additional factors that could be affecting centriole orientation beyond core centrosome components alone. While such experiments would be interesting, as I currently do not have a clear understanding of centriole orientation in this system, I opted to attempt to characterise a putative mechanism under conditions were there would be as few influences to centriole movement as possible.

I have also noticed that the proportion of Ring-oriented centrioles is lower at the start of S-phase and increases as S-phase progresses. This is possibly due to the growth of daughter centrioles orthogonally to mother centrioles (Fig. 1.4B). At early S-phase, new mothers have disengaged from old mothers (as

evidenced by loading of Asl) but many new mother centrioles are still perpendicular to Ring-oriented old mothers and are thus Bar-oriented. Throughout S-phase, new mothers tend to flip up into a Ring-oriented state, however, it is not known how this occurs. Imaging of embryos during very early S-phase may have an impact on the proportions of Ring- and Bar- oriented centrioles. Due to this observation, I actively try to image centrioles in mid to late S-phase where possible going forward.

4.3.2. Usage of Centrilyze to quantify centriole orientation

Centrilyze was developed to enable high-throughput analysis of centriole orientation, allowing me to increase the scale of my experiments. In comparison to manual quantification, Centrilyze is also more reliable in that it does not get tired leading to mis-categorisation of data like a human would. Errors that Centrilyze makes are systematic in nature and trackable with error rates, allowing us not only to quantify data but quantify how accurately data is sorted. Quantifiable error rates allow us to take results in context as compared to vague means of error if I were to manually quantify data. Centriole orientation has definable features such as shape and fluorescence levels at different points throughout the image that make up different orientation categories. Yet, visual differences between categories are subtle enough that they can appear subjective, especially when categorising images over time. This makes an ANN an ideal method of automating centriole orientation quantification, as units interrogate defined aspects of data which does not increase in its subjectivity as input increases (Kriegeskorte and Golan, 2019).

Centriylze sorts data into four categories, Ring, Bar, Slanted and Unidentified. The Unidentified category in theory contains images that do not match any other defined category. However, it is important to note that the Unidentified category is itself a category, and is not the summation of images that do not sufficiently meet the parameters of any other category. In Centrilyze's training dataset, images of centrioles in the dataset that did not fit any other category (were out of focus, overprocessed or otherwise unidentifiable) were annotated as Unidentified. Thus, Centrilyze has learned to recognise Unidentified centrioles using a set of parameters based on the training dataset, and would only be able to categorise centrioles as unidentified, given that they appear similar to Unidentified centrioles in the training dataset. Thus, if Centrilyze attempted to categorise centrioles from compromised WT or non-WT embryos, it may be worse at categorising

Unidentified centrioles as centrioles that do not meet the Ring, Bar or Slanted categories may look different than those identified in the training dataset. This may result in centrioles that are actually Unidentified ending up in other categories. However, checking centriole images sorted into Ring, Bar, Slanted or Unidentified categories in both WT and non-WT datasets show that most centrioles in the Unidentified category tend to represent out of focus centrioles. Moreover, images that contain very poor-quality data are manually removed from experiments before quantification. It is possible to create a category that contains images that do not sufficiently meet the prerequisites for other defined categories. However, such a function would be convoluted and time-consuming to create given that Centrilyze is, for the most part, identifying Unidentified centrioles correctly.

4.3.2. Explaining the presence of Bar and Slanted states given that centrioles have a preference to be oriented as Rings

It was found that most centrioles in WT centrioles are not only oriented as Rings, presumably with their distal end facing the cell cortex (as found in Chapter 3), but are also highly stable in S-phase. Of all orientation states measured, Ring-oriented centrioles also appeared the most stable, which is in line with previous observations from the Raff lab showing that centrioles tend to appear as rings (Fig. 3.1) (Aydogan et al., 2018; Gartenmann et al., 2017). In *Drosophila* where the length and width of centrioles are similar and the few conserved DAPs are dispensable at the distal end in ciliogenesis, we would assume that centrioles are randomly oriented. However, data thus far has shown that centrioles not only have a preferred orientation as distal-ended Rings, but are also relatively stable in that orientation, suggesting an active mechanism holding centrioles in a Ring-oriented state.

When centriole orientation does change, centrioles tend to pass through the Slanted state, which has the lowest stability in WT embryos suggesting that it is an inherently transitionary state. When Centrilyze sorts centrioles into orientation categories and error rates between categories are calculated, the highest rates of error tend to result from mis-sorting into categories that are morphologically adjacent to the desired category (Fig. 4.5D). This makes sense as centriole orientation is an inherently continuous measure. For example, centrioles within the Bar category that are mis-categorised as Slanted likely represent centrioles that are

morphologically between Slanted and Bar-oriented states. These patterns of error rates support the hypothesis that the Slanted state is a transitional state between more stable Ring- or Bar-oriented states.

Bar centrioles are less stable than the Rings but not as unstable as Slanted centrioles. This may be due to most mother centrioles being oriented in a Ring state. Thus, new mothers are likely to separate from old mothers in a Bar-oriented state in S-phase (Nigg and Holland, 2018). Bar-oriented new mother centrioles may then flip into a Ring orientation as S-phase progresses, explaining the slight instability of Bar-oriented centrioles. Although less frequent, I also observe Ring-oriented centrioles that transition into Bar-oriented centrioles which contradicts my initial hypothesis that Ring centrioles are the preferred orientation state in embryos (Fig. 4.6E, top panel). I propose that these transitions may be due to the initiation of a putative centriole orientation mechanism on new mother centrioles taking some time to stably transition Bar-oriented centrioles into a Ring-oriented state, resulting in new mother centrioles wobbling between Ring and Bar states for a few minutes before ending up as a stable Ring. Transitions from Rings to Bars may also be due to passive changes in orientation by MT- or actin-mediated pulling of centrosomes during actin cap formation or as centrioles are equidistantly positioned close to the cell cortex in S-phase (Buttrick et al., 2008; Foe et al., 2000; Kotadia et al., 2010). Given that usually one and at most two transitions are seen over the length of each movie taken in WT embryos (Fig. 4.6B), I speculate that centrioles take about 3 to 5 min to complete a transition from Ring to Bar or vice versa through the Slanted state. Notably, when two transitions are involved, I have observed that it is more likely for Rings to transition to Bars and back, as compared to Bars transitioning to Rings and back to Bars (Fig. 4.6B). These observations are further in line with Rings being the preferred orientation state of centrioles. The stability of Ring-oriented centrioles as compared to other orientation categories, as well as patterns of state transition between centrioles of different categories highlight the potential for an active centriole orientation mechanism, establishing and maintaining distally oriented, Ring-oriented centrioles at the cell cortex in *Drosophila* embryos.

I also wondered what influences the transition from Ring to Bar, and if orientation states beyond 20 sec before the current state play a role in determining how centrioles will be oriented in the future. I hypothesise that the amount of time spent in the Slanted state may influence how centriole orientation changes. I observed that the longer a centriole remains Slanted, the more likely it is to transition to an orientation state other than

the state it was in before it entered the Slanted state. For example, a Ring-oriented centriole that transitioned into a Slanted state for over 1 min would be more likely to transition to a Bar than go back to a Ring. However, if a Ring-oriented centriole transitions to the Slanted state for merely 20 sec, it is more likely to flip back into the Ring than fall into a Bar-oriented state. Therefore, I postulate that likelihood of going back to the original state decreases as time in the Slanted state increases.

Quantifying these observations would require using a mathematical model that measures the probability of centrioles transitioning to different orientation states while taking into account the states they have already been in. This endeavour would be complex and take a full-time statistician to develop. Alternatively, it is also possible for me to manually quantify transitions in WT embryos to investigate how centrioles transition from one orientation state to the next. However, such a method would be time-consuming going forward as different embryo conditions and mutants are tested. One of my aims in establishing an analysis pipeline to quantify centriole orientation was to minimise human error and allow high-throughput analysis. Thus, though it would no doubt yield interesting results, manually quantifying the patterns of orientation state transitions exhibited by centrioles over time is not currently a high-priority.

5. Mechanisms establishing and maintaining centriole orientation

5.1 Introduction

5.1.1. A need to understand why centrioles are oriented

Based on our current knowledge, ciliogenesis is the only process where centriole orientation has any functional significance (Roque et al., 2018; Vieillard et al., 2016). Centrioles converted into basal bodies are always oriented with their distal end facing the cell cortex as axonemes grow from the plus-ends of the basal body MTs (Fig. 1.4C, D) (Avidor-Reiss and Leroux, 2015; Ishikawa and Marshall, 2011). Various studies have shown that inability to dock in a distal-ended orientation at the cell cortex is often accompanied by changes in centriole orientation that overall impair ciliogenesis (Mansour et al., 2021; Roque et al., 2018; Vieillard et al., 2016). In non-ciliated polarised epithelia, the position of the centrosome appears to be important (Carvajal-Gonzalez et al., 2016a; Elric and Etienne-Manneville, 2014; Januschke et al., 2011). In tissues and processes where centrioles are positioned close to the cell cortex such as asymmetric division (Januschke et al., 2011), immune cell migration (Higginbotham et al., 2006), IS formation and mitosis (Moritz et al., 1995b; Stinchcombe et al., 2006), it is possible that centrioles are randomly oriented or that any specific orientation adds no additional functionality to the centriole.

However, I have previously shown in this thesis that in *Drosophila* embryos, most centrioles are oriented as Rings, with their distal end facing the cell cortex (Fig. 3.3C, Fig, 4.6B). In embryos, centrioles being positioned close to the apical cell cortex at regulated distances from each other are important factors in specifying the position of actin caps, which themselves ensure regulated nuclear divisions and eventual cellularisation (Baker et al., 1993; Buttrick et al., 2008; Foe et al., 2000; Kotadia et al., 2010). Given that centrioles in this cell type have a preferred orientation, together with the inherent polarity of centrioles

themselves (Guichard et al., 2013; Uzbekov and Alieva, 2018; Winey and O'Toole, 2014), it is possible that centriole orientation in the *Drosophila* embryo plays a role in embryo polarity and development.

Throughout this thesis, I have been developing methods to measure centriole orientation dynamics in *Drosophila* embryos. In this chapter, I select proteins and cytoskeletal networks that have been previously shown to have roles in centriole positioning in non-ciliated polarised epithelia, and in centriole docking during ciliogenesis on centriole orientation in the embryo, and I investigate the potential for these proteins and networks to be involved in centriole orientation in the embryo. These experiments may provide insights into novel roles for centriole orientation in non-ciliated polarised epithelia.

5.1.2. The importance of microtubules and actin in centrosome function

Centrosomes, consisting of a centriole and its surrounding PCM (Mennella et al., 2012), are well-known MTOCs (Kuriyama and Borisy, 1981). Most of the centrosome's MT binding capability comes from its PCM (Kuriyama and Borisy, 1981). Many proteins facilitate the binding and retainment of MTs. In this chapter, I examine the role of Cnn which is able to bind MT-nucleating complex γ-TuRC through its conserved CM1 domain (Fong et al., 2008; Zhang and Megraw, 2007). MT nucleation from centrosomes is most prominent when centrosomes nucleate MTs contributing to the mitotic spindle in mitosis and to facilitate increased intracellular trafficking to specified apical cortices (Elric and Etienne-Manneville, 2014; Moritz et al., 1995a; Stinchcombe et al., 2006). During this process, Cnn forms a large and stable scaffold aided by Spd2-dependent recruitment and Plk1 activation (Alvarez-Rodrigo et al., 2019; Conduit et al., 2014a; Feng et al., 2017; Wong et al., 2022).

MT nucleation at the centrosome also allows centrosomes to be accurately positioned by pulling centrosomes to the desired location via dynein, typically attached to the cell membrane with other positioning proteins such as Pins and Mud (Bowman et al., 2006; Izumi et al., 2006; Januschke et al., 2013). Dynein is a motor protein that walks towards the minus ends of MTs (Goodson and Jonasson, 2018). As it processes along the MT, MTs can shorten through catastrophe at its plus end (Hunter and Wordeman, 2000; Knoblich, 2010; Tournebize et al., 2000), thus pulling centrosomes to the cell cortex (Fig. 1.6B). Conversely, it has also been

shown that decreasing centrosome MT-nucleating capabilities by decreasing the PCM around centrioles causes centrosomes to drift away from the cell cortex (Fig. 1.9B) (McNally, 2013; Reinsch and Gönczy, 1998; Roque et al., 2018; Wang et al., 2009b). Thus, pulling of centrosomes via their PCM by MTs may be indirectly exerting push/pull forces on centrioles, perhaps changing their orientation as they are pulled.

In addition to their well-known role as an MTOC, it was recently established that centrosomes are also capable of nucleating actin, which contextualises long-standing observations of interactions between centrosomes and actin (Bearer, 1991; Euteneuer and Schliwa, 1985; Farina et al., 2016). Actin based movement has often been implicated in centriole positioning (Garrido-Jimenez et al., 2018; Solecki et al., 2009; Wu et al., 2018). Conversely, centrosomes also appear to influence actin positioning, such as during actin cap and furrow formation in *Drosophila* embryos (Fig. 1.7B) (Kotadia et al., 2010; Ojas et al., 2021; Riggs et al., 2003). Positioning centrosomes in this and other systems often includes MT/actin crosstalk. This may be via proteins that interact with both MTs and actin (Calvo and Izquierdo, 2021; Cheng et al., 2019), or the physical presence of one network influencing the other (Inoue et al., 2019; Jimenez et al., 2021).

Studies showing how actin and MTs work in concert to establish centriole position, together with how centrosomes interact with the MTs and actin cytoskeleton individually suggest that centrioles are subject to push and pull forces from these cytoskeletal networks through their PCM (Copeland, 2020; Goshima et al., 2005; Hunter and Wordeman, 2000; Lucas and Raff, 2007). As a side effect, these forces may also be passively pulling centrioles into different orientations.

5.1.4. The roles of distal cap proteins CP110 and Cep97

In *Drosophila*, distal cap proteins CP110 and Cep97 are the distalmost centriolar proteins and thus in distally oriented centrioles are the closest known proteins to the cell cortex (Fig. 1.3B) (Paintrand et al., 1992; Winey and O'Toole, 2014). Thus, both could potentially play roles in maintaining the distal-ended orientation of centrioles in *Drosophila* embryos.

In vertebrate cells, CP110 is a well-known inhibitor of ciliogenesis which is moved on and off the distal end by Cep97 (CEP97 in humans) (Bettencourt-Dias and Carvalho-Santos, 2008; Song et al., 2022; Spektor et al., 2007). Both CP110 and Cep97 are thought to be co-regulated, such that species which have a conserved copy of CP110 also tend to have Cep97 (Aydogan et al., 2022; Carvalho-Santos et al., 2011). More recently, it has been shown that CP110 and Cep97 also interact with positive regulators of ciliogenesis that facilitate transition zone formation and membrane docking (Dobbelaere et al., 2020; Yadav et al., 2016). This data is in line with how *CP110*$^{-/--}$ mice show ciliogenesis-related defects (Yadav et al., 2016). In contrast, *CP110*$^{-/-}$ flies appear viable with minimal ciliogenesis defects (Franz et al., 2013). This makes *Drosophila* a convenient system to study CP110 function (Aydogan et al., 2022; Franz et al., 2013). However, it is possible that the distal cap does mediate ciliogenesis in *Drosophila,* as *Cep97*$^{-/-}$ flies show some ciliogenesis-related defects and centrioles were unable to maintain their membrane-docked position in ciliated cells (Dobbelaere et al., 2020).

Another prominent function of CP110 and Cep97 is in regulating centriole length, a function that is highly conserved between vertebrates and flies (Delgehyr et al., 2012; Franz et al., 2013; Kobayashi et al., 2011; Kohlmaier et al., 2009; Schmidt et al., 2009). Depletion of either protein leads to centriole lengthening or shortening in a tissue-dependent manner (Delgehyr et al., 2012; Dobbelaere et al., 2020; Franz et al., 2013). It has also been hypothesised that these changes in centriole length ultimately lead to disrupted ciliogensis in CP110-depleted cells (Kobayashi et al., 2011). In *Drosophila* embryos in particular, the Raff lab has previously shown that CP110 and Cep97 likely cap mature centrioles at the same time in each cycle (Aydogan et al., 2022). This function is particularly interesting in the context of my project. As shown in Chapter 4 and published elsewhere, daughter centrioles grow at right angles to mother centrioles (Paintrand et al., 1992). When the daughter centriole matures and moves apart from the mother centriole to become a new mother centriole itself, it tends to flip from a Bar to a Ring orientation. The roles of CP110 and Cep97 in centrosome length control together with centriole maturation (Aydogan et al., 2022; Dobbelaere et al., 2020; Schmidt et al., 2009), in addition to their well-established roles in membrane docking in ciliogenesis (Dobbelaere et al., 2020; Walentek et al., 2016; Yadav et al., 2016), makes them attractive candidates to potentially regulate centriole orientation.

5.1.5. Key Findings

In this chapter I use the live assay and quantification workflow established in Chapter 4 to elucidate potential mechanisms influencing centriole orientation in *Drosophila* embryos. Centrosomes are well-known MTOCs that also influence actin (Conduit et al., 2015; Farina et al., 2016). Their connections to both cytoskeletal networks help to position centrioles close to the cell cortex in a variety of polarised epithelia and ciliated cells (Buttrick et al., 2008; Dobbelaere et al., 2020; Garrido-Jimenez et al., 2018; Higginbotham et al., 2006; Izumi et al., 2006; Quann et al., 2009; Yadav et al., 2016). Thus, I first inject embryos with cytoskeletal depolymerising drugs such as Colchicine and Cytochalasin to investigate if MTs, actin or both contribute to centriole orientation in addition to established roles in positioning. I find that while actin has minimal effects on centriole orientation, push and pull forces generated from MTs may be responsible for indirectly changing centriole orientation over time.

Following on from injections, I employ a candidate-based approach. I focus on the PCM scaffold protein Cnn. In embryos expressing a mutant form of Cnn, centrioles show characteristic disorganised movement that has been published elsewhere (Conduit et al., 2014a; Lucas and Raff, 2007). However, centrioles from these embryos also showed a significant decrease in centriole stability. By injecting them with colchicine to reduce their movement, I suggest that the decrease in centriole stability is in these mutants may be partially due to the depletion of Cnn or the lack of a properly formed PCM.

Lastly, I quantify centriole orientation in embryos lacking either distal cap protein CP110 or Cep97. Both are present at the distal end closest to the cell cortex, and given their established roles in ciliogenesis and centriole maturation, both presented good candidates for maintaining distally oriented centrioles. I show that, remarkably, in the absence of Cep97 the proportion of stable Bar-oriented centrioles significantly increased as the proportion of Ring centrioles decreased, suggesting that not only are Ring-oriented centrioles the default orientation in embryos, but that the distal cap plays a major role in keeping centrioles upright. However, while similar trends were observed in *CP110*$^{-/-}$ embryos, the phenotypes were much milder, suggesting that the involvement of distal cap proteins in centriole orientation may be complex.

5.2 Results

5.2.1. Role of cytoskeletal components in centriole orientation

5.2.1.1. Loss of microtubules appears to decrease centriole movement

In Chapter 4, I found that although most centrioles appear relatively stable, there are instances of centrioles that may be flipping from a Ring to Bar or vice versa, and occasionally flip through various different orientation states in quick succession. As the PCM through which MTs act on centrosomes is directly connected to the centriole walls (Lawo et al., 2012; Lerit et al., 2015), prior observations of MT forces positioning centrioles led me to hypothesise that MT-based attachment leading to push and pull forces on the centrosome may be contributing to changes in centriole orientation (Camuglia et al., 2022; Kotak and Gönczy, 2013; Merdes et al., 1996).

To test this, I used WT embryos expressing NG-Asl and Jupiter mCherry (Jup-mch). I injected embryos in S-phase at cycle 12 or 13 with 1 mM colchicine, which inhibits MT growth by binding to individual tubulin subunits, preventing them from polymerising with growing MT filaments. Colchicine at this concentration or higher has been previously used in embryos and showed desired reduction of MTs around centrioles (Conduit et al., 2014b; Lucas and Raff, 2007; Raff et al., 1990). Colchicine has also shown anti-inflammatory properties by inhibiting neutrophil chemotaxis and adhesion (required in cell movement, see Fig. 1.10). It does this by blocking the release of key crystal-derived chemotactic factors needed in intercellular signalling and selective tyrosine phosphorylation of kinases involved in neutrophil activation (Leung et al., 2015; Roberge et al., 1993). Control embryos were injected with Schnieder's Medium, which was used as a Buffer for colchicine (hereafter referred to as "Buffer").

Initially, I wanted to establish how long it would take for the drug to significantly deplete MTs in the embryo. As Colchicine-injected embryos tend to eventually arrest in mitosis, injections were performed in early S-phase to ensure that centrioles would still be in S-phase as imaging began. Injected embryos were imaged on an Olympus SoRa system at 0, 4 or 8 min post-injection for total of 6 min and 20 sec, with images taken every 20 sec. Embryos were not imaged for longer than this due to bleaching of the sample. Buffer-injected

embryos maintained a cloud of MTs around centrioles for up to 13 min post-injection (Figure 5.1A). In contrast, embryos injected with Colchicine showed a gradual decrease in MTs up to approximately 4 min post-injection, where there were typically negligible MTs around centrioles as indicated by a decrease in red fluorescence around green centrioles (Fig. 5.1A). Phenotypes exhibited by Colchicine-injected embryos at ~4 min post-injection were maintained for up to 13 min post-injection (Fig 5.1A). These observations show that at 4 min post-injection Colchicine had effectively depleted MTs around centrioles. Thus, all further movies were taken starting approximately 4 min post-injection (Fig. 5.1B).

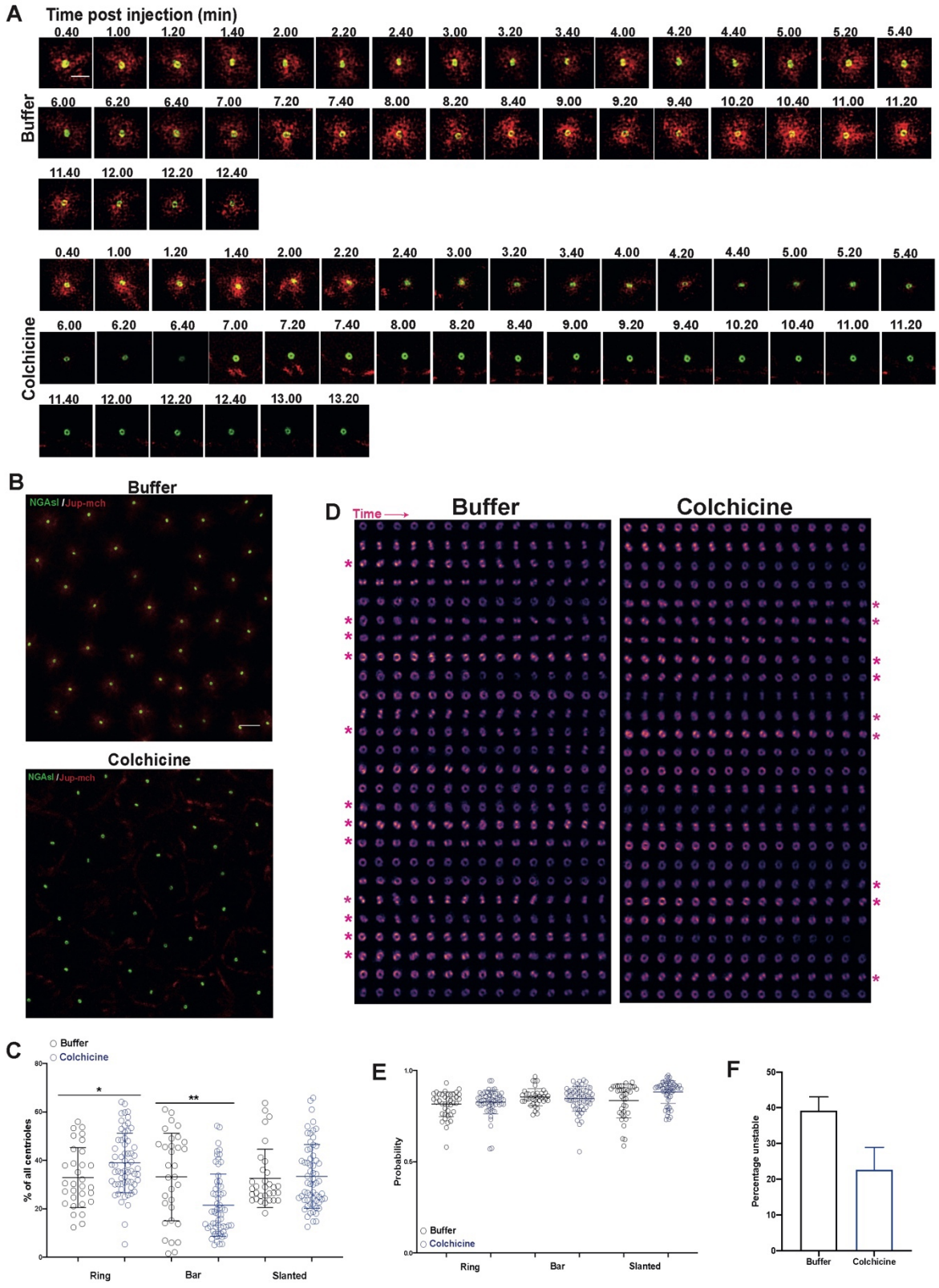

Figure 5.1 Loss of microtubules appears to decrease centriole movement

(A) Z-projected, merged images of centrioles from a WT embryo expressing NG-Asl (labels centrioles, *green*) and Jupiter-mcherry (Jup-mch, labels microtubules, *red*) that was injected either with buffer (top panels) or colchicine (bottom panels). Images of one centriole were taken every 20 sec for 6 min and 20 sec. Imaging period ended at 7 min post-injection. Then, another centriole from the same embryo was imaged starting from 7 min post-injection for 6 min and 20 sec. Imaging period of the second centriole ended at 13 min and 20 sec post-injection. Timepoints of each image post-injection shown as min.sec.

Scale Bar = 1μm. **(B)** Z-projected, merged images of centrioles from an embryo expressing NG-Asl (labels centrioles, *green*) and Jup-mch (labels MTs, *red*) injected with buffer (top) or Colchicine (bottom) at approximately 4 min post-injection. In the embryo injected with Colchicine, MTs appear greatly reduced. Scale bar = 3μm. **(C)** Scatter plot showing the mean (±SD) of the proportion of centrioles in Ring, Bar or Slanted orientations expressed as a percentage of total number of centrioles (with centrioles from multiple timepoints being considered as individual centriole images) in embryos injected with buffer (*black*) or Colchicine (*blue*). All movies taken as in B. Each open circle represents the proportion of centrioles in the orientation state shown on the x-axis for one embryo. Data was compared using an unpaired t-test. *=$p<0.05$; **=$p<0.01$. **(D)** Timelapse montages of centriole images in one buffer- (left) or colchicine-injected (right) embryo. Each row shows same centriole at successive timepoints (20 sec intervals). *Pink* asterisks indicate centrioles which clearly change orientation at some point during the movie. **(E)** Scatter plot shows the mean (±SD) stability of centrioles in embryos injected with buffer (*black*) or Colchicine (*blue*). All movies taken as in B. Each open circle represents the stability of the orientation state indicated on the x-axis for one embryo. Stability is defined as the probability that any given centriole will remain in its current orientation state (indicated on the x-axis) in the next frame. (C, E) Data pooled from 3 independent experiments. N = 10-15 embryos per experimental repeat; n≥40 centrioles per embryo. **(F)** Bar graph shows manual quantification of the mean (±SD) number of centrioles in embryos injected with buffer (*black*) or Colchicine (*blue*) which were "Unstable" (defined as centrioles that exhibit more than 2 state changes throughout the entire movie). N = 3-4 embryos per treatment; n≥1,000 centrioles per treatment.

Movies were input into Centrilyze as described in Chapter 4 to quantify the orientation and stability of the centrioles. 3 independent repeats of the same experiment were performed and data was pooled to eliminate any one-off changes in orientation or stability that may not be conserved in repeat experiments, thus simplifying analysis of results. Pooled data show that that proportion of Ring centrioles in Colchicine-injected embryos moderately increased, while the proportion of Bar-oriented centrioles significantly decreased as compared to Buffer-injected controls (Fig 5.1C).

Observational data shows that centrioles in colchicine-injected embryos exhibited less movement and were less likely to change orientation over time compared to Buffer-injected controls (Fig. 5.1D, *pink* asterisks indicate centrioles that have changed their orientation during the time-course of observation, Movie2 and Movie3), suggesting perhaps that MT forces play a role in passively pushing or pulling centrioles into different orientations as they position centrosomes. Quantification of stability shows a mild increase in the stability of Slanted centrioles in Colchicine-injected embryos as compared to Buffer-injected controls (Fig. 5.1E). This change suggests that centrioles are less likely to change orientation in Colchicine-injected embryos, as Slanted centrioles are likely in a transitionary state between Ring and Bar orientations (Fig. 4.6E, F). However, this change is not statistically significant. I hypothesise that the similarity in quantified stability between Colchicine and Buffer-injected embryos may be due to centriole stability in Buffer-injected controls being close to 1 (defined as the probability for a centriole in a particular orientation state to remain in that state in the next frame) and is near the upper limit of what is able to be quantified by our assay. To

test this, I quantified by eye the number of centrioles per embryo where "Unstable" centrioles change orientation more than once throughout the movie, this is a different method from how I measure stability using Centrilyze, as a human could not accurately determine Centrilyze's definition of stability. Quantifying stability by this definition across ~1,000 centrioles from 3 or 4 embryos per treatment showed that the percentage of centrioles that appeared "Unstable" was on average 40% in control embryos as compared to 20% in Colchicine-injected embryos (Fig. 5.1F). Therefore, even if changes are not statistically significant, data quantified by Centrilyze can provide an estimate as to the trends in orientation and stability that are similar to trends I would find if I were to sort data manually.

Taken together, these stability data suggest that in the absence of functional microtubules, centrioles are potentially less likely to change orientation over time. These results support the idea that MTs may be exerting dynamic pushing or pulling forces on centrioles through PCM connections, as has been reported for centrioles in other systems (Knoblich, 2010; Kotak and Gönczy, 2013; Merdes et al., 1996; Solecki et al., 2004). Orientation proportions in Colchicine-injected embryos also show that in a state where centrioles are not pulled by MT forces, the Ring-oriented state is even more common than in controls. This supports my results in previous Chapters that centrioles have a preference to be oriented as Rings.

5.2.1.2 Centriole orientation appears to be mildly affected by reduction of F-Actin

In addition to being MTOCs, centrosomes also localise actin (Farina et al., 2016; Inoue et al., 2019). In ciliated cells, focal adhesion complex proteins, typically associated with actin bundles at the cell membrane, are directly responsible for docking basal bodies to the cell cortex (Antoniades et al., 2014; Pan et al., 2007). In *Drosophila* embryos specifically, centrosomes position actin caps at the cell cortex that reorganise into furrows during mitosis. These furrows ensure that neighbouring mitotic spindles do not interact with each other during nuclear divisions within the syncytium (Fig. 1.7B) (Raff and Glover, 1989). Furthermore, actin and MTs often interact through common proteins, as well as spatially influencing each other (Buttrick et al., 2008; Inoue et al., 2019; Kao and Megraw, 2009; Ojas et al., 2021). These results support the idea that actin could also be involved in orienting centrioles.

To test if the actin organising functions of centrioles affected orientation in *Drosophila* embryos, I injected WT embryos expressing NG-Asl with Cytochalasin at 1 mg/ml which disables elongation of actin filaments. These concentrations have been previously documented to reduce filamentous actin within *Drosophila* embryos by promoting the activity of actin depolymerising protein CP1 (MacLean-Fletcher and Pollard, 1980; Raff et al., 1990). Controls were injected with Buffer alone which consisted of a 10% DMSO solution. While *Drosophila* embryos are able to undergo mitosis when injected with up to 50% DMSO (Pers. Comm. Isaac Wong, data not shown), quantification shows that when injected with 10% DMSO, the stability of Slanted and Bar-oriented centrioles mildly decreases (Fig. 5.2B). This is an intriguing result because as discussed previously, centriole orientation is particularly important during ciliogenesis (Section 1.1.3.). If centrioles are unable to orient themselves with their distal end facing the cell cortex, basal bodies are unable to properly form and ciliogenesis is impaired (Roque et al., 2018; Vieillard et al., 2016). One of the common symptoms of impaired ciliogenesis in flies and ciliopathies in humans is the lack of co-ordination (Dobbelaere et al., 2020; Kumar et al., 2021; Mansour et al., 2021). A recent study has shown that at low, non-toxic levels of DMSO, adult flies show co-ordination defects similar to those seen in flies with impaired ciliogenesis (Cabrita et al., 2022; Dobbelaere et al., 2020). It is possible, therefore, that the decrease in centriole stability in response to non-toxic levels of DMSO may be in line with previous observations showing that this treatment affects adult fly co-ordination, perhaps through the impairment of ciliogenesis caused by decreased centriole stability.

Injected embryos were imaged at the SoRa as previously described for 5 min, with Z-stacks taken every 20 sec. While old mother and new mother (referring to daughter centrioles that have disengaged from mother centrioles and have become mature centrioles themselves) centriole pairs in DMSO-injected embryos moved apart during S-phase in a similar manner to un-injected controls, centrioles in Cytochalasin-injected embryos started to cluster together (Fig 5.2A, blue arrows, Movie4, Movie5). This phenotype is likely due to the depolymerisation of actin used to ensure equidistant positioning of centrioles at the cell cortex (Foe et al., 2000; Raff and Glover, 1989). Similar patterns have previously been shown in *Drosophila* embryos injected with actin-depolymerising drugs (Raff et al., 1990). Quantification of data shows that embryos injected with 10% DMSO show similar orientation compared to un-injected controls (Fig. 5.2B). Data points near the bottom of the y-axis indicate that in a sample, centrioles in that particular orientation state almost never

maintain the same orientation state for more than 20 sec. This could be due to centrioles in this orientation state being highly unstable, or due to centrioles sinking into the embryo, such that centrioles are constantly changing between a Bar or Slanted state and Unidentified as they drift in and out of focus. Nevertheless, such data is still included as it gives me a more complete picture of the nature of centriole stability compromised embryos. While the orientation of centrioles does not significantly change when centrioles are injected with Cytochalasin (Fig. 5.2C), Slanted centrioles appeared less stable in Cytochalasin-injected embryos, perhaps suggesting that centrioles are flipping between Ring and Bar orientations at a faster rate (Fig. 5.2D). Observed data also show that a higher proportion of centrioles in Cytochalasin-injected embryos flip quickly between all three orientation states as compared to 10% DMSO controls (Fig. 5.2E, *purple* asterisks indicate centrioles which change orientation more than twice in the course of the movie), further suggesting that the depolymerisation of actin mildly decreases centriole stability.

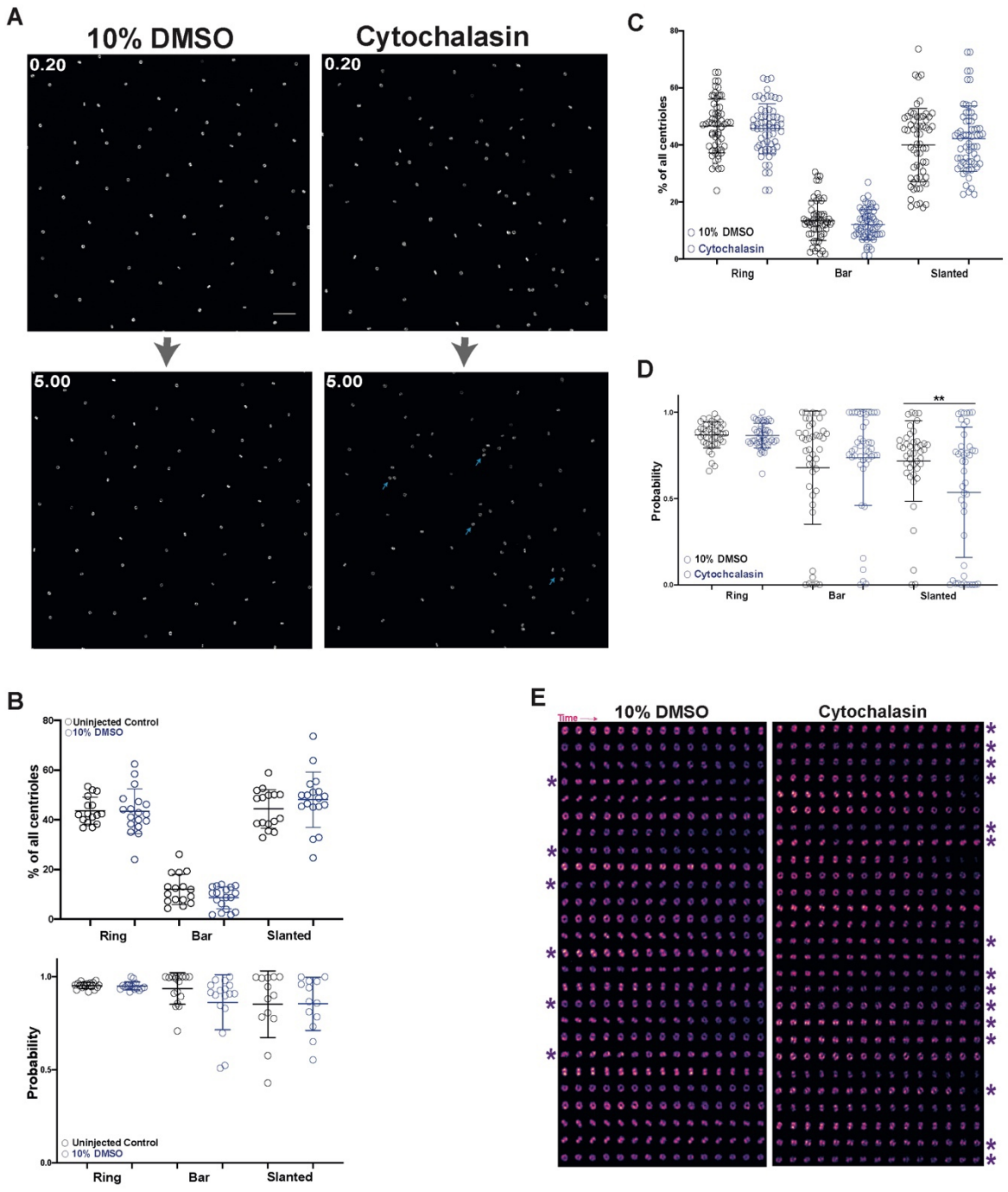

Figure 5.2. Centriole orientation appears to be unaffected by reduction of F-Actin

(A) Z-projected images of centrioles from a WT embryo expressing NG-Asl (labels centrioles, *grey*) injected with 10% DMSO (left) or Cytochalasin (right). Top and bottom images show the same embryo at approximately 4 min post-injection, 20 sec into the start of the imaging period, and at 9 min post-injection at the end of the imaging period. *Blue* arrows indicate clusters of centrioles in the Cytochalasin B image at 9 min post-injection, indicating that actin has likely been depolymerised in the embryo. Timepoints of each image shown as min.sec. Scale bar = 3µm. **(B)** Scatter plot shows the mean (±SD) of the proportion of centrioles (top) or the mean (±SD) stability of centrioles (bottom) in Ring, Bar or Slanted orientations expressed as a percentage of total number of centriole images in un-injected control (*black*) as compared to 10% DMSO (*blue*) injected embryos. Each open circle represents the proportion or stability of centrioles in the orientation state shown on the x-axis for one embryo. N = 10-15 embryos per experimental repeat; n≥40 centrioles per embryo. **(C)** Scatter plot shows the mean (±SD) of the proportion of centrioles in Ring, Bar or Slanted orientations expressed as a percentage of total number of centriole images in embryos injected with 10% DMSO (*black*) or 1mg/ml Cytochalasin (*blue*). Each open circle represents the proportion of centrioles in the orientation state shown on the x-axis for one embryo. **(D)** Scatter plot shows the mean (±SD)

stability of centrioles in embryos injected with 10% DMSO (*black*) or 1 mg/ml Cytochalasin (*blue*). Each open circle represents the stability of the orientation state indicated on the x-axis for one embryo. Data was compared using an unpaired t-test. **=p<0.01. (C, D) Data pooled from 3 independent experiments. N = 10-15 embryos per experimental repeat; n≥40 centrioles per embryo. **(E)** Timelapse montages of centriole images in one 10% DMSO (left), or Cytochalasin (right), injected embryo. Each row shows same centriole at successive timepoints (20 sec intervals). *Purple* asterisks indicate centrioles which change orientation multiple times through the movie.

At present, my results show that injection of Cytochalasin does not significantly affect centriole orientation in *Drosophila* embryos, however there is a slight reduction in stability of centrioles, likely due to centrioles flipping more frequently through Bar and Ring orientation states as indicated by decrease in stability of the transitionary Slanted state. This may be due to more disorganised MT forces acting on centrosomes in the absence of actin, as MTs and actin are well-known to work together to position centrosomes (Buttrick et al., 2008; Elric and Etienne-Manneville, 2014; Sullivan and Theurkauf, 1995). MTs being the dominant mechanism providing push and pull forces on centrosomes also falls in line with existing conclusions about the roles of MTs in centriole positioning in *Drosophila* embryos (Foe et al., 2000; Inoue et al., 2019; Ojas et al., 2021). In future experiments, injections should be performed on embryos expressing fluorescent actin and/or MTs, so that reduction in actin could be visualised post-injection in addition to any changes in centriole orientation. An actin depolymerising drug that is not dissolved in DMSO should also be tested to eliminate the potential effects of low-level DMSO on centriole orientation and stability. The amount of MTs in actin-depleted embryos could also be compared against controls in order to validate my interpretations of this preliminary data.

5.2.2. The role of Cnn and the PCM in centriole orientation

5.2.2.1 In Cnn^{f} embryos, centriole stability is decreased

After concluding that MTs have more effect on centriole orientation and stability compared to actin, I tested the effect of Cnn, a well-conserved scaffolding protein that plays an important part in assembling the mitotic PCM as well as binding and maintaining MT-nucleating γ-TuRC (Alves-Cruzeiro et al., 2014; Conduit et al., 2014a; Conduit et al., 2015; Zhang and Megraw, 2007). Studies in various organisms including *Drosophila* embryos have previously shown that mutating Cnn influences centrosome assembly, causing centrioles to rocket around the cell (Conduit et al., 2014a; Lerit et al., 2015; Lucas and Raff, 2007; Richens et al., 2015). I wondered how this movement and the lack of PCM would affect centriole orientation.

To this end, I used a *cnn*^{f04547} mutation which contained an insertion of the piggyBac sequence in the middle of the *cnn* gene (Woodard and Wilson, 2015). It has been previously shown by western blot that 2 hr old embryos laid by this mutant do not produce any detectable Cnn protein (Lucas and Raff, 2007). Mutants heterozygous for *cnn*^{f04547} expressing either NG-Asl or Jupmch were then made by Isaac Wong. I crossed these flies and selected mothers homozygous for *cnn*^{f04547} with one copy of NG-Asl and one copy of Jupmch. I then imaged embryos laid by these flies (hereafter referred to as *cnn*^{f} embryos). In line with published data (Conduit et al., 2014a; Lerit et al., 2015; Lucas and Raff, 2007), centrioles in *cnn*^{f} embryos were unable to effectively nucleate MTs, appear much less organised and move quickly around the embryo in a rocketing motion (Fig 5.3A, Movie6). However, my movies suggest that some MTs do attempt to nucleate from centrioles (Fig. 5.3A, B) (Lucas and Raff, 2007). Perhaps nucleation is possible through any remaining PCM components surrounding centrioles such as PLP and Spd2 (Conduit et al., 2014b; Lerit et al., 2015). Previous studies have shown that both Spd2 and PLP have MT-nucleating roles that are maintained at the centriole with some functionality in the absence of Cnn (Giansanti et al., 2008; Lerit et al., 2015; Roque et al., 2018). While centrioles generally move in the direction of long nucleated MT filaments, they are also seen to move away from MTs that may be forming blobs around them (Fig. 5.3B). This suggests that in addition to clustering MTs, causing a pushing rocketing motion around embryos as previously described (Lucas and Raff, 2007), MTs may also be capable of pulling on centrosomes in *cnn*^{f} embryos through MT filament nucleation in a similar manner to how MTs position centrioles observed in other systems (Bowman et al., 2006; Izumi et al., 2006; Merdes et al., 1996; Yi et al., 2013). Therefore, given that the lack of MTs increases the stability of centrioles and increases the proportion of centrioles in a Ring orientation (Fig. 5.1C, D, E), rapid centriole movement seen in *cnn*^{f} embryos may be due to centrioles being pushed and pulled by asymmetrically organised MTs (Fig 5.3B).

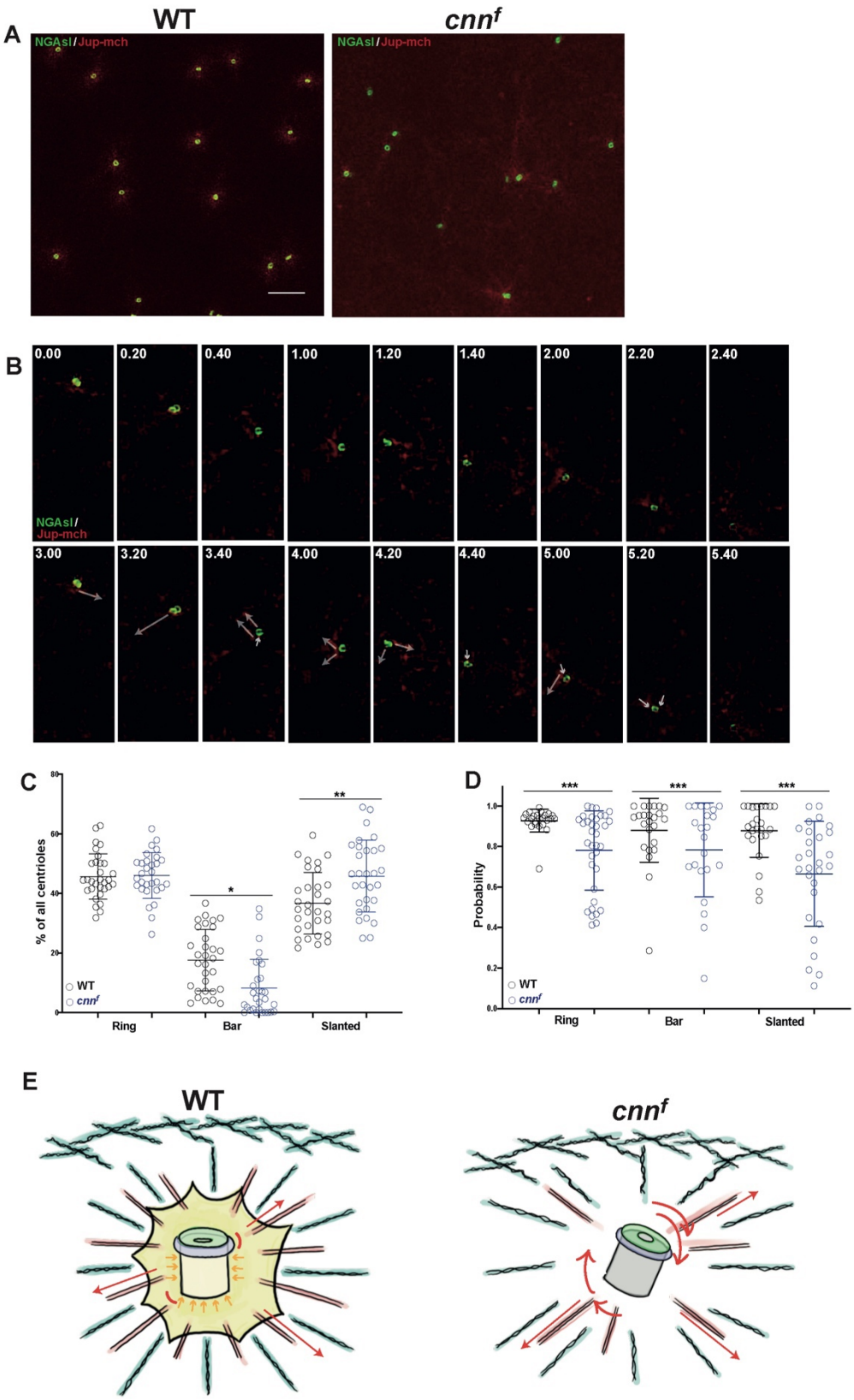

Figure 5.3. In *cnn*^{f} embryos centriole stability is decreased

(A) Z-projected, merged images of centrioles from either a WT or *cnn*^{f} embryo expressing NG-Asl (labels centrioles, *green*) and Jupmch (labels MTs, *red*). In the *cnn*^{f} embryo MTs appear greatly reduced and centrioles are highly disorganised. Scale bar = 3µm. **(B)** Z-projected, merged images of a single centriole over time from a *cnn*^{f} embryo expressing NG-Asl (*green*) and Jupmch (*red*) in the same field of view. Images were taken every 20 sec. Lower panels show *off-white* arrows to indicate the

direction of MTs nucleating from the centriole and if MTs are likely to be pushing or pulling the centriole given the position of the centriole in the next frame. Timepoints of each image shown as min.sec. **(C)** Scatter plot shows the mean (±SD) of the proportion of centrioles in Ring, Bar or Slanted orientations expressed as a percentage of total number of centriole images in WT (*black*) as compared to *cnn*^{f} (*blue*) embryos. Each open circle represents the proportion of centrioles in the orientation state shown on the x-axis for one embryo. **(D)** Scatter plot shows the mean (±SD) stability of centrioles in WT (*black*) as compared to *cnn*^{f} (*blue*) embryos. Each open circle represents the stability of the orientation state indicated on the x-axis for one embryo. (C, D) Data was compared using multiple unpaired t-tests. *=p<0.05; **=p<0.01; ***=p<0.001. Data pooled from 3 independent experiments. N = 10-15 embryos per experimental repeat; n≥40 centrioles per embryo. **(E)** Illustration showing a centriole (*gray*) with pericentriolar material (*yellow*), CP110 (*green*), Cep97 *(purple*), MTs (*pale red*) and actin (*blue*). Direction of pulling MTs forces on centrosomes (*red* arrows) changing centriole orientation (*red* action lines) and inertia provided by an intact PCM (*yellow* arrows). In *cnn*^{f} embryos, PCM is greatly reduced, decreasing inertia needed to tilt centrioles, resulting in a greater rate of centrioles flipping between ring and bar orientation states due to asymmetrically nucleating MTs forces.

Quantification of centriole orientation shows that in *cnn*^{f} embryos a significantly higher proportion of centrioles appear Slanted, while the proportion of Bar-oriented centrioles moderately decreases (Fig 5.3C). The increase in Slanted centrioles appears in line with stability data, which show that centrioles of all orientations in *cnn*^{f} embryos are significantly less stable compared to WT controls (Fig 5.3D). As centrioles are more unstable, it would make sense that they are transitioning more frequently through the Slanted state, as explained in Chapter 4. An interesting observation is that the proportion of Bar-oriented centrioles decreases slightly and proportion of Ring-oriented centrioles remains constant between *cnn*^{f} and WT control embryos (Fig. 5.3C). Thus, while centrioles are flipping between Bar and Ring orientations more often, Ring centrioles are still the preferred state, suggesting that any potential mechanism maintaining centriole orientation has not been significantly perturbed. Therefore, centriole stability and orientation may be maintained by independent mechanisms, and presence of Cnn may solely affect centriole stability. Given that the PCM is known to be a dense, fibrous matrix that may contain phase-separated liquid and solid states (Raff, 2019), I speculate that the presence of PCM nucleated by Cnn may increase the inertia needed to flip a centriole between Ring and Bar orientation states (Fig. 5.3E). Thus, in the absence of a properly formed PCM, less MT-mediated force at the centrosome is required to passively pull centrioles out of a preferred Ring orientation. This hypothesis would agree with results obtained from Colchicine-injected embryos, where the proportion of Ring-oriented centrioles increase in the absence of pulling MT forces and an intact PCM (Fig. 5.1C, D, E).

5.2.2.2 Decrease in stability of centrioles in cnn mutant embryos is not solely due to asymmetric MT forces in cnn^{f} embryos

In addition to the lack of PCM, I wondered if the lack of Cnn itself contributes to changes in centriole stability beyond nucleating the PCM to allow MT-mediated pulling. To this end I injected *cnn^{f}* embryos as described in 5.2.2.1. with the MT-inhibiting drug Colchicine. A previous study from the Raff lab has shown that injection of colchicine into *cnn^{f}* embryos slowed the rapid and disorganised movement of centrioles (Lucas and Raff, 2007). My data agree with these conclusions, as *cnn^{f}* embryos injected with colchicine showed reduced centriole movement as compared to those injected with Buffer alone (Fig. 5.4A). Drug injected *cnn^{f}* embryos embryos showed a reduced proportion of Bar-oriented centrioles as compared to *cnn^{f}* embryos injected with Buffer alone (Fig. 5.4B), in line with the decrease in proportion of Bar-oriented centrioles when WT embryos are injected with colchicine (Fig. 5.1C). Stability of centrioles in *cnn^{f}* embryos was similar when injected with colchicine or with Buffer alone (Fig 5.4C). These results suggest that beyond asymmetric MT forces causing rapid centriole movement, other factors are involved in decreasing the stability of centrioles in *cnn^{f}* embryos that may be more directly related to the absence of Cnn or PCM in general. In *Drosophila* spermatocytes, it was shown that depletion of PCM in PLP mutants was correlated with aberrant, side-on orientation of centrioles (Roque et al., 2018). Therefore, it is possible that the presence of the PCM alone, independent from MT push and pull forces, is sufficient to achieve a Ring orientation due to the balance of forces imparted by the PCM onto the centriole itself (Fig 5.4D).

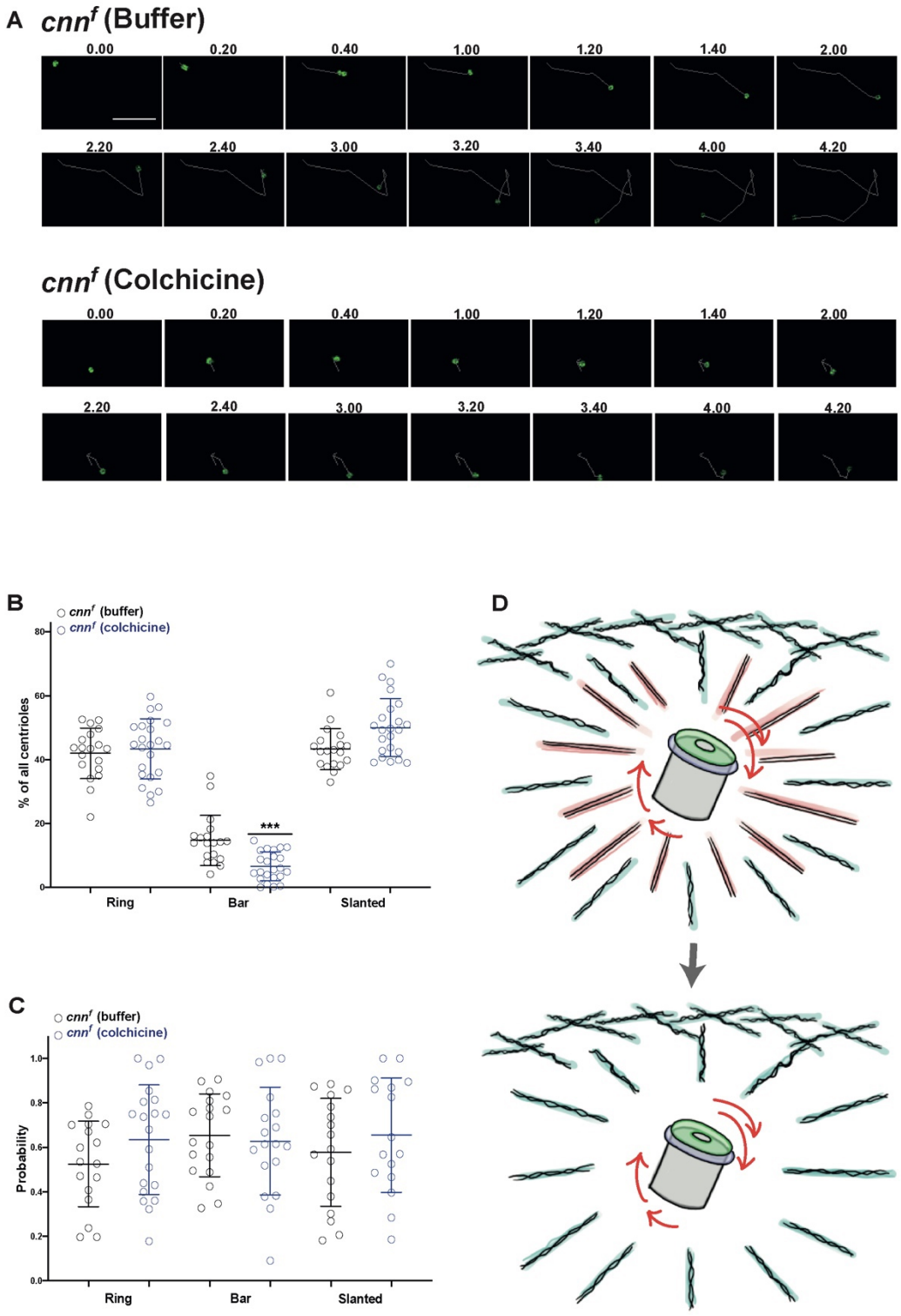

Figure 5.4. Decrease in stability of centrioles in Cnn mutant embryos is not solely due to asymmetric MT forces in *cnn*^{f} embryos

(A) Images showing a single centriole over time from a *cnn*^{f} embryo injected with Buffer (top two panels) or Colchicine (bottom two panels). *Grey* lines show recent centriole tracks. Images were taken every 20 sec. Timepoints of each image shown as min.sec. Scale Bar = 1μm. **(B)** Scatter plot shows the mean (±SD) of the proportion of centrioles in Ring, Bar or Slanted orientations expressed as a percentage of total number of centriole images in *cnn*^{f} embryos injected with Buffer (*black*) or Colchicine (*blue*). Each open circle represents the proportion of centrioles in the orientation state shown on the x-axis for one embryo. ***=p<0.001. **(C)** Scatter plot shows the mean (±SD) stability of centrioles in *cnn*^{f} embryos injected with Buffer

(*black*) or Colchicine (*blue*). Each open circle represents the stability of the orientation state indicated on the x-axis for one embryo. (A, B) Data pooled from 2 independent experiments. N = 10-15 embryos per experimental repeat; n≥40 centrioles per embryo. **(D)** Illustration coloured as in Fig. 5.3E, showing a centriole in a *cnn*^{f} embryo that has negligible PCM, and then injected with colchicine which reduces MTs. Movement is retained even as MTs are depleted.

5.2.3. Distal cap proteins appear to help orient centrioles

5.2.3.1. Cep97 is implicated in Ring-oriented centrioles

Cep97 is part of a well-conserved distal cap protein complex, typically known to function together with CP110 to control ciliogenesis in vertebrate cells (Carvalho-Santos et al., 2011; Kobayashi et al., 2011; Paintrand et al., 1992; Spektor et al., 2007; Tsang et al., 2008). It has also been implicated in controlling centriole length in a variety of organisms (Aydogan et al., 2022; Dobbelaere et al., 2020; Schmidt et al., 2009). In the absence of Cep97, cells show inability to dock centrioles to the putative site of ciliogenesis in both *Drosophila* and vertebrate systems (Dobbelaere et al., 2020; Lee et al., 2022; Nagai et al., 2018). Furthermore, in the absence of DAPs, distal cap proteins Cep97 and CP110 make up the distalmost centriolar proteins (Paintrand et al., 1992; Winey and O'Toole, 2014), which have been shown to be present while centrioles are docked with (Stinchcombe et al., 2015), or without DAPs (Dobbelaere et al., 2020). Both Cep97 function and localisation make it a likely candidate in a potential centriole orientation mechanism.

To test this hypothesis, I crossed a Cep97 mutant to flies expressing NG-Asl to obtain flies that were *Cep97*$^{-/-}$ *; NG-Asl* (Dobbelaere et al., 2008). 2 to 2.5 hr old embryos laid by these flies do not express any detectable Cep97 protein (Fig 5.5A). Remarkably, in embryos laid by *Cep97*$^{-/-}$ *; NG-Asl* flies (hereafter referred to as *Cep97*$^{-/-}$ embryos) centrioles appear to have a high proportion of Bar-oriented centrioles (Fig. 5.5B, Movie7). The increase in Bar-oriented centrioles is also reported by Centrilyze, which shows that the proportion of Bar-oriented centrioles increases at the expense of Ring centrioles, which decrease (Fig. 5.5C). Not only did the proportion of Bar-oriented centrioles increase, but their stability also increased. Notably, of all orientation states, only the stability of Bar-oriented centrioles increased, while the stability of other orientations remained similar to WT controls (Fig. 5.5D). Montages of individual centrioles over time also show a greater proportion of centrioles are Bar-oriented, and these Bar-oriented centrioles are less likely to flip up into a Ring orientation as compared to WT controls (Fig 5.5E). These results strongly indicate that in *Cep97*$^{-/-}$ embryos, centrioles have more of a preference to be stably oriented as Bars, side-on to the cell cortex, as

compared to Rings (Fig. 5.5F). I hypothesise that the presence of Cep97, perhaps in complex with CP110, may bind to an unknown component that establishes distally oriented, Ring-oriented centrioles as a default state, such that if centrioles are putatively pulled out of distal orientation by MT forces, a mechanism employed by Cep97 allows centrioles to tend back to a Ring-oriented state.

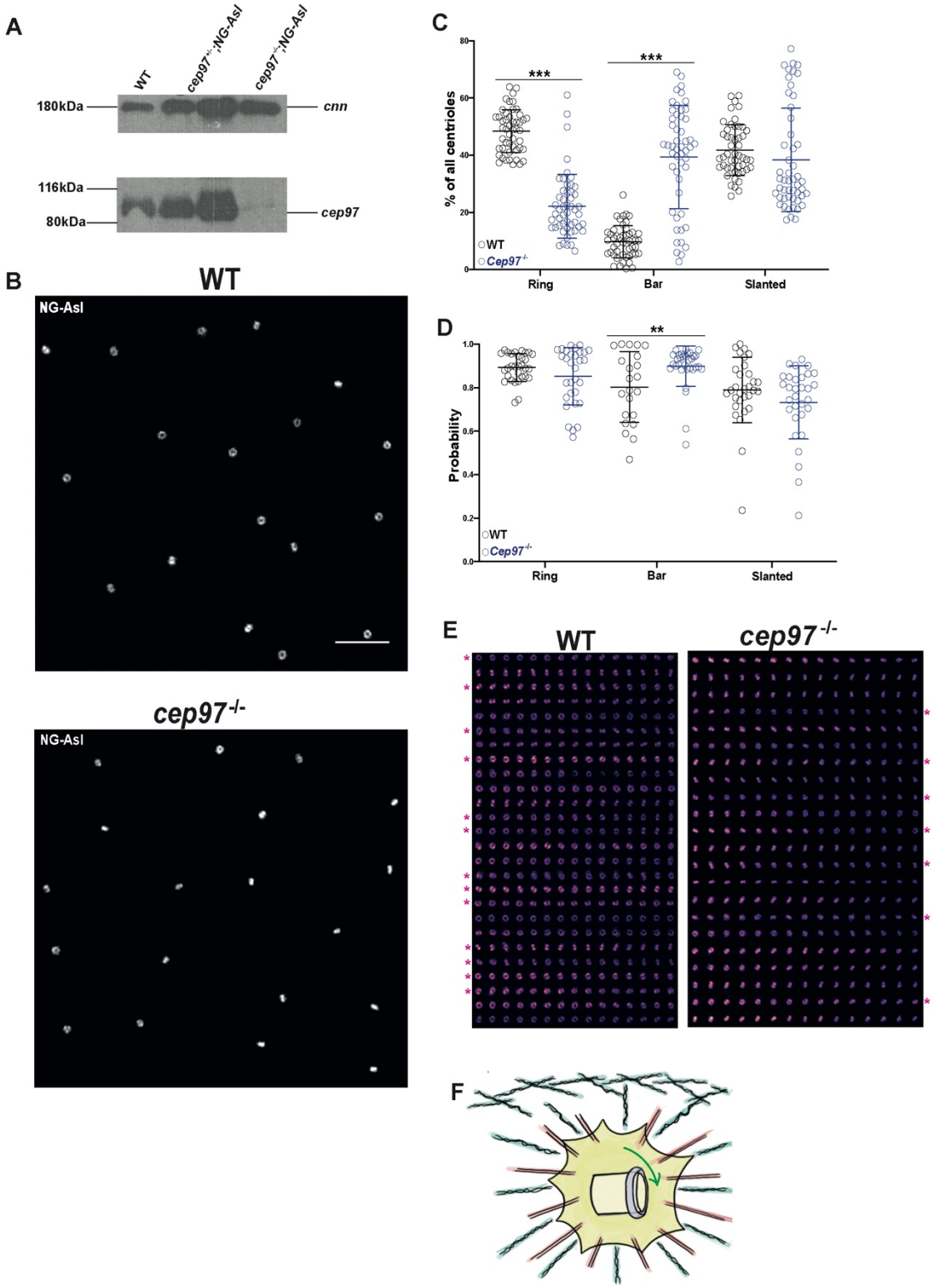

Figure 5.5. Cep97 is implicated in Ring-oriented centrioles

(A) Western blot showing that *;Cep97*$^{-/-}$ embryos do not produce Cep97 protein. The leftmost lane shows WT positive control, both middle lanes show a *Cep97*$^{+/-}$ heterozygous deletion which has moderate Cep97 signal and the rightmost lane shows *;Cep97*$^{-/-}$ embryos with minimal enrichment in Cep97 signal. Cnn is shown as a loading control. N = 2. **(B)** Z-projected images of centrioles from either WT or *Cep97*$^{-/-}$ embryo expressing NG-Asl. Centrioles in *Cep97*$^{-/-}$ embryos appear disorganised with a higher proportion of Bar-oriented centrioles. Scale bar = 3µm. **(C)** Scatter plot shows the mean (±SD) of the proportion of centrioles in Ring, Bar or Slanted orientations expressed as a percentage of total number of centriole images in WT (*black*) as compared to *Cep97*$^{-/-}$ (*blue*) embryos. Each open circle represents the proportion of centrioles in the

orientation state shown on the x-axis for one embryo. **(D)** Scatter plot shows the mean (±SD) stability of centrioles in WT (*black*) as compared to *Cep97*$^{-/-}$ (*blue*) embryos. Each open circle represents the stability of the orientation state indicated on the x-axis for one embryo. (C, D) Data analysed using multiple unpaired t-tests. **=p<0.01, ***=p<0.001. Data pooled from 3 independent experiments. N = 10-15 embryos per experimental repeat; n≥40 centrioles per embryo. **(E)** Timelapse montages of centriole images in one WT (left) or *Cep97*$^{-/-}$ (right) embryo. Each row shows same centriole at successive timepoints (20 sec intervals). *Pink* asterisks indicate centrioles which clearly change orientation at some point during the movie. **(F)** Illustration coloured as in Fig 5.3E showing centrioles falling over into a Bar orientation in the absence of Cep97 (*green* in Fig. 5.3E) as indicated by a *green* arrow.

This hypothesis is in line with observations in both Colchicine-injected embryos and *cnn*^{f} embryos, which show that the proportion of Ring centrioles increases when forces acting on centrosomes are decreased by the depletion of MTs. Conversely, when inertia is lowered for centrioles to change orientation in *cnn*^{f} embryos, centrioles may change orientations more frequently, but Ring-oriented centrioles remain as the preferred state, suggesting that there is a mechanism that tends to bring centrioles back to a Ring orientation when they are pulled out of this orientation state.

5.2.3.2. Orientation is only moderately affected in CP110 mutants

CP110 is a highly conserved protein present at the distal ends of *Drosophila* centrioles and makes up part of the distal cap alongside Cep97 (Paintrand et al., 1992). Removal of CP110 is essential for ciliogenesis in vertebrate cells (Spektor et al., 2007; Tsang et al., 2008; Walentek et al., 2016), however in mice defects in CP110 have also been associated with lack of cilia and ciliopathy phenotypes, suggesting that the roles of CP110 in ciliogenesis lie beyond inhibition (Walentek et al., 2016; Yadav et al., 2016). Despite this, *CP110*$^{-/-}$ *Drosophila* are viable with minimal ciliogenesis defects (Franz et al., 2013), making *Drosophila* an ideal system to study its function. CP110 together with Cep97 also regulate centriole length (Aydogan et al., 2022; Schmidt et al., 2009), in *Drosophila* embryos in particular, centrioles are slightly shortened in the absence of CP110 (Franz et al., 2013). However, in our hands this modest decrease in centriole length does not appear to significantly change the shape or fluorescence intensity of centrioles when viewed at the SoRa or 3D-SIM (Aydogan et al., 2022; Gartenmann et al., 2017). Given that the absence of Cep97 had such a significant effect on centriole orientation, I hypothesised that depleting CP110 may similarly increase the proportion of stably oriented Bar-oriented centrioles.

To investigate how CP110 may regulate centriole orientation I crossed flies with a CP110 deletion with flies expressing NG-Asl to obtain flies with the genotype *CP110*$^{-/-}$ *;; NG-Asl* (Dobbelaere et al., 2008). 2 – 2.5 hr

old embryos laid by these flies do not express any CP110 protein (Fig 5.6A). In embryos laid by *CP110*$^{-/-}$ *;; NG-Asl* flies (hereafter referred to as *CP110*$^{-/-}$ embryos), I rarely observed centrioles clearly organised in old mother and new mother pairs (Fig 5.6B). However, centrioles are still able to divide as normal as has been previously described (Aydogan et al., 2022; Franz et al., 2013). This observation is consistent with previous studies showing that CP110 is dispensable for embryo development (Franz et al., 2013). Embryos laid by *CP110*$^{-/-}$ *;; NG-Asl* flies also showed a significant increase in the proportion of Bar-oriented centrioles and a corresponding moderate, but not statistically significant, decrease in the proportion of Slanted centrioles (Fig. 5.6C). However, the proportion of Ring centrioles did not change between *CP110*$^{-/-}$ embryos and controls, as it did in *Cep97*$^{-/-}$ embryos (Fig. 5.6C). Like in *Cep97*$^{-/-}$ embryos, the stability of Bar-oriented centrioles also increases significantly (Fig. 5.6D). The increase in Bar centriole stability is in line with the decrease in proportion of Slanted centrioles as Bar-oriented centrioles are likely transitioning less through the Slanted state. This quantification appears consistent with observational data, which shows that centrioles in *CP110*$^{-/-}$ embryos are more likely to appear as Bars and remain as Bars for the entire duration of the movie, whilst in WT controls, Bar-oriented centrioles appear more likely to flip into a Ring-oriented state (Fig. 5.6E, Movie8). Taken together, my results suggest that any potential mechanisms holding centrioles in a preferential Ring orientation have been somewhat disrupted in *CP110*$^{-/-}$ mutants such that some centrioles have adopted a Bar-oriented, side-on orientation and do not easily flip back up into a Ring orientation (Fig. 5.6F).

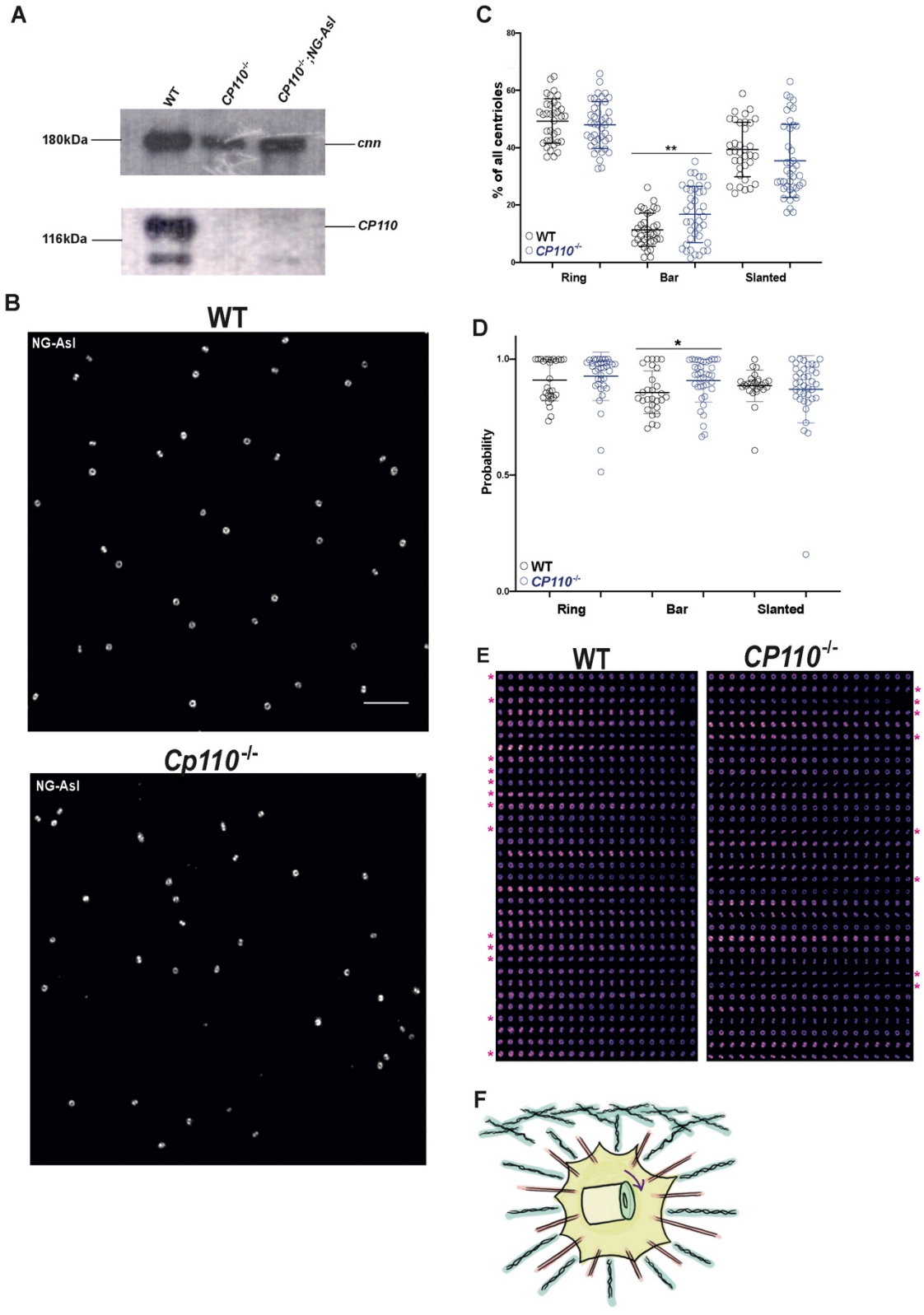

5.6. Orientation is only moderately affected in CP110 mutants

(A) Western blot showing that *CP110*$^{-/-}$ embryos do not produce CP110 protein. The leftmost lane shows a WT positive control, the middle lane shows a *CP110*$^{-/-}$ negative control and the rightmost lane shows *CP110*$^{-/-}$ embryos. Both middle and right lanes show no significant CP110 signal. Cnn is shown as a loading control. N = 2. **(B)** Z-projected images of centrioles from either a WT or *CP110*$^{-/-}$ embryo expressing NG-Asl. Centrioles in *CP110*$^{-/-}$ embryos appear disorganised. Scale bar = 3µm. **(C)** Scatter plot shows the mean (±SD) of the proportion of centrioles in Ring, Bar or Slanted orientations expressed as a percentage of total number of centriole images in WT (*black*) as compared to *CP110*$^{-/-}$ (*blue*) embryos. Each open circle

represents the proportion of centrioles in the orientation state shown on the x-axis for one embryo. **(D)** Scatter plot shows the mean (±SD) stability of centrioles in WT (*black*) as compared to *CP110*$^{-/-}$ (*blue*) embryos. Each open circle represents the stability of the orientation state indicated on the x-axis for one embryo. (C, D) Data analysed using multiple unpaired t-tests. *=p<0.05; **=p<0.01. Data pooled from 3 independent experiments. N = 10-15 embryos per experimental repeat; n≥40 centrioles per embryo. **(E)** Timelapse montages of centriole images in one WT (left) or *CP110*$^{-/-}$ (right) embryo. Each row shows same centriole at successive timepoints (20 sec intervals). *Pink* asterisks indicate centrioles which clearly change orientation at some point during the movie. **(F)** Illustration coloured as in Fig 5.3E showing centrioles falling over into a Bar orientation in the absence of CP110 (*purple* in Fig. 5.3E) as indicated by a *purple* arrow.

5.2.3.3. Addressing the difference in data from Cep97$^{-/-}$ *compared to CP110*$^{-/-}$ *embryos*

CP110 and Cep97 are commonly known to function as a complex. However, despite similar trends across both mutants, centrioles in *Cep97*$^{-/-}$ embryos show much more dramatic changes in centriole orientation and stability as compared to *CP110*$^{-/-}$ embryos. I also noticed that centrioles in *Cep97*$^{-/-}$ embryos appeared slightly smaller compared to those in *CP110*$^{-/-}$ embryos. To test this hypothesis, I measured the radii of 20 Ring-oriented centrioles in *Cep97*$^{-/-}$ and *CP110*$^{-/-}$ embryos as compared to WT controls. These plots show that the diameter of the centrioles in *Cep97*$^{-/-}$ embryos is smaller than centrioles in *CP110*$^{-/-}$ or control embryos (Fig. 5.7A, B). This is possibly due to the change in position of NG-Asl due to the loss of Cep97. As mentioned previously, Asl is ~150 nm in length and the diameter of *Drosophila* centrioles is typically 250 nm. Thus, shifts in how NG-Asl is positioned may significantly affect centriole diameter. As centrioles in *Cep97*$^{-/-}$ embryos are smaller, there is an increased level of fluorescence signal in the centre of Rings. As mentioned in Chapter 4, these features make the absence of fluorescence in the centre of Ring-oriented centrioles more difficult to identify (Fig. 4.3B), thus making it more difficult to manually determine if centrioles are Rings. This could potentially explain, at least in part, why the proportion of Ring-oriented centrioles is reduced in the *Cep97*$^{-/-}$ embryos.

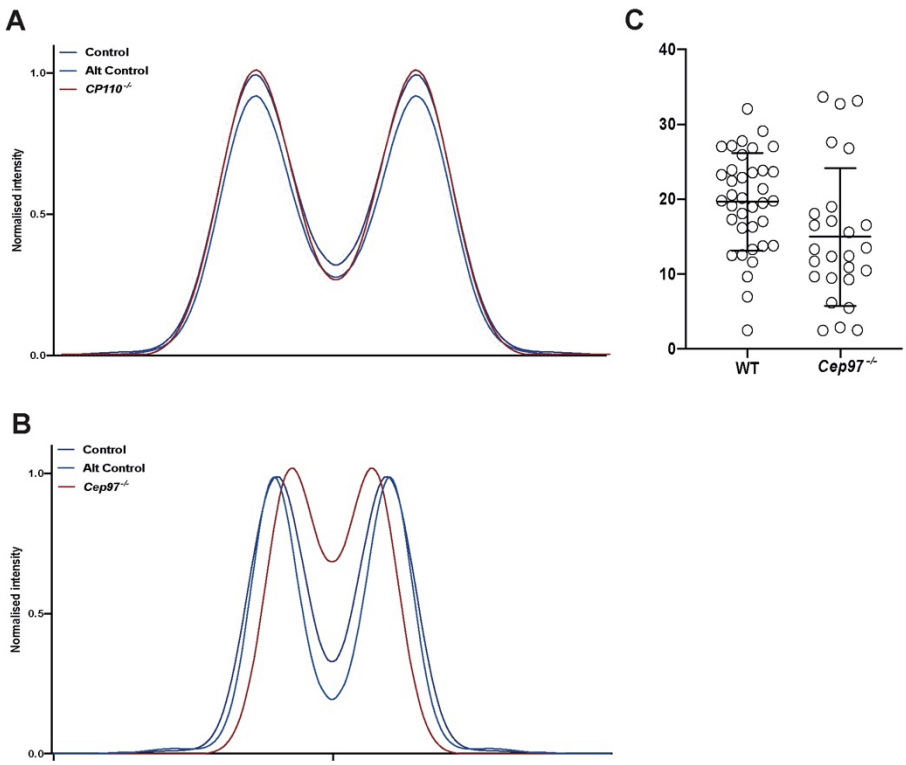

5.7 Addressing the difference in data from Cep97$^{-/-}$ compared to CP110$^{-/-}$ embryos

(A) Graph shows the radial profiles of Ring-oriented centrioles in *CP110*$^{-/-}$ embryos (*red*) as compared to two independent sets of WT control embryos (*dark blue* and *bright blue*). **(B)** Graph shows the radial profiles of Ring-oriented centrioles in *Cep97*$^{-/-}$ embryos (*red*) as compared to two independent sets of WT control embryos (*dark blue* and *bright blue*). (A,B) Graph was generated by measuring the fluorescence intensity at 70 points from the centre of Ring-oriented centrioles with background subtracted. n = 20 Ring-oriented centrioles per condition. **(C)** Scatter plot shows the mean (±SD) of the proportion of centrioles in the Unidentified orientation category, not included in quantifications of orientation shown in Fig. 5.5C, expressed as a percentage of total number of centriole images in WT (left) as compared to *Cep97*$^{-/-}$ (right) embryos. Each open circle represents the proportion of centrioles for one embryo. N = 10-20 embryos; n≥40 centrioles per embryo.

If the decrease in centriolar radius impacted Centrilyze's ability to categorise Ring-oriented centrioles, however, then it would presumably be placing rightfully Ring centrioles into the Unidentified or Slanted category, as those are the categories with the highest error rates for Ring-oriented centrioles (Fig. 4.5D). However, the proportion of centrioles in these categories is not significantly different between *Cep97*$^{-/-}$ embryos and WT controls (Fig. 5.7C, Fig. 5.5C). Furthermore, it is highly unlikely that Ring-oriented centrioles would be mis-sorted as Bar-oriented centrioles, as the probability of error between Ring and Bar-oriented centrioles is very low at <0.01 (Fig. 4.5D). Therefore, Ring-shaped centrioles would have to be near unrecognisable to be mis-sorted as Bars, which is not the case in *Cep97*$^{-/-}$ embryos where Ring-oriented centrioles still appear as Rings, albeit smaller than in WT centrioles. While it may be more difficult to categorise centriole orientation by eye, the decrease in centriole radius seems unlikely to significantly affect

the ability of Centrilyze to effectively categorize Ring-oriented centrioles in *Cep97*$^{-/-}$ embryos, effectively underlining the utility of an ANN to categorize centriole orientation data.

It is unknown why the proportion of stable Bar-oriented centrioles increases more dramatically in *Cep97*$^{-/-}$ compared to *CP110*$^{-/-}$ embryos. However, previous data has shown that in flies, Cep97 mutants seem to show more severe phenotypes compared to CP110 (Delgehyr et al., 2012; Dobbelaere et al., 2020). As a whole, *Cep97*$^{-/-}$ flies are more uncoordinated and also show ciliogenesis defects, whereas *CP110*$^{-/-}$ flies are healthier and more viable (Delgehyr et al., 2012; Dobbelaere et al., 2020; Franz et al., 2013). In the future, a complementation experiment should be performed on *Cep97*$^{-/-}$ embryos to assess if introduction of exogenous Cep97 is capable of reversing the phenotype observed in *Cep97*$^{-/-}$ embryos. It would also be interesting to generate *CP110*$^{-/-}$*; Cep97*$^{-/-}$ *; NG-Asl* embryos and investigate if the increase in Bar-oriented centrioles is additive. Taken together, while the preference for centrioles to be Bar-oriented in *Cep97*$^{-/-}$ embryos is very striking, the milder phenotypes seen with its well-studied binding partner CP110, led me to believe that regulation of centriole orientation via distal cap proteins is more complicated than initially expected, and further experiments would need to be performed in order to make detailed conclusions about the effects of Cep97 and CP110 on centriole orientation.

5.3. Discussion

In this chapter I use Centrilyze to quantify centriole orientation and stability in drug-injected embryos as well as embryos from various mutant fly lines to investigate how lack of cytoskeletal networks, PCM or distal end proteins affects centriole orientation. Quantification by Centrilyze appears broadly consistent with observed trends in centriole orientation seen at the microscope. This shows that Centrilyze is able to accurately categorize centriole orientation close to how I would quantify centrioles manually, even in mutant embryos where the embryo and thereby the centrosomes may be less healthy. By comparing changes in proportions of Ring, Bar and Slanted centrioles as well as their stability over time, I infer how different centrosome components may be part of an overall centriole orientation mechanism.

5.3.1. The subtle effects of actin depletion on centriole orientation and stability

In *Drosophila* embryos, centrosomes regulate cell shape and size by positioning actin. *Drosophila* embryos are syncytial and cellularise at cycle 14 in their development. The size and shape of the eventual cells are determined by the positions of cortical actin caps that form actin-based cleavage furrows in mitosis (Foe et al., 2000; Lv et al., 2021; Riggs et al., 2003; Stevenson et al., 2001). However, my analysis shows that a lack of actin filaments does not significantly affect centriole orientation and only mildly affects stability, exemplified by centrioles flipping more often between the Ring and Bar states through the Slanted state (Fig. 5.2B, C).

I initially hypothesised slight reduction in stability could be due to the increased amount of MTs at the centrosome in response to the reduction in actin, as has been demonstrated in other systems (Farina et al., 2019; Inoue et al., 2019). However, studies in *Drosophila* embryos have not documented a compensatory effect between MTs and actin. Instead, they show that MT asters and the PCM are not significantly perturbed in the absence of actin (Lv et al., 2021; Telley et al., 2012). MTs have also been shown to rely on actin to position centrioles in *Drosophila* (Jimenez et al., 2021; Ojas et al., 2021; Telley et al., 2012). The slight but significant decrease in stability of Cytochalasin-injected embryos could be related not to an increased amount of MTs, but more disorganised push and pull forces from existing MTs in the absence of actin as they attempt to move centrioles into position. This is exemplified perhaps by how centrioles remain close to the cell

cortex, but tend to cluster together in the absence of actin (Fig. 5.2A). Additionally, data from *cnn*^{f} embryos suggest that the PCM may be providing inertia which increases the stability of centrioles by increasing the amount of force needed for centrioles to change orientation. Taken together, the absence of actin for MTs to pull upon resulting in more disorganised MT forces, together with the presence of PCM increasing inertia for centriole orientation to change, collectively may be the reason for the relatively subtle effects of the lack of filamentous actin on changes in centriole orientation and stability.

I have suggested above that the subtle changes to centriole orientation and stability in absence of actin may be due to compensatory effects from other forces acting on the centriole, such as that of MTs and inertia from the PCM. In contrast, it is also possible that centrioles are somehow anchored to the cell cortex through interaction with distal cap proteins like Cep97 and the depletion of actin does not significantly perturb this anchorage. This latter hypothesis would also explain why proportions of centrioles oriented as Rings, Bars and Slanted do not change significantly in Cytochalasin-injected embryos. However, given that the stability of Bar and Slanted centrioles decreases, it is most likely that changes in centriole orientation upon actin depletion are due to a combination of both compensatory forces and an unknown, but intact, anchorage mechanism.

It may also be possible that the concentration of Cytochalasin injected was too low to sufficiently perturb the actin-cytoskeleton and so affect centriole orientation in embryos. In the future, Cytochalasin should be injected into embryos with a fluorescent actin marker in order to observe the extent of actin depletion in tandem with any changes in centriole dynamics. Higher concentrations of Cytochalasin could also be injected to investigate if these trends correlate to increasing concentrations of Cytochalasin. It would also be useful to inject Cytochalasin into embryos expressing a fluorescent MT marker such as Jupmch to identify if MTs do increase and exert more disorganised forces on centrosomes as compared to 10% DMSO-injected controls. Alternatively, another actin depleting drug that is not dissolved in DMSO could be used, as it is possible that low, non-toxic levels of DMSO could have some effect on centriole positioning and orientation (Cabrita et al., 2022; Dobbelaere et al., 2020).

5.3.2. The effect of centriole movement on the stability of centriole orientation in *cnn*^{f} embryos

Even though Colchicine-injected embryos show that the presence of MTs does contribute to destabilising centrioles over time (Fig. 5.1E, F), I find that a lack of Cnn may destabilise centriole orientation in a manner at least partially independent from the effects of asymmetric MTs. To this end I injected *cnn*^{f} embryos with Colchicine which reduced the movement of centrioles as previously reported (Fig. 5.4) (Lucas and Raff, 2007). These embryos are predictably very sick, and so not many samples were able to be imaged per experiment. Of those that were, centriole stability was unchanged between Colchicine- and Buffer-injected *cnn*^{f} embryos (Fig. 5.4B), suggesting that at least some of the decrease in stability seen in *cnn*^{f} embryos was due to the lack of Cnn and not an effect of MT forces. However, decrease in stability could still be due to the lack of PCM, and not lack of Cnn specifically as there may be other forces in the cytoplasm that may be indirectly changing centriole orientation. In absence of inertia provided by the PCM, the act of injection itself could provide enough cytoplasmic flow to change centriole orientation. In the future, a more precise way to test this association would be to use a CM1 mutant of Cnn which maintains Cnn's scaffolding ability in interphase but decreases MT nucleation from centrosomes as the CM1 domain binds the γ-TuRC MT nucleator (Choi et al., 2010; Fong et al., 2008).

5.3.3. The discrepancy between Cep97$^{-/-}$ and CP110$^{-/-}$ embryos

I showed that in *Cep97*$^{-/-}$ embryos, the proportion of Bar-oriented centrioles greatly increases. The stability of Bar-oriented centrioles also increased as the stability of other orientations stayed the same. These results put forward an exciting possibility that Ring-oriented centrioles are the default orientation, and when centrioles lack a distal cap, centrioles are unable to efficiently maintain a Ring-oriented orientation, they then fall into a Bar-oriented state and are unable to reorient into a Ring.

However, results from depleting the other distal cap protein, CP110, while following similar trends, were much more modest compared to those obtained in *Cep97*$^{-/-}$ embryos despite both showing minimal production of CP110 and Cep97 protein respectively (Fig. 5.5A, 5.6A). This is in conflict with previously published data showing that CP110 and Cep97 act as a complex during centriole length regulation and

ciliogenesis (Aydogan et al., 2022; Prosser et al., 2022; Spektor et al., 2007). Moreover, CP110 is better studied compared to Cep97 and presumably has a greater effect on membrane docking compared to Cep97, so much so that removal of CP110, not Cep97, is known as a hallmark of ciliogenesis (Bettencourt-Dias and Carvalho-Santos, 2008; Kobayashi et al., 2011; Schmidt et al., 2009; Song et al., 2014; Spektor et al., 2007; Tsang et al., 2008; Tsang and Dynlacht, 2013). Like in other systems, CP110 and Cep97 are shown to be co-regulated in *Drosophila,* suggesting that either the *Cep97*$^{-/-}$ embryos used in this thesis have other unknown defects that affect centriole orientation, or that in the context of centriole orientation, CP110 and Cep97 have different functions. However, some published data in *Drosophila* show that *Cep97*$^{-/-}$ flies are uncoordinated with ciliopathy-like defects and deformed cilia (Dobbelaere et al., 2020). In contrast, *CP110*$^{-/-}$ flies appear healthier with no ciliogenesis-related defects (Delgehyr et al., 2012; Franz et al., 2013; Martinez-Campos et al., 2004), supporting my observation that centrioles in *Cep97*$^{-/-}$ flies have a smaller radius (Fig. 5.7B).

One of those functions may be the establishment of centriole orientation, however, it is unlikely that Cep97 alone facilitates Ring orientation of centrioles. Conversely, CP110 has been previously shown to associate with Rab11 endosomes which are recruited to the site of ciliogenesis to aid in IFT in vertebrate cells (Hehnly et al., 2012; Kobayashi et al., 2011). In the *Drosophila* embryo, there are large Rab11 endosomes close to the cell cortex that aid in development, cortex polarity and orientation of the mitotic spindle (Calero-Cuenca and Sotillos, 2018; Riggs et al., 2003; Roeth et al., 2009). It is possible that CP110 at the distal end of centrioles in embryos contact Rab11 endosomes, thus leading to Ring-oriented centrioles. Such an association would be consistent with Rab11's other roles given that centrosomes have also been implicated in cell polarity, especially when positioned close to the cell cortex (Carvajal-Gonzalez et al., 2016a; Solecki et al., 2009; Stinchcombe et al., 2006). Cep97 is important in this association as its depletion results in destabilisation of CP110 at the centriole due to being outcompeted by other untimely CP110 removal proteins (Song et al., 2022).

Given the complex roles of CP110 in membrane docking and ciliogenesis, especially across species (Delgehyr et al., 2012; Kobayashi et al., 2011; Schmidt et al., 2009; Spektor et al., 2007; Tsang et al., 2008; Walentek et al., 2016; Yadav et al., 2016), depletion of CP110 may have milder effects on orientation than Cep97 as the contradictory effects of CP110 removal (in ciliogenesis it is an inhibitor yet also required for

ciliogenesis to occur) may be compensatory in embryos, whereas the main function of Cep97 as we know it is to position CP110. Thus, depletion of Cep97 has more straightforward effects on processes involving the distal cap such as potentially centriole orientation. Perhaps as more is uncovered about the functions of Cep97, we can make further conclusions as to how it may act in determining the orientation of centrioles in non-ciliated epithelia such as the embryo.

5.3.4. Ring-oriented centrioles are the default state

Throughout different drug injections and mutations, my data is broadly consistent with the initial hypothesis that mature mother centrioles are preferentially oriented in a Ring-oriented state. When MTs which exert pulling forces on centrioles are perturbed by Colchicine injection, the proportion of centrioles in a Ring-oriented state increase (Fig. 5.1C), suggesting that centrioles prefer to be oriented as Rings in the absence of external forces. Conversely, in *cnn*^{f} embryos where MTs could perhaps more easily cause changes in centriole orientation due to a decrease in inertia around centrioles, centrioles are more likely to be pulled into a Slanted than Bar-oriented state (Fig. 5.3C), suggesting that the latter is the furthest from its default Ring orientation.

It is likely that Ring-oriented orientation of embryo centrioles is facilitated by distal cap proteins CP110 and Cep97. When either are mutated, the proportion and stability of Bar-oriented centrioles increases (Fig. 5.5C, D; 5.6C, D), suggesting that not only are centrioles losing their Ring-oriented orientation, but they are also less able to tend back towards a Ring-oriented state in the absence of a distal cap. Moreover, I have previously observed that new mother centrioles tend to exhibit a Bar orientation and at some point in S-phase, typically flip up into a Ring-oriented state. This may be concurrent with the loading of CP110 and Cep97, which have previously been shown to time their loading with the cell cycle (Aydogan et al., 2022). It is possible that the onset of CP110 and Cep97 loading primes centrioles for being oriented as a Ring, thus in the absence of CP110 or Cep97, centrioles fall back into a Bar-oriented state similar to new mother centrioles at the start of S-phase. However, by the start of S-phase, CP110 and Cep97 are already loaded onto the centriole, suggesting further steps may be required in order to establish a Ring orientation.

5.3.5. A preliminary model for centriole orientation

On the basis of my results, I would like to propose a preliminary model for centriole orientation in *Drosophila* embryos (Figure 5.8A, B). Previous data in vertebrates has shown that CP110 is important in maintaining centriole docking in ciliated cells (Yadav et al., 2016), and that distal cap proteins can remain present while centrioles are docked, as seen in vertebrate IS formation (Stinchcombe et al., 2015; Tsun et al., 2011). Moreover, Cep97 has been shown to play roles in cilia integrity and centriole docking during ciliogenesis in multiple organisms (Dobbelaere et al., 2020; Lee et al., 2022; Nagai et al., 2018). Therefore, despite the differences in severity of centriole orientation changes between *Cep97*$^{-/-}$ and *CP110*$^{-/-}$ embryos, taken together I believe that Cep97, and probably to some extent CP110, play a role in maintaining Ring-oriented centriole orientation via attachment to the cell cortex by some unknown mechanism (Fig. 5.8A). In *CP110*$^{-/-}$ or *Cep97*$^{-/-}$ embryos, not only did the proportion of Bar-oriented centrioles increase at the expense of Ring-oriented centrioles (particularly in *Cep97*$^{-/-}$ embryos) (Fig. 5.5D, 5.6D), but the stability of Bar-oriented centrioles also increased (Fig. 5.5E, 5.6E), suggesting that any mechanism that is in place to help centrioles flip up into a Ring-oriented state, or to be maintained in that state, has been perturbed. Meanwhile, forces generated by MTs nucleated by the PCM may be indirectly pulling centrioles out of a Ring orientation into other orientations. This change is gradual due to the inertia exerted by the PCM (Fig. 5.8B). In conditions that reduce pulling forces on centrioles such as in Colchicine-injected embryos (Fig. 5.1A, B), the proportion of Ring-oriented centrioles increases as MTs are not pulling on centrioles (Fig. 5.1E, F).

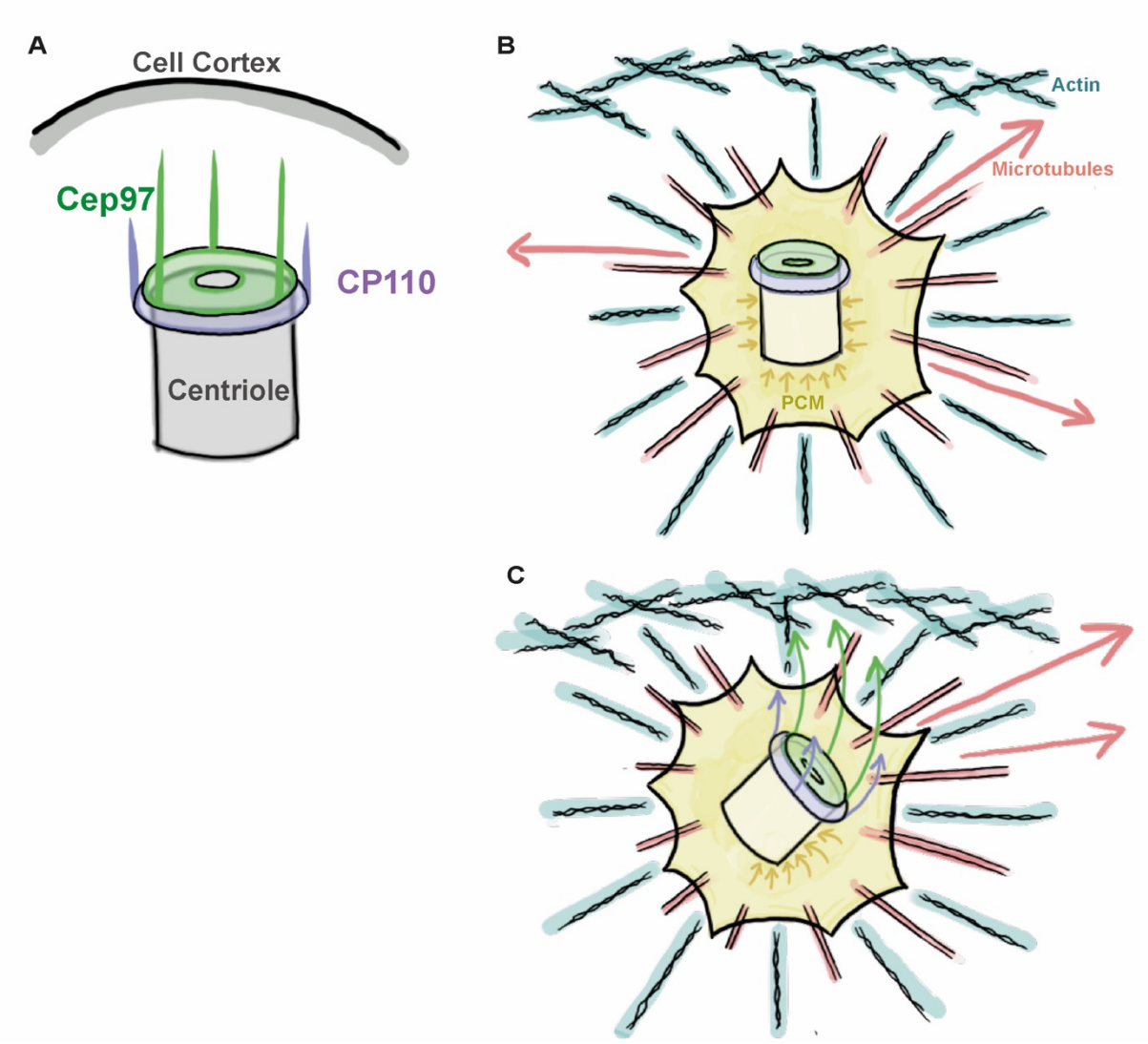

5.8. A Putative Centriole Orientation Mechanism

(A) Illustration showing a centriole with its distal end facing the cell cortex (*gray*). Distal cap proteins CP110 (*green*), Cep97 *(purple*) are present at the distal end. Extensions towards the cell cortex represent potential interactions or attachments from Cep97 and CP110 with the cell cortex (*green* and *purple* respectively). Extensions are longer from Cep97 as centrioles in *Cep97*$^{-/-}$ embryos showed more dramatic changes in orientation and stability as compared to centrioles in *CP110*$^{-/-}$ embryos. **(B)** Top panel illustration showing a centriole coloured as in (A) with pericentriolar material (*yellow*), MTs (*pale red*) and actin (*blue*). Potential direction of forces exerted by MTs shown by *pale red* arrows while inertia provided by an intact PCM is shown by *yellow* arrows. Bottom panel shows illustration as above showing forces generated by MTs (*pale red* arrows) pulling centrioles into a Slanted orientation gradually due to inertia exerted by the PCM (*yellow* arrows). Meanwhile, a putative centriole orientation mechanism facilitated by mainly by Cep97, aided by CP110 allows centrioles to tend back to their preferred orientation state (*green* and *purple* arrows respectively).

Moreover, in *cnn*^{f} embryos where centrosomes do not have a properly formed PCM, asymmetric MT forces from residual PCM cause a decrease in centriole stability (Fig. 5.3.D), likely because centrioles were in a state where MT pulling forces could more easily perturb centriole orientation (Fig. 5.3E). Yet, centrioles still tended back to the Ring-oriented state, as shown by how the proportion of Ring-oriented centrioles was unchanged between *cnn*^{f} and WT embryos (Fig. 5.3C), suggesting that Rings are the default centriole

orientation. Taken together, in WT embryos, centrioles are in a preferential Ring-oriented state, but do change orientation due to pulling forces exerted by MTs to position centrioles throughout nuclear divisions. Change in orientation is often gradual due to the presence of the PCM providing increased inertia to tilting forces. Finally, the presence of the distal cap formed of CP110 and Cep97 are part of a putative centriole orientation mechanism that maintains centrioles in a Ring orientation, but also allows centrioles to tend back to this orientation when perturbed by surrounding forces (Fig. 5.8C).

6 Discussion

6.1. Summary of Key Findings

The Raff lab initially observed that the majority of centrioles in syncytial *Drosophila* embryos appear as rings (Fig. 3.1A, B). This was an unusual phenomenon as embryos do not produce cilia. Moreover, DAPs, which are typically responsible for docking centrioles to the cell membrane (Stinchcombe et al., 2015; Tanos et al., 2013), are mostly not conserved in *Drosophila* and those that show some sequence homology with *Drosophila* proteins are dispensable for their original function (Hodges et al., 2010; Hou et al., 2023; Tischer et al., 2021). I found that centrioles in syncytial fly embryos do have a preferred orientation by using differential fluorescence labelling to measure the relative position of the distal end of centrioles with respect to the centriole midpoint (Fig. 3.2A, 3.3B). Taking into account chromatic aberration (Fig. 3.2B), I find that the distal end is consistently closer to the cell cortex as compared to the centriole midpoint (Fig. 3.3C), suggesting that centrioles have a preferred, distal-ended orientation, much like in ciliated cells (Fig. 3.3D).

With this in mind, I sought to develop a live-assay in order to robustly quantify this inherently subjective measure. I find that the microscope used to capture centrioles ultimately leads to a conservative estimate of the proportion of centrioles that are oriented as Ring (Fig. 4.3C, D). However, this was a trade-off for being able to image centrioles over time, as a higher resolution microscope would be too light hungry. I worked with a collaborator to establish an ANN in order to automate quantification, allowing high-throughput, accurate analysis of centriole orientation throughout multiple experiments. Once a network with a satisfactory error rate (<0.05) was established (Fig. 4.5C), called Centrilyze, we also used it to calculate the stability of centrioles. We find that not only do many centrioles exhibit a distal-ended, Ring orientation, but these Rings tend to also be highly stable and unlikely to change orientation over the 5 - 6 minutes in S-phase during which they were imaged (Fig. 4.6B).

I then use Centrilyze to quantify the centriole orientation and stability between embryos treated with different cytoskeletal depolymerising drugs. Reduction of MTs using Colchicine led to a moderate increase in stability

(Fig. 5.1D, E, F). In contrast, reduction of actin-filaments using Cytochalasin led to a relatively subtle decrease in stability (Fig. 5.2. D, E) From these results I concluded that MTs are likely the main force-generator acting on centrosomes, consistent with other published data. Push and pull MT forces acting on centrosomes (which are connected to the centrioles themselves) may then be indirectly changing centriole orientation. By quantifying centriole orientation and stability in cnn^{f} embryos, I found that general changes in orientation tend to be gradual, perhaps due to inertia provided by the PCM (Fig. 5.3C, D, E). However, there may also be some intrinsic role for Cnn in maintaining centriole stability that has yet to be uncovered (Fig. 5.4).

Investigations into the roles of distal cap proteins CP110 and Cep97 yielded the most clear-cut results. In the absence of Cep97, Bar-oriented centrioles became the preferred centriole orientation as compared to Rings in WT controls (Fig. 5.5C), the increased stability of Bar-oriented centrioles also suggested that in WT controls Rings were the default state and in the absence of Cep97, Bar-oriented centrioles were unable to tend back to a Ring orientation (Fig. 5.5D, E). However, while data from $CP110^{-/-}$ embryos appears consistent with $Cep97^{-/-}$ embryos, $CP110^{-/-}$ embryos showed comparatively milder changes in orientation and stability (Fig. 5.6C, D). Therefore, while it is likely that both distal cap proteins play a role in maintaining the preferred, upright and distal-ended orientation of centrioles, additional experiments will need to be performed in order to make detailed conclusions regarding the role of Cep97, and potentially CP110, in maintaining centriole orientation.

6.2. Quantifying highly subjective measurements

The central phenotype quantified throughout this thesis, centriole orientation, is an inherently subjective measure. As centrioles change orientation between Rings and Bars, different researchers will define a Ring in different ways, and indeed some centrioles within the Slanted category may appear as Rings or Bars to other people. I acknowledge that the question of when a Ring becomes a Bar is arbitrary and my definition of this transition is but an opinion. However, I hope it is clear throughout this work that I have taken steps to minimise my subjectivity as much as possible. Reducing subjectivity was one of the reasons why Centrilyze took such a long time to develop. Throughout its development, I annotated 36,278 individual

centriole images into 6 orientation categories (some of which were later combined) (Fig. 4.4B). In addition to this, my collaborator and I also attempted to best calculate my own error rate when annotating by having me annotate a subset of images several times over the course of a week. In addition to the large sample sizes and multiple error rates, I can also assume that by using an ANN like Centrilyze to quantify data, any subjectivity employed by Centrilyze due to being based on my annotations will stay the same between quantification of multiple datasets. Centrilyze as a program does not get tired or distracted as humans do, thus, any inherent subjectivity in Centrilyze represents at worse a systematic error in calculating centriole orientation, which still enables me to observe differences in centriole orientation between different embryos.

As Centrilyze is trained on images of centrioles from WT embryos, it may be worse at categorising centrioles from mutant or drug-treated embryos. In these embryos centrioles may exhibit shapes and sizes previously unseen by Centrilyze. For example, in *cnn*^{f} embryos where centrioles move very fast (Fig. 5.3A, B), centriole images sometimes appear with shadows due to centrioles moving between Z-stacks. In theory, Centrilyze should sort any unseen centriole morphology into the Unidentified category, but as discussed previously, "Unidentified" centrioles themselves are a morphological category and is not a category that simply contains centrioles that do not match any other category. Therefore, it is possible that the error rate for all orientation categories increases as Centrilyze sorts centrioles from non-WT embryos. Because of this, my collaborator and I have considered training Centrilyze using mutant centriole data as well as WT data, thus potentially making Centrilyze better at categorising centrioles from the mutants it is trained on. However, this would narrow the usage of Centrilyze as an ANN (Kriegeskorte and Golan, 2019), and would lead to the researcher then having to manually annotate a new training dataset for every new mutant or embryo condition passed through Centrilyze, making it inefficient as a method to automate quantification. Instead, we hope that the storied robustness of the Resnet18 network architecture used would allow ample generalisation of the network towards centrioles from mutant embryos (He et al., 2016), as has been shown in consistent error rates between WT and considerably smaller centrioles from *Cep97*$^{-/-}$ embryos.

As a biologist, I believe that even as artificial intelligence continues to improve that we can and should continue to trust what our eyes can perceive, especially as we become familiar with the images we are looking at. It is for these reasons that I have attempted to include as much visual representation of my data

as possible throughout my thesis. That is not to say that quantification is not useful, especially in increasing the robustness of my datasets and to ensure repeatability of results. However, when centriole shape and size start to significantly deviate from the shapes that Centrilyze has become familiar with, using a combination of by-eye observation and ANN quantification can be helpful. Indeed, in the field of microscopy especially, being able to visually observe differences remains a powerful biological tool even as methods of quantification become more complex (Bond et al., 2022; Gartenmann et al., 2017; Reilly and Obara, 2021; Song et al., 2022; Wong et al., 2022). Thus, I hope that providing microscopy images and time-lapse montages of centrioles work together with quantified data in order to form a more nuanced picture of how centriole orientation is affected under different conditions than would be understood from quantified data alone.

6.3. Centriole orientation as an ancient function of the centriole itself

It is theorised that LECA had a centriole-like structure capable of forming flagella (Azimzadeh et al., 2012; Carvalho-Santos et al., 2011). The PCM and thus the centrosome may have evolved later, presumably to aid in centriole segregation and spindle organisation during mitotic division. These functions are indispensable to prevent genomic instability and ensure robust cell division in each cycle (Bazzi and Anderson, 2014; Domínguez-Calvo et al., 2021; Meraldi, 2016). However, plants, which do not possess centrosomes or PCM, have evolved acentrosomal mechanisms to organise the spindle and prevent genomic instability (Hamada, 2014).

Therefore, it is possible that the most ancient conserved function of centrioles is in ciliogenesis, which requires distal ended centriole orientation for axoneme extension (Azimzadeh, 2014; Marshall, 2009). In certain mammalian cell types, it was shown that removal of ciliogenesis inhibitor CP110 from cycling cells resulted in elongated centrioles related to axoneme extension (Schmidt et al., 2009; Spektor et al., 2007), showing that centrioles in non-ciliated cells may possess latent ciliogenesis-related capabilities. Thus, the

upright orientation of centrioles in the *Drosophila* embryo may be vestigial in nature and an orientation mechanism potentially in place in embryos could be relevant to how centrioles dock in ciliated cells.

There is still a lot we do not understand about how centrioles dock during *Drosophila* ciliogenesis. We know that they dock via transition fibres like in vertebrate cells (Gottardo et al., 2018; Hou et al., 2023). However, while vertebrate cells dock to the cell membrane using DAPs, this does not seem to be the case in *Drosophila.* The few DAPs that do have sequence homology with *Drosophila* proteins seem mostly dispensable for ciliogenesis. Their pattern of fluorescence also does not perfectly localise to transition fibres (Basiri et al., 2014; Hou et al., 2023; Lapart et al., 2019). Yet, transition fibres in *Drosophila* appear robust and difficult to perturb. Even when the PCM or transition zone proteins are mutated and abolish centriole docking to the cell membrane, EM images show that transition fibres are still able to form from the side or distal end of centrioles (Fig. 1.8C) (Roque et al., 2018; Vieillard et al., 2016). These observations suggest that the PCM, specialist ciliogenesis proteins, and/or proteins inherent to the centriole itself could be responsible for forming transition fibres. Notably, one study has shown that in the absence of distal cap protein Cep97 in *Drosophila* spermatocytes, centrioles are unable to maintain a docked position at the cell membrane in ciliated cells (Dobbelaere et al., 2020). *Cep97*$^{-/-}$ flies also appear somewhat uncoordinated and show some ciliogenesis defects. These results correlate with the reduction in Ring-oriented centrioles seen in the embryo. It is thus possible that mechanisms governing centriole orientation in ciliogenesis also govern centriole orientation in other non-ciliated epithelia. Therefore, understanding how centrioles may be oriented in the embryo could be a gateway to understanding centriole-to-membrane docking in many other systems.

It is also possible that any regulated centriole orientation in *Drosophila* embryos has evolved its own functionality beyond being a vestigial component of conserved ciliogenesis machinery. In many systems, including *Drosophila* embryos, centrioles are specifically positioned at the apical cell cortex. Current literature describes positioning to be important in polarised trafficking and eventual asymmetrical cell division (Cabernard and Doe, 2009; Calvo and Izquierdo, 2021; Elric and Etienne-Manneville, 2014; Januschke et al., 2011; Stinchcombe and Griffiths, 2014). However, in systems where both centriole positioning and orientation is known, orientation of the centriole itself appears to be key in polarised cell function (Stinchcombe et al., 2015; Tanos et al., 2013), for example, in IS formation in immune cells,

whereby distal-ended docking of centrioles to the cell membrane ensures directionality and amount of granzyme released from lytic granules to kill the attached APC (Stinchcombe et al., 2015; Tamzalit et al., 2020). It is possible to draw parallels between centriole positioning in IS formation with other cell types where centriole positioning is important for increased trafficking and formation of a specialised structure, such as in *Drosophila* wing-disc cells where an actin hair is formed on the apical side of each cell (Carvajal-Gonzalez et al., 2016b). In this cell type, centrioles are often positioned close to the cell cortex right below these actin-rich hairs, aided by the Fz-PCP pathway as well as cortical actin (Carvajal-Gonzalez et al., 2016b; Garrido-Jimenez et al., 2018). When the Fz-PCP pathway is mutated, actin hairs do not form and the centriole drifts away from the apical cortex (Carvajal-Gonzalez et al., 2016b). It is possible that, as in IS formation, the centriole in this cell type is positioned with its distal end facing the cortex thus using its inherent polarity not only to reliably dock to the cell membrane and maintain its position, but also to inform directionality of intracellular trafficking towards making the actin-rich hair similar to the roles of oriented centrioles at the IS.

Like in *Drosophila* wing-discs, centrioles in *Drosophila* embryos are also specifically positioned to define a specialised structure. It has been previously shown that the apical positioning of centrosomes at regulated distances from each other specify the position of actin-rich cortical caps (Foe et al., 2000; Raff and Glover, 1989), which in turn specify the position of pseudo-cleavage and cleavage furrows during nuclear divisions and cellularisation respectively (Kotadia et al., 2010). Given the interactions between centrosome MTs and cortical actin in centriole positioning and function (Buttrick et al., 2008; Inoue et al., 2019), as well as the potential for centrosomal MTs to exhibit directionality in response to centriole orientation (Liu and Huse, 2015), distally oriented, Ring centrioles at the cell cortex may be important for the formation of actin caps in addition to their position.

6.5. Future Directions

Centrilyze represents a powerful tool to understand changes in centriole orientation and stability between centrioles in embryos in different conditions. Given time, there are many more experiments I would like to perform using Centrilyze to elucidate a potential centriole orientation mechanism in *Drosophila* embryos.

6.5.1. Improving methods of actin depletion in *Drosophila* embryos

Injection of embryos with Cytochalasin showed that loss of actin had a relatively subtle effect on centriole stability (Fig. 5.2C, D, E). Future experiments should focus on injecting Cytochalasin into embryos expressing fluorescent actin to confirm that the concentration of Cytochalasin I have injected into embryos is successfully depleting actin within embryos. I would also like to inject Cytochalasin into embryos expressing a fluorescent MT marker to investigate if the increase in MT-mediated forces is indeed decreasing the stability of centrioles. Given that centrioles are known to interact with cortical actin (Buttrick et al., 2008; Calvo and Izquierdo, 2021; Farina et al., 2016), and given the many adverse effects that depleting actin as a whole can have on various cell types including the *Drosophila* embryo, it may also be useful to quantify centriole orientation and stability in embryos where only cortical actin has been depleted. We do not currently possess a characterised mutant that specifically depletes cortical actin in the syncytial embryo, however mutants have been found that cause cortical actin disorganisation during embryo gastrulation and in other *Drosophila* systems (Kanesaki et al., 2013; Kiss et al., 2020; Tsarouhas et al., 2019). In particular, mutations in the gene *scrambled* resulted in reduction of cortical actin cap size in syncytial *Drosophila* embryos. While these actin caps were able to organise centrioles at the cell cortex, they were unable to expand into pseudo-cleavage furrows during mitosis (Fig. 1.7B) (Stevenson et al., 2001). Thus, *Sced* mutant embryos could potentially be useful in understanding the relationship between cortical actin and centriole orientation. In the future it would be interesting to investigate centriole orientation and stability in the embryos of these mutants to elucidate the effects of cortical actin on centriole orientation as well as positioning.

6.5.2. Exploring other ways to deplete the PCM

In *cnn*^{f} embryos, centrioles show a rocketing motion as previously described, and centriole stability significantly decreased (Fig. 5.3B, D). I hypothesised that the decrease in stability may be due to the sensitivity of centrosomes to the push and pull forces of MTs on the centrosome in the absence of the inertia provided by an intact PCM. To further validate this claim, I would like to quantify centriole orientation and stability in embryos expressing a mutant form of Cnn with a non-functional CM1 domain which binds to γ-TuRC (Choi et al., 2010; Tovey et al., 2021; Zhang and Megraw, 2007). Thus, in these embryos, centrioles

would have an intact PCM, but would be unable to bind MTs, thus reducing the push/pull forces of MTs on centrosomes in a more precise manner than using a drug injection. I would predict that stability would increase in this mutant due to the lack of MT-mediated force on a centriole with a properly formed PCM.

I would also like to attempt to deplete the PCM in other ways beyond mutating Cnn. Unfortunately, mutating the other key PCM scaffolding protein, Spd2, results in sterile flies that lay embryos that fail in pronuclear fusion, and so fail to develop (Giansanti et al., 2008). However, embryos can be injected with anti-Spd2 RNAi and direct effects of Spd2 depletion can be observed for several minutes as has been previously shown in *C.elegans* (Stevenson et al., 2002). It is also possible to generate flies lacking endogenous PLP as PLP is shown to be dispensable in early development (Richens et al., 2015). It would be interesting to see if lack of PLP has any effect on centriole stability in particular as mutants seem to subtly disrupt PCM formation (Lerit et al., 2015; Richens et al., 2015; Roque et al., 2018).

6.5.3. Investigating centriole orientation in embryos where proteins implicated in centriole positioning have been depleted

Beyond depleting the PCM, there are two other proteins that would be interesting to investigate as they are both involved in centriole positioning. One is Mud, which was recently shown to be involved in positioning the proximal end of centrioles in syncytial *Drosophila* embryos towards the nucleus (Cunningham et al., 2022). Mud mutants are male sterile and it would not be possible to obtain embryos that are $Mud^{-/-}$. However, Mud does have 4 isoforms (Taniguchi et al., 2014), and generating mutants which are heterozygous for different isoform deletions could result in viable adult flies. The second protein that would be interesting to deplete is Rab11, as mentioned previously, *Drosophila* embryos have large Rab11 recycling endosomes close to the cell cortex (Calero-Cuenca and Sotillos, 2018; Riggs et al., 2003; Roeth et al., 2009). In the context of ciliogenesis, it has also been shown that distal cap protein CP110 is able to interact with Rab11 in order to promote trafficking towards the site of ciliogenesis (Hehnly et al., 2012; Kobayashi et al., 2011). By depleting Rab11 and quantifying changes in centriole orientation and stability, I could infer if endosome-based attachment is involved in a potential centriole anchorage mechanism facilitating the preferred distal-ended orientation of centrioles in *Drosophila* embryos (as concluded in Chapter 3).

6.5.4. Further experiments investigating a Cep97 led mechanism of centriole orientation

In *Cep97*$^{-/-}$ embryos Bar-oriented centrioles become the preferred orientation state as compared to Rings in WT embryos (Fig. 5.5C), strongly suggesting that Cep97 plays a crucial role in a putative centriole orientation mechanism maintaining Ring-oriented centrioles. However, while data in *CP110*$^{-/-}$ embryos followed this trend, the effect was much milder (Fig. 5.6C). In the future I would like to perform a complementation experiment to see if exogenous Cep97 rescues the phenotype seen in *Cep97*$^{-/-}$ embryos. This can be done by crossing functional exogenous Cep97 into *Cep97*$^{-/-}$ flies. If Bar centrioles are still the preferred, most stable orientation in these flies, then I can conclude that these changes are likely not due to the lack of Cep97 itself but due to other defects in the *Cep97*$^{-/-}$ fly stock.

Shortly after the submission of this thesis, a study was published showing that Cep104, a protein previously localised to the distal end of *Drosophila* centrioles and involved in ciliogenesis in human cells (Frikstad et al., 2019; Valente et al., 2014), was part of the distal cap complex in *Drosophila* together with Cep97 and CP110 (Ryniawec et al., 2023). The authors showed that Cep104 associated with MTs and promoted centriole elongation. Cep104 was also recruited to the distal cap by Cep97. Interestingly, despite its cooperative roles with Cep97 in ciliogenesis and centriole length control, Cep104 does not seem to interact with CP110. Given the striking changes in centriole orientation observed in *Cep97*$^{-/-}$ embryos as compared to the more modest changes in *CP110*$^{-/-}$ embryos, Cep104 could be involved in a putative Cep97-driven centriole orientation mechanism. In the future, it would be important to observe how centriole orientation and stability changes in *Cep104*$^{-/-}$ mutant embryos and compare any changes to those seen in *Cep97*$^{-/-}$ embryos.

6.5.5. Exploring centriole orientation in other *Drosophila* tissues

It would also be interesting to see if changes in centriole orientation in the embryo are also conserved in other tissues in the fly that have centrioles specifically positioned close to the cell cortex, such as in the wing-disc (Carvajal-Gonzalez et al., 2016b; Garrido-Jimenez et al., 2018). However, Centrilyze would need

to be recalibrated in order to effectively quantify centrioles. The oocyte also has a highly polarised epithelium but given its roundness, some assay optimisation would need to be carried out before centriole orientation can be robustly measured in this tissue.

6.5.6. Understanding centriole orientation in non-ciliated systems

These experiments would ultimately provide insights into how specifically positioned centrioles are oriented, which is an unusual question within centriole biology especially in non-ciliated tissues. Understanding how centrioles may be oriented is a potentially interesting field of study because while centrioles are positioned close to the apical cortex in many polarised cell types (Carvajal-Gonzalez et al., 2016b; Elric and Etienne-Manneville, 2014; Januschke et al., 2011; Shinohara et al., 2013; Solecki et al., 2009), it is mostly unknown how they are oriented. Yet, in the few systems where centriole orientation has been established, such as ciliated cells and IS-forming cells (Shinohara et al., 2013; Stinchcombe et al., 2015; Tanos et al., 2013), orientation seems to have a functional role in directional trafficking and building polarised structures. Broadening our understanding of how centrioles might be oriented in other polarised cells might provide an idea of just how important centriole positioning can be in these cell types. Additionally, such data interrogates arguably the most ancient, conserved function of the centriole itself, which is as a template to polarised cell structures (Azimzadeh, 2014; Carvalho-Santos et al., 2011). Understanding centriole orientation across different organisms, especially those without DAPs and which are therefore closer in structure to the centriole LECA possessed, might bring to light a deeply conserved function of centrioles as a positional organiser.

References

Alvarez-Rodrigo, I., Steinacker, T.L., Saurya, S., Conduit, P.T., Baumbach, J., Novak, Z.A., Aydogan, M.G., Wainman, A., Raff, J.W., 2019. Evidence that a positive feedback loop drives centrosome maturation in fly embryos. Elife 8.

Alvarez-Rodrigo, I., Wainman, A., Saurya, S., Raff, J.W., 2021. Ana1 helps recruit Polo to centrioles to promote mitotic PCM assembly and centriole elongation. J Cell Sci 134.

Alves-Cruzeiro, J.M., Nogales-Cadenas, R., Pascual-Montano, A.D., 2014. CentrosomeDB: a new generation of the centrosomal proteins database for Human and Drosophila melanogaster. Nucleic Acids Res 42, D430-436.

Alzubaidi, L., Zhang, J., Humaidi, A.J., Al-Dujaili, A., Duan, Y., Al-Shamma, O., Santamaría, J., Fadhel, M.A., Al-Amidie, M., Farhan, L., 2021. Review of deep learning: concepts, CNN architectures, challenges, applications, future directions. Journal of Big Data 8, 53.

Antoniades, I., Stylianou, P., Skourides, Paris A., 2014. Making the Connection: Ciliary Adhesion Complexes Anchor Basal Bodies to the Actin Cytoskeleton. Developmental Cell 28, 70-80.

Arquint, C., Gabryjonczyk, A.M., Imseng, S., Böhm, R., Sauer, E., Hiller, S., Nigg, E.A., Maier, T., 2015. STIL binding to Polo-box 3 of PLK4 regulates centriole duplication. Elife 4.

Avidor-Reiss, T., Leroux, M.R., 2015. Shared and Distinct Mechanisms of Compartmentalized and Cytosolic Ciliogenesis. Curr Biol 25, R1143-1150.

Aydogan, M.G., Hankins, L.E., Steinacker, T.L., Mofatteh, M., Saurya, S., Wainman, A., Wong, S.S., Lu, X., Zhou, F.Y., Raff, J.W., 2022. Centriole distal-end proteins CP110 and Cep97 influence centriole cartwheel growth at the proximal end. J Cell Sci 135.

Aydogan, M.G., Wainman, A., Saurya, S., Steinacker, T.L., Caballe, A., Novak, Z.A., Baumbach, J., Muschalik, N., Raff, J.W., 2018. A homeostatic clock sets daughter centriole size in flies. The Journal of cell biology 217, 1233-1248.

Azimzadeh, J., 2014. Exploring the evolutionary history of centrosomes. Philos Trans R Soc Lond B Biol Sci 369.

Azimzadeh, J., Marshall, W.F., 2010. Building the centriole. Curr Biol 20, R816-825.

Azimzadeh, J., Wong, M.L., Downhour, D.M., Sánchez Alvarado, A., Marshall, W.F., 2012. Centrosome loss in the evolution of planarians. Science (New York, N.Y.) 335, 461-463.

Azuma, T., Kei, T., 2015. Super-resolution spinning-disk confocal microscopy using optical photon reassignment. Opt Express 23, 15003-15011.

Baker, J., Theurkauf, W.E., Schubiger, G., 1993. Dynamic changes in microtubule configuration correlate with nuclear migration in the preblastoderm Drosophila embryo. J Cell Biol 122, 113-121.

Baker, K., Beales, P.L., 2009. Making sense of cilia in disease: the human ciliopathies. Am J Med Genet C Semin Med Genet 151c, 281-295.

Basiri, M.L., Ha, A., Chadha, A., Clark, N.M., Polyanovsky, A., Cook, B., Avidor-Reiss, T., 2014. A migrating ciliary gate compartmentalizes the site of axoneme assembly in Drosophila spermatids. Current Biology 24, 2622-2631.

Basto, R., Lau, J., Vinogradova, T., Gardiol, A., Woods, C.G., Khodjakov, A., Raff, J.W., 2006. Flies without centrioles. Cell 125, 1375-1386.

Basu, S., Roberts, E.L., Jones, A.W., Swaffer, M.P., Snijders, A.P., Nurse, P., 2020. The Hydrophobic Patch Directs Cyclin B to Centrosomes to Promote Global CDK Phosphorylation at Mitosis. Curr Biol 30, 883-892.e884.

Bazzi, H., Anderson, K.V., 2014. Acentriolar mitosis activates a p53-dependent apoptosis pathway in the mouse embryo. Proceedings of the National Academy of Sciences 111, E1491-E1500.

Bearer, E.L., 1991. Actin in the Drosophila embryo: is there a relationship to developmental cue localization? Bioessays 13, 199-204.

Ben Hamida, A., Devanne, M., Weber, J., Truntzer, C., Derangère, V., Ghiringhelli, F., Forestier, G., Wemmert, C., 2021. Deep learning for colon cancer histopathological images analysis. Computers in Biology and Medicine 136, 104730.

Bettencourt-Dias, M., Carvalho-Santos, Z., 2008. Double life of centrioles: CP110 in the spotlight. Trends in Cell Biology 18, 8-11.

Bond, C., Santiago-Ruiz, A.N., Tang, Q., Lakadamyali, M., 2022. Technological advances in super-resolution microscopy to study cellular processes. Mol Cell 82, 315-332.

Bowler, M., Kong, D., Sun, S., Nanjundappa, R., Evans, L., Farmer, V., Holland, A., Mahjoub, M.R., Sui, H., Loncarek, J., 2019. High-resolution characterization of centriole distal appendage morphology and dynamics by correlative STORM and electron microscopy. Nature Communications 10, 993.

Bowman, S.K., Neumüller, R.A., Novatchkova, M., Du, Q., Knoblich, J.A., 2006. The Drosophila NuMA Homolog Mud regulates spindle orientation in asymmetric cell division. Dev Cell 10, 731-742.

Buttrick , G.J., Beaumont , L.M.A., Leitch , J., Yau , C., Hughes , J.R., Wakefield , J.G., 2008. Akt regulates centrosome migration and spindle orientation in the early Drosophila melanogaster embryo. Journal of Cell Biology 180, 537-548.

Cabernard, C., Doe, C.Q., 2009. Apical/basal spindle orientation is required for neuroblast homeostasis and neuronal differentiation in Drosophila. Dev Cell 17, 134-141.

Cabrita, A., Medeiros, A.M., Pereira, T., Rodrigues, A.S., Kranendonk, M., Mendes, C.S., 2022. Motor dysfunction in Drosophila melanogaster as a biomarker for developmental neurotoxicity. iScience 25, 104541.

Čajánek, L., Nigg, E.A., 2014. Cep164 triggers ciliogenesis by recruiting Tau tubulin kinase 2 to the mother centriole. Proc Natl Acad Sci U S A 111, E2841-2850.

Calero-Cuenca, F.J., Sotillos, S., 2018. Nuf and Rip11 requirement for polarity determinant recycling during Drosophila development. Small GTPases 9, 352-359.

Callaini, G., Whitfield, W.G., Riparbelli, M.G., 1997. Centriole and centrosome dynamics during the embryonic cell cycles that follow the formation of the cellular blastoderm in Drosophila. Exp Cell Res 234, 183-190.

Calvo, V., Izquierdo, M., 2021. Role of Actin Cytoskeleton Reorganization in Polarized Secretory Traffic at the Immunological Synapse. Front Cell Dev Biol 9, 629097.

Camuglia, J., Chanet, S., Martin, A.C., 2022. Morphogenetic forces planar polarize LGN/Pins in the embryonic head during Drosophila gastrulation. eLife 11, e78779.

Cao, J., Shen, Y., Zhu, L., Xu, Y., Zhou, Y., Wu, Z., Li, Y., Yan, X., Zhu, X., 2012. miR-129-3p controls cilia assembly by regulating CP110 and actin dynamics. Nature Cell Biology 14, 697-706.

Carvajal-Gonzalez, J.M., Mulero-Navarro, S., Mlodzik, M., 2016a. Centriole positioning in epithelial cells and its intimate relationship with planar cell polarity. Bioessays 38, 1234-1245.

Carvajal-Gonzalez, J.M., Roman, A.-C., Mlodzik, M., 2016b. Positioning of centrioles is a conserved readout of Frizzled planar cell polarity signalling. Nature communications 7, 11135-11135.

Carvalho-Santos, Z., Azimzadeh, J., Pereira-Leal, J.B., Bettencourt-Dias, M., 2011. Evolution: Tracing the origins of centrioles, cilia, and flagella. J Cell Biol 194, 165-175.

Carvalho-Santos, Z., Machado, P., Branco, P., Tavares-Cadete, F., Rodrigues-Martins, A., Pereira-Leal, J.B., Bettencourt-Dias, M., 2010. Stepwise evolution of the centriole-assembly pathway. J Cell Sci 123, 1414-1426.

Cassioli, C., Baldari, C.T., 2019. A Ciliary View of the Immunological Synapse. Cells 8.

Chavali, P.L., Pütz, M., Gergely, F., 2014. Small organelle, big responsibility: the role of centrosomes in development and disease. Philos Trans R Soc Lond B Biol Sci 369.

Cheng, H.W., Hsiao, C.T., Chen, Y.Q., Huang, C.M., Chan, S.I., Chiou, A., Kuo, J.C., 2019. Centrosome guides spatial activation of Rac to control cell polarization and directed cell migration. Life Sci Alliance 2.

Choi, Y.-K., Liu, P., Sze, S.K., Dai, C., Qi, R.Z., 2010. CDK5RAP2 stimulates microtubule nucleation by the γ-tubulin ring complex. Journal of Cell Biology 191, 1089-1095.

Chong, W.M., Wang, W.-J., Lo, C.-H., Chiu, T.-Y., Chang, T.-J., Liu, Y.-P., Tanos, B., Mazo, G., Tsou, M.-F.B., Jane, W.-N., Yang, T.T., Liao, J.-C., 2020. Super-resolution microscopy reveals coupling between mammalian centriole subdistal appendages and distal appendages. eLife 9, e53580.

Churchill, G.A., 1992. Hidden Markov chains and the analysis of genome structure. Computers & Chemistry 16, 107-115.

Cizmecioglu, O., Arnold, M., Bahtz, R., Settele, F., Ehret, L., Haselmann-Weiss, U., Antony, C., Hoffmann, I., 2010. Cep152 acts as a scaffold for recruitment of Plk4 and CPAP to the centrosome. J Cell Biol 191, 731-739.

Cliffe, A., Mieszczanek, J., Bienz, M., 2004. Intracellular shuttling of a Drosophila APC tumour suppressor homolog. BMC Cell Biol 5, 37.

Colicino, E.G., Hehnly, H., 2018. Regulating a key mitotic regulator, polo-like kinase 1 (PLK1). Cytoskeleton 75, 481-494.

Conduit, P.T., Feng, Z., Richens, J.H., Baumbach, J., Wainman, A., Bakshi, S.D., Dobbelaere, J., Johnson, S., Lea, S.M., Raff, J.W., 2014a. The centrosome-specific phosphorylation of Cnn by Polo/Plk1 drives Cnn scaffold assembly and centrosome maturation. Dev Cell 28, 659-669.

Conduit, P.T., Raff, J.W., 2010. Cnn Dynamics Drive Centrosome Size Asymmetry to Ensure Daughter Centriole Retention in Drosophila Neuroblasts. Current Biology 20, 2187-2192.

Conduit, P.T., Richens, J.H., Wainman, A., Holder, J., Vicente, C.C., Pratt, M.B., Dix, C.I., Novak, Z.A., Dobbie, I.M., Schermelleh, L., Raff, J.W., 2014b. A molecular mechanism of mitotic centrosome assembly in Drosophila. eLife 3, e03399.

Conduit, P.T., Wainman, A., Raff, J.W., 2015. Centrosome function and assembly in animal cells. Nat Rev Mol Cell Biol 16, 611-624.

Copeland, J., 2020. Actin-based regulation of ciliogenesis – The long and the short of it. Seminars in Cell & Developmental Biology 102, 132-138.

Cowan, C.R., Hyman, A.A., 2004. Asymmetric Cell Division in C. elegans: Cortical Polarity and Spindle Positioning. Annual Review of Cell and Developmental Biology 20, 427-453.

Cunningham, N.H.J., Bouhlel, I.B., Conduit, P.T., 2022. Daughter centrioles assemble preferentially towards the nuclear envelope in Drosophila syncytial embryos. Open Biol 12, 210343.

Currie, G., Hawk, K.E., Rohren, E., Vial, A., Klein, R., 2019. Machine Learning and Deep Learning in Medical Imaging: Intelligent Imaging. J Med Imaging Radiat Sci 50, 477-487.

Delgehyr, N., Rangone, H., Fu, J., Mao, G., Tom, B., Riparbelli, M.G., Callaini, G., Glover, D.M., 2012. Klp10A, a microtubule-depolymerizing kinesin-13, cooperates with CP110 to control Drosophila centriole length. Curr Biol 22, 502-509.

Delgehyr, N., Sillibourne, J., Bornens, M., 2005. Microtubule nucleation and anchoring at the centrosome are independent processes linked by ninein function. Journal of Cell Science 118, 1565-1575.

Dobbelaere, J., 2023. Cytoskeleton: The many flavors of cilia transition fibers. Current Biology 33, R150-R153.

Dobbelaere, J., Josué, F., Suijkerbuijk, S., Baum, B., Tapon, N., Raff, J., 2008. A genome-wide RNAi screen to dissect centriole duplication and centrosome maturation in Drosophila. PLoS Biol 6, e224.

Dobbelaere, J., Schmidt Cernohorska, M., Huranova, M., Slade, D., Dammermann, A., 2020. Cep97 Is Required for Centriole Structural Integrity and Cilia Formation in Drosophila. Current Biology 30, 3045-3056.e3047.

Domínguez-Calvo, A., Gönczy, P., Holland, A.J., Balestra, F.R., 2021. TRIM37: a critical orchestrator of centrosome function. Cell Cycle 20, 2443-2451.

Dzhindzhev, N.S., Tzolovsky, G., Lipinszki, Z., Schneider, S., Lattao, R., Fu, J., Debski, J., Dadlez, M., Glover, D.M., 2014. Plk4 phosphorylates Ana2 to trigger Sas6 recruitment and procentriole formation. Curr Biol 24, 2526-2532.

Dzhindzhev, N.S., Yu, Q.D., Weiskopf, K., Tzolovsky, G., Cunha-Ferreira, I., Riparbelli, M., Rodrigues-Martins, A., Bettencourt-Dias, M., Callaini, G., Glover, D.M., 2010. Asterless is a scaffold for the onset of centriole assembly. Nature 467, 714-718.

Efimov, A., Kharitonov, A., Efimova, N., Loncarek, J., Miller, P.M., Andreyeva, N., Gleeson, P., Galjart, N., Maia, A.R., McLeod, I.X., 2007. Asymmetric CLASP-dependent nucleation of noncentrosomal microtubules at the trans-Golgi network. Developmental cell 12, 917-930.

Elric, J., Etienne-Manneville, S., 2014. Centrosome positioning in polarized cells: common themes and variations. Exp Cell Res 328, 240-248.

Espigat-Georger, A., Dyachuk, V., Chemin, C., Emorine, L., Merdes, A., 2016. Nuclear alignment in myotubes requires centrosome proteins recruited by nesprin-1. J Cell Sci 129, 4227-4237.

Euteneuer, U., Schliwa, M., 1985. Evidence for an involvement of actin in the positioning and motility of centrosomes. Journal of Cell Biology 101, 96-103.

Farina, F., Gaillard, J., Guérin, C., Couté, Y., Sillibourne, J., Blanchoin, L., Théry, M., 2016. The centrosome is an actin-organizing centre. Nature Cell Biology 18, 65-75.

Farina, F., Ramkumar, N., Brown, L., Samandar Eweis, D., Anstatt, J., Waring, T., Bithell, J., Scita, G., Thery, M., Blanchoin, L., 2019. Local actin nucleation tunes centrosomal microtubule nucleation during passage through mitosis. The EMBO journal 38, e99843.

Feldman, J.L., Priess, J.R., 2012. A role for the centrosome and PAR-3 in the hand-off of MTOC function during epithelial polarization. Curr Biol 22, 575-582.

Feng, Z., Caballe, A., Wainman, A., Johnson, S., Haensele, A.F.M., Cottee, M.A., Conduit, P.T., Lea, S.M., Raff, J.W., 2017. Structural Basis for Mitotic Centrosome Assembly in Flies. Cell 169, 1078-1089.e1013.

Foe, V.E., Field, C.M., Odell, G.M., 2000. Microtubules and mitotic cycle phase modulate spatiotemporal distributions of F-actin and myosin II in Drosophila syncytial blastoderm embryos. Development 127, 1767-1787.

Fong, K.W., Choi, Y.K., Rattner, J.B., Qi, R.Z., 2008. CDK5RAP2 is a pericentriolar protein that functions in centrosomal attachment of the gamma-tubulin ring complex. Mol Biol Cell 19, 115-125.

Franz, A., Roque, H., Saurya, S., Dobbelaere, J., Raff, J.W., 2013. CP110 exhibits novel regulatory activities during centriole assembly in Drosophila. J Cell Biol 203, 785-799.

Frikstad, K.M., Molinari, E., Thoresen, M., Ramsbottom, S.A., Hughes, F., Letteboer, S.J.F., Gilani, S., Schink, K.O., Stokke, T., Geimer, S., Pedersen, L.B., Giles, R.H., Akhmanova, A., Roepman, R., Sayer, J.A., Patzke, S., 2019. A CEP104-CSPP1 Complex Is Required for Formation of Primary Cilia Competent in Hedgehog Signaling. Cell Rep 28, 1907-1922.e1906.

Fry, A.M., Sampson, J., Shak, C., Shackleton, S., 2017. Recent advances in pericentriolar material organization: ordered layers and scaffolding gels. F1000Res 6, 1622.

Fu, J., Glover, D.M., 2012. Structured illumination of the interface between centriole and peri-centriolar material. Open Biol 2, 120104.

Garrido-Jimenez, S., Roman, A.-C., Alvarez-Barrientos, A., Carvajal-Gonzalez, J.M., 2018. Centriole planar polarity assessment in Drosophila wings. Development 145, dev169326.

Gartenmann, L., Vicente, C.C., Wainman, A., Novak, Z.A., Sieber, B., Richens, J.H., Raff, J.W., 2020. Drosophila Sas-6, Ana2 and Sas-4 self-organise into macromolecular structures that can be used to probe centriole and centrosome assembly. J Cell Sci 133.

Gartenmann, L., Wainman, A., Qurashi, M., Kaufmann, R., Schubert, S., Raff, J.W., Dobbie, I.M., 2017. A combined 3D-SIM/SMLM approach allows centriole proteins to be localized with a precision of ~4-5 nm. Curr Biol 27, R1054-r1055.

Giansanti, M.G., Bucciarelli, E., Bonaccorsi, S., Gatti, M., 2008. Drosophila SPD-2 is an essential centriole component required for PCM recruitment and astral-microtubule nucleation. Curr Biol 18, 303-309.

Goetz, S.C., Liem, K.F., Anderson, K.V., 2012. The spinocerebellar ataxia-associated gene Tau tubulin kinase 2 controls the initiation of ciliogenesis. Cell 151, 847-858.

Gönczy, P., 2012. Towards a molecular architecture of centriole assembly. Nat Rev Mol Cell Biol 13, 425-435.

Goodson, H.V., Jonasson, E.M., 2018. Microtubules and Microtubule-Associated Proteins. Cold Spring Harb Perspect Biol 10.

Goshima, G., Wollman, R., Goodwin, S.S., Zhang, N., Scholey, J.M., Vale, R.D., Stuurman, N., 2007. Genes required for mitotic spindle assembly in Drosophila S2 cells. Science 316, 417-421.

Goshima, G., Wollman, R., Stuurman, N., Scholey, J.M., Vale, R.D., 2005. Length control of the metaphase spindle. Curr Biol 15, 1979-1988.

Gottardo, M., Persico, V., Callaini, G., Riparbelli, M.G., 2018. The “transition zone” of the cilium-like regions in the Drosophila spermatocytes and the role of the C-tubule in axoneme assembly. Experimental Cell Research 371, 262-268.

Grallert, A., Patel, A., Tallada, V.A., Chan, K.Y., Bagley, S., Krapp, A., Simanis, V., Hagan, I.M., 2013. Centrosomal MPF triggers the mitotic and morphogenetic switches of fission yeast. Nat Cell Biol 15, 88-95.

Graser, S., Stierhof, Y.D., Lavoie, S.B., Gassner, O.S., Lamla, S., Le Clech, M., Nigg, E.A., 2007. Cep164, a novel centriole appendage protein required for primary cilium formation. J Cell Biol 179, 321-330.

Gudima, G.O., Vorobjev, I.A., Chentsov Yu, S., 1988. Centriolar location during blood cell spreading and motion in vitro: an ultrastructural analysis. J Cell Sci 89 (Pt 2), 225-241.

Guichard, P., Hachet, V., Majubu, N., Neves, A., Demurtas, D., Olieric, N., Fluckiger, I., Yamada, A., Kihara, K., Nishida, Y., Moriya, S., Steinmetz, M.O., Hongoh, Y., Gönczy, P., 2013. Native architecture of the centriole proximal region reveals features underlying its 9-fold radial symmetry. Curr Biol 23, 1620-1628.

Guichard, P., Hamel, V., Le Guennec, M., Banterle, N., Iacovache, I., Nemčíková, V., Flückiger, I., Goldie, K.N., Stahlberg, H., Lévy, D., Zuber, B., Gönczy, P., 2017. Cell-free reconstitution reveals centriole cartwheel assembly mechanisms. Nat Commun 8, 14813.

Hamada, T., 2014. Chapter One - Microtubule Organization and Microtubule-Associated Proteins in Plant Cells, in: Jeon, K.W. (Ed.), International Review of Cell and Molecular Biology. Academic Press, pp. 1-52.

Hassabis, D., Kumaran, D., Summerfield, C., Botvinick, M., 2017. Neuroscience-Inspired Artificial Intelligence. Neuron 95, 245-258.

Hatch, E.M., Kulukian, A., Holland, A.J., Cleveland, D.W., Stearns, T., 2010. Cep152 interacts with Plk4 and is required for centriole duplication. J Cell Biol 191, 721-729.

Hayashi, S., Okada, Y., 2015. Ultrafast superresolution fluorescence imaging with spinning disk confocal microscope optics. Mol Biol Cell 26, 1743-1751.

Hayward, D., Metz, J., Pellacani, C., Wakefield, James G., 2014. Synergy between Multiple Microtubule-Generating Pathways Confers Robustness to Centrosome-Driven Mitotic Spindle Formation. Developmental Cell 28, 81-93.

He, K., Zhang, X., Ren, S., Sun, J., 2016. Deep Residual Learning for Image Recognition, 2016 IEEE Conference on Computer Vision and Pattern Recognition (CVPR). IEEE Computer Society, pp. 770-778.

Hehnly, H., Chen, C.T., Powers, C.M., Liu, H.L., Doxsey, S., 2012. The centrosome regulates the Rab11-dependent recycling endosome pathway at appendages of the mother centriole. Curr Biol 22, 1944-1950.

Higginbotham, H., Tanaka, T., Brinkman, B.C., Gleeson, J.G., 2006. GSK3β and PKCζ function in centrosome localization and process stabilization during Slit-mediated neuronal repolarization. Molecular and Cellular Neuroscience 32, 118-132.

Hobro, A.J., Smith, N.I., 2017. An evaluation of fixation methods: Spatial and compositional cellular changes observed by Raman imaging. Vibrational Spectroscopy 91, 31-45.

Hodge, S.H., Watts, A., Marley, R., Baines, R.A., Hafen, E., MacDougall, L.K., 2021. Twitchy, the Drosophila orthologue of the ciliary gating protein FBF1/dyf-19, is required for coordinated locomotion and male fertility. Biol Open 10.

Hodges, M.E., Scheumann, N., Wickstead, B., Langdale, J.A., Gull, K., 2010. Reconstructing the evolutionary history of the centriole from protein components. J Cell Sci 123, 1407-1413.

Holland, A.J., Fachinetti, D., Zhu, Q., Bauer, M., Verma, I.M., Nigg, E.A., Cleveland, D.W., 2012. The autoregulated instability of Polo-like kinase 4 limits centrosome duplication to once per cell cycle. Genes Dev 26, 2684-2689.

Holland, A.J., Lan, W., Niessen, S., Hoover, H., Cleveland, D.W., 2010. Polo-like kinase 4 kinase activity limits centrosome overduplication by autoregulating its own stability. J Cell Biol 188, 191-198.

Homem, C.C.F., Knoblich, J.A., 2012. Drosophila neuroblasts: a model for stem cell biology. Development 139, 4297-4310.

Hou, Y., Zheng, S., Wu, Z., Augière, C., Morel, V., Cortier, E., Duteyrat, J.L., Zhang, Y., Chen, H., Peng, Y., Durand, B., Wei, Q., 2023. Drosophila transition fibers are essential for IFT-dependent ciliary elongation but not basal body docking and ciliary budding. Curr Biol 33, 727-736.e726.

Huang, N., Xia, Y., Zhang, D., Wang, S., Bao, Y., He, R., Teng, J., Chen, J., 2017. Hierarchical assembly of centriole subdistal appendages via centrosome binding proteins CCDC120 and CCDC68. Nature communications 8, 15057-15057.

Hung, H.F., Hehnly, H., Doxsey, S., 2016. The Mother Centriole Appendage Protein Cenexin Modulates Lumen Formation through Spindle Orientation. Curr Biol 26, 793-801.

Hunter, A.W., Wordeman, L., 2000. How motor proteins influence microtubule polymerization dynamics. J Cell Sci 113 Pt 24, 4379-4389.

Inoue, D., Obino, D., Pineau, J., Farina, F., Gaillard, J., Guerin, C., Blanchoin, L., Lennon-Duménil, A.-M., Théry, M., 2019. Actin filaments regulate microtubule growth at the centrosome. The EMBO Journal 38, e99630.

Ishikawa, H., Kubo, A., Tsukita, S., Tsukita, S., 2005. Odf2-deficient mother centrioles lack distal/subdistal appendages and the ability to generate primary cilia. Nat Cell Biol 7, 517-524.

Ishikawa, H., Marshall, W.F., 2011. Ciliogenesis: building the cell's antenna. Nat Rev Mol Cell Biol 12, 222-234.

Izumi, Y., Ohta, N., Hisata, K., Raabe, T., Matsuzaki, F., 2006. Drosophila Pins-binding protein Mud regulates spindle-polarity coupling and centrosome organization. Nature Cell Biology 8, 586-593.

Jana, S.C., Mendonça, S., Machado, P., Werner, S., Rocha, J., Pereira, A., Maiato, H., Bettencourt-Dias, M., 2018. Differential regulation of transition zone and centriole proteins contributes to ciliary base diversity. Nature Cell Biology 20, 928-941.

Januschke, J., Llamazares, S., Reina, J., Gonzalez, C., 2011. Drosophila neuroblasts retain the daughter centrosome. Nat Commun 2, 243.

Januschke, J., Reina, J., Llamazares, S., Bertran, T., Rossi, F., Roig, J., Gonzalez, C., 2013. Centrobin controls mother-daughter centriole asymmetry in Drosophila neuroblasts. Nat Cell Biol 15, 241-248.

Jelinek, F., Bahl, L., Mercer, R., 1975. Design of a linguistic statistical decoder for the recognition of continuous speech. IEEE Transactions on Information Theory 21, 250-256.

Jimenez, A.J., Schaeffer, A., De Pascalis, C., Letort, G., Vianay, B., Bornens, M., Piel, M., Blanchoin, L., Théry, M., 2021. Acto-myosin network geometry defines centrosome position. Curr Biol 31, 1206-1220.e1205.

Joo, K., Kim, C.G., Lee, M.S., Moon, H.Y., Lee, S.H., Kim, M.J., Kweon, H.S., Park, W.Y., Kim, C.H., Gleeson, J.G., Kim, J., 2013. CCDC41 is required for ciliary vesicle docking to the mother centriole. Proc Natl Acad Sci U S A 110, 5987-5992.

Jurczyk, A., Gromley, A., Redick, S., San Agustin, J., Witman, G., Pazour, G.J., Peters, D.J., Doxsey, S., 2004. Pericentrin forms a complex with intraflagellar transport proteins and polycystin-2 and is required for primary cilia assembly. J Cell Biol 166, 637-643.

Kanesaki, T., Hirose, S., Grosshans, J., Fuse, N., 2013. Heterotrimeric G protein signaling governs the cortical stability during apical constriction in Drosophila gastrulation. Mech Dev 130, 132-142.

Kao, L.R., Megraw, T.L., 2009. Centrocortin cooperates with centrosomin to organize Drosophila embryonic cleavage furrows. Curr Biol 19, 937-942.

Kasioulis, I., Das, R.M., Storey, K.G., 2017. Inter-dependent apical microtubule and actin dynamics orchestrate centrosome retention and neuronal delamination. Elife 6.

Kask, P., Palo, K., Ullmann, D., Gall, K., 1999. Fluorescence-intensity distribution analysis and its application in biomolecular detection technology. Proc Natl Acad Sci U S A 96, 13756-13761.

Khodjakov, A., Cole, R.W., Oakley, B.R., Rieder, C.L., 2000. Centrosome-independent mitotic spindle formation in vertebrates. Curr Biol 10, 59-67.

Kiss, V., Jipa, A., Varga, K., Takáts, S., Maruzs, T., Lőrincz, P., Simon-Vecsei, Z., Szikora, S., Földi, I., Bajusz, C., Tóth, D., Vilmos, P., Gáspár, I., Ronchi, P., Mihály, J., Juhász, G., 2020. Drosophila Atg9 regulates the actin cytoskeleton via interactions with profilin and Ena. Cell Death Differ 27, 1677-1692.

Kitagawa, D., Flückiger, I., Polanowska, J., Keller, D., Reboul, J., Gönczy, P., 2011. PP2A phosphatase acts upon SAS-5 to ensure centriole formation in C. elegans embryos. Dev Cell 20, 550-562.

Kiyomitsu, T., Cheeseman, I.M., 2012. Chromosome- and spindle-pole-derived signals generate an intrinsic code for spindle position and orientation. Nat Cell Biol 14, 311-317.

Klebba, J.E., Buster, D.W., Nguyen, A.L., Swatkoski, S., Gucek, M., Rusan, N.M., Rogers, G.C., 2013. Polo-like kinase 4 autodestructs by generating its Slimb-binding phosphodegron. Curr Biol 23, 2255-2261.

Klena, N., Pigino, G., 2022. Structural Biology of Cilia and Intraflagellar Transport. Annual Review of Cell and Developmental Biology 38, 103-123.

Knoblich, J.A., 2010. Asymmetric cell division: recent developments and their implications for tumour biology. Nature reviews Molecular cell biology 11, 849-860.

Kobayashi, T., Tanaka, K., Mashima, Y., Shoda, A., Tokuda, M., Itoh, H., 2020. CEP164 Deficiency Causes Hyperproliferation of Pancreatic Cancer Cells. Front Cell Dev Biol 8, 587691.

Kobayashi, T., Tsang, W.Y., Li, J., Lane, W., Dynlacht, B.D., 2011. Centriolar kinesin Kif24 interacts with CP110 to remodel microtubules and regulate ciliogenesis. Cell 145, 914-925.

Kohlmaier, G., Loncarek, J., Meng, X., McEwen, B.F., Mogensen, M.M., Spektor, A., Dynlacht, B.D., Khodjakov, A., Gönczy, P., 2009. Overly long centrioles and defective cell division upon excess of the SAS-4-related protein CPAP. Curr Biol 19, 1012-1018.

Kollman, J.M., Merdes, A., Mourey, L., Agard, D.A., 2011. Microtubule nucleation by γ-tubulin complexes. Nat Rev Mol Cell Biol 12, 709-721.

Kotadia, S., Crest, J., Tram, U., Riggs, B., Sullivan, W., 2010. Blastoderm Formation and Cellularisation in Drosophila melanogaster, Encyclopedia of Life Sciences, eLS.

Kotak, S., Gönczy, P., 2013. Mechanisms of spindle positioning: cortical force generators in the limelight. Current Opinion in Cell Biology 25, 741-748.

Kriegeskorte, N., Golan, T., 2019. Neural network models and deep learning. Curr Biol 29, R231-r236.

Kruger, P.B., Mathews, S., Aggarwala, K.R., Sanchez, N., 1993. Chromatic aberration and ocular focus: Fincham revisited. Vision Res 33, 1397-1411.

Kuijpers, M., Hoogenraad, C.C., 2011. Centrosomes, microtubules and neuronal development. Mol Cell Neurosci 48, 349-358.

Kumar, D., Rains, A., Herranz-Pérez, V., Lu, Q., Shi, X., Swaney, D.L., Stevenson, E., Krogan, N.J., Huang, B., Westlake, C., Garcia-Verdugo, J.M., Yoder, B.K., Reiter, J.F., 2021. A ciliopathy complex builds distal appendages to initiate ciliogenesis. Journal of Cell Biology 220.

Kuriyama, R., Borisy, G.G., 1981. Microtubule-nucleating activity of centrosomes in Chinese hamster ovary cells is independent of the centriole cycle but coupled to the mitotic cycle. J Cell Biol 91, 822-826.

Kwak, S.G., Kim, J.H., 2017. Central limit theorem: the cornerstone of modern statistics. Korean J Anesthesiol 70, 144-156.

Lapart, J.-A., Gottardo, M., Cortier, E., Duteyrat, J.-L., Augière, C., Mangé, A., Jerber, J., Solassol, J., Gopalakrishnan, J., Thomas, J., Durand, B., 2019. Dzip1 and Fam92 form a ciliary transition zone complex with cell type specific roles in Drosophila. eLife 8, e49307.

Lattao, R., Kovács, L., Glover, D.M., 2017. The Centrioles, Centrosomes, Basal Bodies, and Cilia of Drosophila melanogaster. Genetics 206, 33-53.

Lawo, S., Hasegan, M., Gupta, G.D., Pelletier, L., 2012. Subdiffraction imaging of centrosomes reveals higher-order organizational features of pericentriolar material. Nat Cell Biol 14, 1148-1158.

LeCun, Y., Bengio, Y., Hinton, G., 2015. Deep learning. Nature 521, 436-444.

Lee, M., Nagashima, K., Yoon, J., Sun, J., Wang, Z., Carpenter, C., Lee, H.K., Hwang, Y.S., Westlake, C.J., Daar, I.O., 2022. CEP97 phosphorylation by Dyrk1a is critical for centriole separation during multiciliogenesis. J Cell Biol 221.

Lerit, D.A., Jordan, H.A., Poulton, J.S., Fagerstrom, C.J., Galletta, B.J., Peifer, M., Rusan, N.M., 2015. Interphase centrosome organization by the PLP-Cnn scaffold is required for centrosome function. J Cell Biol 210, 79-97.

Lerit, D.A., Rusan, N.M., 2013. PLP inhibits the activity of interphase centrosomes to ensure their proper segregation in stem cells. J Cell Biol 202, 1013-1022.

Leung, Y.Y., Yao Hui, L.L., Kraus, V.B., 2015. Colchicine--Update on mechanisms of action and therapeutic uses. Semin Arthritis Rheum 45, 341-350.

Lindsley, D.L., Zimm, G.G., 1992. The genome of Drosophila melanogaster. :viii +1133pp. Academic press.

Liu, X., Huse, M., 2015. Immunological synapse formation: Cell polarity during T cell–APC interaction. Cell Polarity 1: BIological Role and Basic Mechanisms, 247-275.

Liu, Y., She, G.-r., Chen, S.-x., 2021. Magnetic resonance image diagnosis of femoral head necrosis based on ResNet18 network. Computer Methods and Programs in Biomedicine 208, 106254.

Lopes, C.A., Jana, S.C., Cunha-Ferreira, I., Zitouni, S., Bento, I., Duarte, P., Gilberto, S., Freixo, F., Guerrero, A., Francia, M., Lince-Faria, M., Carneiro, J., Bettencourt-Dias, M., 2015. PLK4 trans-Autoactivation Controls Centriole Biogenesis in Space. Dev Cell 35, 222-235.

Lopez, J.F., S; Doi, A; tsunomiya, H, 2019. A deconvolution revolution for confocal image enhancement. BioOptics World 55, 85-88.

Lucas, E.P., Raff, J.W., 2007. Maintaining the proper connection between the centrioles and the pericentriolar matrix requires Drosophila Centrosomin. Journal of Cell Biology 178, 725-732.

Luxton, G.W., Gundersen, G.G., 2011. Orientation and function of the nuclear-centrosomal axis during cell migration. Curr Opin Cell Biol 23, 579-588.

Lv, Z., de-Carvalho, J., Telley, I.A., Großhans, J., 2021. Cytoskeletal mechanics and dynamics in the Drosophila syncytial embryo. Journal of Cell Science 134.

Ma, D., Wang, F., Teng, J., Huang, N., Chen, J., 2023. Structure and function of distal and subdistal appendages of the mother centriole. Journal of Cell Science 136.

MacLean-Fletcher, S., Pollard, T.D., 1980. Mechanism of action of cytochalasin B on actin. Cell 20, 329-341.

Mansour, F., Boivin, F.J., Shaheed, I.B., Schueler, M., Schmidt-Ott, K.M., 2021. The Role of Centrosome Distal Appendage Proteins (DAPs) in Nephronophthisis and Ciliogenesis. Int J Mol Sci 22.

Marshall, W.F., 2009. Centriole evolution. Curr Opin Cell Biol 21, 14-19.

Martinez-Campos, M., Basto, R., Baker, J., Kernan, M., Raff, J.W., 2004. The Drosophila pericentrin-like protein is essential for cilia/flagella function, but appears to be dispensable for mitosis. J Cell Biol 165, 673-683.

McCartney, B.M., McEwen, D.G., Grevengoed, E., Maddox, P., Bejsovec, A., Peifer, M., 2001. Drosophila APC2 and Armadillo participate in tethering mitotic spindles to cortical actin. Nat Cell Biol 3, 933-938.

McNally, F.J., 2013. Mechanisms of spindle positioning. J Cell Biol 200, 131-140.

Meitinger, F., Anzola, J.V., Kaulich, M., Richardson, A., Stender, J.D., Benner, C., Glass, C.K., Dowdy, S.F., Desai, A., Shiau, A.K., Oegema, K., 2016. 53BP1 and USP28 mediate p53 activation and G1 arrest after centrosome loss or extended mitotic duration. J Cell Biol 214, 155-166.

Meitinger, F., Ohta, M., Lee, K.Y., Watanabe, S., Davis, R.L., Anzola, J.V., Kabeche, R., Jenkins, D.A., Shiau, A.K., Desai, A., Oegema, K., 2020. TRIM37 controls cancer-specific vulnerability to PLK4 inhibition. Nature 585, 440-446.

Mennella, V., Keszthelyi, B., McDonald, K.L., Chhun, B., Kan, F., Rogers, G.C., Huang, B., Agard, D.A., 2012. Subdiffraction-resolution fluorescence microscopy reveals a domain of the centrosome critical for pericentriolar material organization. Nat Cell Biol 14, 1159-1168.

Meraldi, P., 2016. Centrosomes in spindle organization and chromosome segregation: a mechanistic view. Chromosome Research 24, 19-34.

Merdes, A., Ramyar, K., Vechio, J.D., Cleveland, D.W., 1996. A complex of NuMA and cytoplasmic dynein is essential for mitotic spindle assembly. Cell 87, 447-458.

Miller, D.E., Cook, K.R., Hawley, R.S., 2019. The joy of balancers. PLoS Genet 15, e1008421.

Mitchison, T., Kirschner, M., 1984. Dynamic instability of microtubule growth. Nature 312, 237-242.

Mogessie, B., Scheffler, K., Schuh, M., 2018. Assembly and Positioning of the Oocyte Meiotic Spindle. Annu Rev Cell Dev Biol 34, 381-403.

Mondal, M.R.H., Bharati, S., Podder, P., 2021. Diagnosis of COVID-19 Using Machine Learning and Deep Learning: A Review. Curr Med Imaging 17, 1403-1418.

Mönnich, M., Borgeskov, L., Breslin, L., Jakobsen, L., Rogowski, M., Doganli, C., Schrøder, J.M., Mogensen, J.B., Blinkenkjær, L., Harder, L.M., Lundberg, E., Geimer, S., Christensen, S.T., Andersen, J.S., Larsen, L.A., Pedersen, L.B., 2018. CEP128 Localizes to the Subdistal Appendages of the Mother Centriole and Regulates TGF-β/BMP Signaling at the Primary Cilium. Cell Rep 22, 2584-2592.

Morin, X., Bellaïche, Y., 2011. Mitotic spindle orientation in asymmetric and symmetric cell divisions during animal development. Dev Cell 21, 102-119.

Moritz, M., Braunfeld, M.B., Fung, J.C., Sedat, J.W., Alberts, B.M., Agard, D.A., 1995a. Three-dimensional structural characterization of centrosomes from early Drosophila embryos. J Cell Biol 130, 1149-1159.

Moritz, M., Braunfeld, M.B., Sedat, J.W., Alberts, B., Agard, D.A., 1995b. Microtubule nucleation by gamma-tubulin-containing rings in the centrosome. Nature 378, 638-640.

Moyer, T.C., Clutario, K.M., Lambrus, B.G., Daggubati, V., Holland, A.J., 2015. Binding of STIL to Plk4 activates kinase activity to promote centriole assembly. J Cell Biol 209, 863-878.

Mutch, S.A., Fujimoto, B.S., Kuyper, C.L., Kuo, J.S., Bajjalieh, S.M., Chiu, D.T., 2007. Deconvolving single-molecule intensity distributions for quantitative microscopy measurements. Biophys J 92, 2926-2943.

Nabais, C., Pessoa, D., de-Carvalho, J., van Zanten, T., Duarte, P., Mayor, S., Carneiro, J., Telley, I.A., Bettencourt-Dias, M., 2021. Plk4 triggers autonomous de novo centriole biogenesis and maturation. J Cell Biol 220.

Nagai, T., Mukoyama, S., Kagiwada, H., Goshima, N., Mizuno, K., 2018. Cullin-3–KCTD10-mediated CEP97 degradation promotes primary cilium formation. Journal of Cell Science 131.

Nigg, E.A., Holland, A.J., 2018. Once and only once: mechanisms of centriole duplication and their deregulation in disease. Nature Reviews Molecular Cell Biology 19, 297-312.

Noatynska, A., Gotta, M., 2012. Cell polarity and asymmetric cell division: the C. elegans early embryo. Essays Biochem 53, 1-14.

Novak, Z.A., Conduit, P.T., Wainman, A., Raff, J.W., 2014. Asterless licenses daughter centrioles to duplicate for the first time in Drosophila embryos. Curr Biol 24, 1276-1282.

Novak, Z.A., Wainman, A., Gartenmann, L., Raff, J.W., 2016. Cdk1 Phosphorylates Drosophila Sas-4 to Recruit Polo to Daughter Centrioles and Convert Them to Centrosomes. Dev Cell 37, 545-557.

Oda, T., Iwasa, M., Aihara, T., Maéda, Y., Narita, A., 2009. The nature of the globular-to fibrous-actin transition. Nature 457, 441-445.

Ohta, M., Ashikawa, T., Nozaki, Y., Kozuka-Hata, H., Goto, H., Inagaki, M., Oyama, M., Kitagawa, D., 2014. Direct interaction of Plk4 with STIL ensures formation of a single procentriole per parental centriole. Nature Communications 5, 5267.

Ojas, D., Jorge, d.-C., Diana, V.V., Ivo, A.T., 2021. Astral microtubule crosslinking safeguards uniform nuclear distribution in the Drosophila syncytium. bioRxiv, 859975.

Paintrand, M., Moudjou, M., Delacroix, H., Bornens, M., 1992. Centrosome organization and centriole architecture: their sensitivity to divalent cations. J Struct Biol 108, 107-128.

Pan, J., You, Y., Huang, T., Brody, S.L., 2007. RhoA-mediated apical actin enrichment is required for ciliogenesis and promoted by Foxj1. J Cell Sci 120, 1868-1876.

Pitaval, A., Senger, F., Letort, G., Gidrol, X., Guyon, L., Sillibourne, J., Théry, M., 2017. Microtubule stabilization drives 3D centrosome migration to initiate primary ciliogenesis. Journal of Cell Biology 216, 3713-3728.

Plessner, M., Knerr, J., Grosse, R., 2019. Centrosomal actin assembly is required for proper mitotic spindle formation and chromosome congression. IScience 15, 274-281.

Pollard, T.D., Cooper, J.A., 2009. Actin, a central player in cell shape and movement. Science 326, 1208-1212.

Prosser, S.L., Tkach, J., Gheiratmand, L., Kim, J., Raught, B., Morrison, C.G., Pelletier, L., 2022. Aggresome assembly at the centrosome is driven by CP110-CEP97-CEP290 and centriolar satellites. Nat Cell Biol 24, 483-496.

Quann, E.J., Liu, X., Altan-Bonnet, G., Huse, M., 2011. A cascade of protein kinase C isozymes promotes cytoskeletal polarization in T cells. Nat Immunol 12, 647-654.

Quann, E.J., Merino, E., Furuta, T., Huse, M., 2009. Localized diacylglycerol drives the polarization of the microtubule-organizing center in T cells. Nature Immunology 10, 627-635.

Rabiner, L.R., 1989. A tutorial on hidden Markov models and selected applications in speech recognition. Proceedings of the IEEE 77, 257-286.

Rabiner, L.R., Juang, B.-H., 1999. Fundamentals of speech recognition. Tsinghua University Press.

Raff, J.W., 2019. Phase Separation and the Centrosome: A Fait Accompli? Trends Cell Biol 29, 612-622.

Raff, J.W., Glover, D.M., 1989. Centrosomes, and not nuclei, initiate pole cell formation in Drosophila embryos. Cell 57, 611-619.

Raff, J.W., Whitfield, W.G.F., Glover, D.M., 1990. Two distinct mechanisms localise cyclin B transcripts in syncytial Drosophila embryos. Development 110, 1249-1261.

Rahman, M.A., Sultana, N., Ayman, U., Bhakta, S., Afrose, M., Afrin, M., Haque, Z., 2022. Alcoholic fixation over formalin fixation: A new, safer option for morphologic and molecular analysis of tissues. Saudi J Biol Sci 29, 175-182.

Ramdas Nair, A., Singh, P., Salvador Garcia, D., Rodriguez-Crespo, D., Egger, B., Cabernard, C., 2016. The Microcephaly-Associated Protein Wdr62/CG7337 Is Required to Maintain Centrosome Asymmetry in Drosophila Neuroblasts. Cell Rep 14, 1100-1113.

Rebollo, E., Sampaio, P., Januschke, J., Llamazares, S., Varmark, H., González, C., 2007. Functionally unequal centrosomes drive spindle orientation in asymmetrically dividing Drosophila neural stem cells. Dev Cell 12, 467-474.

Reilly, W.M., Obara, C.J., 2021. Advances in Confocal Microscopy and Selected Applications. Methods Mol Biol 2304, 1-35.

Reinsch, S., Gönczy, P., 1998. Mechanisms of nuclear positioning. J Cell Sci 111 (Pt 16), 2283-2295.

Reiter, J.F., Blacque, O.E., Leroux, M.R., 2012. The base of the cilium: roles for transition fibres and the transition zone in ciliary formation, maintenance and compartmentalization. EMBO reports 13, 608-618.

Renkawitz, J., Kopf, A., Stopp, J., de Vries, I., Driscoll, M.K., Merrin, J., Hauschild, R., Welf, E.S., Danuser, G., Fiolka, R., Sixt, M., 2019. Nuclear positioning facilitates amoeboid migration along the path of least resistance. Nature 568, 546-550.

Richens, J.H., Barros, T.P., Lucas, E.P., Peel, N., Pinto, D.M., Wainman, A., Raff, J.W., 2015. The Drosophila Pericentrin-like-protein (PLP) cooperates with Cnn to maintain the integrity of the outer PCM. Biol Open 4, 1052-1061.

Riggs , B., Rothwell , W., Mische , S., Hickson , G.R.X., Matheson , J., Hays , T.S., Gould , G.W., Sullivan , W., 2003. Actin cytoskeleton remodeling during early Drosophila furrow formation requires recycling endosomal components Nuclear-fallout and Rab11. Journal of Cell Biology 163, 143-154.

Ríos, R.M., Sanchís, A., Tassin, A.M., Fedriani, C., Bornens, M., 2004. GMAP-210 recruits gamma-tubulin complexes to cis-Golgi membranes and is required for Golgi ribbon formation. Cell 118, 323-335.

Roberge, C.J., Gaudry, M., de Médicis, R., Lussier, A., Poubelle, P.E., Naccache, P.H., 1993. Crystal-induced neutrophil activation. IV. Specific inhibition of tyrosine phosphorylation by colchicine. J Clin Invest 92, 1722-1729.

Roeth, J.F., Sawyer, J.K., Wilner, D.A., Peifer, M., 2009. Rab11 helps maintain apical crumbs and adherens junctions in the Drosophila embryonic ectoderm. PLoS One 4, e7634.

Roque, H., Saurya, S., Pratt, M.B., Johnson, E., Raff, J.W., 2018. Drosophila PLP assembles pericentriolar clouds that promote centriole stability, cohesion and MT nucleation. PLoS genetics 14, e1007198-e1007198.

Royou, A., Field, C., Sisson, J.C., Sullivan, W., Karess, R., 2004. Reassessing the role and dynamics of nonmuscle myosin II during furrow formation in early Drosophila embryos. Mol Biol Cell 15, 838-850.

Rumelhart, D.E., Hinton, G.E., Williams, R.J., 1985. Learning internal representations by error propagation. Institute for Cognitive Science, University of California, San Diego La ….

Rusan, N.M., Peifer, M., 2007. A role for a novel centrosome cycle in asymmetric cell division. J Cell Biol 177, 13-20.

Ryniawec, J.M., Hannaford, M.R., Zibrat, M.E., Fagerstrom, C.J., Galletta, B.J., Aguirre, S.E., Guice, B.A., Dean, S.M., Rusan, N.M., Rogers, G.C., 2023. Cep104 is a component of the centriole distal tip complex that regulates centriole growth and contributes to Drosophila spermiogenesis. Curr Biol 33, 4202-4216.e4209.

Sánchez, I., Dynlacht, B.D., 2016. Cilium assembly and disassembly. Nature cell biology 18, 711-717.

Schmidt, T.I., Kleylein-Sohn, J., Westendorf, J., Le Clech, M., Lavoie, S.B., Stierhof, Y.D., Nigg, E.A., 2009. Control of centriole length by CPAP and CP110. Curr Biol 19, 1005-1011.

Shao, W., Yang, J., He, M., Yu, X.-Y., Lee, C.H., Yang, Z., Joyner, A.L., Anderson, K.V., Zhang, J., Tsou, M.-F.B., Shi, H., Shi, S.-H., 2020. Centrosome anchoring regulates progenitor properties and cortical formation. Nature 580, 106-112.

Shinohara, H., Sakayori, N., Takahashi, M., Osumi, N., 2013. Ninein is essential for the maintenance of the cortical progenitor character by anchoring the centrosome to microtubules. Biol Open 2, 739-749.

Shoda, T., Yamazoe, K., Tanaka, Y., Asano, Y., Inoue, Y.H., 2021. Orbit/CLASP determines centriole length by antagonising Klp10A in Drosophila spermatocytes. J Cell Sci 134.

Shukla, A., Kong, D., Sharma, M., Magidson, V., Loncarek, J., 2015. Plk1 relieves centriole block to reduplication by promoting daughter centriole maturation. Nat Commun 6, 8077.

Siegrist, S.E., Doe, C.Q., 2007. Microtubule-induced cortical cell polarity. Genes Dev 21, 483-496.

Sir, J.H., Pütz, M., Daly, O., Morrison, C.G., Dunning, M., Kilmartin, J.V., Gergely, F., 2013. Loss of centrioles causes chromosomal instability in vertebrate somatic cells. J Cell Biol 203, 747-756.

Solecki, D.J., Model, L., Gaetz, J., Kapoor, T.M., Hatten, M.E., 2004. Par6α signaling controls glial-guided neuronal migration. Nature Neuroscience 7, 1195-1203.

Solecki, D.J., Trivedi, N., Govek, E.E., Kerekes, R.A., Gleason, S.S., Hatten, M.E., 2009. Myosin II motors and F-actin dynamics drive the coordinated movement of the centrosome and soma during CNS glial-guided neuronal migration. Neuron 63, 63-80.

Song, R., Walentek, P., Sponer, N., Klimke, A., Lee, J.S., Dixon, G., Harland, R., Wan, Y., Lishko, P., Lize, M., Kessel, M., He, L., 2014. miR-34/449 miRNAs are required for motile ciliogenesis by repressing cp110. Nature 510, 115-120.

Song, T., Yang, Y., Zhou, P., Ran, J., Zhang, L., Wu, X., Xie, W., Zhong, T., Liu, H., Liu, M., Li, D., Zhao, H., Zhou, J., 2022. ENKD1 promotes CP110 removal through competing with CEP97 to initiate ciliogenesis. EMBO Rep 23, e54090.

Sonnen, K.F., Schermelleh, L., Leonhardt, H., Nigg, E.A., 2012. 3D-structured illumination microscopy provides novel insight into architecture of human centrosomes. Biol Open 1, 965-976.

Sorokin, S., 1962. Centrioles and the formation of rudimentary cilia by fibroblasts and smooth muscle cells. J Cell Biol 15, 363-377.

Spektor, A., Tsang, W.Y., Khoo, D., Dynlacht, B.D., 2007. Cep97 and CP110 suppress a cilia assembly program. Cell 130, 678-690.

Steinacker, T.L., Wong, S.S., Novak, Z.A., Saurya, S., Gartenmann, L., van Houtum, E.J.H., Sayers, J.R., Lagerholm, B.C., Raff, J.W., 2022. Centriole growth is limited by the Cdk/Cyclin-dependent phosphorylation of Ana2/STIL. J Cell Biol 221.

Stevens, N.R., Dobbelaere, J., Brunk, K., Franz, A., Raff, J.W., 2010. Drosophila Ana2 is a conserved centriole duplication factor. J Cell Biol 188, 313-323.

Stevenson, V., Hudson, A., Cooley, L., Theurkauf, W.E., 2002. Arp2/3-dependent pseudocleavage [correction of psuedocleavage] furrow assembly in syncytial Drosophila embryos. Curr Biol 12, 705-711.

Stevenson, V.A., Kramer, J., Kuhn, J., Theurkauf, W.E., 2001. Centrosomes and the Scrambled protein coordinate microtubule-independent actin reorganization. Nature Cell Biology 3, 68-75.

Stinchcombe, J.C., Griffiths, G.M., 2014. Communication, the centrosome and the immunological synapse. Philos Trans R Soc Lond B Biol Sci 369.

Stinchcombe, J.C., Majorovits, E., Bossi, G., Fuller, S., Griffiths, G.M., 2006. Centrosome polarization delivers secretory granules to the immunological synapse. Nature 443, 462-465.

Stinchcombe, J.C., Randzavola, L.O., Angus, K.L., Mantell, J.M., Verkade, P., Griffiths, G.M., 2015. Mother Centriole Distal Appendages Mediate Centrosome Docking at the Immunological Synapse and Reveal Mechanistic Parallels with Ciliogenesis. Curr Biol 25, 3239-3244.

Sullivan, W., Daily, D.R., Fogarty, P., Yook, K.J., Pimpinelli, S., 1993. Delays in anaphase initiation occur in individual nuclei of the syncytial Drosophila embryo. Mol Biol Cell 4, 885-896.

Sullivan, W., Theurkauf, W.E., 1995. The cytoskeleton and morphogenesis of the early Drosophila embryo. Curr Opin Cell Biol 7, 18-22.

Tamzalit, F., Tran, D., Jin, W., Boyko, V., Bazzi, H., Kepecs, A., Kam, L.C., Anderson, K.V., Huse, M., 2020. Centrioles control the capacity, but not the specificity, of cytotoxic T cell killing. Proceedings of the National Academy of Sciences 117, 4310-4319.

Tan, C.H., Gasic, I., Huber-Reggi, S.P., Dudka, D., Barisic, M., Maiato, H., Meraldi, P., 2015. The equatorial position of the metaphase plate ensures symmetric cell divisions. Elife 4, e05124.

Tang, N., Marshall, W.F., 2012. Centrosome positioning in vertebrate development. J Cell Sci 125, 4951-4961.

Taniguchi, K., Kokuryo, A., Imano, T., Minami, R., Nakagoshi, H., Adachi-Yamada, T., 2014. Isoform-specific functions of Mud/NuMA mediate binucleation of Drosophila male accessory gland cells. BMC Dev Biol 14, 46.

Tanos, B.E., Yang, H.J., Soni, R., Wang, W.J., Macaluso, F.P., Asara, J.M., Tsou, M.F., 2013. Centriole distal appendages promote membrane docking, leading to cilia initiation. Genes Dev 27, 163-168.

Tariq, A., Green, L., Jeynes, J.C.G., Soeller, C., Wakefield, J.G., 2020. In vitro reconstitution of branching microtubule nucleation. eLife 9, e49769.

Telley, I.A., Gáspár, I., Ephrussi, A., Surrey, T., 2012. Aster migration determines the length scale of nuclear separation in the Drosophila syncytial embryo. Journal of Cell Biology 197, 887-895.

Thibos, L.N., Bradley, A., Still, D.L., Zhang, X., Howarth, P.A., 1990. Theory and measurement of ocular chromatic aberration. Vision Res 30, 33-49.

Tischer, J., Carden, S., Gergely, F., 2021. Accessorizing the centrosome: new insights into centriolar appendages and satellites. Curr Opin Struct Biol 66, 148-155.

Tournebize, R., Popov, A., Kinoshita, K., Ashford, A.J., Rybina, S., Pozniakovsky, A., Mayer, T.U., Walczak, C.E., Karsenti, E., Hyman, A.A., 2000. Control of microtubule dynamics by the antagonistic activities of XMAP215 and XKCM1 in Xenopus egg extracts. Nat Cell Biol 2, 13-19.

Tovey, C.A., Tsuji, C., Egerton, A., Bernard, F., Guichet, A., de la Roche, M., Conduit, P.T., 2021. Autoinhibition of Cnn binding to γ-TuRCs prevents ectopic microtubule nucleation and cell division defects. J Cell Biol 220.

Tsang, W.Y., Bossard, C., Khanna, H., Peränen, J., Swaroop, A., Malhotra, V., Dynlacht, B.D., 2008. CP110 suppresses primary cilia formation through its interaction with CEP290, a protein deficient in human ciliary disease. Dev Cell 15, 187-197.

Tsang, W.Y., Dynlacht, B.D., 2013. CP110 and its network of partners coordinately regulate cilia assembly. Cilia 2, 9.

Tsarouhas, V., Liu, D., Tsikala, G., Fedoseienko, A., Zinn, K., Matsuda, R., Billadeau, D.D., Samakovlis, C., 2019. WASH phosphorylation balances endosomal versus cortical actin network integrities during epithelial morphogenesis. Nat Commun 10, 2193.

Tsou, M.F., Stearns, T., 2006. Mechanism limiting centrosome duplication to once per cell cycle. Nature 442, 947-951.

Tsun, A., Qureshi, I., Stinchcombe, J.C., Jenkins, M.R., de la Roche, M., Kleczkowska, J., Zamoyska, R., Griffiths, G.M., 2011. Centrosome docking at the immunological synapse is controlled by Lck signaling. J Cell Biol 192, 663-674.

Uzbekov, R., Alieva, I., 2018. Who are you, subdistal appendages of centriole? Open biology 8, 180062.

Valente, E.M., Rosti, R.O., Gibbs, E., Gleeson, J.G., 2014. Primary cilia in neurodevelopmental disorders. Nat Rev Neurol 10, 27-36.

van Bon, B.W., Oortveld, M.A., Nijtmans, L.G., Fenckova, M., Nijhof, B., Besseling, J., Vos, M., Kramer, J.M., de Leeuw, N., Castells-Nobau, A., Asztalos, L., Viragh, E., Ruiter, M., Hofmann, F., Eshuis, L., Collavin, L., Huynen, M.A., Asztalos, Z., Verstreken, P., Rodenburg, R.J., Smeitink, J.A., de Vries, B.B., Schenck, A., 2013.

CEP89 is required for mitochondrial metabolism and neuronal function in man and fly. Hum Mol Genet 22, 3138-3151.

van Breugel, M., Hirono, M., Andreeva, A., Yanagisawa, H.A., Yamaguchi, S., Nakazawa, Y., Morgner, N., Petrovich, M., Ebong, I.O., Robinson, C.V., Johnson, C.M., Veprintsev, D., Zuber, B., 2011. Structures of SAS-6 suggest its organization in centrioles. Science 331, 1196-1199.

Varmark, H., Llamazares, S., Rebollo, E., Lange, B., Reina, J., Schwarz, H., Gonzalez, C., 2007. Asterless Is a Centriolar Protein Required for Centrosome Function and Embryo Development in Drosophila. Current Biology 17, 1735-1745.

Vasquez-Limeta, A., Loncarek, J., 2021. Human centrosome organization and function in interphase and mitosis. Semin Cell Dev Biol 117, 30-41.

Vavylonis, D., Kovar, D.R., O'Shaughnessy, B., Pollard, T.D., 2006. Model of formin-associated actin filament elongation. Molecular cell 21, 455-466.

Veleri, S., Manjunath, S.H., Fariss, R.N., May-Simera, H., Brooks, M., Foskett, T.A., Gao, C., Longo, T.A., Liu, P., Nagashima, K., Rachel, R.A., Li, T., Dong, L., Swaroop, A., 2014. Ciliopathy-associated gene Cc2d2a promotes assembly of subdistal appendages on the mother centriole during cilia biogenesis. Nature communications 5, 4207-4207.

Vertii, A., Hehnly, H., Doxsey, S., 2016. The Centrosome, a Multitalented Renaissance Organelle. Cold Spring Harb Perspect Biol 8.

Vieillard, J., Paschaki, M., Duteyrat, J.-L., Augière, C., Cortier, E., Lapart, J.-A., Thomas, J., Durand, B., 2016. Transition zone assembly and its contribution to axoneme formation in Drosophila male germ cells. The Journal of cell biology 214, 875-889.

Viterbi, A., 1967. Error bounds for convolutional codes and an asymptotically optimum decoding algorithm. IEEE transactions on Information Theory 13, 260-269.

Walentek, P., Quigley, I.K., Sun, D.I., Sajjan, U.K., Kintner, C., Harland, R.M., 2016. Ciliary transcription factors and miRNAs precisely regulate Cp110 levels required for ciliary adhesions and ciliogenesis. Elife 5.

Wang, X., Tsai, J.-W., Imai, J.H., Lian, W.-N., Vallee, R.B., Shi, S.-H., 2009a. Asymmetric centrosome inheritance maintains neural progenitors in the neocortex. Nature 461, 947-955.

Wang, X., Tsai, J.W., Imai, J.H., Lian, W.N., Vallee, R.B., Shi, S.H., 2009b. Asymmetric centrosome inheritance maintains neural progenitors in the neocortex. Nature 461, 947-955.

Wei, Q., Ling, K., Hu, J., 2015. The essential roles of transition fibers in the context of cilia. Curr Opin Cell Biol 35, 98-105.

Wieczorek, M., Bechstedt, S., Chaaban, S., Brouhard, G.J., 2015. Microtubule-associated proteins control the kinetics of microtubule nucleation. Nature Cell Biology 17, 907-916.

Winey, M., O'Toole, E., 2014. Centriole structure. Philos Trans R Soc Lond B Biol Sci 369.

Wong, S.S., Wilmott, Z.M., Saurya, S., Alvarez-Rodrigo, I., Zhou, F.Y., Chau, K.Y., Goriely, A., Raff, J.W., 2022. Centrioles generate a local pulse of Polo/PLK1 activity to initiate mitotic centrosome assembly. Embo j 41, e110891.

Wong, Y.L., Anzola, J.V., Davis, R.L., Yoon, M., Motamedi, A., Kroll, A., Seo, C.P., Hsia, J.E., Kim, S.K., Mitchell, J.W., Mitchell, B.J., Desai, A., Gahman, T.C., Shiau, A.K., Oegema, K., 2015. Cell biology. Reversible centriole depletion with an inhibitor of Polo-like kinase 4. Science 348, 1155-1160.

Woodard, L.E., Wilson, M.H., 2015. piggyBac-ing models and new therapeutic strategies. Trends Biotechnol 33, 525-533.

Woodruff, J.B., Wueseke, O., Hyman, A.A., 2014. Pericentriolar material structure and dynamics. Philos Trans R Soc Lond B Biol Sci 369.

Wu, C.-T., Chen, H.-Y., Tang, T.K., 2018. Myosin-Va is required for preciliary vesicle transportation to the mother centriole during ciliogenesis. Nature cell biology 20, 175-185.

Wu, Z., Pang, N., Zhang, Y., Chen, H., Peng, Y., Fu, J., Wei, Q., 2020. CEP290 is essential for the initiation of ciliary transition zone assembly. PLoS Biol 18, e3001034.

Xie, S., Dierlam, C., Smith, E., Duran, R., Williams, A., Davis, A., Mathew, D., Naslavsky, N., Iyer, J., Caplan, S., 2022. The retromer complex regulates C. elegans development and mammalian ciliogenesis. J Cell Sci 135.

Yadav, S.P., Sharma, N.K., Liu, C., Dong, L., Li, T., Swaroop, A., 2016. Centrosomal protein CP110 controls maturation of the mother centriole during cilia biogenesis. Development 143, 1491-1501.

Yamamoto, S., Kitagawa, D., 2019. Self-organization of Plk4 regulates symmetry breaking in centriole duplication. Nat Commun 10, 1810.

Yang, T.T., Chong, W.M., Wang, W.-J., Mazo, G., Tanos, B., Chen, Z., Tran, T.M.N., Chen, Y.-D., Weng, R.R., Huang, C.-E., Jane, W.-N., Tsou, M.-F.B., Liao, J.-C., 2018. Super-resolution architecture of mammalian centriole distal appendages reveals distinct blade and matrix functional components. Nature Communications 9, 2023.

Ye, X., Zeng, H., Ning, G., Reiter, J.F., Liu, A., 2014. C2cd3 is critical for centriolar distal appendage assembly and ciliary vesicle docking in mammals. Proc Natl Acad Sci U S A 111, 2164-2169.

Yeow, Z.Y., Lambrus, B.G., Marlow, R., Zhan, K.H., Durin, M.A., Evans, L.T., Scott, P.M., Phan, T., Park, E., Ruiz, L.A., Moralli, D., Knight, E.G., Badder, L.M., Novo, D., Haider, S., Green, C.M., Tutt, A.N.J., Lord, C.J., Chapman, J.R., Holland, A.J., 2020. Targeting TRIM37-driven centrosome dysfunction in 17q23-amplified breast cancer. Nature 585, 447-452.

Yi, J., Wu, X., Chung, A.H., Chen, J.K., Kapoor, T.M., Hammer, J.A., 2013. Centrosome repositioning in T cells is biphasic and driven by microtubule end-on capture-shrinkage. J Cell Biol 202, 779-792.

Zhang, J., Megraw, T.L., 2007. Proper recruitment of gamma-tubulin and D-TACC/Msps to embryonic Drosophila centrosomes requires Centrosomin Motif 1. Mol Biol Cell 18, 4037-4049.

Zhang, Y., Lin, H., Yang, Z., Wang, J., Sun, Y., Xu, B., Zhao, Z., 2019. Neural network-based approaches for biomedical relation classification: A review. Journal of Biomedical Informatics 99, 103294.

Zimmerman, W.C., Sillibourne, J., Rosa, J., Doxsey, S.J., 2004. Mitosis-specific anchoring of gamma tubulin complexes by pericentrin controls spindle organization and mitotic entry. Mol Biol Cell 15, 3642-3657.

Appendix

Written by Conor Wild, XChem (beamline i04-1), Life Sciences (Diamond Light Source). c.wild@diamond.ac.uk.

A1 Centrilyze

Centrilyze is trained on fluorescence microscope image data preprocessed to produce flattened 2d, 28x28 pixel PNG images (via a Python script written by Isaac Wong) in matplotlib's magma colourmap. Datasets are annotated as one of seven classes indicating the angle between the axis of the centriole and the focal plane.

A1.1. Data Classes

Centrilyze training data and test data is assigned to one of seven categories:

- "Oriented": A centriole whose axis is approximately perpendicular to the focal plane, called "Clear Ring" in thesis.
- "Precieved_Oriented": A centriole whose axis is almost perpendicular to the focal plane, called "Perceived Ring" in thesis.
- "Slanted": A centriole at approximately 45 degrees to the microscope, called "Slanted" in thesis.
- "Precieved_Not_Oriented": A centriole whose axis is almost parallel to the focal plane, called "Perceived Bar" in thesis.
- "Not_Oriented": A centriole whose axis is approximately parallel to the focal plane, called "Clear Bar" in thesis.
- "Unidentified": An image that either cannot be identified as a centriole or one in which the axis is not possible to determine, called "Unidentified" in thesis.

- "No_sample": An image that can be determined not to contain a centriole i.e. “is empty” of meaningful fluorescence. This data was not included in the thesis.

A1.2. Train/Test Split

The dataset was preprocessed as described in section 2.5.3. and then split into 10,378 samples from 5 videos for testing and 25,117 samples from 9 videos for training. The split was performed so that samples from the same video were not in both the training and testing set to ensure that the resulting trained network would be able to generalize to novel experiments.

A1.3. Architecture

Centrilyze is a Convolutional Neural Network (CNN) based centriole data classifier. Centrilyze is implemented in Pytorch (Paszke et al., 2019), a python library for tensor algebra and machine learning.

Centrilyze uses a Resnet 18 architecture with 1 input layer and seven output classes: "Oriented", "Precieved_Oriented", "Slanted", "Precieved_Not_Oriented", "Not_Oriented", "Unidentified" and "No_sample". This architecture was chosen as it is simple and known to perform well on image classification problems (He et al., 2016).

A1.4. Training

A1.4.1. Regularization and Data Augmentation

The network is trained without dropout layers. This is based on the size of the training data and the relatively small variation between samples relative to the parameterization of the network. Data is augmented with an affine transformation and a blur in order to prevent the network from overfitting. Input samples to the network are first subject to a random affine transform with a random angle and translated between -7 and 7 pixels in the x and y directions. Interpolation is bilinear. Samples then undergo a gaussian blur with a sigma between 0.01 and 2.0.

A1.4.2. Data Transformations

In training and testing input samples are transformed to grayscale and then each pixel is normalized to between 0.0 and 1.0.

A1.4.3. Loss Function

The network is trained with the typical CC-E loss function for classification CNNs.

A1.4.4. Optimizer

The network's parameters are optimized with the Adam optimizer with a learning rate of 0.001 (Kingma and Ba, 2014).

A2 Stability Analysis using a Hidden Markov Model

A2.1. Stability Analysis Premise

Classification errors and censored data due to missing frames, before, after and during the experiment, mean that a naive analysis of the expected time for a centriole to stay in its current state, and the relative probabilities of transitions to other states are difficult to determine. This is an appropriate problem to address with a hidden markov model (HMM) of the evolution of states.

A2.2. Theory and Assumptions

A2.2.1. Hidden Markov Models

A Hidden Markov Model specifies a time series of observed states (for centrilyze the orientation classification) and hidden states (for centrilyze the "true" orientation of the centriole).

Furthermore the model specifies that the observed state at any time only depends on the current hidden state, and that the current hidden state only depends on the previous hidden state. The model is thus characterized

by the transition probabilities, the probabilities one hidden state changes to another, and the emission probabilities, the probability a hidden state gives an observed state.

From these assumptions it is possible to estimate the most likely hidden state. If the hidden states can be associated with meaningful states, such as by having known emission probabilities, then this allows one to include information from the time series data in the estimate of the probability of the true state. This is the use to which this model is put in centrilyze.

To illustrate this, consider a series of three observed states: oriented, unknown, oriented. It may be more plausible that a true oriented state be misclassified as unknown than that an oriented state would transition to unknown, be correctly classified, and transfer back to oriented. This exact situation occurs when a centriole drifts out of the microscope plane for a frame. The Hidden Markov Model allows one to quantify how likely these two situations are and hence what the most likely true state of the unknown frame is.

These can be compared to expectations one might have from random changes in centriole orientation. Most important of these is that under random changes in orientation, a slanted centriole is more likely to become unoriented than oriented because there are more orientations that would be considered unoriented than oriented: if transitions towards orientation are found to be more likely it means that a biological process is biassing transition towards orientation.

A2.2.2. Centriole Orientation Dynamics Assumptions

- Centriole orientation dynamics are memoryless. This is plausible as the fluid dynamics of centriole orientation would be at very low Reynolds numbers (viscosity dominated rather than inertia dominated), however it is *possible* that biological processes do impart memory (the next state depends on previous states, not just the current one - an example might be a centriole that has remained oriented for some time is more likely to remain oriented) on time scales comparable to experiments.

- Centrioles reorientation is expected to happen on a timescale longer than between frames collected in an experiment. This is necessary in order for the estimates of the hidden markov model to be accurate, as otherwise the time dependence between states is lost.
- Transition probabilities between states are consistent within an experiment
    - Spatial differences in transition rates, for example because of the location of production of a protein which biassed state transitions, may challenge this
- Emission probabilities (Centrilyze classification errors relative to human) are consistent across experiments
    - Differences in data quality might lead to higher error rates, which can complicate this assumption

A2.3. Stability Analysis

The transition probability matrix of the Hidden Markov Model can, under reasonable assumptions, indicate how long a centriole is likely to stay in its current state. This is given by treating the self transition probability as failure probability of a geometric distribution (giving a mean time in the state as 1-the self transition probability). From this the number of frames the centriole is likely to stay in this state before transitioning can be determined, and then this can be multiplied by the time between frames to determine the time before a centriole transitions to another state. The transition matrix can also indicate bias in the transitions: for example, bias in transitions from unoriented states towards oriented ones.

A2.4 Implementation

Centrilyze stability analysis is implemented in python using the hmmlearn module. The Multinomial HMM class is used, and the emission matrix is not initialised randomly as it is known.

A2.5. Usage

A2.5.1. Training Emission Probabilities

Centrilyze's stability analysis is trained against the Cerntrilyze's annotations of its test set. Emission probabilities are first calculated from the error rates of Centrilyze against the human annotations in its test dataset.

A2.5.2. Training

For a new experiment the Hidden Markov Model is then trained with fixed emission probabilities using the Baum-Welch algorithm (Rabiner, 1989). This gives the transition probability matrix. Training is performed for 1000 iterations, and all centriole videos in the experiment are used in training.

A2.5.3. Evaluation

From the emission probabilities estimated from Centrilyze's error against humans and the transition probabilities estimated from Centrilyze's test dataset and the transition matrix estimated for an experiment using the Baum-Welch algorithm the model can be evaluated on novel data from that experiment to determine the most probable series of hidden states. The Viterbi algorithm is used in order to determine the most likely hidden states for each centriole video (Viterbi, 1967).

Supplementary References

He, K., Zhang, X., Ren, S., Sun, J., 2016. Deep Residual Learning for Image Recognition, 2016 IEEE Conference on Computer Vision and Pattern Recognition (CVPR). IEEE Computer Society, pp. 770-778.

Kingma, D.P., Ba, J., 2014. Adam: A method for stochastic optimization. arXiv preprint arXiv:1412.6980.

Paszke, A., Gross, S., Massa, F., Lerer, A., Bradbury, J., Chanan, G., Killeen, T., Lin, Z., Gimelshein, N., Antiga, L., 2019. Pytorch: An imperative style, high-performance deep learning library. Advances in neural information processing systems 32.

Rabiner, L.R., 1989. A tutorial on hidden Markov models and selected applications in speech recognition. Proceedings of the IEEE 77, 257-286.

Viterbi, A., 1967. Error bounds for convolutional codes and an asymptotically optimum decoding algorithm. IEEE transactions on Information Theory 13, 260-269.